192(1), 2023

PTNSS

COMBUSTION ENGINES

Wrocław University of Science and Technology

X INTERNATIONAL
CONGRESS ON COMBUSTION ENGINES

POLISH SCIENTIFIC SOCIETY
OF COMBUSTION ENGINES

June 19th-21st, 2023

congress.ptnss.pl

Wrocław University of Science and Technology
Faculty of Mechanical Engineering
27 Wybrzeże Wyspiańskiego Street, 50-370 Wrocław, Poland

Due to the dynamic development of machine and vehicle powertrains, the "Combustion Engines" scientific journal, while retaining its historical title, currently publishes works related not only to internal combustion engines, but also other powertrains, including hybrid drives, electric drives and fuel cells.

PTNSS Supporting Members
Członkowie wspierający PTNSS

BOSMAL Automotive Research and Development Institute Ltd
Instytut Badań i Rozwoju Motoryzacji BOSMAL Sp. z o.o

Motor Transport Institute
Instytut Transportu Samochodowego

Institute of Aviation
Sieć Badawcza Łukasiewicz – Instytut Lotnictwa

Automotive Industry Institute
Sieć Badawcza Łukasiewicz – Przemysłowy Instytut Motoryzacji

Sieć Badawcza Łukasiewicz – Poznański Instytut Technologiczny

AVL List GmbH

Solaris Bus & Coach S.A.

Air Force Institute of Technology
Instytut Techniczny Wojsk Lotniczych

Military Institute of Armoured & Automotive Technology
Wojskowy Instytut Techniki Pancernej i Samochodowej

Toyota Motor Poland Ltd. Sp. z o.o.

RADWAG Balances and Scales
RADWAG Wagi Elektroniczne

MS Mechatronic Solutions Group

FOGO Sp. z o.o.

COMBUSTION ENGINES
A Scientific Magazine

2023, 192(1)

Year LXII

PL ISSN 2300-9896
PL eISSN 2658-1442

Publisher:
Polish Scientific Society of Combustion Engines
60-965 Poznan, pl. M. Skłodowskiej-Curie 5, Poland
tel.: +48 61 6475966, fax: +48 61 6652204
E-mail: sekretariat@ptnss.pl
WebSite: http://www.ptnss.pl
Papers available on-line: http://combustion-engines.eu

Contents

Borkowski A, Zawiślak M. Comparative analysis of the life-cycle emissions of carbon dioxide emitted by battery electric vehicles using various energy mixes and vehicles with ICE 3

Ejilah RI, Ogbaneme AA, Agboneni OO, Adekunle SO. Analysis of jatropha oil-kerosene fuel mixtures on the performance of a variable-load direct injection CI engine 11

Kęska A, Janicka A, Zawiślak M. Numerical optimization of the BAT-CELL Bio-Ambient-Tests method for engine exhausts toxicity evaluation 19

Wozniak M, Siczek K, Zakrzewski S, Just P, Ozuna G, Onescu C. Deposition effect of carbon deposits on charge flow in EGR valve equipped CI engine 26

Andrych-Zalewska M, Sitnik L, Sroka Z, Mihaylov V. Fuel with a higher content of bio components in greenhouse effect aspects 36

Adamczyk P, Zięty A, Grygier D. Evaluation of materials used for coatings of electrical connectors used in the electrical harness of passengers cars 43

Regulski P. The material and economic assessment of the life cycle of city buses in the operational phase 50

Bienek F, Szczygiel I, Rutczyk B. Economical analysis of electric vehicles in Poland 55

Fąfara J-M, Modliński N. Numerical study of internal flue gas recirculation system applied to methane-hydrogen powered gas microturbine combustor 63

Stępień Z. Synthetic automotive fuels 78

Żurawski P. Optimization of the combustion chamber strength of aluminum pistons in diesel engines using the DuralBowl technology 91

Krakowski R. The effect of adding effective microorganism and silver compounds to flash point of engine oil 97

Publisher:
Polish Scientific Society of Combustion Engines
60-965 Poznan, pl. M. Sklodowskiej-Curie 5, Poland
tel.: +48 61 6475966, fax: +48 61 6652204
E-mail: sekretariat@ptnss.pl
WebSite: http://www.ptnss.pl

Subscriptions
Send subscription requests to the Publisher's address.
Cost of a single issue PLN 65.

Preparation for print
ARS NOVA Publishing House
60-782 Poznan, ul. Grunwaldzka 17/10A

Circulation: 80 copies

Printing and binding

Zakład Poligraficzny Moś i Łuczak, sp. j.,
Poznań, ul. Piwna 1

The journal is under the patronage of the Transport Committee of the Polish Academy of Sciences

The journal is registered and listed in the Polish and international database

Papers published in the
Combustion Engines
quarterly receive 70 points as stated by the Notification of the Minister of Science and Education dated 1 December 2021.

Declaration of the original version
The original version of the Combustion Engines journal is the printed version.

Cover
I – AVL RACETECH, hydrogen 2.0 dm^3 turbo engine *(www.avl.com)*;
background *(sun, stones, horizon – www.peakpx.com)*
IV – AVL and SuperTurbo™ Technologies on Hydrogen Engine Application *(www.hydrogen-central.com)*

Article citation info:
Borkowski A, Zawiślak M. Comparative analysis of the life-cycle emissions of carbon dioxide emitted by battery electric vehicles using various energy mixes and vehicles with ICE. Combustion Engines. 2023;192(1):3-10. https://doi.org/10.19206/CE-147159

Adam BORKOWSKI
Maciej ZAWIŚLAK

Combustion Engines
Polish Scientific Society of Combustion Engines

Comparative analysis of the life-cycle emissions of carbon dioxide emitted by battery electric vehicles using various energy mixes and vehicles with ICE

ARTICLE INFO

Received: 31 December 2021
Revised: 16 February 2022
Accepted: 6 March 2022
Available online: 13 March 2022

The research aims to find an effective way to reduce real-world CO_2 emissions of passenger vehicles, by answering the question of what kind of vehicles in various countries generates the smallest carbon footprint. Emissions were calculated for vehicles from three of the most popular segments: small, compact, and midsize, both with conventional body and SUVs. Each type of vehicle was analyzed with various types of powertrain: petrol ICE (internal combustion engine), diesel ICE, LPG ICE, petrol hybrid, LPG hybrid and BEV (battery electric vehicle) with four different carbon intensity of electric energy source. The final conclusion provides guidelines for environmentally responsible decision-making in terms of passenger vehicle choice.

Key words: *sustainable mobility, vehicle CO_2 emission, Life Cycle Assessment, carbon footprint, GHG reduction*

1. Introduction

According to the current state of scientific knowledge about the environment and climate, global warming caused mainly by anthropogenic CO_2 emissions is a problem that requires global action aimed at the fastest and most effective reduction of greenhouse gases (GHG) emissions [20]. The results of scientists' research contributed to the signing of the Paris Agreement. It is a legally binding agreement, signed by 190 countries from around the world. Its goal is to limit the phenomenon of global warming below 2 degrees Celsius and the effects of climate change as effectively as possible.

As a result, one of the activities of the European Parliament and the EU Council was to establish a regulation (EC) 443/2009 [9], setting CO_2 emission standards for new passenger cars. For 2020, the fleet-wide average emissions target was set at 95 g CO_2/km, which corresponds to fuel consumption of around 4.2 dm^3/100 km of petrol, 3.7 dm^3/100 km of diesel or 6.2 dm^3/100 km of LPG (*Liquefied Petroleum Gas*). The levels of average fuel consumption seem very unlikely to be obtained, but due to a few additional rules, manufacturers do not really have to obtain such low values of average fuel consumption. Some of the most questionable rules are as follows:

- excluding 5% of the most emitting new cars in calculations (in 2020),
- granting bonuses for eco-innovations that do not demonstrate a CO_2 reduction effect during the test procedures (up to 7 g/km credit),
- giving additional incentives for cars emitting less than 50 g/km (in 2020 these cars are counted as 2 vehicles, in 2021 as 1.67, in 2022 as 1.33),
- considering only direct emissions (TTW, tank to wheel),
- basing CO_2 emissions on unrealistic and outdated NEDC driving cycle, while fuel consumption levels are already measured with more realistic WLTP cycle,
- considering electric cars as vehicles with zero emission.

The exclusions described above are the result of a compromise between the EU authorities and the automotive industry lobby, linking interests of car manufacturers with alleged success in limiting the impact of passenger vehicles in the EU on global warming. Assuming that the global warming is a real and serious threat to the Earth and humanity, the success of achieving 95 g CO_2/km goal on paper, because of its simplifications and exceptions, should not be qualified as real progress in reducing the influence of transport on climate changes. The result of research carried out by Jato Dynamics [15] shows growing average CO_2 emissions of a new passenger cars in Europe in the years 2016-2019, despite increase in electric vehicle market and considering outdated NEDC driving cycle. In 2016, the average CO_2 emission of new car in Europe was 117.7 g/km, and by 2019 it had increased to 121.6 g/km. In 2020, thanks to increased sales of plug-in hybrids and pure electric vehicles, the number dropped to 106.7 g/km, so theoretically average CO_2 emissions of new cars in the EU started to decrease. As electric vehicles are treated as zero-emission, while in real life they emit CO_2 indirectly, mainly due to electric energy consumption, the success may not be as beneficial for climate as it may appear. The problem of emission from BEVs has already been described in the paper [23], with recommendation to use well-to-wheels methodology for calculating GHG emissions. It provides much more realistic results of GHG emissions of BEVs, but still does not account for emissions from vehicle production and maintenance, which may be very important, especially for BEVs used in countries with very low carbon intensity of electric energy production.

The main goal of the scientific research is to find solutions that could help limit real CO_2 emissions of passenger vehicles in Europe and potentially also in other countries by estimating a life-cycle CO_2 emissions of a variety of vehicles used in a few countries with different carbon intensity of energy production. The research aims to show the most effective way to limit real CO_2 emissions by passenger vehicles, and to answer the question what kind of vehicle people should use if they intend to limit the carbon footprint.

2. Methodology

From the perspective of climate change, tailpipe greenhouse gases emissions are as important as emissions related to all other activities, such as:

– extraction of materials for production of vehicle, fuel, spare parts, tires, fluids,
– production of vehicle, fuel, spare parts, tires, fluids,
– generation of energy for charging BEVs (Battery Electric Vehicles) and PHEVs (Plug-in Hybrid Electric Vehicles),
– vehicle maintenance,
– end of vehicle's life.

As there are no methods to directly measure GHG emission associated with all the activities above, to assess the life cycle emissions there is a need to use other methods, such as Life Cycle Assessment (LCA). The method allows to estimate the impact of the whole life cycle of a product or service on various environmental aspects. Based on the principles of the LCA method, the paper presents a simplified method of assessing lifetime emissions of passenger vehicles, that could potentially replace current standards of assessing GHG emissions of vehicles that include only tailpipe CO_2 emissions. The new method allows for obtaining more realistic values of GHG emissions than tailpipe emission itself and could be implemented to better assess the real influence of vehicles on global warming.

Total GHG emission of a vehicle during its life (E_{tot}) can be estimated as a sum of 5 main contributors with the greatest global warming potential:

– emission of vehicle production (E_{vp}), excluding battery cells in hybrid vehicles and BEVs,
– emission related to production of battery cells (E_{bp}),
– tailpipe emission (E_t),
– emission related to production of fuel and energy for use of the vehicle (E_{ep}),
– emission related to basic maintenance activities (E_m): replacement of engine oil, tires, and brakes.

The relation is represented by formula (1):

$$E_{tot} = E_{vp} + E_{bp} + E_t + E_{ep} + E_m \quad (1)$$

Based on a literature review [5, 12, 21, 22], it was concluded that end-of-life emission is still very difficult to estimate, especially as an industry-scale process of recycling batteries from electric vehicles is still under development. There are different methods for the end of life of each part of a vehicle, such as reuse, upcycling, recycling, downcycling, combustion, or landfill. Each method for each part of vehicle would result in different carbon footprint, so calculating the footprint without knowledge about processes that will be available in 10–20 years, at the end of life of currently new vehicles, could result in significant errors. Additionally, considering that in other studies the end-of-life carbon footprint is very low relative to other parts of vehicle life cycle, this component is excluded from the calculations.

Based on the results of LCA research of 10 Audi vehicles with different material composition [19, 26–29], carried out in accordance with ISO 14040 standard and verified by TÜV NORD CERT GmbH, the influence of the content of the materials of which passenger cars are mainly built was determined using the least squares method and set to 3 kg CO_2-eq per kg of steel, 12 kg CO_2-eq per kg of light metals (aluminum alloys, magnesium alloys) and 6 kg CO_2-eq per kg of the rest of the vehicles. For vehicles with low content of light metals (60% of steel, 10% of light metals, 30% of other materials), the calculated average GHG (greenhouse gas) emission of production stage is equal to 4.8 kg CO_2-eq per 1 kg of vehicle's empty weight without driver. For vehicles with high content of light metals (40% of steel, 30% of light metals, 30% of other materials), the calculated average GHG emission of production stage equals 6.6 kg CO_2-eq per 1 kg. For hybrid vehicles, PHEVs and BEVs, the weight of the materials for calculation of emission from production stage should exclude weight of battery cells. Therefore, emission of vehicle production can be estimated using the formula (2):

$$E_{vp} = 3 \cdot M_{steel} + 12 \cdot M_{al} + 6 \cdot M_{other} \quad (2)$$

where: E_{vp} – GHG emission of vehicle production excluding battery cells [kg CO_2-eq], M_{steel} – mass of steel and iron in vehicle [kg], M_{al} – mass of aluminum and aluminum alloys in vehicle [kg], M_{other} – mass of other materials in vehicle, apart from battery cells [kg].

Mass of each material may be calculated or estimated using mass of the vehicle (without battery cells) and the content percentage of each material type.

Although this method can be applied to estimate vehicle production stage emissions for most currently manufactured vehicles, it is not appropriate for vehicles with high content of carbon fiber reinforced polymers (CRFP).

One of the biggest source of uncertainty in determining greenhouse gases emission of vehicles is battery production. The production of 1 kWh battery cells generates, depending on the literature sources, from 38 to 490 kg of CO_2-eq. According to the review of 50 LCA publications from the years 2005-2020 [3], the median value of battery cells GWP is 120 kg CO_2-eq per 1 kWh of battery capacity. There is a possibility that real emissions of battery production for certain vehicles may be significantly smaller, as producers may reduce the emissions related to the production processes, e.g. by investing in renewable energy sources. The level of emissions may be as well much higher, when batteries are produced with high-carbon energy sources. The lower level of uncertainty was set to 70 kg CO_2-eq per 1 kWh of battery capacity, level corresponding to 25th percentile from the review [3], while the higher level was set to 175 kg CO_2-eq per 1 kWh of battery capacity, the 75th percentile from the same review. Emission of battery cells production can be estimated using the formula (3):

$$E_{bp} = 120 \cdot B_{ec} \quad (3)$$

where: E_{bp} – GHG emission of battery cells production [kg CO_2-eq], B_{ec} – overall energy capacity of battery cells [kWh].

Fuel and energy consumption of various types of vehicles has been determined by analysis of a few different sources: tests conducted by the ADAC association (ADAC Ecotest) [2], fuel consumption results submitted by users of spritmonitor.de website [24], honestjohn.co.uk website

[13], official website of the United States Environmental Protection Agency dedicated to fuel economy of vehicles (fueleconomy.gov) [10] and author's own research on fuel economy of LPG-powered vehicle.

Life cycle tailpipe emission can be estimated using the formula (4):

$$E_t = \frac{FC}{100} \cdot CI_{fb} \cdot TDD \quad (4)$$

where: E_t – total tailpipe GHG emission [kg CO_2-eq], FC - average fuel consumption of vehicle [dm^3/100 km], CI_{fb} - carbon intensity of burning particular fuel [kg CO_2-eq/dm^3], TDD – total distance driven by vehicle [km].

Carbon intensity of burning different fuels (CI_{fb} – carbon intensity of fuel burning) was assumed on the basis of Defra (Department for Environment, Food & Rural Affairs)/DECC (Department of Energy & Climate Change) guidelines [7]:

- gasoline (average biofuel blend): 2.2423 kg CO_2-eq/dm^3,
- diesel (average biofuel blend): 2.5835 kg CO_2-eq/dm^3,
- LPG: 1.5326 kg CO_2-eq/dm^3.

Production of fuel and electricity also contributes to total GHG emissions and it is included in the proposed estimation method in form of the formula (5):

$$E_{ep} = \left(\frac{FC}{100} \cdot CI_{fp} + \frac{EC}{100 * CH_{eff}} \cdot CI_e\right) \cdot TDD \quad (5)$$

where: E_{ep} – total GHG emission related to the production of fuel and energy for use of the vehicle [kg CO_2-eq], FC - average fuel consumption of vehicle [dm^3/100 km], CI_{fp} – carbon intensity of the production of particular fuel [kg CO_2-eq/dm^3], EC – average electric energy consumption of vehicle [kWh/100 km], CH_{eff} – overall efficiency of charging electric vehicle [-], CI_e – carbon intensity of electricity production [kg CO_2-eq/kWh], TDD – total distance driven by vehicle [km].

Emission related to production of fuel (CI_{fp} – carbon intensity of fuel production) was assumed on the basis of data available in Defra/DECC guidelines [7] and the following values were assumed for the calculations:

- gasoline (av. biofuel blend): 0.4750 kg CO_2-eq/dm^3,
- diesel (average biofuel blend): 0.5837 kg CO_2-eq/dm^3,
- LPG: 0.1918 kg CO_2-eq/dm^3.

Emission related to production of electricity (CI_e – carbon intensity of electricity) for BEVs assumed for the calculations:

- Poland: 0.724 kg CO_2-eq/kWh [8], as a representation of high-carbon intensity of electricity generation,
- USA: 0.417 kg CO_2-eq/kWh [14], as a representation of medium-carbon intensity of electricity generation,
- EU-27 average: 0.226 kg CO_2-eq/kWh [8], as a representation of low-carbon intensity of electricity generation,
- Sweden: 0.013 kg CO_2-eq/kWh [8], as a representation of very low-carbon intensity of electricity generation.

Emission related to maintenance activities can be estimated using the formula (6):

$$E_m = Oil_{cap} \cdot Oil_n \cdot CI_{oilp} + Br_{wt} \cdot Br_n \cdot CI_{brp} + 4 \cdot Tire_{wt} \cdot Tire_n \cdot CI_{tirep} \quad (6)$$

where: E_m – emission related to maintenance of vehicle [kg CO_2-eq], Oil_{cap} – average amount of engine oil for oil change [dm^3], Oil_n – number of oil changes over vehicle's life cycle [-], CI_{oilp} – carbon intensity of engine oil production [kg CO_2-eq/dm^3], Br_{wt} – weight of brake components that need to be periodically replaced [kg], Br_n – number of replacements of brake components over vehicle's life cycle [-], CI_{brp} – average carbon intensity of brake components production [kg CO_2-eq/kg], $Tire_{wt}$ – weight of single tire in size corresponding to vehicle specification [kg], $Tire_n$ - number of tire sets changes over vehicle's life cycle [-], CI_{tirep} – carbon intensity of tires production [kg CO_2-eq/kg].

The weight of replaceable brake components is assumed to be proportional to the weight of the vehicle, and can be estimated using the formula (7), based on [4] and [11]:

$$Br_{wt} = \frac{EVWT}{64} \quad (7)$$

where: Br_{wt} – weight of brake components that need to be periodically replaced [kg], EVWT – empty vehicle weight [kg].

Additional assumptions for GHG emission assessment:

- CH_{eff} – overall efficiency of charging electric vehicles: assumed value of 0.9,
- annual distance travelled: 15,000 km,
- vehicle lifespan: 20 years, TDD (total distance driven) = 300,000 km,
- battery of electric vehicles lasts for the whole lifespan of the car,
- energy density of battery cells: 250 Wh/kg, used to calculate empty vehicle weight without battery cells,
- Oil_n (number of engine oil changes) = 20, change of engine oil every year (all vehicles with internal combustion engines),
- Br_n (brakes changes over vehicle's life cycle) = 2 for petrol, diesel and LPG vehicles, 1 for hybrid petrol, hybrid LPG and LPG with eco-driving (thanks to reduced brake wear achieved by limited use of braking system), 0 for BEVs (thanks to greatly reduced brake wear achieved by highly effective regenerative braking),
- $Tire_n$ (tires changes) = 3 (75,000 km lifespan of tires, all vehicles),
- CI_{oilp} (life cycle GHG emission of engine oil production) = 5 kg CO_2-eq/dm^3 [17],
- CI_{brp} (average carbon intensity of brake components production) = 4 kg CO_2-eq/kg, based on [4] and [11],
- CI_{tirep} (carbon intensity of tires production) = 4 kg CO_2-eq/kg [25],

Assumptions concerning parameters of all analyzed types of vehicles are presented in Table 1. The author has made every effort to ensure that the assumptions about the vehicles are as close as possible to the values that characterise typical vehicles from each group. The list of exemplary vehicles from which the data were collected is as follows:

- small (B-segment) – e.g. Ford Fiesta, Honda Jazz, Hyundai i20, Opel Corsa, Peugeot 208, Peugeot e-208, Renault Clio, Renault ZOE, Toyota Yaris, and Volkswagen Polo as small cars with conventional body, Ford EcoSport, Honda HR-V, Hyundai Bayon, Hyundai Kona, Hyundai Kona Electric, Opel Crossland, Opel

Mokka, Opel Mokka-e, Peugeot 2008, Peugeot e-2008, Renault Captur, Toyota Yaris Cross, Volkswagen T-Cross, and Volkswagen T-Roc as small SUVs,
– compact (C-segment) – e.g. Ford Focus, Honda Civic, Hyundai i30, Opel Astra, Peugeot 308, Renault Megane, Toyota Corolla, Volkswagen ID.3, and Volkswagen Golf as compact cars with conventional body, Hyundai Tucson, Kia Sportage, Nissan Qashqai, Opel Grandland, Peugeot 3008, Renault Kadjar, Toyota C-HR, and Volkswagen Tiguan as compact SUVs,
– midsize (D-segment) – e.g. Ford Mondeo, Opel Insignia, Peugeot 508, Tesla Model 3, Toyota Camry, and Volkswagen Passat as midsize cars with conventional body, Ford Mustang Mach-E, Honda CR-V, Hyundai Santa-Fe, Kia Sorento, Nissan X-Trail, Peugeot 5008, Renault Koleos, Tesla Model Y, Toyota RAV-4 as midsize SUVs.

Values of empty weight and battery capacity are based on data gathered from technical specifications of vehicles from each vehicle type, as well as from tests conducted by the ADAC association [1]. Data concerning fuel and energy consumption are based on tests conducted by the ADAC association (ADAC Ecotest) [1], official U.S. Environmental Protection Agency website concerning fuel economy of vehicles [10] and data collected by users of websites Spritmonitor.de [24] and Honestjohn.co.uk [16]. Fuel consumption of LPG vehicles is based on consumption of petrol vehicles of the same type, with assumption of 30% increase of volumetric fuel consumption. The value is higher than frequently indicated 20% to compensate for additional petrol consumption during vehicle start-up and warm-up. Fuel consumption of LPG vehicles using eco-driving techniques is based on author's long-term research of LPG consumption of compact vehicle and extrapolated for other vehicle types. Data concerning tire weight are based on technical specifications of tires in typical sizes for each segment, gathered from the catalog of Continental Tires [6]. A higher tire weight was observed in BEVs compared to equivalent vehicles with ICE, probably due to the higher weight of the vehicles caused by lower energy density of battery cells compared to traditional fuels.

3. Results

The results of life cycle GHG emissions were estimated using formulas (1)–(7) and are presented in Fig. 1. The emissions were calculated for vehicles of three of the most popular segments: small (B-segment), compact (C-segment), and midsize (D-segment), divided into cars with conventional body and SUVs. For each type of vehicle, 10 different subtypes were analyzed:

1. Petrol vehicle.
2. Diesel vehicle.
3. LPG vehicle.
4. LPG vehicle used with eco-driving techniques.
5. Hybrid (petrol–electric) vehicle.
6. Hybrid (LPG–electric) vehicle.
7. Battery electric vehicle powered by electric energy in Poland.
8. Battery electric vehicle powered by an average electric energy in the USA.
9. Battery electric vehicle powered by an average electric energy in EU-27.
10. Battery electric vehicle powered by electric energy in Sweden.

Emission of vehicle is divided into five sources:

1. Vehicle production GHG emission (without battery cells production).
2. Tailpipe GHG emission.
3. Fuel/energy production GHG emission.
4. Maintenance GHG emission.
5. Battery cells production GHG emission, with lower and higher uncertainty level according to the values presented in the method section.

The most important results of the research are the values of total life cycle GHG emissions, which determine the impact of vehicle on global warming. In case of the same total distance driven for each vehicle, total emission is directly proportional to emission per kilometer, marked on the right axis of Fig. 1.

To visualize how the estimated total emission is distributed over the lifetime of vehicles with different fuel types and energy sources, Fig. 2 presents calculated cumulative greenhouse gases life cycle emissions over 20 years of compact car usage.

4. Discussion

By analyzing obtained calculation results, they can be summarized as follows:

1. In each type of vehicle, petrol vehicles generate the highest total GHG emission.
2. The average calculated reduction in emission, compared to petrol vehicles was found as follows:
   – 3.7% for diesel vehicles,
   – 10% for BEVs used in Poland,
   – 15% for LPG vehicles,
   – 18% for petrol hybrid vehicles,
   – 25% for LPG vehicles with eco-driving techniques,
   – 30% for LPG hybrid vehicles,
   – 37.5% for BEVs used in the USA, 54.5% for BEVs used in EU-27,
   – 74% for BEVs used in Sweden.
3. The average emission of SUV is 18.6% higher than emission of car with conventional body, 14% in small segment, 20% in compact segment, and 20.9% in midsize segment.
4. The average emission of electric SUV is 17.3% higher than emission of electric car with conventional body, 14.4% in small segment, 19.1% in compact segment, and 18% in midsize segment.
5. The average difference between emission of electric SUV and electric car in Poland is 32 g CO_2-eq/km (17.8% increase), while in Sweden the average difference is smaller: 8.3 g CO_2-eq/km (15.8%).
6. Total emission of electric vehicle used in Poland is 230–250% higher than in Sweden.
7. In countries with high-carbon intensity of electric energy production (such as Poland), total CO_2 emission of conventional cars, regardless of their fuel type is likely to be lower than emissions of BEV SUVs of the same segment, with reduction at the level of approximately:
   – 34% for hybrid LPG car,

Table 1. Assumed parameters of various vehicle types

Vehicle type	Fuel, energy source	Empty weight without battery cells	Empty weight with battery cells	Steel & iron content	Aluminum alloys content	Other materials content	Average fuel/energy consumption	Battery energy capacity	Engine oil capacity	Tire weight
		kg	kg	%	%	%	dm^3/100 km or kWh/100 km	kWh	dm^3	kg
Small car	Petrol	1100	1100	60	10	30	5.5	0	3.5	7
	Diesel	1150	1150	60	10	30	4.5	0	4	7
	LPG	1130	1130	60	10	30	7.2	0	3.5	7
	LPG eco-driving	1130	1130	60	10	30	6.2	0	3.5	7
	Hybrid Petrol	1170	1176	60	10	30	4.4	1.5	3.5	7
	Hybrid LPG	1200	1206	60	10	30	5.7	1.5	3.5	7
	BEV Poland	1200	1400	56	14	30	14	50	0	8
	BEV USA	1200	1400	56	14	30	14	50	0	8
	BEV EU-27 Avg	1200	1400	56	14	30	14	50	0	8
	BEV Sweden	1200	1400	56	14	30	14	50	0	8
Small SUV	Petrol	1200	1200	60	10	30	6.3	0	3.5	9.5
	Diesel	1250	1250	60	10	30	5.2	0	4	9.5
	LPG	1230	1230	60	10	30	8.2	0	3.5	9.5
	LPG eco-driving	1230	1230	60	10	30	7.1	0	3.5	9.5
	Hybrid Petrol	1270	1278	60	10	30	5	2	3.5	9.5
	Hybrid LPG	1300	1308	60	10	30	6.5	2	3.5	9.5
	BEV Poland	1300	1540	56	14	30	16	60	0	10.5
	BEV USA	1300	1540	56	14	30	16	60	0	10.5
	BEV EU-27 Avg	1300	1540	56	14	30	16	60	0	10.5
	BEV Sweden	1300	1540	56	14	30	16	60	0	10.5
Compact car	Petrol	1250	1250	60	10	30	6.4	0	4	8.5
	Diesel	1330	1330	60	10	30	5.2	0	4.5	8.5
	LPG	1280	1280	60	10	30	8.3	0	4	8.5
	LPG eco-driving	1280	1280	60	10	30	7.2	0	4	8.5
	Hybrid Petrol	1350	1356	60	10	30	5	1.5	4	8.5
	Hybrid LPG	1380	1386	60	10	30	6.5	1.5	4	8.5
	BEV Poland	1400	1640	56	14	30	16	60	0	10
	BEV USA	1400	1640	56	14	30	16	60	0	10
	BEV EU-27 Avg	1400	1640	56	14	30	16	60	0	10
	BEV Sweden	1400	1640	56	14	30	16	60	0	10
Compact SUV	Petrol	1400	1400	60	10	30	7.8	0	4	11
	Diesel	1500	1500	60	10	30	6.3	0	4.5	11
	LPG	1430	1430	60	10	30	10.1	0	4	11
	LPG eco-driving	1430	1430	60	10	30	8.8	0	4	11
	Hybrid Petrol	1500	1508	60	10	30	6.1	2	4	11
	Hybrid LPG	1530	1538	60	10	30	7.9	2	4	11
	BEV Poland	1600	1900	56	14	30	19	75	0	12
	BEV USA	1600	1900	56	14	30	19	75	0	12
	BEV EU-27 Avg	1600	1900	56	14	30	19	75	0	12
	BEV Sweden	1600	1900	56	14	30	19	75	0	12
Midsize car	Petrol	1500	1500	60	10	30	7.2	0	4.5	10
	Diesel	1600	1600	60	10	30	5.9	0	5	10
	LPG	1530	1530	60	10	30	9.4	0	4.5	10
	LPG eco-driving	1530	1530	60	10	30	8.1	0	4.5	10
	Hybrid Petrol	1600	1608	60	10	30	5.7	2	4.5	10
	Hybrid LPG	1630	1638	60	10	30	7.4	2	4.5	10
	BEV Poland	1600	1900	56	14	30	18	75	0	11
	BEV USA	1600	1900	56	14	30	18	75	0	11
	BEV EU-27 Avg	1600	1900	56	14	30	18	75	0	11
	BEV Sweden	1600	1900	56	14	30	18	75	0	11
Midsize SUV	Petrol	1650	1650	60	10	30	9	0	4.5	12
	Diesel	1750	1750	60	10	30	7.3	0	5	12
	LPG	1680	1680	60	10	30	11.7	0	4.5	12
	LPG eco-driving	1680	1680	60	10	30	10.1	0	4.5	12
	Hybrid Petrol	1750	1758	60	10	30	7.1	2	4.5	12
	Hybrid LPG	1780	1788	60	10	30	9.2	2	4.5	12
	BEV Poland	1800	2140	56	14	30	22	85	0	13
	BEV USA	1800	2140	56	14	30	22	85	0	13
	BEV EU-27 Avg	1800	2140	56	14	30	22	85	0	13
	BEV Sweden	1800	2140	56	14	30	22	85	0	13

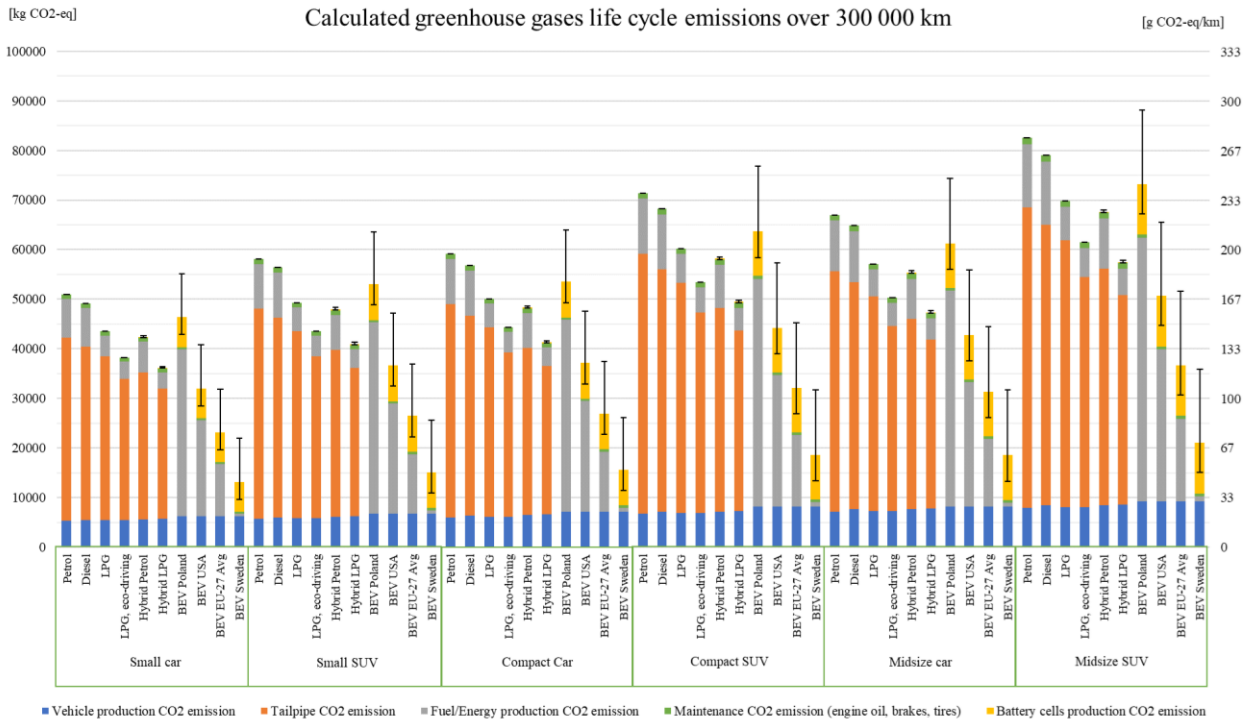

Fig. 1. Calculated greenhouse gases life cycle emissions of passenger vehicles over 300 000 km

Fig. 2. Calculated cumulative greenhouse gases life cycle emissions over 20 years of compact car usage

- 30% for LPG car with eco-driving techniques,
- 23% for hybrid petrol car,
- 20.5% for LPG car,
- 10% for diesel car,
- 6.5% for petrol car.

8. In countries with medium-carbon intensity of electric energy production (such as the USA) total GHG emissions of BEV SUVs are similar to emissions of cars of the same segment with conventional body and LPG hybrid (on average 5% lower total emission than BEV SUV in the USA) and economically driven LPG powertrain (on average 1% higher total emission than BEV SUV in the USA). Some more emissions are generated by cars with petrol hybrid (on average 11.4% higher total emission than BEV SUV in the USA) and LPG powertrain (on average 15% higher total emission than BEV SUV in the USA). Emissions of diesel and petrol cars are on average higher than BEV SUVs in the USA by respectively 30% and 35%.
9. In countries with low-carbon intensity of electric energy production (EU-27 average), total emissions of electric vehicles are much lower than vehicles with internal combustion engines of the same segment, on average by 46.4%. However, average emission per 1 km of electric

vehicles: compact SUV (107.2 g CO_2-eq/km), midsize car (104.5 g CO_2-eq/km) and midsize SUV (122.3 g CO_2-eq/km) exceeds 95 g CO_2-eq/km level set by UE authorities as a target tailpipe emission level for passenger vehicles in 2020, while small SUVs (88.2 g CO_2-eq/ km) and compact cars (89.9 g CO_2-eq/km) are also close to the value. The small differences between emission of midsize BEV SUV in EU-27 (122.3 g CO_2-eq/km) and smaller vehicles with internal combustion engines: small hybrid LPG car (120.6 g CO_2-eq/km, 1.4% less than midsize BEV SUV), economically driven small LPG car (127.5 g CO_2-eq/km, 4.2% more than midsize BEV SUV) and compact hybrid LPG car (137.7 g CO_2-eq/km, 12.6% more than midsize BEV SUV) shows that even with low-carbon intensity of electric energy production not all BEVs offer significant potential to reduce CO_2 emission compared to vehicles with internal combustion engines with relatively low level of CO_2 emission.

10. Even in countries with very low-carbon intensity of electric energy production such as Sweden, BEVs are not completely zero emission vehicles, as there are still emissions related to production of vehicle, battery and maintenance. Total calculated GHG emissions for BEVs in Sweden range from around 13 tonnes CO_2-eq for small car (43.9 g CO_2-eq/km) to around 21 tonnes CO_2-eq (70.2 g CO_2-eq/km) for midsize SUV. However, the total emissions of electric vehicles in Sweden are much lower than vehicles with internal combustion engines of the same segment, on average by 69%.
11. Results visualized in Fig. 2 show that increased GHG emission of the production stage of BEVs can be compensated in just 3–5 years compared to vehicle with ICE, but only with very low carbon intensity of electricity production. The higher the carbon intensity of electricity production, the longer it takes to compensate.

The results of the study demonstrate similarities with other studies on assessing the impact of vehicles on global warming. Study [18] also found that "… in Polish conditions, introducing cars with electric engines into circulation at the expense of withdrawing cars with internal combustion engines is not unequivocally positive." It also found that not only GHG emission of BEVs may be at similar level to those of vehicles with ICE, but also other pollutants, such as NO_x (nitrogen oxides), PM (particulate matter), and SO_2 (sulphur dioxide).

Another study [16] concluded that LPG may be a good alternative to petrol in terms of emissions and showed a 15–18% decrease in CO_2 emission, which is in line with findings in the current paper.

Each method of assessing GHG emission has its own limitation and is susceptible to input data. The presented method was developed to compare GHG emissions of different vehicles in a simple, yet effective way, with data available for customers of vehicles. Currently, customers are informed only about TTW (tank to wheel, tailpipe) CO_2 emission, which in case of battery electric vehicles does not exist. As there is a strong need to limit CO_2 emissions, the method can effectively help people choose the right vehicle that under certain conditions of use would also be the least harmful in terms of climate changes.

5. Conclusion

The final conclusions resulting from the conducted research are summarized as follows:

- in countries with high and medium-carbon intensity of electric energy production, driving a fuel-efficient hybrid or LPG vehicle may result in less total CO_2 emission than driving a battery electric vehicle (BEV), therefore BEVs are not always the best solution for limiting CO_2 emissions of transport,
- in countries with low and very low-carbon intensity of electric energy production, total CO_2 emission of BEVs is lower than that of similar vehicles with internal combustion engines,
- SUVs with both electric and internal combustion powertrains generate around 18% more CO_2 emissions than vehicles with conventional body of the same class and powertrain. In order to achieve real reductions of CO_2 emissions, popularity of SUVs should be reversed as soon as possible,
- LPG installation can decrease total CO_2 emission of petrol and hybrid vehicles by around 15%,
- eco-driving techniques can decrease total CO_2 emission of LPG vehicles by around 12% compared to normal, non-aggressive driving,
- national policies concerning passenger vehicles and their impact on climate change, covering aspects such as subsidies, excise duties, and taxes should take into account not tailpipe, but life cycle emissions of vehicles,
- low energy consumption of electric vehicle is essential in limiting its indirect CO_2 emissions, therefore it should be treated as a crucial parameter in the design process,
- high longevity is crucial in decreasing CO_2 emission per kilometer driven of electric vehicles. Reduced longevity would significantly increase emission of BEV per kilometer, as the emissions related to production of vehicle and battery would be divided by a shorter distance.

Battery electric vehicles are possibly the future of individual passenger transport, but it is crucial to recognize not only their advantages, but also their drawbacks. In order to minimize the impact of passenger transport on the environment, it is too early to simply replace all internal combustion vehicles with BEVs. In order to make these cars friendly to climate, they should use as little energy as it is possible and have a long service life. Electric vehicles with high energy consumption may hamper and prolong the transition to renewable energy, without which BEVs are not necessarily less harmful to the climate than fuel-efficient vehicles with internal combustion engines.

Nomenclature

BEV	battery electric vehicle
ICE	internal combustion engine
LPG	liquefied petroleum gas
CO_2-eq	carbon dioxide equivalent
GHG	greenhouse gas
SUV	sport utility vehicle

Bibliography

[1] ADAC Autotest. Available online: https://www.adac.de/infotestrat/tests/auto-test/alltests.aspx

[2] ADAC Ecotest. Available online: https://www.adac.de/rund-ums-fahrzeug/tests/ecotest/

[3] Aichberger C, Jungmeier G. Environmental life cycle impacts of automotive batteries based on a literature review. Energies. 2020;13:23. https://doi.org/10.3390/en13236345

[4] Anderson C, Dettmann T. Environmental footprint and performance analysis of a brake disc production line using discrete event simulation. 2013. Available online: https://odr.chalmers.se/bitstream/20.500.12380/182182/1/182182.pdf

[5] Bieker G. A global comparison of the life-cycle greenhouse gas emissions of combustion engine and electric passenger cars. International Council on Clean Transportation. 2021. https://theicct.org/publications/global-LCA-passenger-cars-jul2021

[6] Continental Tire Catalog. Available online: https://continentaltire.com/tire-search

[7] DEFRA/DECC Guidelines to Defra/DECC GHG conversion factors for company reporting. Department of Energy and Climate Change. 2012.

[8] Energiewende A. Agora Energiewende and Ember (2021):The European Power Sector in 2020: Up-to-Date Analysis on the Electricity Transition. 2021. https://static.agora-energiewende.de/fileadmin/Projekte/2021/2020_01_EU-Annual-Review_2020/A-EW_202_Report_European-Power-Sector-2020.pdf

[9] European Parliament. Council of the European Union. Regulation (EC) 2009, 443(140). https://eur-lex.europa.eu/legal-content/EN/ALL/?uri=celex%3A32009R0443

[10] FuelEconomy.gov. The Official U.S. Government source for fuel economy information. https://www.fueleconomy.gov/

[11] Gradin KT, Åström AH. Comparative life cycle assessment of car disc brake systems–case study results and method discussion about comparative LCAs. Int J Life Cycle Ass. 2020;25:2. https://doi.org/10.1007/s11367-019-01704-9

[12] Hill N, Amaral S, Morgan-Price S, Nokes T, Bates J, Helms H et al. Determining the environmental impacts of conventional and alternatively fuelled vehicles through LCA. Final Report for the European Commission. 2020.

[13] Honest John RealMPG. Available online: https://www.honestjohn.co.uk/real-mpg/

[14] How much carbon dioxide is produced per kilowatthour of U.S. electricity generation? Available online: https://www.eia.gov/tools/faqs/faq.php?id=74&t=11

[15] Jato Dynamics, Munoz F. Increased demand for EVs in 2020 contributed to 12% fall in Europe's average CO_2 emissions. 2021. Available online: https://www.jato.com/wp-content/uploads/2021/04/CO2-Europe-2021-Release-Final.pdf

[16] Jaworski A, Lejda K, Lubas J, Mądziel M. Comparison of exhaust emission from Euro 3 and Euro 6 motor vehicles fueled with petrol and LPG based on real driving conditions. Combustion Engines. 2019;178(3):106-111. https://doi.org/10.19206/CE-2019-318

[17] Kettunen M. No more room for friction in our sustainability efforts. Available online: https://www.neste.com/blog/base-oils/no-more-room-friction-our-sustainability-efforts

[18] Laskowski PP, Zimakowska-Laskowska M, Zasina D, Wiatrak M. Comparative analysis of the emissions of carbon dioxide and toxic substances emitted by vehicles with ICE compared to the equivalent emissions of BEV. Combustion Engines. 2021;187(4):102-105. https://doi.org/10.19206/CE-141739

[19] Life Cycle Assessment. Audi looks one step ahead. 2011. Available online: https://docplayer.net/21911056-Life-cycle-assessment-audi-looks-one-step-ahead.html

[20] Masson-Delmotte V, Zhai P, Pirani A et al. Climate change 2021. The physical science basis. Contribution of Working Group I to the Sixth Assessment Report of the Intergovernmental Panel on Climate Change. 2021, 6. https://www.ipcc.ch

[21] Merkisz J, Pielecha J, Fuć P. Badania i analizy zużycia energii i emisji zanieczyszczeń przez pojazdy w sieci drogowej. Komitet Inżynierii Lądowej i Wodnej PAN, Warszawa, 2013.

[22] Prussi M, Yugo M, De Prada L, Padella M, Edwards R, Lonza L. JEC well-to-wheels report v5, EUR 30284 EN. Publications Office of the European Union. 2020. https://doi.org/10.2760/959137

[23] Sitnik L. Emissions of e-mobility. Combustion Engines. 2019;178(3):135-139. https://doi.org/10.19206/CE-2019-323

[24] Spritmonitor. Available online: https://www.spritmonitor.de/

[25] Sun X, Zheng J H, Zhang P, Zhao MN, Wu HX, Yan YT. Comparative life cycle assessment of Chinese radial passenger vehicle tire. Mater Sci Forum. 2017;898:2432-2445. https://doi.org/10.4028/www.scientific.net/MSF.898.2432

[26] The new Audi A3 Life Cycle Assessment. 2012. Available online: https://docplayer.net/29037623-The-new-audi-a3-life-cycle-assessment.html

[27] The new Audi A8 Life Cycle Assessment. 2018. Available online: https://www.audi.com/content/dam/gbp2/company/sustainability/downloads/documents-and-policies/umweltbilanzen/en/ONLINE_Booklet_Umweltbilanzierung_Audi_A8_EN_2018.pdf

[28] The new Audi R8 Life Cycle Assessment. 2015. Available online: https://www.audi.com/content/dam/gbp2/company/sustainability/downloads/documents-and-policies/umweltbilanzen/en/Audi_R8_LCA_English.pdf

[29] The new Audi TT Coupé Life Cycle Assessment. 2015. Available online: https://www.audi.com/content/dam/gbp2/company/sustainability/downloads/documents-and-policies/umweltbilanzen/en/Audi_TT_LCA_English.pdf

Adam Borkowski, MEng. – Faculty of Mechanical Engineering, Wroclaw University of Science and Technology.
e-mail: *adam.borkowski@pwr.edu.pl*

Maciej Zawiślak, DSc., DEng. – Faculty of Mechanical Engineering, Wroclaw University of Science and Technology.
e-mail: *macej.zawislak@pwr.edu.pl*

Article citation info:
Ejilah RI, Ogbaneme AA, Agboneni OO, Adekunle SO. Analysis of jatropha oil-kerosene fuel mixtures on the performance of a variable-load direct injection CI engine. Combustion Engines. 2023;192(1):11-18. https://doi.org/10.19206/CE-153463

Robinson I. EJILAH
Abiodun A. OGBANEME
Osazoduwa O. AGBONENI
Sikiru O. ADEKUNLE

Combustion Engines
Polish Scientific Society of Combustion Engines

Analysis of jatropha oil-kerosene fuel mixtures on the performance of a variable-load direct injection CI engine

ARTICLE INFO

Received: 14 June 2022
Revised: 25 August 2022
Accepted: 2 September 2022
Available online: 4 September 2022

Jatropha oil was blended with kerosene in ratios; JOK0, JOK20, JOK30, JOK40 and JOK50 and benchmarked against conventional diesel fuel. The blended fuel samples was test-run on a TD110-TD115 TQ small CI engine test rig, and emission levels for the fuel samples were examined using an SQV automobile exhaust gas analyser. The JOK20 fuel sample offered a better performance in terms of higher BP, BTE, and EGT followed by; JOK30, JOK40 and JOK50 blends; and also exhibited lower SFC, BSEC and AFR, hence less fuel consuming than diesel fuel. A reduction in CO emission was recorded for JOK20, and a significant cut was also observed for JOK30, JOK40 blends with load increase.; while, JOK30, JOK40 and JOK50 samples exhibited higher CO_2 and lower UHC emission levels than diesel. No traceable level of NO_x emission was recorded for JOK20 fuel sample.

Key words: *jatropha oil, kerosene, CI engine, performance, emission*

1. Introduction

Over the years there has been a worldwide search and move towards the application of alternative, and renewable fuels with low environmental impact. Crude oil reserve depletion, price uncertainty and negative effect of fossil fuels on the environmental are responsible for this move. Alternative fuels have superior performance and environmental emission reduction abilities. Oils from plant sources have demonstrated very good potentials to be used as alternative fuels; due to their renewability, and ability to lower greenhouse emission while improving energy security [1].

Jatropha curcas is one of such promising energy crops, with high seed oil content ranging from 30 to 50% by weight [2]. Studies have shown that the usage of non-edible oils in neat form is possible but not preferable [3]. The crude jatropha oil contains 21% saturated fatty acids and 75% fuel diesel fuel blends produce remarkable results in fuel economy, brake power and minimal combustion chamber wear in compression ignition engines. Nonetheless, in longer term usage, the high viscosity of non-edible oils and the low volatility affects the atomization and spray pattern of fuel, leading to incomplete combustion and severe carbon deposits, clogging of fuel filter, coking of injector tips, and piston ring sticking, would be common place engine durability challenges [4–13]. However, to surmount these challenges, the transesterification or blending of jatropha curcus oil would be required to reduce the oil's viscosity profile [14–16].

Azad et al. [17] found that the result of; calorific value (CV), brake specific fuel consumption (BSFC) and brake thermal efficiency (BTF) of mustard seed oil blended with kerosene at 20% and 30% of the blends, were close to that of the diesel fuel. The resulting blends also gave better engine performance behavior when compared with other fuel blends in the group, thus making it suitable for use in compression ignition (CI) engines.

Ghormade et al. [18] in a study compared the performance of two vegetable oil blends with kerosene (i.e. soybean oil with kerosene, and rapeseed oil with kerosene) with conventional diesel fuel. It was observed that; blends of 20% vegetable oil with 80% kerosene by volume fairly improves the thermal efficiency of the test engine under high loading conditions. Huzayyin et al. [19] reported fairly improved thermal efficiency in the case of heavy loading for high pressure injection engine during the performance test of blends of heavy fuel, and low grade oil kerosene compared with diesel fuel at 60% fuel oil and 40% kerosene by volume.

Sanjid et al. [20] found that the palm and jatropha oil blend (PBJB10) showed 20.49% reduction in carbon monoxide (CO) emission compared with diesel fuel. This blend demonstrated better results with unburnt hydrocarbon (UHC) emissions and sound levels. In a related study, Nalgundwar et al. [21] tested dual biodiesel palm and jatropha oils with diesel fuel; the blend D70JB15PB15 exhibited a 14.5% CO reduction in emission. While, the blend D90JB5PB5 shows 5.3% increase in NO_x emission. In addition, Agarwal et al. [22] found that CO, UHC and carbon dioxide (CO_2) emissions were less in the B20 engine compared to the emission arising from the use of conventional diesel fuel. However, in the same study, the oxides of nitrogen (NO_x) emission levels was observed to be higher rate of emission due to the presence of fuel oxygen. The use of unprocessed jatropha oil as fuel may be difficult due to its high density and density. However, other than blending with kerosene, the high viscosity could also be significantly reduced with the addition of n-hexane, save that it could generate a negating ecological condition due to the increased concentration of nitrogen oxides, as it is with canola oil [23]. Existing literature has also revealed that that fish waste and jatropha oil can be used as alternate fuel for engines without modifying any specifications of the engine, and also, the emissions from the engine showed a better

result except NO_x which is higher [24]. Jatropha oil is gaining a lot of attention on account of the fact the ecological impact in CO_2 reduction and climate change mitigation as a safe aviation fuel is also been considered. Due to the fact that aviation sector has no near-term alternative to liquid hydrocarbon fuels, the SAF produced from variable renewable feedstock-including jatropha, seems to be the best option for modern aviation fleet [25].

Furthermore, in a study by Hemanandh et al. [26], the performance and emission characteristics of hydro treated jatropha oil and kerosene blends was reported. The results showed a decrease in CO, UHC, CO_2 and NO_x emissions for HK10, HK20 and HK30 blends. An observable increase in BTE, decrease in BSFC and increase in smoke emission for HK10, HK20 and HK30 blends where also reported. Madiwale et al. [27] showed improvement in brake power (BP), BSFC, and BTE at various loading conditions. Several works have been published on the performance and emission behavior of vegetable oils blended with diesel and kerosene, However, the objective of this paper is evaluate the effect of jatropha oil blended with kerosene, and varying engine load on the performance and emission of an air cooled-single cylinder, 4-stroke direct injection (DI) diesel engine, and identify which blended sample(s) offers significant potential as sustainable fuel for modern diesel engines.

2. Materials and Methods

The jatropha, kerosene and diesel oil were used for this experiment. The diesel and kerosene fuel were purchased from a government approved fuel station in Bauchi-Nigeria, while the jatropha oil with fatty acid composition and chemical structure presented in Table 1 below was purchased from a local supplier. The proportion of fuel blends used are presented in Table 2. Physical properties of jatropha oil, kerosene and diesel oil and jatropha oil-kerosene blends (refer to Tables 3 and 4) were determined in accordance with standardized ASTM test procedures; ASTM D97-93, ASTM D2015-85, ASTM D 93-94, ASTM D D613, ASTM D 445 for density, higher heating value, flash point, octane number and kinematic viscosity respectively [28].

Table 1. Fatty acid composition (%) and chemical structure of jatropha curcas oil [13]

Name	Composition [%]	Structure
Palmitic acid	12.6	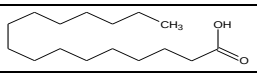
Stearic acid	3.9	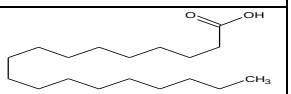
Oleic acid	41.8	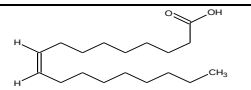
Linoleic acid	41.8	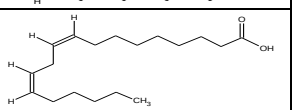
Linolenic acid	7.8	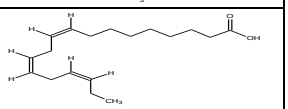

Table 2. Samples of fuel mixtures used

Blend name	Percentage of blends
Diesel	100% Diesel
JOK0	100% jatropha oil
JOK20	80% jatropha oil and 20% kerosene
JOK30	70% jatropha oil and 30% kerosene
JOK40	60% jatropha oil and 40% kerosene
JOK50	50% jatropha oil and 50% kerosene

Table 3. Physico-chemical and fuel properties of jatropha curcas, kerosene, and diesel oil [13, 29]

Properties	Jatropha oil	Kerosene oil	Diesel oil
Viscosity (cp) @35^{o}C	40.4	1.067	2.7
Specific density @35^{o}C	0.917	0.79	0.835
Cetane value	33.7–51	42	47.8
Flash point [^{o}C]	274	37.8	65.5
Carbon residue [%]	0.64	–	< 0.05
Sulfur [%]	0.13	0.04 -0.3	< 1.0
Acid value	38.2	–	–
Saponification value	198	–	–
Iodine value	112.5	–	–
Calorific value	39,862	46,520	45,457

Table 4: Summary of the properties of jatropha oil with kerosene and diesel blends

Fuel property	JOK0	JOK20	JOK30	JOK40	JOK50
Density at 30^{o}C [kg/m^3]	917	884	878	869	856
Kinematic viscosity at 40^{o}C [mm^2/s]	50.93	3.85	3.67	3.51	3.19
Flash point [^{o}C]	274	195	191	187	180
Pour point [^{o}C]	2	< 2	< 2	< 2	< 2
Cloud point [^{o}C]	14	10	7	6	4
Specific gravity	0.917	0.888	0.882	0.873	0.860
Calorific value [MJ/kg]	39,862	40.874	41.122	41.687	42.125

2.1. Experimental setup and procedure

The neat jatropha oil was blended with kerosene at various proportions such as JOK0, JOK20, JOK30, JOK40, and JOK50 on volumetric basis and was tested in a single cylinder, air-cooled, 4 stroke and DI diesel engine mounted on an engine test bed, coupled to a hydraulic dynamometer was used (refer to Fig. 1 for schematic diagram and Table 5 for technical specification of the test rig). A SV-5Q automobile exhaust gas analyzer incorporated to the test rig's exhaust tail pipe was also used to measure the CO, CO_2, UHC and NO_x emissions from the engine. For a constant speed and variable load engine test rig with a hydraulic dynamometer, the time taken by the engine to consume 8 ml of the fuel was recorded at a constant speed 1400 rpm and at varying load of 500 g, 1000 g, 1500 g, 2000 g and 2500 g. The torque, exhaust temperature, oil temperature for all fuel samples were recorded. Engine performance measurements such as BSFC, air flow rate, BP, Brake specific energy consumption (BSEC), BTE, and air-fuel ratio (AFR) were taken. Engine performance test for diesel was also conducted as a basis for comparison. Technical specifications of the engine test rig are shown in Fig 1. A multi

gas analyzer was used to measure the concentration of gaseous emissions CO, CO_2, UHC, and NO_x, in order to determine the emission characteristics of the various blends. The performance and emission characteristics of fuel samples were analyzed and discussed.

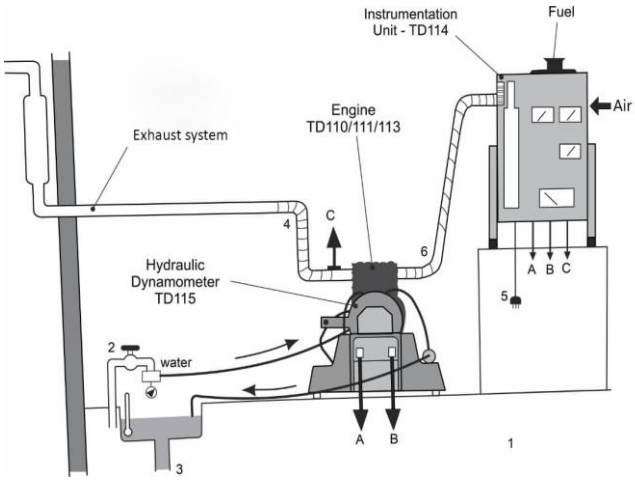

Fig. 1. An illustration of a complete TD110-TD115 TQ small engine test rig [30]

Table 5. Technical specifications of engine [30]

S/N items	Engine data
1. Model	TD110-115
2. Method of starting	manual starting
3. Engine type	single cylinder, 4-stroke diesel
4. Bore stroke	79.5× 955 mm
5. Piston stroke/stroke	115 mm
6. Displacement	1896 cm^3
7. Rated speed	1500 rpm
8. Maximum output	5.6 kW
9. Compression ratio	12:1 to 17.5:1
10. Maximum MEP	1400 kPa
11. Cooling method	air cooled
12. Fuel and lube oil	filter present
13. Injection pump	Bosh VE VP 37

3. Results and discussions

3.1. Effect of load and fuel samples on engine performance

Figure 2 shows the influence of diesel, jatropha oil, jatropha oil and kerosene (JOK) blends on brake power as a function of load. The pure jatropha oil (JOKO) exhibits the same behaviour with diesel as there was no significant change in engine BP at minimum and maximum loads. Nonetheless, the BP of JOK0 increased by 1.73% at 2000 g, while the BP of JOK20 fuel sample increased by 71% and 28% at minimum and maximum loads respectively, and reached a maximum at 2500 g. It was observed that the BP for JOK30 blend increased by 33% at minimum load. At maximum load the change in brake power is negligible. While, it was also noted that the JOK 40 fuel sample exhibited no significant changes in BP at minimum and maximum loads. The brake power for JOK50 increased by 29% at minimum load. There were no significant changes in BP at maximum load even though, a simulation study have shown that engine load some what affects; the axial movements of the rings in the grooves, elastic contact of the ring and cylinder surface asperities, and causes power losses due to the ring friction [31]. Furthermore, it could be seen that all tested fuel samples registered their highest BP under the condition of maximum load. These results show that JOK20 blend exhibited a comparably higher BP at minimum and maximum load points when compared with diesel [27]. The BP increased with increase in the engine load for all test fuels because of the enhanced combustion and decrease in frictional losses at higher loads [32].

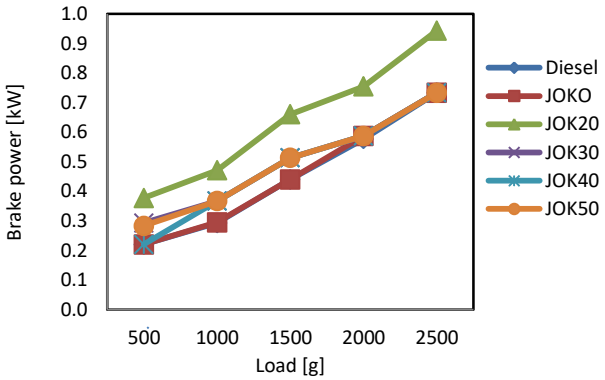

Fig. 2. Variation of BP for JOK blends with increase in load

Figure 3 shows the variation of SFC for JOK blends and diesel under different loading condition. In general, the BSFC was found to decrease with increase in the engine load for all test fuels. This was because of improved combustion in the cylinder at higher loads [32]. The trend of JOK0 fuel sample shows no significant change in SFC when compared with conventional diesel fuel.

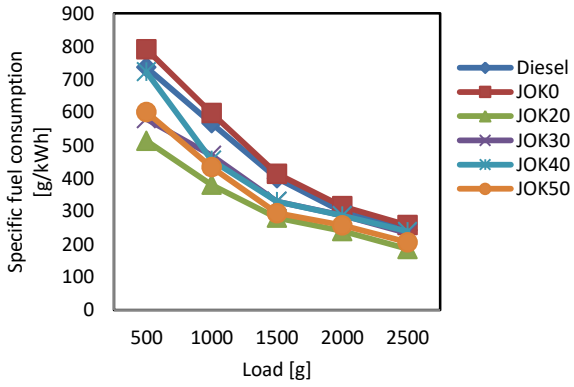

Fig. 3. Variation of SFC for JOK blends with increase in load

The SFC behavior for other blends under consideration at minimum and maximum loads are discussed as follows; JOK20 decreased from 71% to 28%, JOK30 decreased from 33% to 0%, JOK40 exhibits the similar behavior with diesel at minimum and maximum loads. However, at 1000 g engine load JOK20 sample exhibited the best SFC performance. While, JOK50 decreased from 28% to 0% from 1000 g to 1500 g. The improvement in SFC of JOK20 fuel sample ascribed to better combustion behavior of the fuel blend largely influenced by the presence of oxygen in the blend [32], and the addition of higher composition of kerosene lowers the viscosity of the blends (refer to table 4) and improves fuel spray atomization and subsequently the fuel

combustion. However, recent finding have also shown that The use of nanoparticles (such as; Al_2O_3 and TiO_2) in fuels could also be employed to improve engine efficiency and reduce fuel consumption with no observed changes in the exhaust gas temperature after addition of nanoparticles [33].

The Fig. 4 presents the variation of AFR of diesel and other blends as a function of load. The trend of the effect of the variations caused by tested fuel samples at minimum and maximum loads are observed as follows; JOK0 sample decreases by 6.8% and 5.8% respectively with its lowest AFR occurring at 2000 g; JOK20 fuel sample decreases by 16.4%, and increased by 1.7%, exhibiting its highest AFR at maximum load; JOK30 fuel sample decreases by 4.7%, and increased by 4% revealing its highest AFR occurring at the intermediate load points; JOK40 fuel sample increases by 1.8% and 1.7% with its highest AFR recorded at the minimum load; and JOK50 blended sample decreases by 7.9%, and increases by 18%, with its highest AFR is at maximum load.

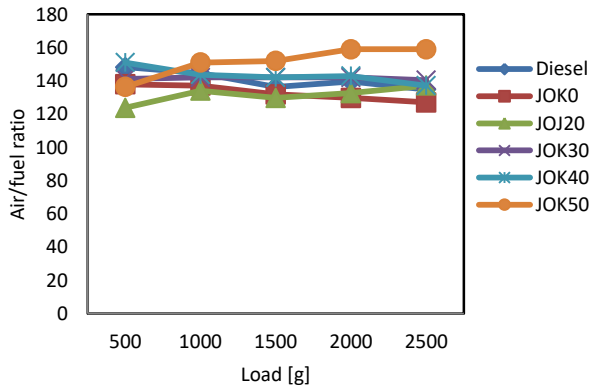

Fig. 4. Variation of AFR for JOK blends with increase in load

The illustration of BSEC variations for tested fuels and blends as a function of load is presented in Fig. 5. The trends in BSEC at minimum and maximum loads are discussed as follows: JOK0 fuel sample decreased from 6.7% to 2.7%; JOK20 blends decreases from 37% to 31.2%; JOK30 fuel decreased from 28.7% to 13.1%; JOK40 sample decreased from 9.9% to 9.8%. JOK50 blended fuel sample decreased from 24.4% to 21.4%. A general decrease in BSEC with increase in load was observed for all tested fuel samples under the varying loading condition.

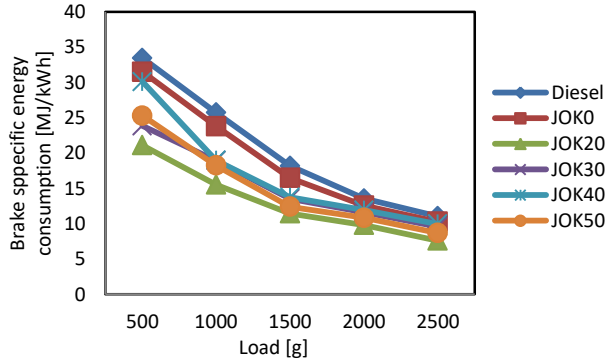

Fig. 5. Variation of BSEC for JOK blends with increase in load

The main reason for this could be credited to the fact that the percent increase in the amount of fuel required to operate the engine is less than the percent increase in BP. The blended samples appear to produced lower BSEC compared to diesel fuel. This lowering of the BSEC could be explained in terms of the availability of the oxygen in the fuel blends. BSEC is the energy input required to develop unit brake power, and is independent of the fuel used. When two different fuels of different heating values are blended together, the fuel consumption may not be reliable, since the heating value and density of the two fuels are different. In such cases, the BSEC will give more reliable value [34].

The BTE gives an idea of the output generated by the engine with respect to heat supplied in the form of fuel. Figure 6 shows variation in thermal efficiency for the fuels with increase in engine load. An increase in BTE was observed for all tested fuel blends for all loading condition. The variations in BTE at minimum and maximum loads for all samples is as follows: JOK0 sample increased from 15.3% to 36.5%; JOK20 blend increased from 17% to 47.5%; JOK30 fuel blend increased from 15.1% to 37.5%; JOK40 fuel sample increased from 11.9% to 36.2%; and JOK50 fuel blends increased from 13.7% to 41.5%. For all tested samples, JOK20 fuel samples exhibited the highest thermal efficiency, this too can be attributed to the commensurate increase in engine power with load increment. The BP increased with increase in the engine load for all test fuels – so does the BTE, because of enhanced combustion and decrease in frictional losses at higher loads [35]. The frictional losses could be further enhanced by the lubricity properties of the jatropha oil occasioned by its high saponification values (refer to Table 3). In addition, the SFC of an engine is inversely proportional to its BTE, hence decrease in SFC resulted in increase of the BTE. From the foregoing, it could be observed that the BTE of JOK fuel samples were observable higher than diesel under varying loading conditions.

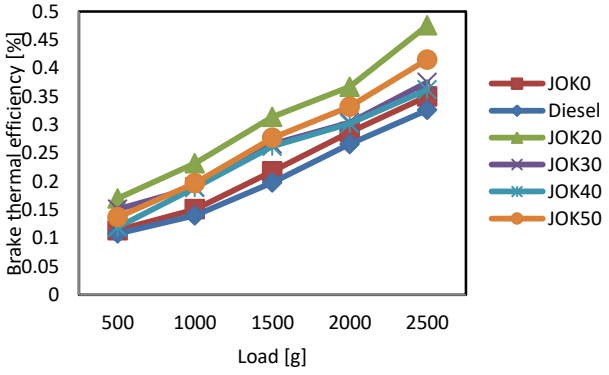

Fig. 6. Variation of BTE for JOK blends with increase in load

Figure 7 illustrates the results of the variation of EGT with load for diesel and various fuel blends under study. Under all loading condition, JOK and blends were found to have lower EGT compared to diesel. JOK30, JOK40 and JOK50 fuel samples demonstrated a comparatively lower EGTs when compared with JOK 20 and JOK0 fuel samples. The high EGT in this case is traceable to the presence

of higher concentration of jatropha oil (JOK0 and JOK20) in the fuel sample, with its relatively lower heating value than kerosene and diesel fuel (refer to Table 3), and this would require higher amount of fuel in the engine to generate that extra power needed to take on the additional loading. From the foregoing engine performance results (refer to Fig. 6), a relationship could also be established between EGT and BP, on account of the fact that, a rise in combustion temperature brings about an increase in the pressure acting on the piston, to improve mechanical power output [36].

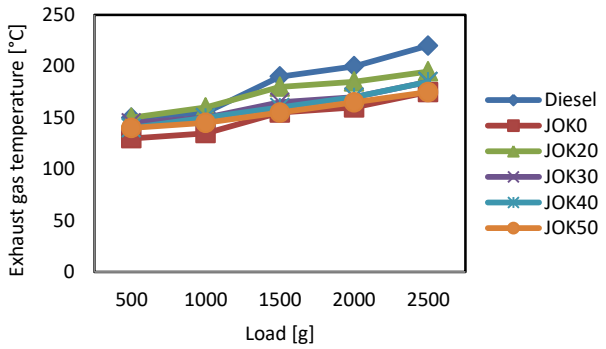

Fig. 7. Variation of EGT for JOK blends with increase in load

3.2. Effect of load and fuel samples on engine tailpipe emission

The variation of CO emission with load is shown in Fig. 8. CO is an intermediate combustion product that is formed mainly due to incomplete combustion of fuel. If combustion is complete, CO is converted to CO_2. If the combustion is incomplete due to shortage of air or low gas temperature, CO will be formed. As the load increases there is a significant decrease in CO emission in fuel blends with lower concentration of jatropha oil [20].

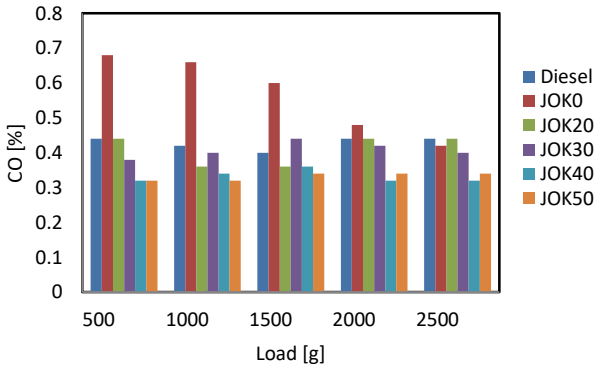

Fig. 8. Variation of CO for JOK blends with increase in load

Figure 9 showed the emission levels of CO_2 for various blends and diesel. JOK0 fuel sample shows lower CO_2 emission at minimum and maximum loads. The following fuel samples; JOK20, JOK30, JOK40 and JOK50 fuel samples exhibited higher CO_2 emission than diesel with load increment.

HC in exhaust occur as a result of incomplete burning of the carbon compounds in the fuel. The trend of UHC emission variation for different blends is illustrated in Fig. 10. Apart from the pure JOK and blended samples exhibited lower UHC values than conventional diesel fuel. The blend with the lowest UHC emission is JOK50 with 84 ppm and 86 ppm at minimum and maximum loads. The lower HC emissions of JOK and blends can be attributed to the presence of oxygen in JOK and blends and its contribution to the give a near complete combustion process.

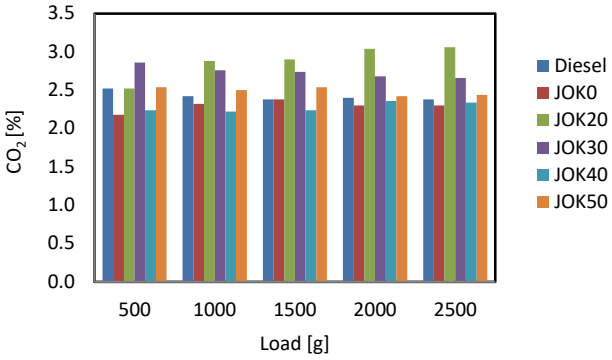

Fig. 9. Variation of CO_2 for JOK blends with increase in load

It could be seen from Fig. 10 that, at lower engine loads oxidation reactions were very slow due to lower temperature and lean mixture. UHC are formed in the core of the spray and the regions just outside the flame zone [37]. They are also formed at the point where the fuel spray touches the wall and thereby gets quenched. UHC emissions increased with load for all the fuels. At higher loads, the mixture was too rich causing incomplete combustion and higher UHC emission [38]. As the load increased, heat released by the fuel also increased which improved combustion and consequently UHC level start decreasing. Above the rated load value UHC emission started increasing due to poor combustion [39]. HC emissions drop at all brake power by doping with kerosene. Increasing the kerosene content reduces the HC emissions significantly. This was caused by the lower viscosity of blends by kerosene blending.

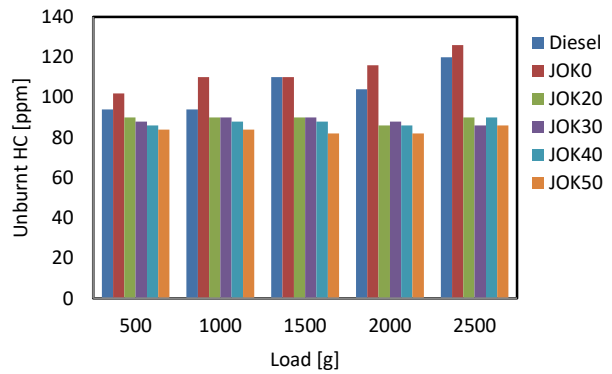

Fig. 10. Variation of UHC for JOK blends with increase in load

Figure 11 shows the variation of NO_x with respect to load and fuel sample variations. It could be seen that conventional diesel fuel produces 31 ppm of NO_x at 1500 g engine load, while JOK30 blended sample produces similar emission level with diesel at 2000 g load. JOK40 fuel sam-

ple also generated similar emission level with diesel under varying engine load condition. The highest emission of 74 ppm was observed for JOK50 samples under all load conditions. There was no noticeable production of NO_x emission for JOK0 and JOK20 blended samples could probably be caused by the reduction of the peak engine temperature due to less excess air, or a slight leak in the sampling system affecting the sensitivity of the analyzer.

It could also be observed that the NO_x emission level exhibited occurred as the oil temperature increased. Hence, it could be inferred that the increase in NO_x emission is very much dependent on the combustion chamber temperature. At the higher chamber temperature, the reaction $N2 + O_2 = 2NO$ takes place, and this promotes the formation of NO_x. Temperature drops rapidly during expansion and exhaust strokes, but the reverse reaction or dissociation of NO is not rapid enough to establish equilibrium and therefore higher amount of NO_x appears in the exhaust at higher loads [39]. Further studies have suggested that addition of antioxidant such as, N,N′-diphenyl-1,4-phenylenediamine (DPPD) has been found to reduce NO_x emissions significantly with a slight penalty in terms of engine power and brake specific been found to reduce NO_x emissions significantly with little negative effect on engine power and brake specific fuel consumption (BSFC) as well as CO and HC emissions [40].

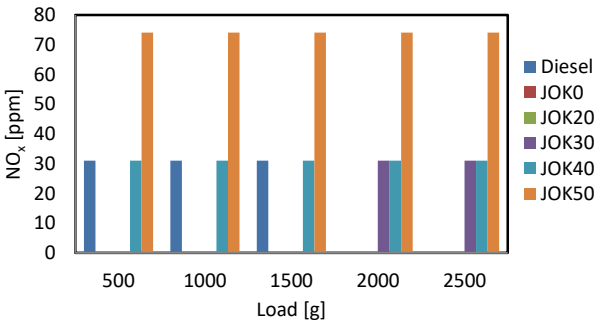

Fig. 11. Variation of NO_x for JOK blends with increase in load

4. Conclusion

This work was an attempt to explore the usability of jatropha oil-kerosene mixtures as combustion fuels for CI engines. From the finding the following conclusions can be drawn:

i. The JOK20 blended samples offered significant potential as sustainable fuel for modern diesel engines.
ii. JOK20 fuel blend exhibited the highest BP, BTE, and EGT followed by JOK30, JOK40 and JOK50 blends than diesel fuel.
iii. JOK20 blended fuel sample exhibited the lowest SFC, and is hence more economical in terms of fuel consumption.
iv. JOK20 sample has the lowest BSEC and AFR followed by JOK30, JOK40 and JOK50 blends than diesel fuel.
v. There was slight reduction in CO emission level for JOK20 compared to diesel fuel.
vi. significant reduction was noticed for JOK30, JOK40 and JOK50 blends as the load increases.
vii. In comparison to diesel fuel, JOK20, JOK30, JOK40 and JOK50 fuel samples exhibited higher CO_2 emission level than diesel as engine load increases.
viii. Other than JOK0 sample, all other fuel blends exhibited lower UHC emission than diesel fuel.
ix. JOK50 fuel sample released the highest NO_x emission. JOK30 and JOK40 had the same level of NO_x formation than diesel fuel, while there was no noticeable trace of NO_x formation in JOK0 and JOK20 fuel samples.

Acknowledgement

This work was assisted by Automotive Engineering Technology Workshop, Federal Polytechnic, Bauchi Nigeria for providing the test facilities throughout the course of this research.

Nomenclature

AFR	air fuel ratio
BMEP	brake mean effective pressure
BP	brake power
BSEC	brake specific energy consumption
BSFC	brake specific fuel consumption
BTE	brake thermal efficiency
CI	compression ignition
CO	carbon monoxide
CO_2	carbon dioxide
DI	direct injection
EGT	Exhaust gas temperature
NO_x	nitrogen oxides
SFC	specific fuel consumption
UHC	unburnt hydrocarbon

Bibliography

[1] Birhanu A, Ayalew S. A review on potential and status of biofuel production in Ethiopia. J Plant Sci. 2017;5(2):82-89. https://doi.org/10.11648/j.jps.20170502.16
[2] Pramanik K. Properties and use of jatropha curcas oil and diesel fuel blends in CI engines. Renew Energ. 2003;28(2): 239-248. https://doi.org/10.1016/S0960-1481(02)00027-7
[3] Hanumantha Rao YV, Voleti RS, Hariharan VS, Sitamara Raju AV, Nageswara Redd P. Use of jatropha methyl ester and its blends as alternative fuel in diesel engine. J Braz Soc Mech Sci. 2009;31(3):253-260. https://doi.org/10.1590/S1678-58782009000300011
[4] Agarwal AK. Vegetable oils verses diesel fuel: development and use of biodiesel in a compression ignition engine. TIDE. 1998;8(3):191-204.
[5] Engelman HW, Guenther DA, Solvis TW. Vegetable oil as diesel fuel. Diesel and Gas Engine Power Division of ASME. 1978, 78-DGP-19.

[6] Sims REH, Raine RR, Mcleod RJ. Rapeseed oil as a fuel for diesel engines. SAE Presented, 1981. Australia.
[7] Basic NJ, Humke AL. Vegetable oils, diesel fuel supplements? Automotive Engineering. 1981;89(4):37-41.
[8] Worgether M. Results of a long term test based on rapeseed oil fuel. Beyond the energy crisis. Opportunity and challenge. 3rd International Conference on Energy Use Management. Berlin. In: FAZZOLORE, R.A., SMITH, C.R. (eds), 1981:1955-1965, Pergamon Press, Oxford.
[9] Sapaun SM, Masjuki HH, Azlan A. The use of palm oil diesel fuel substitute. J Power Energ. 1996;210(1):47-53. https://doi.org/10.1243/PIME_PROC_1996_210_007_02
[10] Ryan TW, Dodge LG, Callahan TJ. The effect of vegetable oil properties on injection and combustion in two different diesel engines. J Am Oil Chem Soc. 1984;61(10):1610-1619. https://doi.org/10.1007/BF02541645
[11] Peterson CL, Cruz RO, Perkins L., Korus R, Auld DL. Transesterification of vegetable oil for use as diesel fuel: A progress report. ASAE. PNWS, 1990, 90-610. ASAE. St Joseph, MI 49085.
[12] Reid JF, Hansen AC, Goering CE. Quantifying diesel injector coking with computer vision. Transactions of the ASAE. 1989;32(5):1503-1506. https://doi.org/10.13031/2013.31179
[13] Ejilah IR, Asere AA, Adisa AB, Ejila A. The effect of diesel fuel jatropha curcas oil methyl ester blends on the performance of a variable speed compression ignition engine. Aust J Agr Eng. 2010:1(3):80-85. https://search.informit.org/doi/10.3316/informit.633130711996398
[14] Al Widyan MI, Al Shyoukh AO. Experimental evaluation of the transesterification of waste palm oil into biodiesel. Bioresource Technol. 2002;85(3):253-256. https://doi.org/10.1016/S0960-8524(02)00135-9
[15] Demirbas A. Biodiesel fuels from vegetable oils via catalytic and non-catalytic supercritical alcohol transesterifications and other method: a survey. Energ Convers Manage. 2003; 44(13):2093-2109. https://doi.org/10.1016/S0196-8904(02)00234-0
[16] Narayana CM. Vegetable oil as engine fuels-prospect, Proceeding on Recent Trend in Automotive Fuels. 2002, Nagpur, India.
[17] Azad AK, Ameer USM, Alam MM. Experimental study of DI Diesel engine performance using biodiesel blend with kerosene. Int J Energ Envoron. 2013;4(2):265-278. https://www.ijee.ieefoundation.org/vol4/issue2/IJEE_10_v4n2.pdf
[18] Ghormade TK, Deshpande NV. Soybean oil as an alternative fuel for I.C. engines. Proceedings of Recent Trends in Automotive Fuels. 2002, Nagpur, India.
[19] Huzayyin AS, Bawady AH, Rady MA, Dawood A. Experimental evaluation of Diesel engine performance and emission using blends of jojoba oil and Diesel fuel. Energ Convers Manage. 2004;45(13-14):2093-2112. https://doi.org/10.1016/j.enconman.2003.10.017
[20] Sanjid A, Masjuki HH, Kalam MA, Ashrafur Rahman SM, Abedin MJ, Palash SM. Production of palm and jatropha based biodiesel and investigation of palm-jatropha combined blend properties, performance, exhaust emission and noise in an unmodified diesel engine. J Clean Prod. 2014; (65):295-303. https://doi.org/10.1016/j.jclepro.2013.09.026
[21] Nalgundwar A, Paul B, Sharma SK. Comparison of performance and emissions characteristics of DI CI engine fueled with dual biodiesel blends of palm and jatropha. Fuel. 2016; 173:172-179. https://doi.org/10.1016/j.fuel.2016.01.022
[22] Agarwal AK, Shrivastava A, Prasad RK. Evaluation of toxic potential of particulates emitted from Jatropha biodiesel fuelled engine. Renew Energ. 2016;99:564-572. https://doi.org/10.1016/j.renene.2016.07.056
[23] Longwic R, Sander P, Tatarynow D. Ecological aspects of using mixtures of canola oil with n-hexane in diesel engine. Combustion Engines. 2022;190(3):56-60. https://doi.org/10.19206/CE-143245
[24] Marszalek N, Lis T. The future of sustainable aviation fuels. Combustion Engines. 2022;191(4):29-40. https://doi.org/10.19206/CE-146696
[25] Kathirvelu B, Subramanian S, Govindan N, Santhanam S. Emission characteristics of biodiesel obtained from Jatropha seeds and fish wastes in a diesel engine. Sustain Environ Res. 2017;27(6):283-290. https://doi.org/10.1016/j.serj.2017.06.004
[26] Hemanandh J, Ganesan S, Sridhar Raja KS, Aakhash Sivan V, Maher Khaliq A. Production of alternate fuel using jatropha oil and kerosene – analysis of their performance and emission characteristics. In: Arockiarajan, A., Duraiselvam, M., Raju, R. (eds) Advances in Industrial Automation and Smart Manufacturing. Lecture Notes in Mechanical Engineering. Springer. https://doi.org/10.1007/978-981-15-4739-3_75
[27] Madiwale S, Karthikeyan A, Bhojwani V. Properties investigation and performance analysis of a diesel engine fuelled with Jatropha, soybean, palm and cottonseed biodiesel using ethanol as an additive. Mater Today-Proc. 2018;5(1):657-664. https://doi.org/10.1016/j.matpr.2017.11.130
[28] American Society for Testing of Materials. Annual Book of ASTM Standards. Philadelphia: ASTM 19103,1983.
[29] Kumar A, Bhattacharya T, Hasnain SM, Nayak AK, Hasnain MS. Applications of biomass-derived materials for energy production, conversion, and storage. Mat Sci Energ Tech. 2020;(3):905-920. https://doi.org/10.1016/j.mset.2020.10.012
[30] TQ. TD110-TD115 Test Bed and Instrumentation Manual for Small Engines, TQ Educational and Training Publishers, London 2000, 1-6.
[31] Wolff A, Koszałka G. Influence of engine load on piston ring pack operation of an automotive IC engine. Combustion Engines. 2022;190(3):88-94. https://doi.org/10.19206/CE-141737
[32] Kumar Kadian A, Khan M, Sharma RP, Mozammil Masnain SM. Performance enhancement and emissions mitigation of DI-CI engine fueled with ternary blends of jatropha biodiesel-diesel-heptanol. Mat Sci Energ Tech. 2022;(5):145-154. https://doi.org/10.1016/j.mset.2022.01.002
[33] Cieśliński JT, Krzyżak J, Kropiwnicki J, Kneba Z. Experiments on compression ignition engine powered by nanofuels. Combustion Engines. 2022;188(1):55-59. https://doi.org/10.19206/CE-142281
[34] Pikonas A, Pukalskas S, Grabys J. Influence of composition of gasoline-ethanol blends on parameters of internal combustion engines. Journal of Kones, Internal Combustion Engines. 2003;10(1-2):205-211. https://www.infona.pl/resource/bwmeta1.element.baztech-article-BUJ6-0026-0027
[35] Bajpai S, Das LM. Feasibility of utilization of fatty acid ethyl esters-diesel blends as an actto fatty acid methyl esters-diesel blend. Proc 7th International Conference of Biofuels. 2010:91-100.
[36] Plint and Partners. Shell-Plint Engine Test Bed Manual. Plint and Partners Publications. England 1984:8-14.
[37] Sen SP. Internal Combustion Engine – Theory and Practice. Khanna Publishers, 2nd edition, Delhi 1994, 133-139.
[38] Devarajan Y, Jayabal KR, Ragupathy D, Venu H. Emissions analysis on second generation biodiesel. Front Env Sci Eng. 2017;11(3):1-6. https://doi.org/10.1007/s11783-017-0891-0

[39] Sethi VP, Salariya KS. Exhaust analysis and performance of a single cylinder diesel engine run on dual fuels. J Ins Engin (India): Series C. 2004;85:1-7.
[40] Palash SM, Kalam MS, Masjuki HH, Arbab MI, Masum BM, Sanjid A. Impacts of NO_x reducing antioxidant additive on performance and emissions of a multi-cylinder diesel engine fueled with Jatropha biodiesel blends. Energ Convers Manage. 2014;77:577-585. https://doi.org/10.1016/j.enconman.2013.10.016

Ass. Prof. Robinson I. Ejilah, PhD. – Faculty of Engineering and Engineering Technology, Dept. of Mechanical/Production Engineering, Abubakar Tafawa Balewa University, Bauchi-Nigeria.
e-mail: *irejilah@atbu.edu.ng; rejilah@gmail.com*

Osazoduwa O. Agboneni – Nenis Automotive Engineering Consultant, Nenis Engineering Co. Ltd., Ikorodu, Lagos.
e-mail: *oduwa.agboneni@gmail.com*

Abiodun A. Ogbaneme, Research Student – Faculty of Engineering and Engineering Technology, Dept. of Mechanical/Production Engineering, Abubakar Tafawa Balewa University, Bauchi-Nigeria.
e-mail: *attegba@yahoo.com*

Sikiru O. Adekunle – School of Engineering Technology, Department of Mechatronics Engineering Tech., Federal Polytechnic, Bauchi-Nigeria.
e-mail: *olusikiru2009@gmail.com*

Article citation info:
Kęska A, Janicka A, Zawiślak M. Numerical optimization of the BAT-CELL Bio-Ambient-Tests method for engine exhausts toxicity evaluation. Combustion Engines. 2023;192(1):19-25. https://doi.org/10.19206/CE-147781

Aleksandra KĘSKA
Anna JANICKA
Maciej ZAWIŚLAK

Combustion Engines
Polish Scientific Society of Combustion Engines

Numerical optimization of the BAT-CELL Bio-Ambient-Tests method for engine exhausts toxicity evaluation

ARTICLE INFO

Received: 14 January 2022
Revised: 19 February 2022
Accepted: 28 March 2022
Available online: 15 April 2022

The BAT-CELL Bio-Ambient-Tests method is based on the assessment of the influence of the actual toxicity of various types of gas mixtures on living cells, taking into account the additive synergism. Work has been carried out on the application of the BAT-CELL method for testing engine exhaust gases. The application of computational fluid mechanics using Ansys Fluent made it possible to analyse the flow of engine exhaust gases through the aspiration system used, including analysis of shear stress values and their uniformity distribution on the bottom wall of the sampler containing cell culture on the bottom wall of the sampler. The appropriate flow rate of exhaust gases through the aspiration system and the shape of aspiration tubing for the sampler were selected in order to enable uniform contact of gas particles with the cell surface and not to damage them mechanically. The simulation results were verified in real-life tests and confirmed the theoretical assumptions.

Key words: *internal combustion engine, Euro norms, new method, in-vitro tests*

1. Introduction

In accordance with the principle of sustainable development, propagated in Europe since the beginning of the 19th century, the economic development must lead to an improvement in the quality of the natural environment by, among other things, limiting the harmful effects of production and consumption on the state of the environment and protecting natural resources. At a time when motorisation is one of the most important trends in the development of society, attention should be paid to the aspect of exposure of a human body to the negative effects of such progress of civilisation. The progress of motorisation in the world has forced the introduction of certain legal restrictions on the control of exhaust emissions. Euro emission standards have been in force in Europe since 1992. The control is carried out by means of various measurement methods, thanks to which the concentration of emitted compounds subject to standards is determined, including hydrocarbons (HC), nitrogen oxides (NO_x), carbon monoxide (CO) and particulate matter (PM/PN). However, all the methods used do not give direct and clear results on their actual toxicity. Actual toxicity should be understood as a harmful effect of a substance on living organisms – tissues, organs or biological processes. It seems appropriate to use a method that will make it possible to determine the actual impact of toxic substances on a living organism in a relatively quick, unambiguous and objective manner. Moreover, the currently binding exhaust emission standards do not take into account many harmful compounds, directly unlimited (Fig. 1), which determine toxicity of exhaust gases. In the group of hydrocarbons we can distinguish compounds from polycyclic aromatic hydrocarbons (PAH) and volatile organic compounds (VOC), such as benzo(a)pyrene or benzene, which exhibit, inter alia, carcinogenic and mutagenic effects even at very low concentrations, which has been repeatedly scientifically proven [3, 18, 21–23].

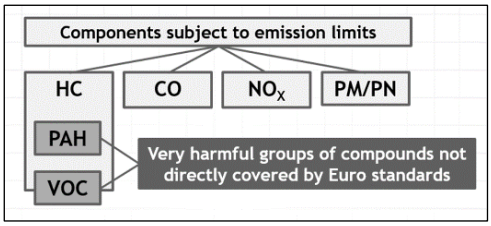

Fig. 1. Location of VOCs and PAHs among the limited components of exhaust gases [19]

This paper proposes a method for measuring the real toxicity of engine exhaust gases, which may be a supplement or alternative to the currently used methods. The method takes into account synergistic interactions of compounds without the need to identify them qualitatively and quantitatively. Moreover, in a relatively simple way, both in terms of conducting the experiment and interpretation of results, it allows for obtaining an answer to the question whether a given gas mixture may cause toxic effects in our body.

2. Review of exhaust emission test methods

Research on exhaust emission measurement methods in the context of changing Euro emission standards is an extremely important and topical issue. Commonly used exhaust emission measurement methods can be divided into those using exhaust gas analysers [33] (including portable emissions measurement system PEMS), analytical methods (e.g. chromatography, spectroscopy) and less popular calculation methods [28]. These methods can be used for testing exhaust emissions in stationary conditions on a chassis dynamometer or in road traffic conditions.

Definitely, the most common method of measurement in the conditions of real vehicle traffic is the method using a special mobile scientific and research apparatus of the PEMS type, appropriately installed in a vehicle [5, 8, 9, 11, 15, 20, 24, 26, 30]. It makes it possible to measure the con-

centration of individual pollutants and the energy consumption of traffic, while measuring the mass flow rate of exhaust gases from a power unit. The apparatus may be used for testing vehicles of various types and homologation categories. Moreover, it provides instantaneous values of the measured parameters, which allows for quick conclusions from the conducted tests.

A common method of measuring pollutant emissions in stationary conditions on a chassis dynamometer are exhaust gas analysers [27, 31]. These are measuring instruments intended for measuring the content of exhaust gas components such as carbon monoxide, carbon dioxide, nitrogen oxides, hydrocarbons, oxygen. The most popular of them are non-dispersive infrared (NDIR) analysers, using spectrometric methods, which consist in measuring with a photometer the total absorption of radiation in a quite narrow band of wavelengths, characteristic of the compound in question. Other analysers used are flame ionisation detection (FID) for the determination of hydrocarbons and methane and chemiluminescent (CLD) for the determination of nitrogen oxides. Other methods used to measure exhaust emissions are analytical methods, mainly chromatographic (including flame ionisation or chemiluminescence detection) and spectroscopic [1, 6, 10, 13, 16, 25, 32]. Among them we can distinguish the less known ones, e.g. the electronic method for the detection of nitric oxide emissions, which is based on absorption spectroscopy using a diode laser [7, 29], or the method using a specialised spectroscopic remote sensing device developed by the University of Denver [4].

Testing of gaseous mixtures by means of in vitro tests is a new method, not commonly used. So far, the only Polish author of papers published in Switzerland, based on tests on living cells exposed to gaseous mixtures, including exhaust gases, is Czerwiński [2]. In this type of research, the key issue is not the selection of an appropriate test, but the selection of appropriate parameters of cell exposure to harmful substances and the knowledge of the dose of the tested gases causing the toxic effect.

3. BAT-CELL method

Innovative, patented BAT-CELL Bio-Ambient-Tests method (Patent. Poland, No 220670. Method for the measurement of the effects of gaseous mixtures on living cells: Int. Cl. C12M 1/34, C12M 1/36, C12M 1/38, G01N 33/00. Application no. 400646 of 04.09.2012. published 30.11. 2015) consists in evaluating the effects of the actual toxicity of different types of gas mixtures on living cells, taking into account additive synergism. It allows direct contact between the test gas and the cell surface, thanks to the elimination of a physicochemical barrier in the form of culture fluid, which distinguishes it among other direct methods of this type.

The cell culture, devoid of the culture fluid, is placed in a sterile closed chamber (sampler). In particular, the fibroblast-like cell line obtained from mouse subcutaneous adipose tissue L929 is dedicated to this type of study. Subsequently, the gas is introduced into the sampler through an inlet tube through an antibacterial filter and by means of an aspiration system (Fig. 2).

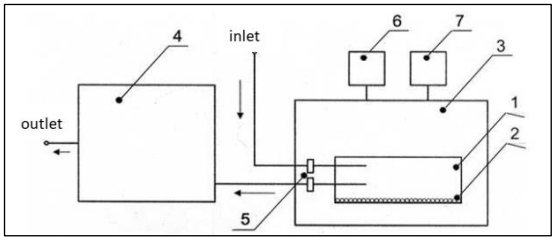

Fig. 2. Diagram of a system for assessing the toxicity of gas mixtures using the BAT-CELL Bio-Ambient-Tests method (1 – sterile sampler, 2 – cell line devoid of culture fluid, 3 – conditioning chamber equipped with pressure (6) and temperature (7) sensors, 4 – aspirating system, 5 – antibacterial filters) [12]

After exposure of the cell culture to the gas, it is flooded with culture fluid and the toxic effect of the gas on the culture is examined by standard toxicological tests according to standard procedures. The exposure time is chosen individually depending on the type of gas mixture. Flow parameters shall be chosen to the shape of the sampler in such a way that uniform contact of the gas molecules with the cell surface is ensured and the cells are not mechanically damaged. Numerical methods of fluid mechanics are used for this purpose.

The conditioning chamber (Fig. 3) is equipped with pressure and temperature sensors to ensure that the vital functions of the cell culture are maintained. The elimination of the culture fluid is possible by maintaining physical parameters appropriate to the requirements of the cell line, a line-safe residence time for the cells outside the incubator atmosphere and no nutrient supply. The culture fluid additionally has an antibiotic function for the cells, therefore the sampler with the cell line is additionally protected at the inlet with an antibacterial filter [12].

Fig. 3. BAT-CELL chamber

4. CFD numerical analysis

Thanks to the application of computational fluid mechanics with the Ansys Fluent software, it was possible to select an appropriate flow rate and shape of the aspiration tubing for the cell culture sampler.

The simulations were carried out for two values of the flue gas flow rate and the shape of the aspiration pipes for the sampler containing the cell culture.

Simulations were carried out for two flow rates – 150 and 250 cm^3/min. Four solutions of the shape of aspiration tubing were proposed, differing in the angle of inclination of the tubing in relation to the bottom wall of the sampler, and thus in their length, as well as in the angle of truncation of the outlet duct (Fig. 4). The length of the aspiration tubing (the section inside the sampler) varied from 18 to 35 mm, depending on the model.

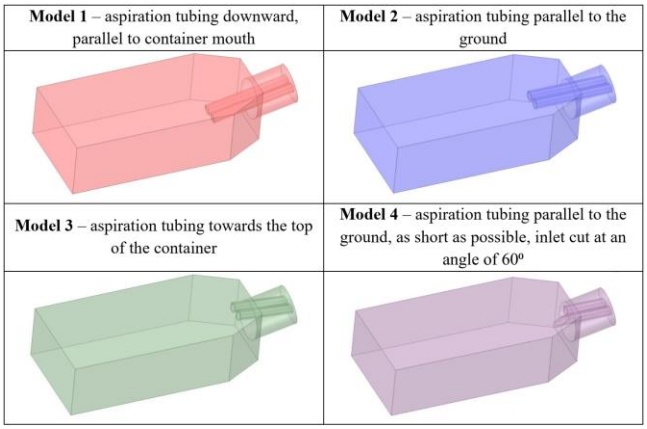

Fig. 4. Different solutions of the shape of aspiration tubing

For the purpose of the simulation, the sampler construction was simplified. The 3D spatial model was discretised. A tetrahedral mesh with an element size of 0.001 m was applied. In order to compact the mesh locally, a wall layer was applied to the lower wall of the sampler.

For a flow rate of 250 cm^3/min, a flow velocity of 0.5895 m/s was calculated, while for a flow rate of 150 cm^3/min the value was 0.3537 m/s. For both cases, the Reynolds number was calculated (an example of calculation for the higher flow rate is given – formula 1). The obtained values $Re_1 = 73$ and $Re_2 = 121$ testified to laminar flow. In laminar motion, the fluid elements move along straight or gently curved paths, depending on the shape of the rigid walls that give shape to all the current lines. In laminar flow, therefore, there is an exchange of mass, and with it an exchange of momentum on a microscopic scale, which is the cause of the occurrence of tangential stresses. In laminar flow, characterised by the dominance of viscous forces over inertial forces, any random disturbances arising are damped, so that the flow is static (stable). Such motion can occur as long as the Reynolds number does not exceed the critical value $Re_{kr} \leq 2300$ [14]. The Reynolds number values were calculated for the medium, which was air. The obtained parameters were set under flow simulation conditions.

$$Re_2 = \frac{\rho \cdot V \cdot d_h}{\mu} = \frac{1.225\,\frac{kg}{m^3} \cdot 0.5895\,\frac{m}{s} \cdot 0.003\,m}{0.000017894\,\frac{kg}{m \cdot s}} = 121 \qquad (1)$$

where: ρ – the density of the medium, V – flow velocity, d_h – hydraulic diameter, μ – dynamic viscosity.

The Navier-Stokes equations (equation 2) [14] were used to describe the flow of a Newtonian viscous fluid in the studied system. These equations describe the principle of conservation of momentum for a moving fluid. According to them, changes in the fluid element depend only on mass forces, external pressure and internal viscous forces in the fluid. In addition to normal stresses, tangential stresses occurring on the walls of the viscous fluid element can also be considered.

$$\frac{\partial v}{\partial t} + v \cdot \nabla v = F - \frac{1}{\rho}\nabla p + v\nabla^2 v \qquad (2)$$

where: $(v \cdot \nabla)v$ – convection: the transfer of local momentum with the movement of a fluid, F – creation of momentum due to mass forces (gravity), $\frac{1}{\rho}\nabla p$ – change of momentum due to pressure forces, $v\nabla^2 v$ – friction forces: dissipation of momentum due to friction processes.

The results show maps and graphs of shear stress distribution on the bottom wall of the sampler depending on the set flow rate value and shape of aspiration tubing (Fig. 5–8). Due to the wide range of stress values in this case, the range of scale values on individual maps and graphs was not standardised, as the exact stress distribution and maximum values of tangential stresses for individual models would not be visible. Therefore, the results are presented unaltered. The diagram of the dependence of shear stress values on the position of a given point in the plane of the bottom wall of the sampler shows the values at a given node of the element mesh.

Maximum values of tangential stresses for particular models of aspiration tubing are presented in the Fig. 9.

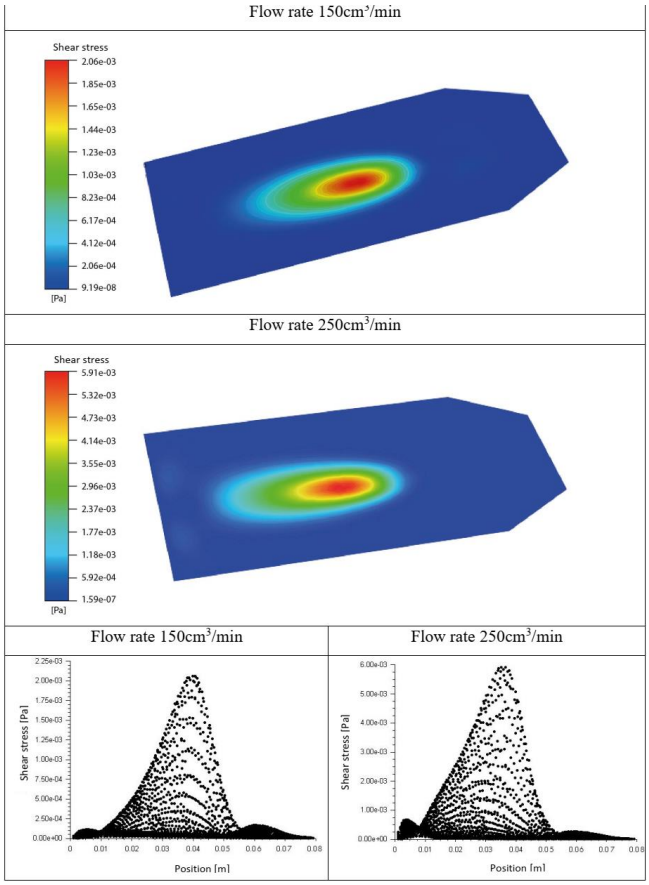

Fig. 5. Maps and diagrams of shear stress distribution on the bottom wall of the test specimen for model 1

The lowest stress values were observed for model 3, in which the designed tubing were directed upwards. On the basis of the analysis performed, it was concluded that the direction of aspiration tubing has an influence on the values of shear stresses. Reducing the flow rate to 150 cm^3/min will reduce the shear stress values several times. Directing the inlet aspiration tubing towards the top of the sampler or cutting its tip at an angle leads to a more uniform distribution of shear stresses on the bottom wall of the container.

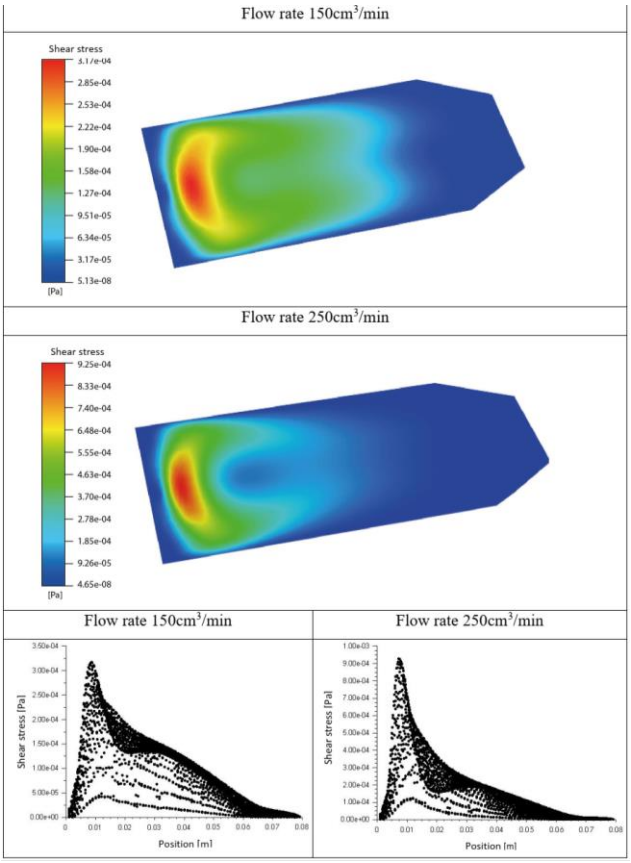

Fig. 6. Maps and diagrams of shear stress distribution on the bottom wall of the specimen for model 2

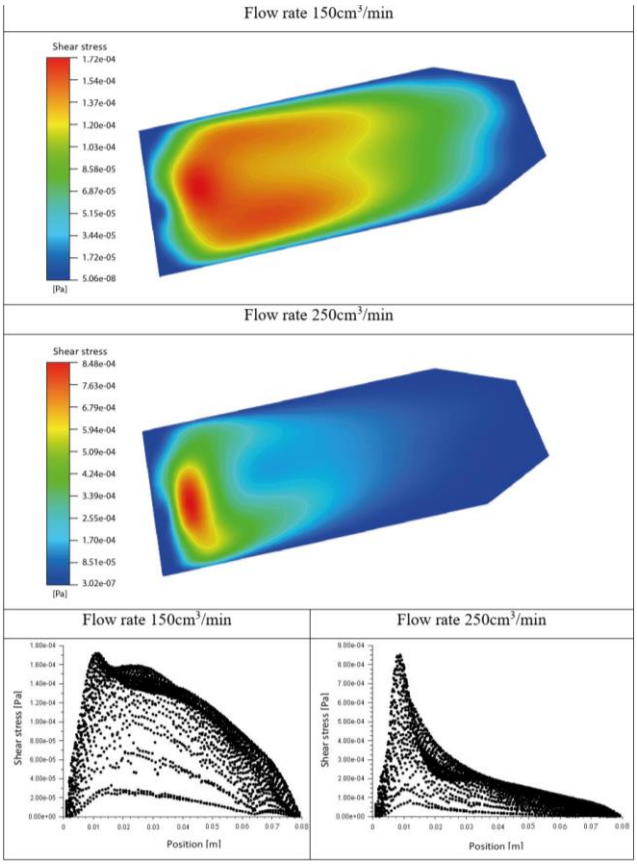

Fig. 8. Maps and diagrams of shear stress distribution on the lower wall of the sampler for model 4

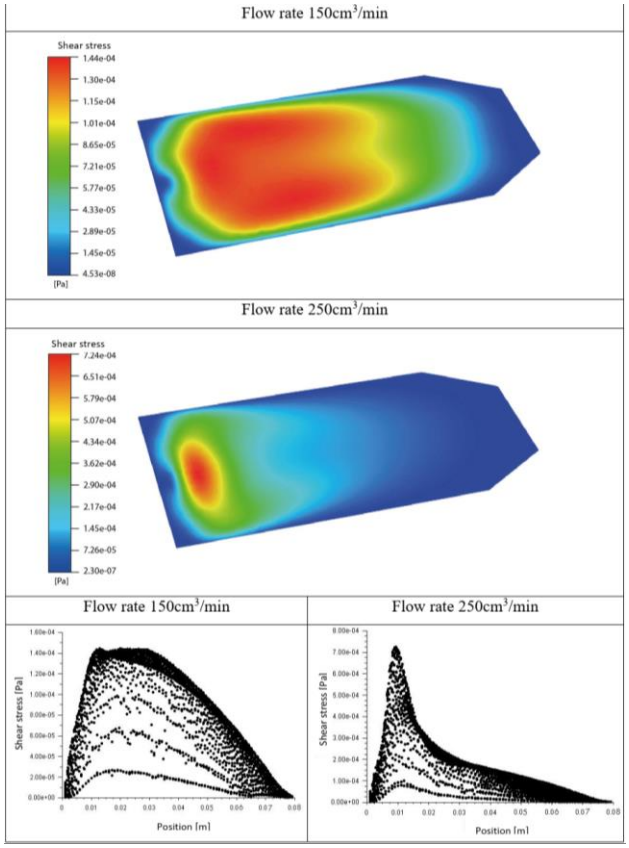

Fig. 7. Maps and diagrams of shear stress distribution on the lower wall of the sampler for model 3

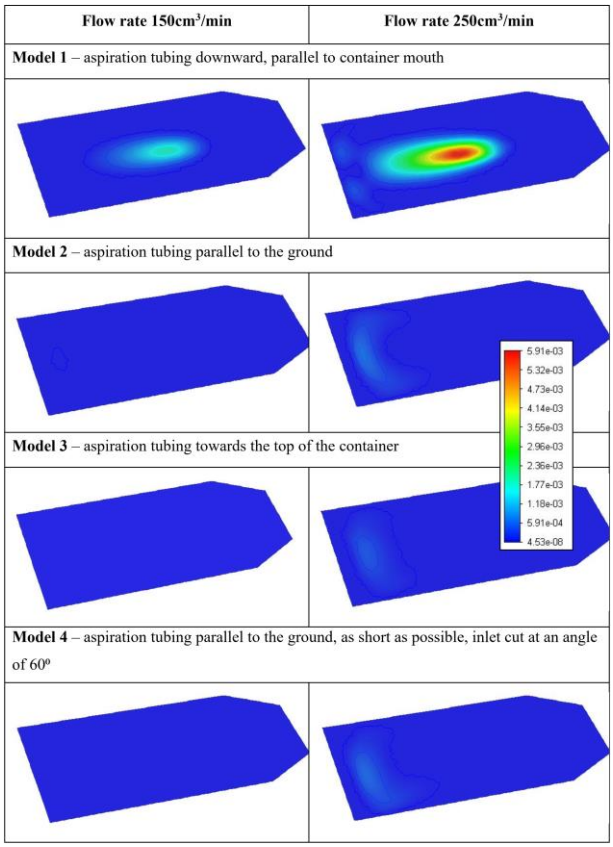

Fig. 9. Comparison of shear stress distributions on the lower wall of the sampler for individual models

In order to compare the models, a table containing distribution maps of shear stress values with a unified measurement scale is also presented (Table 1). Its range is determined by the highest and lowest values of shear stresses selected on the basis of the previous analysis.

Table 1. Maximum shear stresses for various aspiration pipe shapes

Model	Maximum shear stress on the bottom wall of the container [Pa]	
	for the flow rate 150 cm^3/min	for the flow rate 250 cm^3/min
1	$2.06 \cdot 10^{-3}$	$5.91 \cdot 10^{-3}$
2	$3.17 \cdot 10^{-4}$	$9.25 \cdot 10^{-4}$
3	$1.44 \cdot 10^{-4}$	$7.24 \cdot 10^{-4}$
4	$1.72 \cdot 10^{-4}$	$8.48 \cdot 10^{-4}$

Due to the lowest maximum values of shear stress and the most uniform distribution of values on the surface of the bottom wall of the sampler, model 3 and a gas flow rate of 150 cm^3/min were selected for the real tests.

5. Real model

The sampler used is a standard container used for adherent cell culture, made of polystyrene (Fig. 10). The inner surface of the bottom wall of the sampler enables proper adhesion of cells to the substrate, thus their movement inside the sampler is not possible. It should be noted that the samplers used in the BAT-CELL method are subject to constructional modifications by the manufacturer over time. Therefore, it is important to simulate the flow of tested gases through the sampler before commencing the main tests.

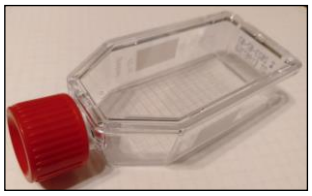

Fig. 10. Sterile closed cell culture container

For cell exposure, the method requires changing the sampler stopper to a different one, which contains aspiration tubing – inlet and outlet. The tubes are made of rigid Teflon, which is resistant to elevated temperature (max. 260°C), in which liquid sterilisation of exchangeable stoppers equipped with tubing. The diameter of the tubing has been selected according to the size of the upper surface of the stopper, so that two holes can be drilled in it. The outer diameter of the tubing was 4 mm and the inner diameter was 3 mm. The tubings were fixed in the holes of the stopper using a suitable VOC-free adhesive. When designing the shape of the tubing, care had to be taken to ensure that they did not mechanically damage the lower wall with the adherent cell culture when the stopper was screwed on. Because of the downward slope of the sampler inlet, it was necessary to design appropriately long aspiration tubing. An important issue was the selection of the angle of the aspiration tubing in relation to the bottom wall of the sampler and their shape.

The actual model of the sampler with the visible aspiration tubing facing upwards inside the sampler is shown in Fig. 11. Antibacterial filters are screwed to the external ends of the aspiration tubing via a specially selected connector.

The selection of an appropriate flow rate is aimed only at the exchange of air, the velocity of which will not cause mechanical damage to the cells, but will lead to a continuous supply of fresh fumes. Therefore, it is not important to select an exact value of the flow rate, but one that does not exceed the critical value that ruptures the cells.

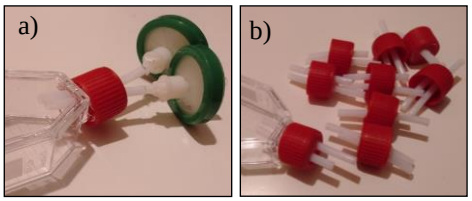

Fig. 11. a) The actual model of the sampler with aspiration tubing terminated with filters, b) prototype series of identical interchangeable caps

The value of the flow rate of exhaust gases flowing through the sampler inlet/outlet system equal to 250 cm^3/min in the first test experiment was selected on the basis of previous experiments [12, 17]. The second tested flow rate value of 150 cm^3/min was selected based on the first trial test, during which cell rupture from the adherent substrate was observed (Fig. 12a, b). The lack of uniformity of cell distribution after exposure indicated that the set flow rate was too high. Previous analyses [12, 17] did not show the problem of cell rupture for a flow rate value of 250 cm^3/min. The reason was most likely due to discrepancies in the methods of adhesion of a given cell line to the sampler substrate.

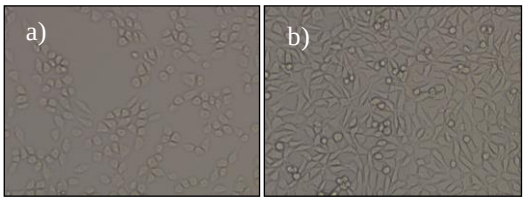

Fig. 12. a) cells detached from the substrate, b) cells multiplying properly

The test gases flowing through the aspiration system exert specific internal forces on the bottom of the adherent cell culture probe. These forces are divided into tangential and normal stresses. The effect of cell detachment from the substrate is related to the occurrence of shear stresses. Therefore, the distribution of shear stresses on the lower wall of the sampler was analysed. The aim was to obtain as uniform a distribution as possible, which would give information that the cell culture would not be disturbed at any point and that no mechanical damage would occur and the tests would have to be repeated.

The research, which confirmed the correctness of BAT-CELL method validation, concerned the survival rate of cells subjected to exposure to engine exhaust fumes emitted from petrol vehicles meeting Euro 3 and Euro 6 emission standards. One of the methods used to determine cell survival rate is the method using a haemocytometer – a glass plate with engraved lines forming a grid, with the help of which it is possible to count degenerated cells. Example results are presented in the diagram below (Fig. 13) [19].

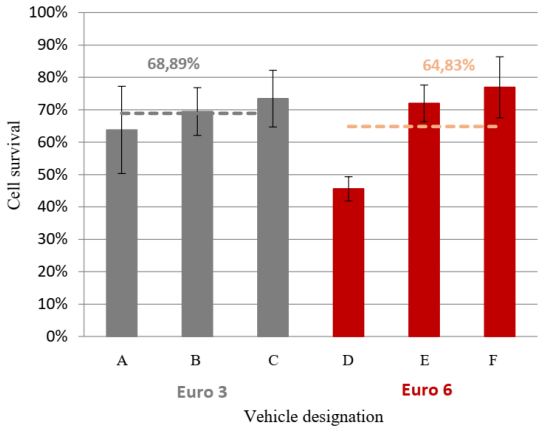

Fig. 13. Mean cell survival calculated with using a hemocytometer [19]

For the tested vehicles complying with the Euro 3 standard, the cell survival was found to be approximately 4% higher in comparison with the vehicles complying with the Euro 6 standard, which means higher toxicity of exhaust gases for the tested vehicles of newer generation [19].

6. Summary and conclusions

Validation of the BAT-CELL Bio-Ambient-Tests method performed by numerical analysis of the exhaust gas flow through the aspiration system was verified in real tests, and simulation results confirmed theoretical assumptions.

Appropriate selection of flow rate values, aimed at air exchange leading to continuous supply of fresh exhaust gases, as well as the shape of aspiration tubing allowed to eliminate the effect of cell detachment from the adherent sampler substrate, allowing for their proper multiplication and elimination of mechanical damage to the cells.

In addition to the sampler design, parameters such as exposure time of the cell culture to the engine exhaust gas and the exhaust gas collection method were validated.

While continuing the research, actions should be taken to improve the BAT-CELL Bio-Ambient-Tests method. Above all, the cell culture samplers for the method should be standardised, the sampling method for the gas mixtures tested should be standardised and a procedure should be developed for the in vitro method used to assess cell cytotoxicity. Undoubtedly, it is also necessary to verify the method on a sufficient number of vehicles to confirm the reliability of performing real toxicity tests of engine exhaust gases on living cells in order to use the method commercially as an alternative to those currently used. Nevertheless, it should be stressed that the test showed that it is worth considering the validity of introducing successively more restrictive exhaust emission standards, which take into account only selected compounds or groups of compounds, but not necessarily those which determine the toxicity of the exhaust gas mixture. Moreover, it is important to take into account the interactions of particular compounds with each other, which may, for example, intensify the toxic effect.

Acknowledgements

The work is a part of the research of the doctoral dissertation *The method for the assessment of the toxicity of engine exhaust gases in the aspect of the analysis of the development of emission standard*.

Nomenclature

CLD	chemiluminescence detector
CO	carbon monoxide
FID	flame ionization detector
HC	hydrocarbons
NDIR	nondispersive infrared sensor
NO_x	oxides of nitrogen
PAH	polycyclic aromatic hydrocarbons
PM	particulate matter
PN	number of particulate matter
VOC	volatile organic compounds

Bibliography

[1] Barro C, Parravicini M, Boulouchos K, Liati A. Neat polyoxymethylene dimethyl ether in a diesel engine; part 2: exhaust emission analysis. Fuel. 2018;(234):1414-1421. https://doi.org/10.1016/j.fuel.2018.07.108

[2] Bisig C, Comte P, Güdel M, Czerwinski J, Mayer A, Müller L et al. Assessment of lung cell toxicity of various gasoline engine exhausts using a versatile in vitro exposure system. Environ Pollut. 2018;(235):263-271 https://doi.org/10.1016/j.envpol.2017.12.061

[3] California Environmental Agency. Available online: https://ww3.arb.ca.gov/research/resnotes/notes/94-22.htm

[4] Carslaw DC, Farren NJ, Vaughan AR. The diminishing importance of nitrogen dioxide emissions from road vehicle exhaust. Atmos Environ. 2019;(1):100002. https://doi.org/10.1016/j.aeaoa.2018.100002

[5] Degraeuwe B, Weiss M. Does the New European Driving Cycle (NEDC) really fail to capture the NO_x emissions of diesel cars in Europe? Environ Pollut. 2017;(222):234-241. https://doi.org/10.1016/j.envpol.2016.12.050

[6] Deng X, Chen Z, Wang X, Zhen H, Xie R. Exhaust noise, performance and emission characteristics of spark ignition engine fuelled with pure gasoline and hydrous ethanol gasoline blends. Case Studies in Thermal Engineering. 2018;(12):55-63. https://doi.org/10.1016/j.csite.2018.02.004

[7] Diemel O, Honza R, Ding C-P, Böhm B, Wagner S. In situ sensor for cycle-resolved measurement of temperature and mole fractions in IC engine exhaust gases. P Combust Inst. 2019;37(2):1453-1460. https://doi.org/10.1016/j.proci.2018.06.182

[8] Dimaratos A, Toumasatos Z, Triantafyllopoulos G, Kontses A, Samaras Z. Real-world gaseous and particle emissions of a bi-fuel gasoline/CNG Euro 6 passenger car. Transport Res D-Tr E D. 2020;(82):102307. https://doi.org/10.1016/j.trd.2020.102307

[9] Gallus J, Kirchner U, Vogt R, Benter T. Impact of driving style and road grade on gaseous exhaust emissions of passenger vehicles measured by a Portable Emission Measurement System (PEMS). Transport Res D-Tr E D. 2017;52(A): 215-226. https://doi.org/10.1016/j.trd.2017.03.011

[10] Hao X, Zhang X, Cao X, Shen X, Shi J, Yao Z. Characterization and carcinogenic risk assessment of polycyclic aro-

matic and nitro-polycyclic aromatic hydrocarbons in exhaust emission from gasoline passenger cars using on-road measurements in Beijing, China. Sci Total Environ. 2018;(645): 347-355. https://doi.org/10.1016/j.scitotenv.2018.07.113
[11] Xie X, Zhang Y, He Y, You K, Fan B, Yu D et al. Parallel attention-based LSTM for building a prediction model of vehicle emissions using PEMS and OBD. Measurement. 2021;(185):110074. https://doi.org/10.1016/j.measurement.2021.110074
[12] Janicka A. Ocena toksyczności mikroatmosfery środowiska wnętrza pojazdu samochodowego. Oficyna Wydawnicza Politechniki Wrocławskiej, Wrocław 2013.
[13] Jasiński R, Markowski J, Pielecha J. Probe positioning for the exhaust emissions measurements. Procedia Engineer. 2017;(192):381-386. https://doi.org/10.1016/j.proeng.2017.06.066
[14] Jeżowiecka-Kabsch K, Szewczyk H. Mechanika płynów. Oficyna Wydawnicza Politechniki Wrocławskiej, Wrocław 2001.
[15] Kamińska M, Andrzejewski M, Daszkiewicz P. Research of ecological indicators of two-way vehicle in stationary conditions. Combustion Engines. 2022;188(1):30-34. https://doi.org/10.19206/CE-142169
[16] Kerbachi R, Chikhi S, Boughedaoui M. Development of real exhaust emission from passenger cars in Algeria by using on-board measurement. Energy Proced. 2017;(136):388-393. https://doi.org/10.1016/j.egypro.2017.10.268
[17] Kęska A, Janicka A. Application of bat-cell bio-ambient tests in exhaust gas emissions examinations for Euro 4 and Euro 6 combustion engines. J Mach Engineer. 2017;17(4): 83-90. https://doi.org/10.5604/01.3001.0010.7007
[18] Kęska A, Janicka A. Determination of volatile organic compounds for combustion engines compliant with Euro 4 and Euro 6. Proceedings of ECOpole. 2017;11(2):387-394. https://doi.org/10.2429/proc.2017.11(2)038
[19] Kęska A. Metoda oceny toksyczności spalin silnikowych w aspekcie analizy rozwoju standardów emisyjnych. Raporty Wydziału Mechanicznego Politechniki Wrocławskiej. 2020; 26(155).
[20] Kuranc A. Exhaust emission test performance with the use of the signal from air flow meter. Eksploat Niezawodn. 2015;17(1):129-134.
[21] Lebrecht G, Czerczak S, Szymczak W. Benzen. Dokumentacja proponowanych wartości dopuszczalnych poziomów narażenia zawodowego. Podstawy i Metody Oceny Środowiska Pracy. 2003, 1(35).
[22] Manahan SE. Toksykologia środowiska. Aspekty chemiczne i biochemiczne. Wydawnictwo Naukowe PWN, Warszawa 2006.
[23] Mendyka B, Radek P, Janicka A, Czarny A, Zaczyńska E, Pawlik M. Cytotoksyczność i mutagenność preparatów zawierających domieszkę estru metylowego oleju rzepakowego. Medycyna Środowiskowa. 2005;8(2).
[24] Merkisz J, Andrzejewski M, Pielecha J. Comparison of carbon dioxide emissions in real traffic conditions of the vehicle with the values obtained in the certification test on the background of European standards. Combustion Engines. 2011-SC-057, 2011.
[25] Poulakis E, Philippopoulos C. Photocatalytic treatment of automotive exhaust emissions. Chem Eng J. 2017;(309): 178-186. https://doi.org/10.1016/j.cej.2016.10.030
[26] Shen X, Shi J, Cao X, Zhang X, Zhang W, Wu H et al. Real-world exhaust emissions and fuel consumption for diesel vehicles fueled by waste cooking oil biodiesel blends. Atmos Environ. 2018;(191):249-257. https://doi.org/10.1016/j.atmosenv.2018.08.004
[27] Szwaja S, Ansari E, Rao S, Szwaja M, Grab-Rogalinski K, Naber JD et al. Influence of exhaust residuals on combustion phases, exhaust toxic emission and fuel consumption from a natural gas fueled spark-ignition engine. Energ Convers Manage. 2018;(165):440-446. https://doi.org/10.1016/j.enconman.2018.03.075
[28] Szymlet N, Kamińska M, Lijewski P, Rymaniak Ł, Tutak P. Use of toxicity indicators related to CO_2 emissions in the ecological assessment of an two-wheel vehicle. Combustion Engines. 2021;187(4):36-41. https://doi.org/10.19206/CE-141487
[29] Wang Z, Liu X, Mu Y, Yang X, Yang L, Jiang Z. The exhaust emission online detection on the diesel engine. Optik. 2018;(164):126-131. https://doi.org/10.1016/j.ijleo.2018.02.047
[30] Wang J, Gui H, Yang Z, Yu T, Zhang X, Liu J. Real-world gaseous emission characteristics of natural gas heavy-duty sanitation trucks. J Environ Sci. 2022;(115):319-329. https://doi.org/10.1016/j.jes.2021.06.023
[31] Yusoff MNAM, Zulkifli NWM, Masjuki HH, Harith MH, Syahir AZ, Khuong LS et al. Comparative assessment of ethanol and isobutanol addition in gasoline on engine performance and exhaust emissions. J Clean Prod. 2018; (190):483-495. https://doi.org/10.1016/j.jclepro.2018.04.183
[32] Zardini AA, Suarez-Bertoa R, Forni F, Montigny F, Otura-Garcia M, Carriero M et al. Reducing the exhaust emissions of unregulated pollutants from small gasoline engines with alkylate fuel and low-ash lube oil. Environ Res. 2019;(170): 203-214. https://doi.org/10.1016/j.envres.2018.12.021
[33] Ziółkowski A, Fuć P, Lijewski P, Rymaniak Ł, Daszkiewicz P, Kamińska M et al. Analysis of exhaust emission measurements in rural conditions from heavy-duty vehicle. Combustion Engines. 2020;182(3):54-58. https://doi.org/10.19206/CE-2020-309

Aleksandra Kęska, DEng. – Faculty of Mechanical Engineering, Wrocław University of Science and Technology.
e-mail: *aleksandra.keska@pwr.edu.pl*

Prof. Anna Janicka, DSc., DEng. – Faculty of Mechanical Engineering, Wrocław University of Science and Technology.
e-mail: *anna.janicka@pwr.edu.pl*

Prof. Maciej Zawiślak, DSc., DEng. – Faculty of Mechanical Engineering, Wrocław University of Science and Technology.
e-mail: *maciej.zawislak@pwr.edu.pl*

Article citation info:
Wozniak M, Siczek K, Zakrzewski S, Just P, Ozuna G, Onescu C. Deposition effect of carbon deposits on charge flow in EGR valve equipped CI engine. Combustion Engines. 2023;192(1):26-35. https://doi.org/10.19206/CE-150503

Marek WOZNIAK
Krzysztof SICZEK
Sergiusz ZAKRZEWSKI
Pawel JUST
Gustavo OZUNA
Constantin ONESCU

Combustion Engines
Polish Scientific Society of Combustion Engines

Deposition effect of carbon deposits on charge flow in EGR valve equipped CI engine

ARTICLE INFO

Received: 14 February 2022
Revised: 11 April 2022
Accepted: 29 May 2022
Available online: 7 July 2022

The exhaust gas recirculation (EGR) valve regulates the exhaust gas flow between the engine exhaust manifold and the inlet one. This allows the inlet air to warm up, improving fuel evaporation and reducing the combustion temperature of the charge. Such a valve reduces the number of harmful substances in the exhaust gases. The valve tends to stick when too much sediment builds on the walls of the exhaust system, especially during driving in urban conditions or when leaks in the vacuum or exhaust pipes occur. A faulty valve causes the engine to run unevenly at idle speed and under light loads. The defective EGR valve weakens the inlet manifold capacity, increases combustion, causes clogging of the particulate filter and damage to the lambda probe. Blocked EGR valve may lead to engine immobilization as a result of its computerized control system operations. A model of an EGR valve for a selected diesel engine was developed to determine velocity distribution of the load flowing in it for different values of the degree of valve opening and the volume of deposits on the valve walls. The volume of accumulated carbon deposits on the walls of the EGR valve was measured using a real engine. Based on the recorded mileage of the vehicle, the assumed average speed of the car and the driving style of the driver and the intensity of deposition of carbon particles on the walls was estimated.

Key words: *CI engine, EGR valve, carbon deposits, CFD analysis*

1. Introduction

The necessity of NO_x emission reduction for different combustion engines caused the development and the common use of various catalytic converters and exhaust gas recirculation systems (EGR). The latter allows for recirculation of a portion of exhaust gases from the exhaust manifold and the inlet manifold via a condenser. During the flow, the exhaust gases are gradually cooled down and the deposition of particulate matter, hydrocarbons, and other entrained species takes place [1]. The deposited particles have forms differing in size and chemical composition depending on the place of deposition: on inner walls of EGR system components such as manifolds, pipes, valves, and coolers. The mentioned size and chemical composition of carbon deposits in the case of spark-ignition (SI) engines supplied with gasoline [2] significantly differ from these in case of compressed-ignition (CI) engines supplied by diesel fuel [3], emulsion fuel [4] or biodiesel [5].

The chosen EGR valve, applied in the compressed ignition (CI) combustion engine is shown in Fig. 1. The inlet gas flows from the EGR cooler and outlet gas are directed to the intake manifold of the CI engine. The EGR rate is controlled by balancing the opposing effects of the electric valve drive and the return spring. The inner walls of the EGR valve are covered with carbon deposits (CDs), affecting the loading of the engine exhaust catalysts during their operation. The presented study is aimed to determine the effect of carbon deposits on the inner surfaces on the charge flow inside the EGR valve applied to the CI engine chosen.

1.1. Role of EGR technology

Exhaust gas recirculation (EGR) is an emission control technology decreasing NO_x emission in various CI engines: from light-duty engines through medium and heavy-duty engine to low-speed, two-stroke marine engines [6].

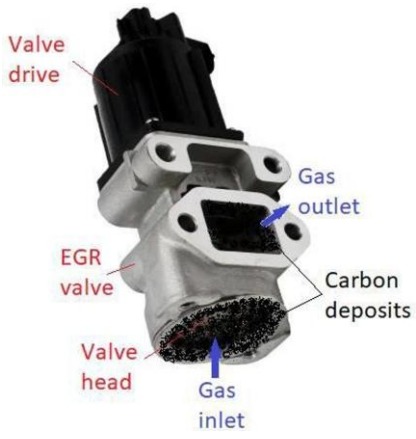

Fig. 1. EGR-valve covered with Carbon Deposits (CDs)

EGR technology is also utilized for enhancing the performance of selective catalytic reduction (SCR) catalysts [7].

Three main NO_x reduction technology pathways are applied in the modern CI engines [6]:
– EGR (without NO_x after treatment),
– EGR combined with SCR after treatment,
– SCR only, without EGR.

EGR systems can be used in HCCI [8] and PCCI engines [9] and in CI engines applied in hybrid vehicles [10–13].

The EGR rate is usually calculated from equation (1) [14]:

$$\text{EGR rate (\%)} = \frac{\text{EGR amount}}{\text{Intake air+EGR amount}} \times 100\% \qquad (1)$$

1.2. Types of EGR systems

There are different classifications for EGR systems. In a hot EGR system, the gas is recycled directly. The EGR-cooler system utilizes a gas-coolant heat exchanger for the operation.

The EGR systems in turbocharged CI engines, depending on the recirculation location, have either high or low pressure loop [15].

The examples of EGR systems utilized in CI engines are presented in Fig. 2, namely: Short-Route-system (SR) (Fig. 2a), Long-Route-system (LR) (Fig. 2b), Hybrid system (Fig. 2c), Venturi system (Fig. 2d), Fast rotating valve system (Fig. 2e) and Pump EGR-system (Fig. 2f) [16]. The EGR valve presented in Fig. 1 has been applied in the Long-Route-system (LR).

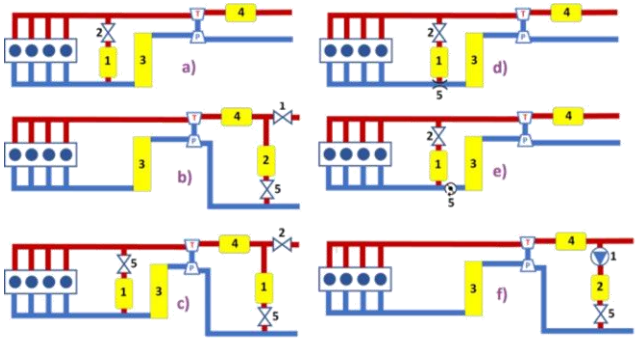

Fig. 2. Example EGR-Systems for CI engines [16]. a) Short-Route-system (SR), 1 – EGR-cooler, 2 – EGR-valve, 3 – Charge Air Cooler (CAC), 4 – Diesel Particulate Filter (DPF); b) Long-Route-system (LR), 1 – Exhaust throttle, 2 – EGR-cooler, 3 – CAC, 4 – DPF, 5 – EGR-valve; c) Hybrid system, 1 – EGR-cooler, 2 – Exhaust throttle, 3 – CAC, 4 – DPF, 5 – EGR-Valve; d) Venturi system, 1 – EGR-cooler, 2 – EGR-valve, 3 – CAC, 4 – DPF, 5 – Venturi; e) Fast rotating valve system, 1 – EGR-cooler, 2 – EGR-valve, 3 – CAC, 4 – DPF, 5 – Fast rotating valve; f) Pump EGR-system, 1 – Pump, 2 – EGR-cooler, 3 – CAC, 4 – DPF, 5 – EGR-valve

Reinfarth [16] discussed the advantages and the drawbacks of the mentioned systems.

The Short-Route System (SR) is simple and responds fast to EGR demands. It needs throttling and is sensitive to soot deposition in the whole intake system. It also needs the turbocharger able to deliver sufficient charging pressure, as only part of the exhaust gas passes the turbine while another part is used as EGR.

In Long-Route-system (LR), the compressor and the charge air cooler are in contact with the exhaust gases. The optimization of the cooling effect of the EGR-cooler prevents any condensation that would be able to damage the compressor wheel. The latter is exposed to exhaust gases accelerating its corrosion.

To avoid clogging in this system the EGR-loop is placed downstream from the particulate filter. To generate the pressure drop needed to drive the flow of EGR throttling the exhaust or the intake air is applied, however, the former manner is preferred due to lower fuel consumption.

The LR-system utilizes long piping filled with EGR causing a delayed reaction to changing EGR demands. Additionally, the exhaust gas with soot particles after the diesel particulate filter (DPF) causes fouling of the intercooler.

Such a system increases mass flow passing through both the turbine and the compressor. Under low loads, this limits the engines fuel consumption as compared to the SR-system. Such a consumption is also decreased due to the higher cooling capacity of the LR-system. As the EGR is cooled by the cooler and by the intercooler, the intake temperatures for the LR-system are lower and thus the heat losses in the engine are minimized.

The Hybrid EGR system allows the application of the EGR-path best fitting the actual driving situation and to reach the best engine efficiency in certain load points.

The Venturi system allows for local increase in the pressure drop that drives the EGR flow. In this system, the pumping effect can be regulated. A higher pumping effect with more EGR flow increases the pressure in the intake piping.

In the EGR system with Fast Rotating Valve, the pressure drop driving the EGR is increased via throttle of the intake air. However, this limits the intake pressure and enhances the pumping resistance. Simultaneously the delivered amount of air decreases, weakening the tolerable EGR rate. This problem is resolved via the application of a system with a fast-rotating throttle, limiting the intake pressure temporarily for better EGR performance, while keeping low values of the average pressure. The intake air pressure is limited just in time for the exhaust pulses to press some EGR into the intake.

The EGR system with the pump can supply the desired amount of EGR in any driving situation without any throttling. It needs an additional energy to drive a pump resulting in higher fuel consumption. Electric drive allows its speed regulation independently from the engine speed. The design of each EGR system is complex and requires [17]:

- limiting the pressure drop of the cooler, particularly in low-pressure-loop EGR systems,
- the compactness requiring high thermal efficiency,
- limiting the coolant flow rate to prevent its boiling,
- a careful thermal fatigue cycle analysis due to difficult and variable operating conditions,
- prevention of unexpected structural failures resulting from pressure pulses in the exhaust gases promoting fluctuating forces,
- limiting the negative effect of the deposition of residue on heat transfer walls, on the gas side and on the thermal efficiency

1.3. Effects of EGR

The use of EGR results in various effects on engine operation and phenomena generated therein. EGR valve is placed in the airpath chain of a combustion engine and routes usually more than 10% of the exhaust gas (or mixture), from the exhaust manifold, back into the inlet one [18].

Such a valve doses the appropriate amount of exhaust gas into the inlet manifold, relative to the engine load and speed. The location of the EGR valve causes diverse formation of NO_x and fumes smokiness from the individual cylinders of the engine, due to an uneven propagation of exhaust gas into the channels of the inlet manifold [19].

Mulenga et al. [20] reported that cooled EGR decreased in-cylinder NO_x formation. Abarham et al. [21] noticed that EGR coolers are usually cooled with engine coolant.

Agarwal et al. [22] explained that EGR controls the NO_x in CI engines via the lowering the O_2 concentration and flame temperature of the charge in the combustion chamber. Higher soot generated by EGR leads to higher carbon deposits, lubricating oil degradation and enhanced engine wear.

Pulkrabek [23] reported that EGR allowed better fuel economy and more efficient drivability. Okubo and Kubahara [24] noticed that EGR weakening NO_x emissions, fuel consumption and pumping loss is suitable for diesel engines with large exhaust gas flow rates. Hussain et al. [25] reported that EGR increased the UHC emission by 40 to 50%. Such an effect is avoided by reutilization of UHC. Parks et al. [9] found that the fuel efficiency and emission of PCCI engine depend on the EGR rate, fuel rail pressure, and fuel injection timing. As EGR enhanced, NO_x emission decreased, but CO and HC emission increased. The emission and efficiency changed significantly as EGR rates increased above 40%. As the EGR rates grew, the fuel efficiency began to drop, and the engine operation became less stable. Simultaneously, CO and HC emission rose due to the instability as incomplete combustion occurred

2. Charge flow in the EGR system

In the literature [26–28], the charge flow in an EGR system is usually considered as an integral part of the charge flow throughout the engine. Only a few papers consider the problem of disturbances in such a charge flow resulting from the presence of fouling of carbon and soot deposits.

Abd-Elhady et al. [29] reported that EGR coolers were affected by severe fouling resulting in the drop of their thermal efficiency by up to 30% within a very short period. The deposited layer was a blend of particulate matter and sticky heavy HCs difficult to remove from the heat exchanger surfaces.

Some authors [30, 31] noticed that the use of the EGR cooler results in higher production of PM.

According to [32–34] EGR operation affects the combustion, and hence NO_x formation and reduction via three mechanisms decreasing the flame temperature:

- dilution: the potentially enhanced mixing time and longer burn duration caused by the EGR's dilution effect. Additionally, the EGR weakens the partial pressure of O_2, due to lower temperature and low availability of O_2 less NO_x is produced,
- thermal: the enhanced heat capacity of an EGR-laced mixture,
- chemical: enhanced dissociation of CO_2 and H_2O,
- Exhaust gas from engines is cooled to decrease the emission via the EGR cooler.

Kowada et al. [35] reported that the use of a catalyzed wall-flow DPF allows limiting PM emission in both mass and small particles. Abarham et al. [36] reported that the soot and hydrocarbon deposition in the EGR cooler may be acidic and corrosive.

Some authors [37, 38] reported that EGR fouling exhibited an asymptotic evolution characterised by the rapid growth of the deposited layer in the first stages and a progressively slower growth until stable conditions are reached.

Authors of refs. [39, 40] noticed that the duration of the entire fouling process generally covers a matter of hours causing the EGR system operation almost its entire lifetime under fouled conditions.

As reported in [41, 42] the deposition of fouling material on heat transfer walls enhanced the thermal resistance due to the low conductivity of the residue.

Hoard et al. [43] reported that the thickness of the deposited layer, soot and hydrocarbons primarily limited the free-flow section, changing the velocity field, boundary layer separation and reattachment locations, compared to clean conditions, and changes in the turbulence field.

Hesselgreaves [44] stated that such changes enhanced the gas pressure drop through the cooler.

Williams et al. [45] explained that the carbon-containing deposits such as the particulate matter, hydrocarbons, and other entrained species having deposited from the flow of exhaust gas cooling down, form in the EGR systems. Reduction of such deposits needed optimized dimensioning of EGR coolers and valves, the use of EGR cooler bypass in the most sensitive cold conditions and the use of oxidation catalysts upstream of the EGR system. CDs forming in the HP-EGR systems caused emission and fuel consumption deterioration, poor performance and drivability, as well as engine failure. It was also report-ed that in the HP-EGR system of a CI engine operating at conditions conducive to EGR deposit formation over 24 hours, such a formation with Fischer-Tropsch Gas-to-Liquid (GTL) Gasoil fuel was less by 72% than that with B7 representative of EN590 diesel fuel.

Tanaka et al. [46] reported that the formation of lacquer with soot on the EGR valve or cooler occurred at 100°C or less, but not at 120°C. After the engine start, water was detected during the initial period for all temperatures studied. After the evaporation of water, aromatic HCs occurred at lower temperatures, while C=O groups occurred at higher temperatures.

3. Modelling of fouling and deposition of carbon and soot deposits

3.1. Models of fouling and deposition of carbon and soot deposits

There are some models created to solve the problem of fouling as well as the deposition of carbon and soot, which are strictly related.

Teng and Regner [47] elaborated a model for soot particle deposition. The soot deposit comprised three characteristic layers:

- a quasi-crystal base layer formed by nanoparticles,
- an intermediate layer of denser packing of soot particles with mesopores,
- a highly porous top layer formed by mechanical interlocking of soot particles.

The EGR performance was affected by the top layer of the deposit. The low contact energy made particles in the top and intermediate layers removable by the shearing force under high EGR flows. The contact energy for the particles

in the base layer was much higher compared to that in the surface and intermediate layers.

The behaviour of the EGR cooler fouling at the transient engine operation differed from that at the steady-state conditions.

Abarham et al. [36] developed a 1-D model to determine EGR cooler fouling amount and distribution across a concentric tube heat exchanger with a constant wall temperature in the CI engine. It well predicts the effectiveness, mass deposition, and pressure drop.

Jafarmadar et al. [48] used the model of the soot formation rate treated as the difference between the soot formation and oxidation, given by the equation (2).

$$\frac{\mathrm{Dm_{soot}}}{\mathrm{dt}} = \frac{\mathrm{dm_{form}}}{\mathrm{dt}} - \frac{\mathrm{dm_{oxid}}}{\mathrm{dt}} = A_f \cdot m_{fv} \cdot p^{0.5} \cdot \exp\left(-\frac{E_a}{R \cdot T}\right) - \frac{6 \cdot M_c}{\rho_s \cdot d_s} \cdot m_s \cdot R_{tot} \quad (2)$$

where: A_f – constant, R – gas constant, T – temperature, p – pressure, E_a – energy of activation, m_{fv} – mass of fuel vapour, m_s – mass of soot, M_c – molecular weight of carbon, ρ_s – soot density, d_s – soot particle size, R_{tot} – soot oxidation rate.

Some models of the fouling process in the EGR cooler system utilize a 1D approximation of the geometry and usually comprise no erosion or re-entrainment mechanisms [36, 49].

Other models utilize a Lagrangian framework for particle transport on a simplified channel of the heat exchanger [50].

Sometimes a complete steady 3D model applied to a single tube us used [51].

The model elaborated by Abarham et al. [49] predicts well a fouling depth. Most of the methods and models are based on bulk conditions or non-local parameters and applies only to simple geometries (1D, axisymmetric, single-channel, etc) where the homogeneity of the flow allows easy definition of those parameters.

3.2. Paz et al. fouling model

From the point of view of modelling of fouling in the EGR valve, the model developed by Paz et al. [52, 53] and presented in Fig. 3 seems to be very useful.

The model is based on the deposition-removal balance, and properly predicts the local fouling thickness under the constant thermal and flow conditions.

It adapts the fouling model [54] based on soot particle deposition neglecting the condensation and considered local effects.

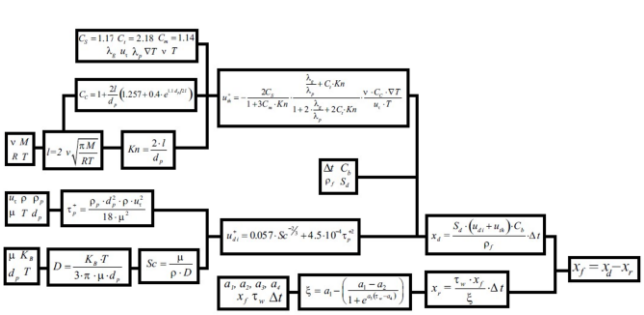

Fig. 3. The Paz et al. [52] fouling model (own source of the scheme)

In the model the sticking probability S_d is equal to one, and the bond strength factor ξ is adjusted experimentally. The model comprises dimensionless deposition and removal velocities. The deposition velocity is the sum of mass diffusion u_{di}^{+} and thermophoresis u_{th}^{+}, which is the highest deposition force when thermal gradients occur [55] with typical soot particle sizes between 10^{-8} to 10^{-5} m [56].

The re-entrainment of deposited particles is quantified via the average velocity or shear stress at the wall [40, 57–59].

The removal dimensionless velocity is proportional to the layer thickness and the wall shear stress [60–62].

After determining the velocities for each cell, the net fouling thickness x_f is determined at the end of the time step. Such a thickness is then accumulated in the cells adjacent to the walls until the height of a cell is exceeded, and then the fluid cell is changed to a solid one with its corresponding physical properties. Such a process is reversible, allowing a fouled cell to become a fluid cell again if the flow conditions change and the newly computed x_f is smaller than the cell size. The deposit properties include an effective density of 36.5 kg/m^3 and thermal conductivity of 0.07 W/m·K [52].

The fouling factor evolution curves are fitted to the asymptotic profile and the deposit mass is weighted under 30 to 60 kg/h exhaust gases flow at 400ºC [53]. Such a methodology allows for time reconstruction of fouling.

3.3. Adaptation of the Paz et al. fouling model to the case of the EGR valve fouling

To adapt the Paz et al. fouling model to the case of the EGR valve fouling it was necessary to do some transformations and make some assumptions.

The assumed dimensionless dependency of the average fouling thickness h/h_{ref} versus mass flow in EGR valve $\dot{M}/\dot{M}_{ref}$ was similar to the one for the average fouling thickness versus tube mass flow [63] (Fig. 4).

The assumed dimensionless dependency of the CD mass in the EGR valve m^{CD}/m_{ref}^{CD} versus time t/t_{ref} is similar to the one for the CD mass in EGR cooler versus time [63] (Fig. 5).

In these dimensionless dependencies the following symbols occurred: $\dot{M}_{ref}$ – the EGR inflow mass flow, $t_{ref} = L/V_{aver}$ – time of car mileage, L = 172,000 km – car mileage, V_{aver}= 60 kph – average car driving speed, $h_{ref} = V^{CD}/A$ – average fouling thickness in EGR valve, V^{CD} – calculated CD volume, A – the calculated area of inner walls of the modelled EGR valve, m_{ref}^{CD} – measured CD mass in the EGR valve after reaching the assumed car mileage.

For the actual EGR gas mass flow $\dot{M}$ the average fouling thickness h was determined and then actual CD mass $m^{CD} = \rho \cdot A \cdot h$ was estimated, where ρ – EGR carbon deposits density, and then time for CD inside EGR valve was determined. The fitting of the Paz et al. fouling model [52] to the obtained function $h = f(t)$ allows estimating the unknow input model parameters.

The situation becomes easier if the values of some parameters can be determined during separate experimental studies or estimated based on the literature data.

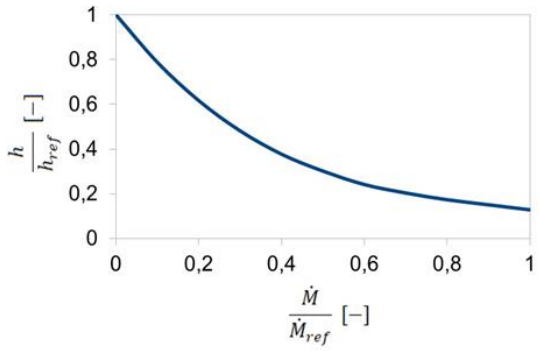

Fig. 4. The average fouling thickness h/h_{ref} vs. mass flow in EGR valve $\dot{M}/\dot{M}_{ref}$

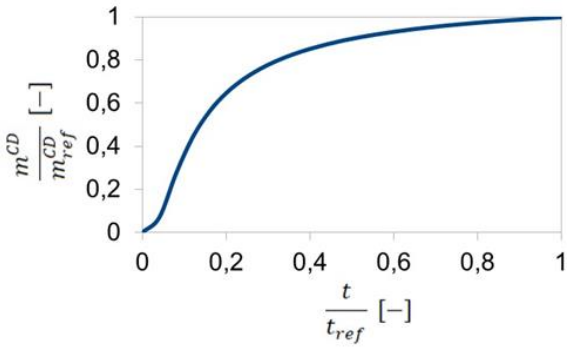

Fig. 5. The CD mass in the EGR valve m^{CD}/m^{CD}_{ref} vs. time t/t_{ref}

4. Methods and materials

4.1. Engine characteristics and operational conditions

During the study, the EGR valve from a CI engine of Opel Zafira 1.7 CDTi was used. The characteristics M(n) and P(n) of such an engine were obtained from the dyno test and are presented in Fig. 6. It was assumed that the engine operated at rotational speed equal to 4000 rpm.

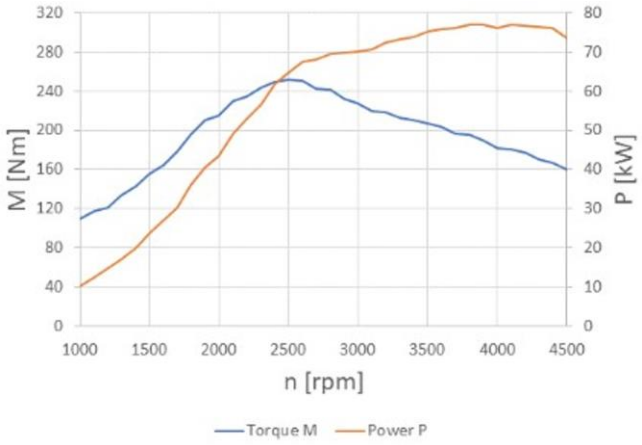

Fig. 6. Characteristics of a CI engine of Opel Zafira 1.7 CDTi (own source)

4.2. CFD model of the EGR valve

To allow the CFD analysis of charge flow in the EGR valve the model of the latter was elaborated. The model of the fluid domain comprising inner volumes of EGR valve (3+4+5–6), part of intake manifold 1 and connecting canal 2 is presented in Fig. 7. As an approximation, for diesel exhaust gas calculations the properties of air were used. The error associated with neglecting the combustion products was below 2%. Air was treated as an ideal gas [64].

The lift of the EGR valve was 3.7 mm (about 30% of full valve opening) corresponding to the EGR rate in the range 30–40%, similarly to the system described in [65].

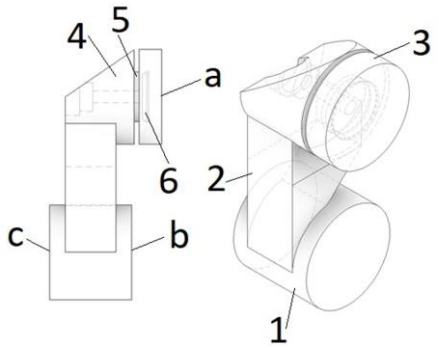

Fig. 7. Model of fluid domain: 1 – intake manifold, 2 – connecting canal, 3 and 4 – the inner volume of EGR valve being the sum of sub volumes, 5 – orifice, 6 – excluding the volume of valve: a – inlet of exhaust flow from EGR cooler, b – an inlet of air, c – outlet of a mixture of air and EGR gas

4.3. Estimation of carbon deposit volume

To consider an occurrence of CDs in the model of the fluid domain (Fig. 7), on the inner surfaces of the connecting canal 2, EGR subvolumes 3 and 4, and on the outer surfaces of the excluded volume of valve 6 the thin layers were added. The thickness of a chosen layer was equal to the average height of the CD structures on the relating wall obtained from optical scanning microscope. The introduced layers (Fig. 8) limited the volume of the flow domain in the model shown in Fig. 5.

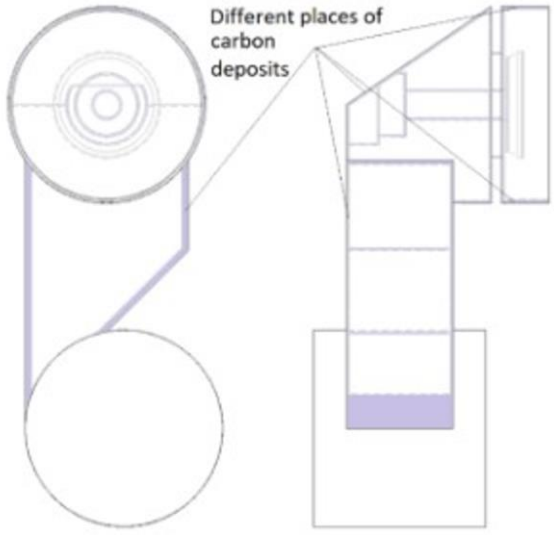

Fig. 8. The corrected model of the fluid domain from Fig. 7 after introducing modelled layers of carbon deposits

4.4. Assumptions and boundary conditions

For the modelled fluid domain, the following assumptions and boundary conditions were introduced:

- a no-slip boundary condition was applied on the walls and a standard wall function option was used for near-wall treatment

- the normal flow velocity of EGR inflow gas (from the EGR cooler) was 18.59 m/s for the case without CDs and 20.13 m/s for the case with CDs. It corresponded to the mass flow rate of 0.038 kg/s, being 30–40% of the mass flow rate in the intake manifold when the EGR rate is 30%, similarly to [66]. The temperature of an inflowing gas was 473 K,
- the normal flow velocity of air from the turbocharger was 44 m/s corresponding to the mass flow rate of 0.09 kg/s and its temperature was 330 K, similarly to the 1.6 L CI engine with variable geometry turbine VGT and Common rail systems [67],
- the outlet flow of the mixture of EGR gas and air was under a pressure outlet boundary condition and temperature of 373 K,
- the temperature of the walls was 373 K and no heat transfer through the walls occurred,
- the fluid flow and heat transfer processes were turbulent and in steady state,
- the mesh comprising tetrahedral finite elements was generated in the fluid domain (Fig. 9), the inflation option was chosen on walls with at least five layers and an average size of an element was 3 mm.

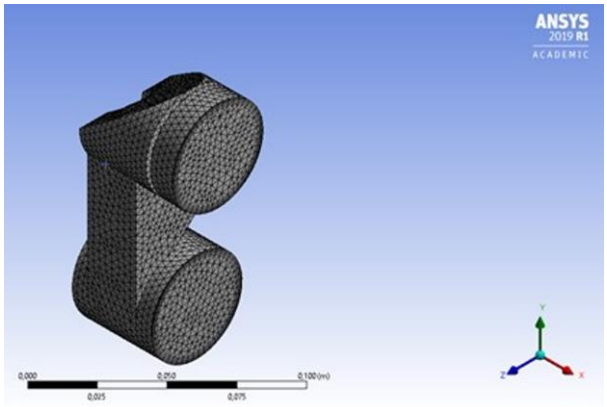

Fig. 9. Mesh of finite elements for the fluid domain of EGR model analyzed

4.5. Carbon deposit thickness

The carbon deposit thickness was estimated by measuring the inner geometry of a new and operated EGR valves with use of optical scanning microscope. An optical scanner, structured light by GOM with an ATOS core head was used for scanning. GOM scan and Geomagic Design X software were used to process the scans. The dimensions were inspected using the GOM Inspect module.

4.6. Carbon deposit mass, volume, and density

Two masses of EGR valves without an electric driver were measured for two cases: of the new valve and the one covered inside with CDs.

The CD volume $V^{CD}$was calculated as a difference of inner volumes of a new EGR valve and EGR covered by CD layers.

The CD mass m_{ref}^{CD} was calculated as a difference between the measured mass of an EGR valve without an electric driver and covered inside with CDs and the one of a new EGR valve, also without an electric driver.

The CD density ρ was calculated as a ratio of the CD mass and its estimated volume. It was compared with the one of graphite equal to 2.25 g cm^{-3}.

5. Results

5.1. Carbon deposit thickness

The obtained carbon deposit thickness measurement results are presented in Fig. 10. The EGR valve measured on side of the valve stem is depicted in Fig. 10a), whereas in Fig. 10b) is presented the side of the valve head. The average values of thickness visible in Fig. 10a) were even twice higher than these visible in Fig.10b.

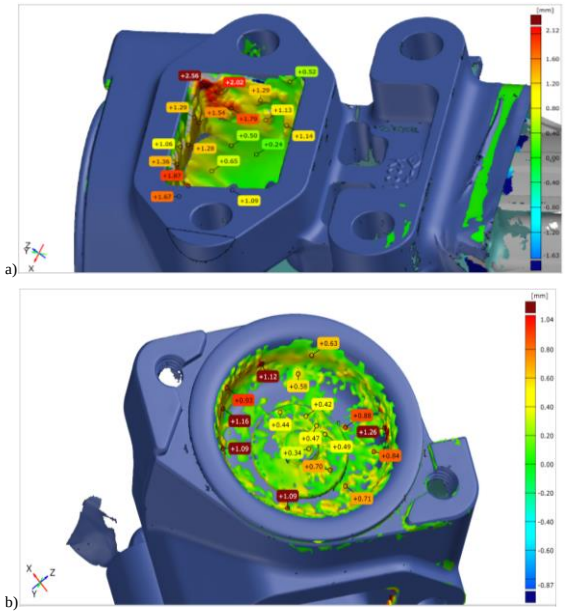

Fig. 10. Thickness of carbon deposits in an EGR valve chamber measured using optical scanning microscopy, a) on side of the valve stem, b) on side of the valve head

5.2. Carbon deposit mass, volume, and density

The masses of EGR valve without an electric drive for two cases: for the new valve and the one covered inside with CDs, the CD mass, CD volume and CD density, the ratio of CD density and that of graphite are presented in Table 1.

The obtained density of carbon deposits inside the EGR valve could be slightly greater than the density of graphite. It was because CDs could contain also other substances than carbon, for example, S, Cl, Ca, and Zn originated from the combustion of lubricating oil [68].

It could be also lower than the density of graphite due to the very uneven and porous structure. Thus, the obtained density of CDs can be treated as the equivalent one.

Table 1. The masses of EGR valve without an electric drive for two cases: the new valve and the one covered inside with CDs, the CD mass, CD volume and CD density, the ratio of CD density and that of graphite

Mass of a new EGR valve	[g]	522.699 ±0.001
Mass of an EGR valve covered inside by CD	[g]	523.669 ±0.001
CD mass	m_{ref}^{CD} [g]	0.97 ±0.002
CD volume	V^{CD} [cm^3]	0.43 ±0.7
CD density	ρ [g cm^{-3}]	2.325 ±0.56
CD density/density of graphite	[–]	1.033 ±0.25

5.3. The flow velocity of charge in the modelled EGR valve

The values of the flow velocity of charge, calculated using the modelled EGR valve are presented in Fig. 11 for the case of the new EGR valve and in Fig. 12 for the case of the EGR valve covered inside by the CD layers. On the left side of each figure is presented the 3D view of the velocity distribution and on the right side the velocity distribution in the XY plane (the orientation of these axes is visible in Fig. 9) containing the main axis of the EGR valve. The values presented in Fig. 12 are higher even by 30% than those in Fig. 11.

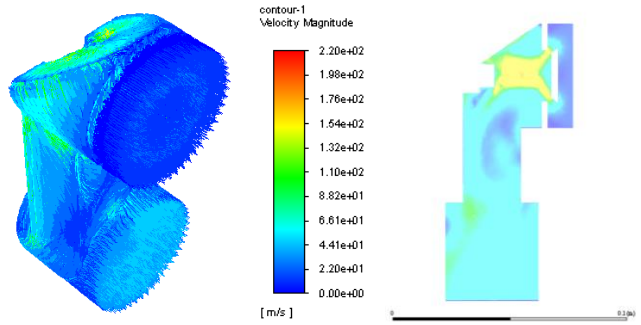

Fig. 11. The flow velocity of the fluid in the new EGR valve

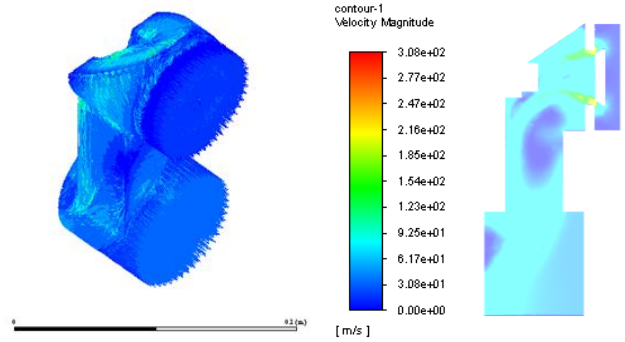

Fig. 12. The flow velocity of the fluid in the EGR valve covered inside by the CD layers

5.4. The total temperature of charge in the modelled EGR valve

The values of the total temperature of charge calculated using the modelled EGR valve are presented in Fig. 13 for the case of the new EGR valve and in Fig. 14 for the case of the EGR valve covered inside by the CD layers. On the left side of each figure is presented the 3D view of the temperature distribution and on the right side the temperature distribution in the XY plane (the orientation of these axes is visible in Fig. 9) containing the main axis of the EGR valve. The values presented in Fig. 14 are higher even by 30% than those in Fig. 13.

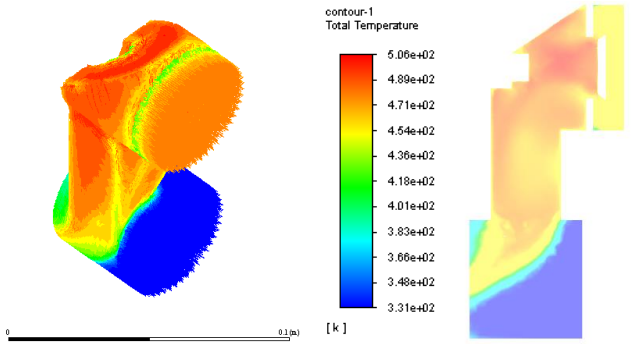

Fig. 13. The total temperature of charge in the new EGR valve

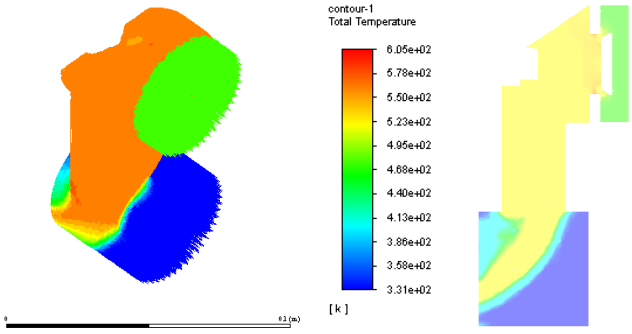

Fig. 14. The total temperature of charge in the EGR valve covered inside by the CD layers

6. Conclusions

Based on the obtained results the following conclusions can be drawn:

- the analysis of the effect of deposition of CDs on the charge flow in the EGR valve in the CI engine was performed,
- only a few models intended for simulation of the fouling process in the EGR system can predict the fouling depth,
- the method allowing determination of the function for average fouling depth inside the EGR valve versus time and the mass flow inside the EGR valve $h = f(t, \dot{M})$ has been proposed. Fitting fouling model of Paz et al. to such a function $h = f(t, \dot{M})$ allows estimation of the model parameters,
- the occurrence of CDs in the EGR valve strongly affects the distribution of the flow velocity of charge therein. The values of the flow velocity when CDs occur can be up to 30% higher than in the case of EGR without CDs,
- the total temperature values of the charge flowing in the EGR valve with CDs can be higher by 100 K as compared to the case without them. In the latter case, the total temperature distribution varies more in value and position than in the case with CDs.

Nomenclature

CI	compression ignition
CD	carbon deposits
CFD	computational fluid dynamics
EGR	exhaust gas recirculation
SCR	selective catalytic reduction

Bibliography

[1] Williams R, Cook S, Woodall K, Clayton, C, Gee M, Mulquen S et al. Development of an engine test to rate the EGR deposit formation propensity of fuels in light-duty diesel engines. SAE Int J Adv & Curr Prac in Mobility. 2021;3(1): 337-348. https://doi.org/10.4271/2020-01-2096

[2] Kikichi G, Miyagawa M, Yamamoto Y, Inayoshi N. Accumulation mechanism of gasoline EGR deposit. SAE Technical Paper 2017-01-0806. 2017. https://doi.org/10.4271/2017-01-0806

[3] Manni M, Florio S, Gommellini C. Impact of fuel and oil quality on deposits, wear and emissions from a light duty diesel engine with high EGR. SAE Transactions. 2000; (109):1534-1547. http://www.jstor.org/stable/44745955.

[4] Hasannuddin AK, Yahya WJ, Sarah S, Ithin AM, Syahrullail S, Sugeng DA et al. Performance, emissions and carbon deposit characteristics of diesel engine operating on emulsion fuel. Energy. 2018;(142):496-506. https://doi.org/10.1016/j.energy.2017.10.044

[5] De Serio D, Oliveira A, Sodre JR. Effects of EGR rate on performance and emissions of a diesel power generator fueled by B7. J Braz Soc Mech Sci. 2017;(39):1919-1927. https://doi.org/10.1007/s40430-017-0777-x

[6] Jaaskelainen H, Khair MK. Exhaust Gas Recirculation. https://dieselnet.com/tech/engine_egr.php, 2021

[7] Zha Y, Cunningham M, Heichelbech J, Lakkireddy V, Kumar A, Srinivasan A et al. Cummins sustained low temperature NO_x reduction (SLTNR). 2016 Annual Merit Review. Washington 9.06.2016. https://energy.gov/sites/prod/files/2016/06/f33/pm068_zha_2016_o_web.pdf

[8] Hassan AO, Abu-Jrai A, Al-Muhatseb AH, Jamil F. Impact of EGR and engine speed on HCCI engine performance and tailpipe emissions. Energy Proced. 2017;(136):208-212. https://doi.org/10.1016/j.egypro.2017.10.321

[9] Parks JE, Prikhodko V, Storey JME, Barone TL, Lewis S.A., Kass MD et al. Emissions from premixed charge compression ignition (PCCI) combustion and effect on emission control devices. Catal Today. 2010;151(3-4):278-284. https://doi.org/10.1016/j.cattod.2010.02.053

[10] Jonasson K. Control of hybrid electric vehicles with diesel engines. Doctoral Dissertation. Lund Institute of Technology, Sweden 2005. https://www.iea.lth.se/publications/Theses/LTH-IEA-1046.pdf

[11] Yamada T, Haga H, Matsumoto I, Tomoda T. Study of diesel engine system for hybrid vehicles. SAE Int J Alt Power. 2012;1(2):560-565. https://doi.org/10.4271/2011-01-2021.

[12] Lee J, Moon JI, Yeon-Hee K. A study on heat exchange efficiency of EGR cooler for diesel hybrid. Transactions of the Korean Society of Automotive Engineers. 2009;17(2): 159-164. https://www.koreascience.or.kr/article/JAKO2009-09651054565.pdf

[13] Song RC. A study on engine performance of EGR valve problem in hybrid vehicles. J Energ Eng. 2015;(24):34-39, https://doi.org/10.5855/ENERGY.2015.24.3.034.

[14] Jeong BG, Won JH, Oh KC, Heo HS, Bae S, Seo HJ et al. Characteristics of integrated air control and low-pressure exhaust gas recirculation valve for diesel engines. Int J Automot Techn. 2020;21(1):239-247. https://doi.org/10.1007/s12239-020-0023-x

[15] Zheng M, Reader GT, Hawley JG. Diesel engine exhaust gas recirculation – a review on advanced and novel concepts. Energ Convers Manage. 2004;(45):883-900. https://doi.org/10.1016/S0196-8904(03)00194-8

[16] Reinfarth S. EGR-systems for diesel engines. Licentiate thesis. Kungliga Tekniska Högskolan (KTH), Stockholm 2010. http://kth.diva-portal.org/smash/get/diva2:305816/-FULLTEXT01

[17] Teng H, Regner G. Characteristics of soot deposits in EGR coolers. SAE Technical Paper 2009-01-2671. 2009. https://doi.org/10.4271/2009-01-2671

[18] Teodorescu CS, Olaru S. Issues in modeling and control of electro-pneumatic EGR valve actuator for automotive engineering. 15th International Conference on System Theory, Control and Computing (ICSTCC), Sinaia 2011:1-8. https://ieeexplore.ieee.org/document/6085657

[19] Krakowian K, Kazmierczak A, Gorniak A, Wróbel R. Influence of the single EGR valve usability on development of the charge directed to individual cylinders of an internal combustion engine. International Conference on Advances in Energy Systems and Environmental Engineering (ASEE17). E3S Web Conf. 2017;22. https://doi.org/10.1051/e3sconf/20172200088

[20] Mulenga MC, Chang DK, Tjong JS, Styles D. Diesel EGR cooler fouling at freeway cruise. SAE Technical Paper 2009-01-1840. 2009. https://doi.org/10.4271/2009-01-1840

[21] Abarham M, Hoard J, Assanis D, Styles D, Cutris EW, Ramesh N. Review of soot deposition and removal mechanisms in EGR coolers. SAE Int J Fuels Lubr. 2010;3(1): 690-704. https://doi.org/10.4271/2010-01-1211

[22] Agarwal D, Singh SK, Agarwal AK. Effect of exhaust gas recirculation (EGR) on performance, emissions, deposits and durability of a constant speed compression ignition engine. Appl Energy. 2011;88(8):2900-2907. https://doi.org/10.1016/j.apenergy.2011.01.066

[23] Pulkrabek WW. Engineering Fundamentals of the Internal Combustion Engine. Prentice Hall, New Jersey 2004.

[24] Okubo M, Kuwahara T. Principle and design of emission control systems. Chapter 3. New Technologies for Emission Control in Marine Diesel Engines. Elsevier 2019. https://doi.org/10.1016/B978-0-12-812307-2.00003-1

[25] Hussain J, Palaniradja K, Alagumurthi N, Manimaran R. Effect of exhaust gas recirculation (EGR) on performance and emission of a compression ignition engine with staged combustion (insertion of unburned hydrocarbon). Int J Energ Eng. 2012:2(6):285-292. https://doi.org/10.5923/j.ijee.20120206.03

[26] Shi Y, Reitz RD. Multi-dimensional modelling of diesel combustion: Review. In: Modelling Diesel Combustion. Mechanical Engineering Series. Springer. Dordrecht 2010. https://doi.org/10.1007/978-90-481-3885-2_15

[27] Abay K, Colak U, Yuksek L. Computational fluid dynamics analysis of flow and combustion of a diesel engine. J Therm Eng.2018;4(2):1878-1895. https://doi.org/10.18186/journal-of-thermal-engineering.388333

[28] Millo F, Pautasso E, Pasero P, Barbero S, Vennettilli N. An experimental and numerical study of an advanced EGR control system for automotive diesel engine. SAE Int J Engines. 2009;1(1):188-197. https://doi.org/10.4271/2008-01-0208

[29] Abd-Elhady MS, Malayeri MR, Muller-Steinhagen H. Fouling problems in exhaust gas recirculation coolers in the automotive industry. Proc Int Conf Heat Exchanger Fouling Clean VIII, Schladming. 2009:125-133. https://heatexchanger-fouling.com/wp-content/uploads/2021/09/17_Malayer_EGR_F.pdf

[30] McKinley TL. Modeling sulfuric acid condensation in diesel engine EGR coolers. SAE Technical Paper 970636. 1997. https://doi.org/10.4271/970636
[31] Lim J, Kang B, Park J et al. A study on the effects of EGR temperature on emission characteristics in a HSDI diesel engine using EGR cooler. Proceedings of KSAE. Fall Conference, 2004:306-312.
[32] Ladommatos N, Abdelhalim SM, Zhao H, Hu Z. The dilution, chemical, and thermal effects of exhaust gas recirculation on diesel engine emissions – part 1: Effect of reducing inlet charge oxygen. SAE Technical Paper 961165. 1996. https://doi.org/10.4271/961165
[33] Ladommatos N, Abdelhalim SM, Zhao H, Hu Z. The dilution, chemical, and thermal effects of exhaust gas recirculation on diesel engine emissions – part 2: Effects of carbon dioxide. SAE Technical Paper 961167, 1996. https://doi.org/10.4271/961167
[34] Ladommatos N, Abdelhalim SM, Zhao H, Hu Z. The dilution, chemical, and thermal effects of exhaust gas recirculation on diesel engine emissions – part 3: Effects of water vapour. SAE Technical Paper 971659, 1997. https://doi.org/10.4271/971659
[35] Kowada M, Hayashi K, Shouyama K, Ihara Y, Sugihara H. Hino's advanced low-emission technologies developed to meet stringent emissions standards. SAE Technical Paper 2006-01-0275, 2006. https://doi.org/10.4271/2006-01-0275
[36] Abarhem M, Hoard J, Assanis DN, Styles D, Curtis EW, Ramesh N et al. Numerical modeling and experimental investigations of EGR cooler fouling in a diesel engine. SAE Technical Paper 2009-01-1506. 2009. https://doi.org/10.4271/2009-01-1506
[37] Thonon B, Grandgeorg S, Jallut C. Effect of geometry and flow conditions on particulate fouling in plate heat exchangers. Heat Transfer Eng. 1999;20(3):12-24. https://doi.org/10.1080/014576399271385
[38] Stolz A, Fleischer K, Knecht W, Nies J, Strähle R. Development of EGR coolers for truck and passenger car application. SAE Technical Paper 2001-01-1748, 2001. https://doi.org/10.4271/2001-01-1748
[39] Grillot JM, Icart G. Fouling of a cylindrical probe and a finned tube bundle in a diesel exhaust environment. Exp Therm Fluid Sci. 1997;(14):442-454. https://doi.org/10.1016/S0894-1777(96)00145-8
[40] Abd-Elhady MS, Malayeri MR, Muller-Steinhagen HM. Fouling problems in exhaust gas recirculation coolers in the automotive industry. Heat Transfer Eng. 2011;(32):248-257. https://doi.org/10.1080/01457632.2010.495612
[41] Bolt TR, Melo LF. Fouling of heat exchangers. Exp Therm Fluid Sci. 1997;14(4):315. https://doi.org/10.1016/S0894-1777(96)00133-1
[42] Park S, Choi K, Kim H, Lee K. Influence of PM fouling on effectiveness of heat exchanges in a diesel engine with fin-type EGR coolers of different sizes. Heat Mass Transfer. 2010;(46):1221-1227. https://doi.org/10.1007/s00231-010-0652-0
[43] Styles D, Giuliano JM, Sluder CS, Storey JME, Hoard J, Abarham M. Diesel EGR cooler fouling. SAE Technical Paper 2008-01-2475. 2008. https://doi.org/10.4271/2008-01-2475
[44] Hesselgreaves JE. The effect of system parameters on the fouling performance of heat exchangers. Proceedings of the 3rd UK National Conference on Heat Transfer and 1st European Conference on Thermal Sciences. 1992.
[45] Williams R, Cook S, Woodall K, Clayton C, Gee M, Mulqueen S et al. Development of an engine test to rate the EGR deposit formation propensity of fuels in light-duty diesel engines. SAE Technical Paper 2020-01-2096. 2020. https://doi.org/10.4271/2020-01-2096
[46] Tanaka K, Hiroki K, Kikuchi T, Konno M, Oguma M. Investigation of mechanism for formation of EGR deposit by in situ ATR-FTIR spectrometer and SEM. SAE Int J Engines. 2016;9(4):2242-2249. https://doi.org/10.4271/2016-01-2351
[47] Teng H, Regner G. Characteristics of soot deposits in EGR coolers. SAE Int J Fuels Lubr. 2010;2(2):81-90. https://doi.org/10.4271/2009-01-2671
[48] Jafarmadar S, Pirouzpanah V, Zehni A. Modeling the effect of EGR on combustion and pollution of direct injection diesel engines with flow field model. 5th International Congress on Chemical Engineering. Kish Island 2008.
[49] Abarham M, Zamankham P, Hoard JW, Styles D, Sluder CS, Storey JME et al. CFD analysis of particle transport in axisymmetric tube flows under the influence of thermophoretic force. Int J Heat Mass Tran. 2013;(61):94-105. https://doi.org/10.1016/j.ijheatmasstransfer.2013.01.071
[50] Nagendra K, Tafti DK, Viswanathan AK. Modeling of soot deposition in wavy-fin exhaust gas recirculator coolers. Int J Heat Mass Tran. 2011;54(7-8):1671-1681. https://doi.org/10.1016/j.ijheatmasstransfer.2010.10.033
[51] Stauch R, Brotz F, Supper J. CFD simulation of the fouling process in EGR coolers. Vehicle Thermal Management Systems. 2011:233-243. https://doi.org/10.1533/9780857095053.3.233
[52] Paz C, Suzarez E, Eiris A. et al. Experimental set up for the determination of fouling behaviour in diesel engine exhaust gas recirculation systems. 10th Conference on Energy for a Clean Environment. Lisbon 2009.
[53] Paz C, Suarez E, Eiris A, Porteiro J. Development of a predictive CFD fouling model for diesel engine exhaust gas systems. Heat Transfer Eng. 2013;34(8-9):674-682. https://doi.org/10.1080/01457632.2012.738321
[54] Suarez E, Paz C, Porteiro J et al. Simulation of the fouling layer evolution in heat transfer surfaces. V European Conference on Computational Fluid Dynamics. Lisbon 2010.
[55] Messerer A, Niessner R, Poschl U. Thermophoretic deposition of soot aerosol particles under experimental conditions relevant for modern diesel engine exhaust gas systems. J Aerosol Sci. 2003;34(8):1009-1021. https://doi.org/10.1016/S0021-8502(03)00081-8
[56] Kittelson DB. Engines and nanoparticles: a review. J Aerosol Sci. 1998;29(5-6):575-588. https://doi.org/10.1016/S0021-8502(97)10037-4
[57] Abd-Elhady MS, Rindt CCM, Wijers JG, Steenhoven AA, Bramer EA, Meer TH. Minimum gas speed in heat exchangers to avoid particulate fouling. Int J Heat Mass Tran. 2004; 47(17-18):3943-3955. https://doi.org/10.1016/j.ijheatmasstransfer.2004.03.024
[58] Abd-Elhady M, Malayeri M. Asymptotic characteristics of particulate deposit formation in exhaust gas recirculation (EGR) coolers. Appl Therm Eng. 2013;60(1-2):96-104. https://doi.org/10.1016/j.applthermaleng.2013.06.038
[59] Sluder CS, Storey J, Lance MJ, Barone T. Removal of EGR cooler deposit material by flow-induced shear. SAE Technical Paper 2013-01-1292. 2013. https://doi.org/10.4271/2013-01-1292
[60] Freeman WB, Middis J, Muller-Steinhagen HM. Influence of augmented surfaces and of surface finish on particulate fouling in double pipe heat exchangers. Chem Eng Process. 1990;27(1):1-11. https://doi.org/10.1016/0255-2701(90)85001-K
[61] Kim NH, Webb RL. Particulate fouling of water in tubes having a two-dimensional roughness geometry. Int J Heat Mass Tran. 1991;34(11):2727-2738. https://doi.org/10.1016/0017-9310(91)90231-3

[62] Bott TR. Fouling of Heat Exchangers. Elsevier Ltd 1995.
[63] Paz C, Suarez E, Concheiro M et al. CFD transient simulation of the fouling of a EGR cooler in a diesel exhaust environment. Proceedings of International Conference on Heat Exchanger Fouling and Cleaning. Budapest 2013.
[64] Jaaskelainen H. Diesel Exhaust Gas. 2020. https://dieselnet.com/tech/diesel_exh.php.
[65] Yang Z, Winward E, Stobart R, Zhao D, O'Brien G. Modelling the exhaust gas recirculation mass flow rate in modern diesel engines. SAE Technical Paper 2016-01-0550. 2016. https://doi.org/10.4271/2016-01-0550
[66] Olsson A. Analysis and measurements of gas flows for engines with EGR. Master of Science Thesis. KTH Industrial Engineering and Management. Stockholm 2012. http://www.diva-portal.org/smash/get/diva2:707659/FULLTEXT01.pdf
[67] Desantes JM, Galindo J, Guardiola C, Dolz V. Air mass flow estimation in turbocharged diesel engines from in-cylinder pressure measurement. Exp Therm Fluid Sci. 2010; 34(1):37-47. https://doi.org/10.1016/j.expthermflusci.2009.08.009
[68] Wo H, Dearn KD, Song R, Hu E, Xu Y, Hu X. Morphology, composition, and structure of carbon deposits from diesel and biomass oil/diesel blends on a pintle-type fuel injector nozzle. Tribol Int. 2015;(91):189-196. https://doi.org/10.1016/j.triboint.2015.07.003

Marek Wozniak, DEng. – Department of Vehicles and Fundamentals of Machine Design, Lodz University of Technology, Poland.
e-mail: *marek.wozniak@p.lodz.pl*

Krzysztof Siczek, DSc., DEng. – Department of Vehicles and Fundamentals of Machine Design, Lodz University of Technology, Poland.
e-mail: *ks670907@p.lodz.pl*

Sergiusz Zakrzewski, DEng. – Department of Vehicles and Fundamentals of Machine Design, Lodz University of Technology, Poland.
e-mail: *sergiusz.zakrzewski@p.lodz.pl*

Paweł Just, DEng. – Department of Materials Engineering and Production Systems, Lodz University of Technology, Poland.
e-mail: *pawel.just@p.lodz.pl*

Prof. Gustavo Ozuna, DSc., DEng. – Department of Industrial Engineering and Systems, University of Sonora, Mexico.
e-mail: *gozuna@industrial.uson.mx*

Prof. Constantin Onescu, DSc., DEng. – Maintenance Department, University of Pitesti, Romania.
e-mail: *constantin.onescu@gmail.com*

Article citation info:
Andrych-Zalewska M, Sitnik L, Sroka Z, Mihaylov V. Fuel with a higher content of bio components in greenhouse effect aspects. Combustion Engines. 2023;192(1):36-42. https://doi.org/10.19206/CE-147741

Monika ANDRYCH-ZALEWSKA
Lech SITNIK
Zbigniew SROKA
Veselin MIHAYLOV

Combustion Engines
Polish Scientific Society of Combustion Engines

Fuel with a higher content of bio components in greenhouse effect aspects

ARTICLE INFO

Received: 31 January 2022
Revised: 11 March 2022
Accepted: 28 March 2022
Available online: 22 April 2022

Transport is an energy-intensive sector of the economy and it is important where energy comes from and how it is used – now and in the future. The presented research results seem to encourage further work, despite the fact that the work had the character of basic research. The results were achieved in idealized conditions by the fact that the internal combustion engine was tested in static conditions on the test bench and the fuels contained components with strictly defined parameters. These conditions are different from everyday life. However, the obtained results seem to be valuable as they lead to conclusions regarding biofuels, and these conclusions are not directly formulated and published in the literature on the subject. The general conclusion from the research carried out is that the introduction of the so-called biofuels can contribute not to the reduction of CO_2 emissions, but to its faster balancing in the environment. This balancing can be achieved but at the cost of increased fuel consumption. This increase in fuel consumption would probably not occur if the "bio" components in the fuel were synthetic hydrocarbons obtained from biomass. However, proving it requires wider studies, including LCA. Data for this LCA, especially about a fuel consumption, may be coming from long term operation of vehicles.

Key words: *energy, fuel, bio-blends, CO_2 balance, engines*

1. Introduction

The global problem is the concentration of CO_2 in the atmosphere which lead to the greenhouse effect. The general problem is that the concentration of CO_2 in the ambient air is too high and is constantly increasing. This trend must be reversed. A number of quick measures should be taken to reduce the amount of CO_2, which in many cases is associated with the simultaneous reduction of emissions of CO_2 and other compounds – mainly harmful to health. Therefore, reducing CO_2 emissions has many benefits. Road transport is one of a a major contributor to CO_2 emissions. As a consequence, the car industry is forced to reduce it [1, 27].

And this means (as is commonly believed) that the problem of CO_2 emissions from transport could be solved immediately if the energy used today and in the future comes from renewable sources[1, 28].

But the world's problem is not CO_2 emissions, but the increasing concentration of CO_2 in the atmosphere, leading to the acceleration of the greenhouse effect. It seems that understanding this problem is not obvious. Confirmation of this observation results from the analysis of various forecasts for the development of transport and energy sources for its supply. For example in Fig. 1 shows historical and forecast energy consumption for the United States by 2050 [1].

But the world's these projections (Fig. 1) show that by 2050 the demand for petroleum fuels will change by approx. 10%, but after the initial decline (until 2035) there will be another increase in demand, which will result in a total decrease of this demand from 2020 to 2050 only by approx. 7.5%. According to this forecast, the minimum demand for petroleum fuels will occur around 2036 and this demand will be similar to what it was in 2008.

The forecasts (for USA) also show that the maximum share of biofuels (approx. 4%) is achieved now, and will practically not change by 2050 (but today the bio-components concentration in fuels, in EU for example, there is up to 10%).

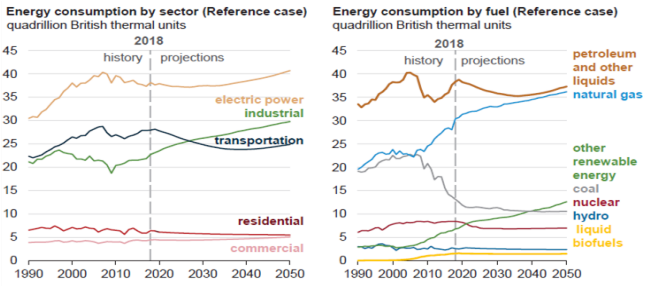

Fig. 1. Historical and projection models of energy and fuel consumption by economy sector in the USA [1]

The forecast of the total consumption of crude oil and other fluids and biofuels shows that the share of biofuels in the fuel blend first will increases (until around 2035) and then decreases. It seems that the increase in the share of bio components is rather unexpected. There is an "old school" opinion (example [2]), that *"The share of renewable transport fuels is minimal and most of those supplied to date (biodiesel) do more harm than good"*. Other point of view is that up to 2030, advanced biofuels will not make a sizeable contribution and will be constrained in the medium term by land availability for achieving of "renewable power" to produce this kinds of fuels.

One could agree with this and similar opinions, were it not for the fact that the raw material for the production of bio components is not only biomass from industrial plants. The real raw material for the production of bio components on a large scale is municipal solid waste (MSW), of which there is an excess of which around the world will increase [3].

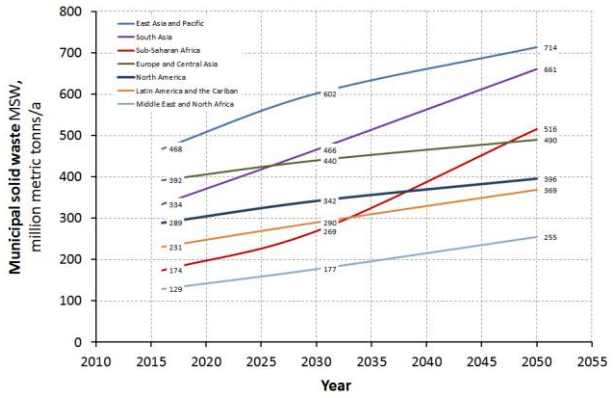

Fig. 2. Municipal waste now and in forecasts (data from [3])

Municipal solid waste (MSW) can be transformed to many fuel components (or fuel). Nowadays a popular technology is achieving from MSW a butanol [4–5]. This technology is relatively simple therefore the find more and more interest. Municipal solid waste can also be converted into synthetic gas (syngas) [6–8], and then into synthetic hydrocarbons that can be used as fuel or fuel components.

Regarding today's practice, there are three basic ways to reduce CO_2 as follows [9].

- The use of alcohols (first of all the ethanol) and their mixtures with petrol (in Europe, for example, the B10 petrol has a 10% ethanol by volume in petrol) [10].
- The use of fatty acids esters (methyl or ethyl esters) of vegetable oils and their mixtures with diesel fuel (nowadays B7 in EU has 7% FAME by volume in commercial diesel fuel) [11–14].
- The use of synthetic hydrocarbons produced from synthesis gas coming from biomass and their mixtures with standard hydrocarbons [15–17].

The article presents another method of obtaining fuel from bio components. For this purpose, a mixture of light and heavy alcohols was used as an additive to fuels for a spark ignition (SI) engine. On the use of alcohols, as fuel components, exist a many papers e.g. [18, 19] but in this work we wanted to conduct research with multi-component fuels, but such that each component had precisely defined composition and properties. Therefore, we used isooctane as the base. Research with the use of isooctane, as a fuel base, has been described in various publications, and the characteristic is, for example.

In [20] studies were conducted to evaluate the effect of mixing iso-octane with ethanol on ignition delay times (IDT). The results showed that the IDT of ethanol/isooctane mixtures decreased with the ethanol ratio and pressure, and decreased with increasing temperature. It has been shown that a large number of active OH groups generated by the added ethanol shorten the IDT of the fuel blend.

In [21] three test fuels were used in the study, namely isooctane, ethanol and n-butanol. The macroscopic spray characteristics and the droplet size distribution of the sprayed liquid were measured. The results showed that properties such as surface tension, fuel density and viscosity, saturation temperature, and latent heat of vaporization play a very important role in the penetration of the fuel plume. Isooctane showed the shortest penetration lengths while butanol showed the longest penetration length. Alcohol sprays consisted of larger diameter droplets.

In [22] the main purpose of this study is to understand the effect of fuel properties on atomization. This was quantified by the length of the liquid penetration and the spray angles. The stream shape was determined for fuel mixtures containing isooctane, hexane and ethanol. The results showed that the addition of ethanol or hexane to isooctane can promote vigorous boiling. The ethanol blend sprays showed sharper boiling compared to the hexane blend sprays. Shorter liquid penetration and better liquid-ethanol dispersion were observed. Compared to the isooctane spray, the droplet size decreased steadily with increasing hexane content. Sprays with ethanol mixtures showed a different trend [22].

In [23] were investigated the size and velocity of the liquid droplets upon impact against the wall. The spay was fed with methanol, ethanol, isooctane, toluene reference fuels (TRF) and gasoline. The results show that in the case of free atomization of methanol, ethanol and TRF, the droplet velocity is lower and the droplet size is larger compared to gasoline fuel. Falling droplets are larger and reflected droplets are smaller compared to free spray droplets. The droplet diameters of ethanol fuel are smaller, and the crushing effect upon hitting a wall is better than that of isooctane fuel.

In [24] the authors concluded that, the petroleum-derived gasoline is the most commonly used fuel for propelling vehicles (especially passenger cars). Its substitutes are sought. Until now, single components or binary mixtures (n-heptane/isooctane) were usually used as substitutes for gasoline in investigations. In the last decade, however, there has been rapid progress in the creation and use of ternary mixtures (n-heptane/isooctane/toluene), as well as multi-component mixtures with hydrocarbons having carbon numbers of C4–C10. The concept of using oxidized components (ethanol, butanol, MTBE, etc.) accelerated research into such compositions. The conclusion is that despite the progress in research into the combustion of alternative fuels for gasoline, there are still serious gaps in knowledge on this subject.

Alcohol components such as butanol and ethanol are considered alternatives to conventional gasoline due to their lower emissions and their renewable nature [25]. This article explores the spray structures and atomization of butanol, ethanol and isooctane. The results clearly show two phases of the stream development; initial (phase 1) and main (phase 2). The developed phase cone angles for butanol and ethanol are consistently stable, while isooctane exhibits relatively large fluctuations. The highest value of the cone angle is observed for ethanol, while butanol shows the lowest. Higher injection pressure leads to a smaller cone angle for any fuel. In phase 2, All three components exhibit consistently smaller droplet sizes in phase 2 compared to phase 1. The higher injection pressure helps isooctane to reduce the droplet size while allowing butanol and ethanol to produce a more uniform stream.

An empirical model of ignition retardation for fuel mixtures of n-heptane, toluene, ethanol and isooctane was developed in [26]. This model has been successfully validated based on the published experimental data on ignition retar-

dation, two-component, three-component and quaternary fuel blends with the above-mentioned components.

2. Research methodology

The main aim of the research, for this article topics, was to clarify whether the addition of bio components must be accompanied by an increase in fuel consumption and whether adding such additives makes sense due to the greenhouse effect.

The article presents research on the use of three-component fuels. The isooctane was mixed with the two alcohols, light (ethanol) and heavy (n-butanol). All three components have a strictly defined chemical composition and properties. Their mixture does not contain any additives improving the fuel. This is a rare situation in research. Typically, tests are performed using a hydrocarbon fuel as the base. This base usually cannot be strictly defined chemically. This makes it much more difficult to evaluate the results obtained.

The main properties of the ingredients used in the tested here fuel mixtures can be found on the websites.

The composition of the mixtures was made in accordance with the mathematical design of the experiment. The variables in the study are the shares of mixture components, which add up to 100%. Experimental design such as Simplex-Lattice and Simplex-Centroid were used.

Assessed was the impact of :

- x_1 – isooctane (EC: 208-759-1) concentration
- x_2 – ethanol (EC: 200-578-6) concentration
- x_3 – butanol (EC: 200-751-6) concentration

as independent variables of mixture components.

The engine was tested on the standard test bench (equipment with standard devices for dynamic fuel consumption and emission measurement.

For each blends, the universal characteristics of the engine were determined (torque and power as function of engine speed in rpm).

On basis of this data was next the minimum of brake specific fuel consumption ($BSFC_{min}$) for each blends calculated.

It is unexpected that the $BSFC_{min}$ position for each blend, in relation to the torque, changes slightly, while in relation to rpm it changes within quite wide limits. There will be a further discussion on the reason for such phenomena. If the minimum of BSFC for each blend is known, then it will be possible to find which blend provides the lowest BSFC. This question can be answered with relevant use of a mathematical model. Such model be found (as result of owner investigations), and here is presented as:

$$BSFC_{min} = 235.75\, x_1 + 334.5\, x_2 + 291\, x_3 + 130\, x_2 x_3 \quad (1)$$

$$x_1 + x_2 + x_3 = 1 \quad (2)$$

For this model the correlation coefficient equals to $R^2 = 0.9678$.

By searching for minimum of the function (1) can be found

$$x_1 = 1,\ x_2 = 0,\ x_3 = 0 \quad (3)$$

From formula (1) it shows that the lowest specific fuel consumption is achieved by supplying the engine with isooctane. The addition of any alcohol or simultaneously of both alcohols to this fuel, leads to an increase in BSFC.

3. Tests results and discussion

The presented data (based on the data from the works [27, 28]) were somewhat surprising. The addition of low energy components was expected to increase the specific fuel consumption. These expectations were confirmed. However, it was not expected that the increase would be as radical as, for example, in the case of the 3V mixture, when the increase in $BSFC_{min}$ by almost 37% was recorded. This result is different confirmed by the literature data. For example in [29] The experiment was conducted in a spark ignition engine to investigate the effects of gasoline components on fuel consumption, combustion and emissions. Isooctane was chosen as the base fuel. Short-chain, medium-chain and long-chain alkanes, ethers and aromas were appropriately blended with isooctane. The results show that the aromas contribute to fuel economy. 20% toluene (C_7H_8) mixed with isooctane shows a relatively lower BSFC. Short chain alkanes (C_nH_{2n+2}) show great potential for improving fuel economy, e.g. a blend of 20% n-pentane mixed with isooctane. In contrast, 20% methyl tert-butyl ether ($C_5H_{12}O$) mixed with isooctane shows a higher BSFC value. Therefore blending with hydrocarbons shows lower BSFC and with oxygen content components lead to higher BSFC.

In [30] are described a comparative analysis of the combustion process, emissions and performance of the PFI SI engine fueled with mixtures of methanol, ethanol and butanol with gasoline. Gasoline and butanol blends showed lower BSFC for higher LHV.

The effect of blending of gasoline with butanol isomers on the combustion and emission characteristics of the PFI SI engine was investigated and described also in [31]. The mixtures accounted for 70% of the volume gasoline and 30% vol. butanol isomers (N30, S30, I30 and T30). Compared to gasoline, all butanol isomeric mixtures have higher cylinder pressure. and the T30 has a higher specific fuel consumption (BSFC).

Acetone-butanol-ethanol (ABE) is an intermediate in the fermentation process for the production of bio-butanol [32]. This product is considered to be a promising alternative fuel. Pure gasoline and ABE blends have been prepared, ranging from 0% to 80% vol. ABE. ABE blending showed an increase in (BSFC); while measurements of exhaust gas temperature and nitrogen oxide emissions show that ABE burns at a lower peak temperature (which is less important due to the widespread use of three-way catalysts in SI engines.

One such alternative fuel may be gasoline-alcohol blends. The work [33] analyzes the operation of the S.I. with variable compression ratio. The mixtures tested in this study were butanol and ethanol in proportions of 10, 20, 30 and 40 percent in gasoline. The thermal efficiency of the brake and the specific fuel consumption (BSFC) were compared for the composed mixtures and for different compression ratios and loads. It was found that the Brake Thermal Efficiency was observed to increase and the BSFC to decrease. The results show that the engine runs smoothly up to 40 percent of the component content, and at this content, its maximum efficiency was found.

It is relatively difficult to draw clear conclusions from this short presentation of the results. Undoubtedly, any mixture of combustible components, if only they can be made into a liquid that can be burned in the engine, changes all combustion parameters, emissions and performance. The only question is whether there is any common denominator of these activities and whether conclusions can be drawn from such studies that will be a guide to the development of fuels useful for achieving the intended goals, e.g. pro-ecological. At what cost (eg increase or decrease of fuel consumption) this will be achieved. This paper is an attempt to answer the presented problems.

Even more interesting values were obtained by analyzing the unit energy consumption in each gram of fuel.

Because the tested fuels consisted of chemicals with strictly defined properties, it was possible to determine calorific value for each blend. Since $BSFC_{min}$ values are known, it was still possible to determine the values of the minimum of specific energy consumption – $BSEC_{min}$. These values are given respectively. This also gives the percentage deviation $BSEC_{min}$ at engine running with each tested fuel in relation to isooctane supplying.

Data on $BSFC_{min}$ and $BSEC_{min}$ are additionally shown in Fig. 3.

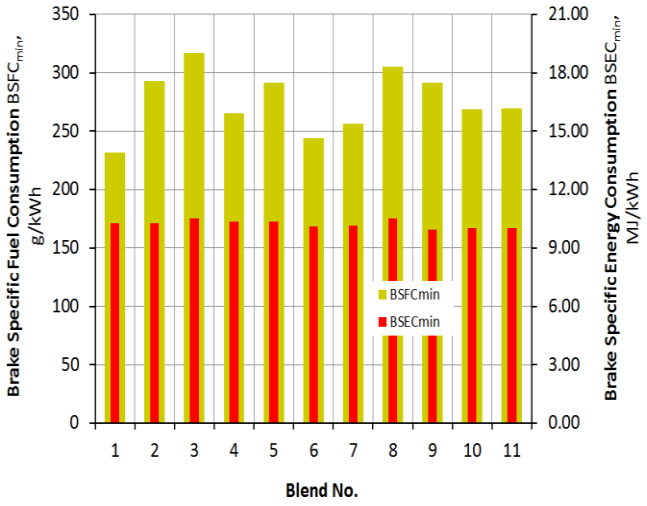

Fig. 3. $BSFC_{min}$ (higher bars – in yellow) and $BSEC_{min}$ (lower bars – red) vs. mixtures

The presented data shows that regardless of the fuel composition, the amount of energy consumed by the engine is quasi constant. It is obvious that with each $BSFC_{min}$ the engine had almost identical torque (Fig. 6). This torque was achieved at various engine speeds. Burning any type of fuel is a chemical reaction. If there are many reactants, each burns at a different rate – which in the case of an internal combustion engine means practically different speeds. Hence the deviations of this speed with BSFC minima from the data on the deviation of BSEC minimum when feeding the engine with tested fuels in relation to its supply with isooctane, it shows that these deviations (D BSEC) – do not exceed a few percent, which can be considered as being within the measurement error (up to 5%). If the composition of blends and the corresponding $BSFC_{min}$ value are taken into account, the resulting data can be represented as shown in Fig. 4.

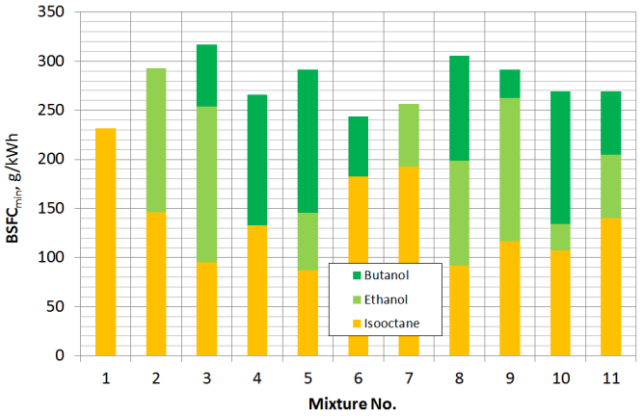

Fig. 4. $BSFC_{min}$ by each blends

One of the main goal of this study was showing the influence of bio-components contained in engine fuel, on the possibility of the greenhouse effect reduction. All the mixtures, used in the tests, contained carbon and hydrogen, and moreover those with alcohol(s) content also oxygen. In CO_2 emissions, only the carbon content is important, independent of its sources, but for greenhouse effect lowering, the source of carbon in CO_2 (renewable or non-renewable), is primary important.

Assuming that the alcohols come from renewable sources and the isooctane comes from crude oil, that is, from non-renewable sources, the use of alcohol additives should reduce the greenhouse effect (with CO_2 as the main influencing factor). Since, as already mentioned, chemically pure components with specific properties were used for the tests, the mass of carbon in each mixture can be calculated. Such calculations were made and the results are shown in Fig. 5.

If one compares BSEC (Fig. 4) with the content of carbon and hydrogen plus oxygen in fuels (Fig. 6), it can be seen that there is a convergence between BSEC and C_{TOTAL} and at the same time there is no relationship between BSEC and $H_2 + O_2$.

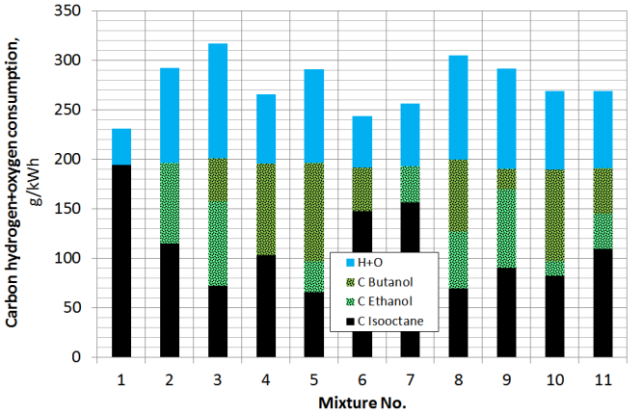

Fig. 5. $BSFC_{min}$ with carbon contents and it's overcoming depends of blends composition

After simple calculations, the relationship is obtained $BSEC_{min} = f(C_{TOTAL})$ as

$$BSEC_{min} = 0.50317 + 0.04993\ C_{TOTAL} \quad (4)$$

with the correlation coefficient $R^2 = 0.96313$. While $BSEC_{min} = f(H + O)$ is given by the equation

$$BSEC_{min} = 9.99160 + 0.00294\ (H + O) \quad (5)$$

with the correlation coefficient $R^2 = 0.13505$ so there is no correlation.

Therefore, the above remark is preliminary confirmed.

It is noteworthy that independent of the origin of carbon in the fuel, its total mass, in individual blends, does not differ significantly. However, the content of carbon from non-renewable and renewable resources is clearly different. These proportions on a mass basis, taking into account $BSFC_{min}$ are important.

These masses obviously refer to BSFC i.e. they are expressed in g/kWh. It was assumed (by every j-th blend; j = = 1 to 11)

$$C_{TOTAL(j)} = C_{Isooctane(j)} + C_{Ethanol(j)} + C_{Butanol(j)} \quad (7)$$

It is already known (on the basis of the research results presented here) that with the increase in the share of components from renewable sources (alcohols), the BSFC also increases, but the share of bio-carbon also increases – which should generally relieve the environment.

The question is whether there are any regularities in the discussed changes. A preliminary analysis of this problem can be made on the basis of the research data collected here.

Using the obtained data in, the change in $BSFC_{min}$ can be determined if carbon from non-renewable sources is replaced with "bio carbon". If

$$C_{BIO}(j) = [C_{Ethanol}(j) + C_{Butanol}(j)]/C_{TOTAL}(j) \quad (8)$$

it can be concluded that the minus of the $C_{BIO}(j)$ is an indicator of this replacement.

The data are graphically presented in Fig. 6.

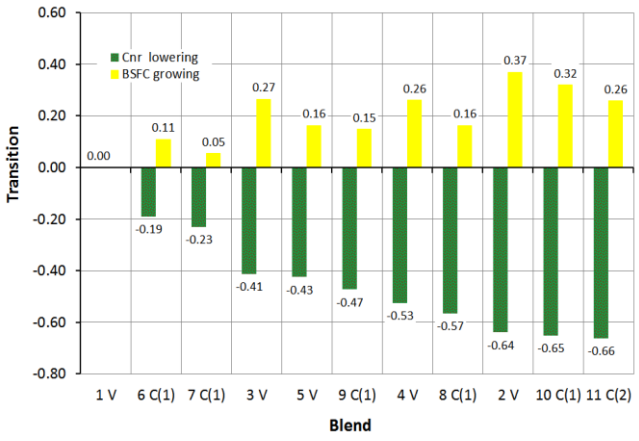

Fig. 6. Carbon from non-renewable sources content lowering and $BSFC_{min}$ grooving

Replacing non-renewable carbon with "bio carbon" leads to an increase in fuel consumption (in this case $BSFC_{min}$). This increase in fuel consumption does not depend only on the carbon resources. As it can be see, other factors are also important

It should be remembered that the engine powered by each of the blends operated normally and reached the "factory" parameters. The obtained results indicate that it is even possible to significantly reduce CO_2 emissions, however, this is always associated with an increase in fuel consumption. There are no linear relationships. Although CO_2 emissions are proportional to carbon consumption. The molar mass of carbon is 12 g and the molar mass of CO_2 is 44 g. Assuming that CO_2 generated from carbon from renewable resources will be completely utilized in the environment, replacing carbon with "bio carbon" seems reasonable, and the mass effect of CO_2 balance may be significant. Replacement by more than 60% of nonrenewable carbon can be achieved with an increase in $BSFC_{min}$ from 26% (blend 11C(2)) to 37% (blend 2V). On the other hand, replacement by "only" 19% (blend 6C(1)), causes an increase in $BSFC_{min}$ by 11% but in turn a greater reduction of 23% (blend 7C(1)) causes an increase in $BSFC_{min}$ by only 5%). A similar lack of regularity can be demonstrated with indirect limits on carbon replacement between 40% and 60%.

4. Summary

The paper shows a possible way to reduce CO_2 generated by road transport by preparing, testing and using of fuels with a higher content of bio-components. High CO_2 concentration in the air is a global problem, and because road transport has here a share of about 17%, therefore the reduction of CO_2 emissions in this economy sector is important. One of the ways, and certainly one of the fastest to implement, is the use of bio-components in fuels. Since the technology of preparing fuel blends seems relatively simple, as well the obtaining of components – from renewable sources such as municipal waste available is, it was decided to carry out research with the aim to clarity of possibility of use a of bio components in bigger amount (volumetric over 10%).

Eleven fuel mixtures were prepared, of which one was the isooctane as reference fuel, six mixtures were two-component and four were three-component.

By testing the spark ignition engine, the minimum specific fuel consumption ($BSFC_{min}$) was determined for each blend, as well as the corresponding values of torque and engine speed.

Although the calorific values of each mixture are different, the location of $BSFC_{min}$ relative to the torque is almost identical, but differ in the engine speed (rpm).

Regardless of the $BSFC_{min}$ location on the operating characteristics, the engine consumes a similar amount of energy, which prompted the authors to introduce a specific energy consumption indicator – $BSEC_{min}$.

Also is shown that the energy "consumption" depends mainly of carbon content in fuel. Other ingredients such hydrogen are from second importance. The explanation of this phenomenon requires further research. However, it can be hypothesized that the energy needed to break down (analyze) the fuel molecules is covered from the synthesis (oxidation) of hydrogen to water, so that the net energy comes from the oxidation of carbon.

Replacing carbon in fuel with "bio carbon" may, as a consequence, lead to the balancing of CO_2 in the environment, but

it leads to an increase in specific fuel consumption. However, these relationships are not of a regular linear nature.

The general conclusion from the research carried out is that the introduction of the so-called biofuels can contribute not to the reduction of CO_2 emissions, but to its faster balancing in the environment. All of this can be achieved but at the cost of increased fuel consumption. This increase in fuel consumption would probably not occur if the "bio" components in the fuel were synthetic hydrocarbons obtained from biomass. However, proving this requires more extensive research, including LCA, because obtaining synthetic hydrocarbons requires additional energy (and the question arrivers what kind of resources will this energy come from).

5. Recommendation

Transport is one of the most energy-consuming sectors of the economy. Its role is constantly growing. Therefore, it is important where the energy used in transport comes from and how it is used – both now and in the future. It is particularly important in terms of ensuring the possibility of storing energy on board vehicles, e.g. in the form of liquid fuels. Here, in turn, it is important to start the circulation of individual elements that make up fuels in nature and to close the one-way directions for example, flow of carbon from the lithosphere to the atmosphere, which consequently must result in an increase in its concentration (e.g. in CO_2) in the latter.

The simplest solution to the problem seemed to be the use of biofuels containing carbon, hydrogen and oxygen. Especially that there is an opinion that oxygen (usually one atom in a biofuel molecule for several carbon atoms and often at least twice as many hydrogen atoms) may play any role here.

In fact, different conclusions can be drawn from the research presented here. In the process of burning, a molecule of a biofuel must first be analyzed (to atoms), which then are synthesized into new compounds (mainly CO_2 and H_2O).

The more complicated the fuels are, the more energy is needed to analyze them. This energy is further recovered during the synthesis, but the net yield depends directly only on the carbon content of the fuel. On the other hand, the more complicated the fuel composition, the more its consumption (and therefore also the price of transport work) increases.

However, it is also worth taking into account that the results presented here were achieved under idealized conditions. These conditions are different from everyday life [34, 35]. Of course, global trends in the development of drive systems must be taken into account, and research must be carried out in the light of regulations on emissions, fuels, lubricants and test methods [36]. Hence, further work in the presented direction is necessary.

Nomenclature

CO_2	carbon dioxide
LCA	life cycles assessment
UE	European Union
MSW	municipal solid waste
IDT	ignition delay times
TRF	toluene reference fuels
BSFC	brake specific fuel consumption
LHV	lower heating value
ABE	acetone-butanol-ethanol
PFI SI	port fuel injected spark ignition

Bibliography

[1] U.S. Energy Information Administration, Annual Energy Outlook 2019 case descriptions. Outlook. 2019.

[2] Thring RH. Alternative fuels for spark-ignition engines. SAE Technical Paper 831685. 1983. https://doi.org/10.4271/831685

[3] Tiseo I. Projection of waste generation worldwide in 2016, 2030, and 2050, by region. Statista 2020. https://www.statista.com/statistics/233613/waste-generation-worldwide-by-region/

[4] Farmanbordar S, Karimi K, Amiri H. Municipal solid waste as a suitable substrate for butanol production as an advanced biofuel. Energ Convers Manage. 2018;(157):396-408. https://doi.org/10.1016/j.enconman.2017.12.020

[5] Meng F, Ibbett R, De Vrije T, Metcalf P, Tucker G, McKenzie J. Process simulation and life cycle assessment of converting autoclaved municipal solid waste into butanol and ethanol as transport fuels. Waste Manage. 2019;(89): 177-189. https://doi.org/10.1016/j.wasman.2019.04.003

[6] Veses A, Sanahuja-Parejo O, Callén MS, Murill R, Garcia T. A combined two-stage process of pyrolysis and catalytic cracking of municipal solid waste for the production of syngas and solid refuse-derived fuels. Waste Manage. 2020; (101):171-179. https://doi.org/10.1016/j.wasman.2019.10.009

[7] Chan WP, Veksha A, Lei J, Oh WD, Dou X, Giannis A et al. A hot syngas purification system integrated with downdraft gasification of municipal solid waste. Appl Energ. 2019;(237):227-240. https://doi.org/10.1016/j.apenergy.2019.01.031

[8] Martínez I, Grasa G, Callén MS, Lopez JM, Murillo R. Optimised production of tailored syngas from municipal solid waste (MSW) by sorption-enhanced gasification. Chem Eng J. 2020;(401):126067. https://doi.org/10.1016/j.cej.2020.126067

[9] Festel GW. Biofuels – economic aspects. Chem Eng Technol. 2008;31(5):715-720. https://doi.org/10.1002/ceat.200700335

[10] Jaya D, Setiyaningtyas R, Prasetyo S. Bioetanol production from green algae spirogyra sp. Eksergi. 2018;15(1):16-19. https://doi.org/10.31315/e.v15i1.2290

[11] Chiavola D, Recco E. Emission performance of a diesel engine fueled with petrol diesel, green diesel, and waste cooking oil blends. J Combust. 2018;ID 4819175. https://doi.org/10.1155/2018/4819175

[12] Singh D, Sharma D, Soni SL, Sharma S, Sharma PK, Jhalani A. A review on feedstocks, production processes, and yield for different generations of biodiesel. Fuel. 2020;(262): 116553. https://doi.org/10.1016/j.fuel.2019.116553

[13] Othman MF, Adam A, Najafi G, Mamat R. Green fuel as alternative fuel for diesel engine: a review. Renew Sustain Energ Rev. 2017;(80):694-709. https://doi.org/10.1016/j.rser.2017.05.140

[14] Abed KA, El Morsi AK, Sayed MM, El Shaib AA, Gad SS. Effect of waste cooking-oil biodiesel on performance and exhaust emissions of a diesel engine. Egypt J Petrol. 2018; 27(4):985-989. https://doi.org/10.1016/j.ejpe.2018.02.008
[15] Veipa A, Kirsanovs V, Barisa A. Techno-economic analysis of biofuel production plants producing biofuels using fisher tropsch synthesis. Environ Clim Technol. 2020;24(2):373-387. https://doi.org/10.2478/rtuect-2020-0080
[16] Gotovsky M, Gotovsky A, Lychakov V, Mikhaylov V, Sukhorukov Y, Sukhorukova E. Formate Fischer-Tropsch process for producing traditional energy carriers with zero carbon balance. WIT Trans Ecol Envir. 2019;(237):155-162. https://doi.org/10.2495/ESUS190141
[17] Nikparsa P, Rauch R, Mirzaei AA. A hybrid of winddiesel technology with biomass-based Fischer–Tropsch synthesis. Monatshefte für Chemie. 2017;(148):1877-1886. https://doi.org/10.1007/s00706-017-1998-5
[18] Puricelli S. The effects of innovative blends of petrol with renewable fuels on the exhaust emissions of a GDI Euro 6d-TEMP car. Fuel. 2021;(294):120483. https://doi.org/10.1016/j.fuel.2021.120483
[19] Srinivasan CA, Saravanan CG. Emission reduction on ethanol-gasoline blend using fuel additives for an SI engine. Energ Source Part A. 2013;35(12):1093-1101. https://doi.org/10.1080/15567036.2011.584114
[20] Qin M, He B, Chen R, Fan X, Wang J, Wang X. Study on the reaction kinetics of ignition characteristics of ethanol/isooctane mixtures at elevated temperatures. J Xi'an Jiaotong Univers. 2019;53(7):38-53. https://doi.org/10.7652/xjtuxb201907006
[21] Kale R, Banerjee R. Experimental investigation on GDI spray behavior of isooctane and alcohols at elevated pressure and temperature conditions. Fuel. 2019;(236):1-12. https://doi.org/10.1016/j.fuel.2018.08.153
[22] Yan J, Gao S, Liu W, Chen T, Lee TH, Lee C-F. Experimental study of flash boiling spray with isooctane, hexane, ethanol and their binary mixtures. Fuel. 2021;(292): 120415. https://doi.org/10.1016/j.fuel.2021.120415
[23] Pei Y, Qin J, Li X, Zhang D, Wang K, Liu Y. Experimental investigation on free and impingement spray fueled with methanol, ethanol, isooctane, TRF and gasoline. Fuel. 2017; (208):174-183. https://doi.org/10.1016/j.fuel.2017.07.011
[24] Sarathy SM, Farooq A, Kalghatgi GT. Recent progress in gasoline surrogate fuels. Prog Energ Combust. 2018;(65): 67-108. https://doi.org/10.1016/j.pecs.2017.09.004
[25] Zhang J, Yao S, Patel H, Fang T. An experimental study on gasoline direct-injection spray and atomization characteristics of alcohol fuels and isooctane. Atomization Sprays. 2011;21(5):363-374. https://doi.org/10.1615/AtomizSpr.2011003624
[26] Ma J, Kwak KH, Lee B, Jung D. An empirical modeling approach for the ignition delay of fuel blends based on the molar fractions of fuel components. Fuel. 2016;(164):305-313. https://doi.org/10.1016/j.fuel.2015.09.069
[27] Hussein A. Experimental investigation on performance of a spark ignition engine runs with alcoholic blend-gasoline. Journal of KONES Powertrain and Transport. 2015;22(3): 249-256. https://doi.org/10.5604/12314005.1181680
[28] Hussein A. The effect of the heavy alcohol additive to base fuel of spark ignition engine. Doctoral Thesis. Wroclaw University of Science and Technology, Wroclaw 2017. https://doi.org/10.13140/RG.2.2.20883.84003
[29] Han Y, Hu S, Tan M, Xu Y, Tian J, Li R et al. Experimental study of the effect of gasoline components on fuel economy, combustion and emissions in GDI engine. Fuel. 2018;(215): 371-380. https://doi.org/10.1016/j.fuel.2017.12.033
[30] Li Y, Gong J, Deng Y, Yuan W, Fu J, Zhang B. Experimental comparative study on combustion, performance and emissions characteristics of methanol, ethanol and butanol in a spark ignition engine. Appl Thermal Eng. 2017;(115):53-63. https://doi.org/10.1016/j.applthermaleng.2016.12.037
[31] Li Y, Ning Z, Yan J, Lee TH, Lee C. Experimental investigation on combustion and unregulated emission characteristics of butanol-isomer/gasoline blends. J Cent South Univ. 2019;(26):2244-2258. https://doi.org/10.1007/s11771-019-4170-z
[32] Nithyanan K, Lee CF, Wu H, Zhang J. Performance and emissions of acetone-butanol-ethanol (ABE) and gasoline blends in a port fuel injected spark ignition engine. ASME 2014 Internal Combustion Engine Division Fall Technical Conference. 2014, ICEF2014-5644. https://doi.org/10.1115/icef2014-5644
[33] Basu D, Phulli S, Kotebavi V. Performance analysis of a VCR SI engine using petrol alcohol blends. 2014 Power and Energy Systems: Towards Sustainable Energy. 2014. https://doi.org/10.1109/PESTSE.2014.6805264
[34] Andrych-Zalewska M, Chłopek Z, Merkisz J, Pielecha J. Evaluation of the test drive cycle conditions impact on exhaust emissions from an internal combustion engine. Combustion Engines. 2018;175(4):3-9. https://doi.org/10.19206/CE-2018-401
[35] Andrych-Zalewska M, Chłopek Z, Merkisz J, Pielecha J. Exhaust emission from a vehicle engine operating in dynamic states and conditions corresponding to real driving. Combustion Engines. 2019;178(3):99-105. https://doi.org/10.19206/CE-2019-317
[36] Bielaczyc P, Woodbum J, Ameya J. World-wide trends in powertrain system development in light of emissions legislation, fuels, lubricants, and test methods. Combustion Engines. 2021;184(1):57-71. https://doi.org/10.19206/CE-134785

Monika Andrych-Zalewska, DEng. – Faculty of Mechanical Engineering, Wroclaw University of Science and Technology.
e-mail: *monika.andrych@pwr.edu.pl*

Prof. Lech Sitnik, DSc., DEng. – Faculty of Mechanical Engineering, Wroclaw University of Science and Technology.
e-mail: *lech.sitnik@pwr.edu.pl*

Prof. Zbigniew Sroka, DSc., DEng. – Faculty of Mechanical Engineering, Wroclaw University of Science and Technology.
e-mail: *zbigniew.sroka@pwr.edu.pl*

Veselin Mihaylov, DSc., DEng. – Department of Technical Engineering, Technical University of Varna.
e-mail: *v_mihaylov@tu-varna.bg*

Article citation info:
Adamczyk P, Zięty A, Grygier D. Evaluation of materials used for coatings of electrical connectors used in the electrical harness of passengers cars. Combustion Engines. 2023;192(1):43-49. https://doi.org/10.19206/CE-150505

Paulina ADAMCZYK
Anna ZIĘTY
Dominika GRYGIER

Combustion Engines
Polish Scientific Society of Combustion Engines

Evaluation of materials used for coatings of electrical connectors used in the electrical harness of passengers cars

ARTICLE INFO

Received: 3 January 2022
Revised: 25 May 2022
Accepted: 29 May 2022
Available online: 7 July 2022

Automotive electrical connectors are the essential components of a wiring harness. They are typically made of copper, which has excellent electrical conductivity. Due to the limited corrosion resistance of pure copper, connectors are often coated with other metals. In this paper, the qualities of coatings made of gold and tin are investigated and compared. The samples were examined by a metallographic microscope and scanning electron microscope (SEM). The examination revealed uneven thickness, delamination of the coatings, and issues with the preparation of the core material for coating. Numerous burrs and irregularities were observed. Selected samples were examined in salt solution to test their corrosion resistance. Even though gold is a noble metal and its electrochemical potential is higher, the tin coating was more resistant to corrosion.

Key words: *automotive electrical connectors, metal coatings, anodic protection, cathodic protection, corrosion*

1. Introduction

Almost every part of a car is supported by electronics, from very obvious examples like radio to brake assist. To make electronics work, the automotive wiring harness is essential. Its main components are circuits, housing, connectors, wrapping material and additional components [1]. A connector is a piece which enables an easy way to connect wires or whole circuits. It provides good electrical conductivity and a stable connection between components [2]. With the development of technology, the number of connectors is increasing, which can range from several hundred to several thousand in one vehicle [3]. As part of the wiring harness, connectors must be characterized by very good electrical conductivity. The conditions in which car connectors work are related not only to weather conditions and season, but also to temperature changes and vibrations caused by the engine operation [4]. Vibration contributes to faster degradation of components and can cause failure [5]. According to Abdi and Benjemâa, the operating temperature of connectors ranges from –40°C to 80–120°C, depending on the location of the connector. The vibration frequency ranges from 10 to 2000 Hz [6]. The operating environmental conditions of the connectors are conducive to the occurrence of corrosion, which promotes faster wear of the components [7]. For this reason, the materials from which the connectors are made should be resistant to high humidity, high and low temperatures and the presence of acid oxides in the air, including nitrogen oxides and sulfur oxides [3].

Automotive connectors are typically made of copper, due to the excellent electrical conductivity of this metal. There is one primary disadvantage of choosing copper as a connector material. Its resistance to harsh environment is not particularly good in comparison to other conducting metals like silver or gold [2]. Noble metals are unfortunately much more expensive than copper, due to limited resources and increasing demand for them [8], and are not used as a material for manufacturing automotive wiring. To preserve electrical properties and achieve anticorrosive abilities, connectors are coated with different metals. Gold, silver and tin are the most commonly used [2].

Noble metals, such as gold and silver, can be used to produce cathodic coatings, which provide anodic protection. These metals have higher electrochemical potential compared to copper and act as a cathode, which means that they are resistant to environmental conditions. They create a barrier between copper and the environment, providing protection against corrosion. Apart from the high price of noble metals, there is one disadvantage of such coatings. The coating must cover a core material evenly to protect it. Every discontinuity can result in a very deep corrosion pit, because copper, as a metal with lower electrochemical potential than gold or silver, will be exposed to environmental conditions. It is important to notice, that copper without any protection would corrode at a slower rate than copper coated with damaged cathodic coating [9].

Tin is a metal with lower electrochemical potential than copper, hence it is used as an anodic coating, which provides cathodic protection. Sometimes such protection is called sacrificial protection, because the coating acts as an anode, which corrodes instead of the core material. This method provides protection of core material even when the coating is not continuous [9, 10]. Another positive aspect of anodic coatings is the lower price compared to coatings made of noble metals.

In this paper, we examine and compare the properties of anodic and cathodic coatings on automotive connectors.

2. Methodology

2.1. Microscopy

Five different samples of automotive connectors were examined. According to the manufacturer, three of them were coated with tin and the other two had coatings made of gold. Energy-Dispersive X-ray Spectroscopy (EDX) was performed to verify the manufacturer's claims and detect possible injections of different metals. Two measurement

points were chosen for each sample, one for coating material and one for core material. Connectors were examined by microscopy (Nikon Eclipse MA200) and Scanning Electron Microscopy (FEI Phenom G2 Pro) to determine coatings quality and thickness.

2.2. Roughness and corrosion tests

Two samples, one coated with tin and one coated with gold, were selected for the topography examination. The roughness of each connector was measured according to PN-87/M-04256/02. The topography picture was prepared via SEM. The corrosion resistance of these two samples was examined. Two tests, open circuit potential and potentiodynamic polarization, were performed on an automated measurements site (Fig. 1), which consisted of a vessel, a potentiostat ATLAS 0531 – ELECTROCHEMICAL UNIT&IMPEDANCE ANALYSER, computer controller and three electrodes: calomel electrode as a reference electrode, platinum electrode as a counter electrode and connector as a working electrode. The open-circuit test in 3% sodium chloride solution lasted 40 minutes and took place at room temperature. This test was performed in order to find a resting potential of a system, which is necessary for the second test. During potentiodynamic polarization measurement, potentiodynamic curves were registered and a pitting susceptibility of material was evaluated.

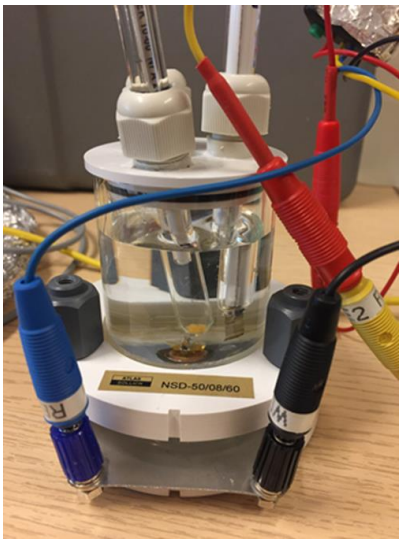

Fig. 1. The measurement site for corrosion tests

3. Results

3.1. EDX analysis

EDX analysis revealed that one of five samples did not match the manufacturer's specification and one of the gold coatings was actually made of silver (Table 1). The core material in each sample was copper, with a small amount of metal of a coating in sample number 1. EDX analysis detected copper injections in all coatings (Table 2). Coating made of gold contained the smallest amount of copper – 2.06%. Tin coatings contained more copper injections. It was especially noticeable in sample number 5, which consisted of 52.77% copper. Sample number 1 was excluded from further analysis due to inconsistency between specification and analysis results.

Table 1. Coating materials according to specification and EDX analysis

Sample	Specification	EDX results
1	Au	Ag
2	Au	Au
3	Sn	Sn
4	Sn	Sn
5	Sn	Sn

Table 2. EDX analysis results

Sample	Coating	Core
1	Ag – 84.17% Cu – 15.83%	Ag – 1.01% Cu – 98.99%
2	Au – 97.94% Cu – 2.06%	Cu – 100%
3	Sn – 73.21% Cu – 26.79%	Cu – 100%
4	Sn – 82.70% Cu – 17.30%	Cu – 100%
5	Sn – 47.23% Cu – 52.77%	Cu – 100%

3.2. Structure and thickness

Four connectors were examined by regular microscopy with magnification from 100× to 500× in order to briefly evaluate the quality of coatings. In some cases, magnification was not sufficient to notice and examine very thin coatings. SEM examination was performed for more accurate observation using magnification 10000×. The coating on sample number 2, which was the only connector coated with gold, was continuous, without any fractures, or delamination, but the thickness was uneven (Fig. 2 and Fig. 3). The gold coating covered the connector partially, only at the point of contact. The core material was prepared correctly before coating deposition. It was even, with no burrs. Connector number 3 was the only one with visible discontinuity of a coating (Fig. 4 and Fig. 5). Delamination was observed within a coating and between coating and core material. The thickness of the coating varied in different areas. Core material preparation was performed poorly, as there was noticeable roughness of the surface and numerous burrs. Sample number 4 had continuous coating (Fig. 6 and Fig. 7). The thickness of the coating was generally even. There were thinner and thicker areas, but not many. Some injections and delamination of the coating were noticed. The core material surface was not smooth, but there were no huge burrs. Coating number 5 was of poor quality (Fig. 8 and Fig. 9). Delamination between coating and core material, delamination within the coating and numerous injections were detected. The coating was continuous but its thickness was uneven. The core material surface was not prepared correctly before coating. It was uneven with visible burrs.

Coating thickness was measured with SEM. For each sample minimum and maximum thickness were measured. Depending on the material used, typical coatings on connectors range in thickness from 0.1 to 30 μm [11]. The average thickness of all coatings was calculated based on eight measurements. Values of all coatings thickness were presented in Table 3. The only gold coating was the thinnest of all samples, with an average thickness of 0.91 μm. Tin coatings were visibly thicker. Sample number 4 had the thickest coating – 6.61 μm. Significant differences between minimum and maximum thickness were noticed for each sample. According to Meyyappan et al. [12], typical gold

coating thickness on connectors ranges from 400 to 800 nm, while the coating of sample 2 exhibited an average thickness of 910 nm. The highest coating thickness was 1420 nm, while in some areas it was only 170 nm. In the publication by Monlevade et al., the thickness of the gold coating ranged from 0.8 to 1.35 μm [13]. The biggest value of maximum thickness was registered for sample number 4 – 8.57 μm. It is worth noting that Yuan et al. [14] showed an inverse relationship between tin coating thickness and connector resistance.

Table 3. Coating thickness

Sample	Material	Coating thickness		Average thickness [μm]
		Minimum [μm]	Maximum [μm]	
2	Au	0.17	1.42	0.91
3	Sn	1.60	4.34	2.71
4	Sn	4.85	8.57	6.61
5	Sn	2.57	8.19	4.98

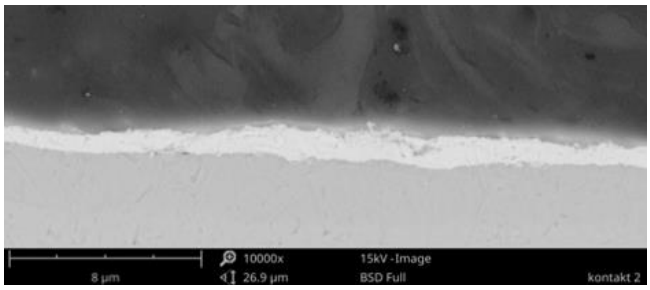

Fig. 2. Scanning microscope image of sample number 2 – a continuous, well-made coating of variable thickness, a substrate for coating application well prepared

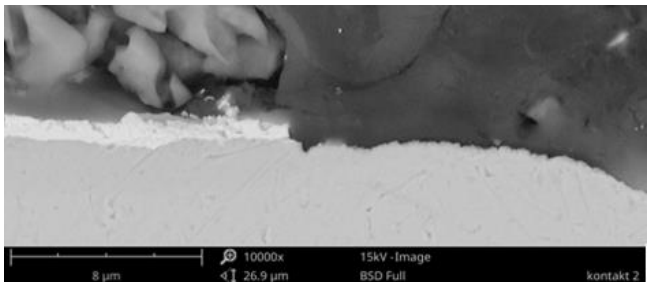

Fig. 3. Scanning microscope image of sample number 2 – the place of the beginning of coating application – visible layer break

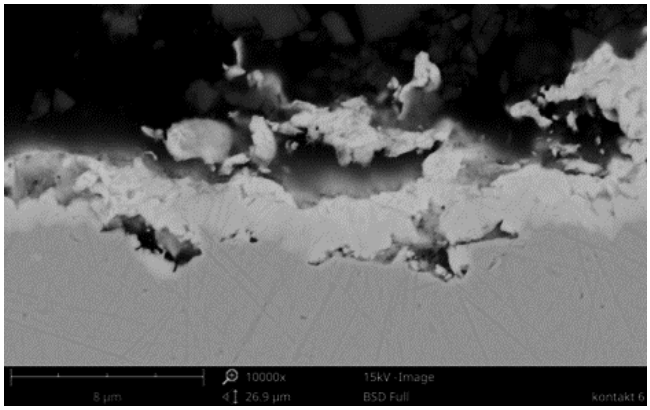

Fig. 4. Scanning microscope image of sample number 3 – a continuous layer, uneven coating thickness, visible delamination

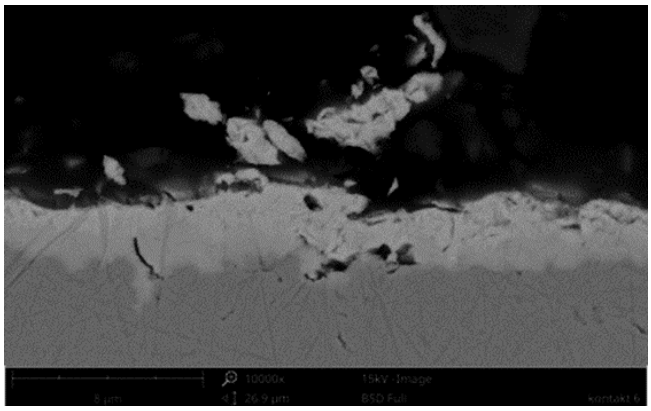

Fig. 5. Scanning microscope image of sample number 3 – differences in coating thickness with continuity, visible delamination at the border of coating and core material

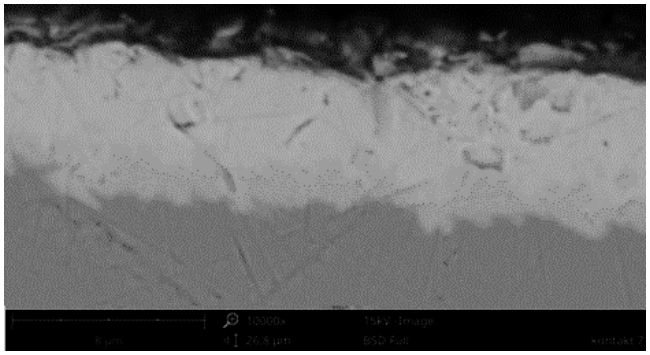

Fig. 6. Scanning microscope image of sample number 4 – a continuous layer with even coating thickness, visible impurities in the coating

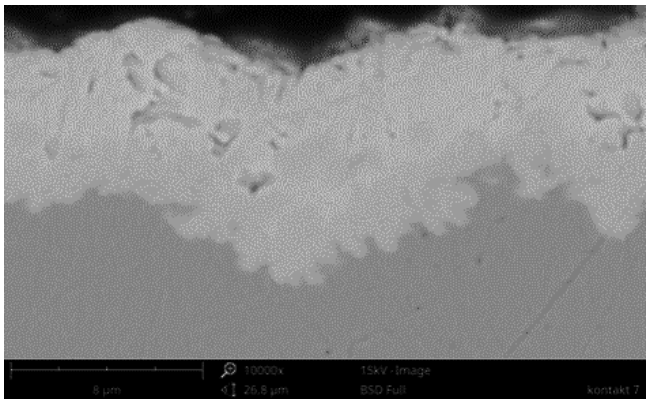

Fig. 7. Scanning microscope image of sample number 4 – a continuous layer with uneven coating thickness. Coating material with numerous irregularities

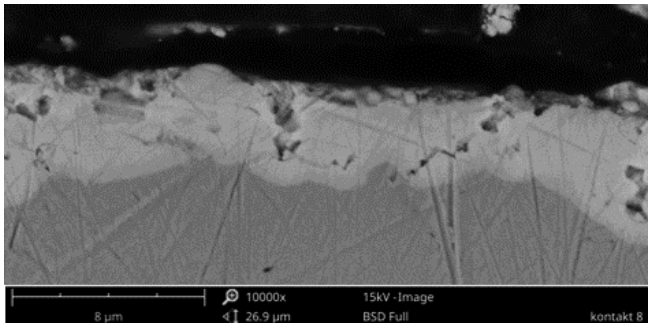

Fig. 8. Scanning microscope image of sample number 5 – a continuous layer, with varied coating thickness, numerous impurities

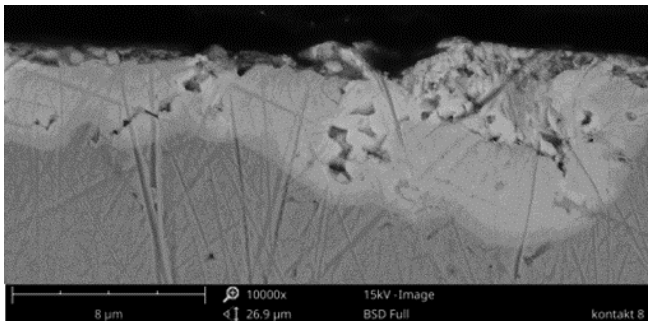

Fig. 9. Scanning microscope image of sample number 5 – a continuous layer, with uneven coating thickness, and numerous impurities

3.3. Roughness

The results of the roughness measurements of the selected specimens, number 2 and 3, were collected and presented in Table 4. It also includes the average roughness values of the Ra and Rz parameters calculated from the two measurements taken for each specimen.

Under each figure showing the measurement of roughness profile is a cross-section of the profile of roughness height in the given measurement lines for the sample indicated in the description.

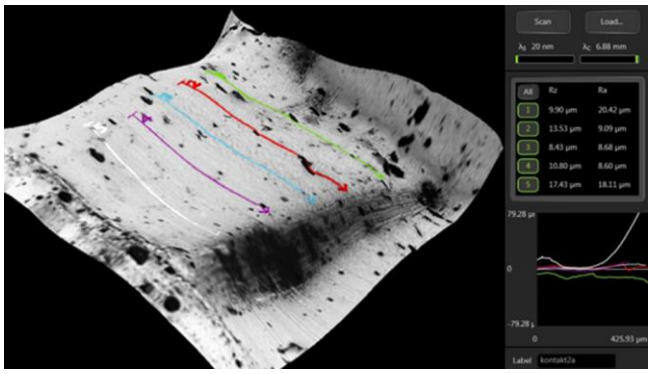

Fig. 10. Sample number 2, measurement 1 – 3D view of the test surface

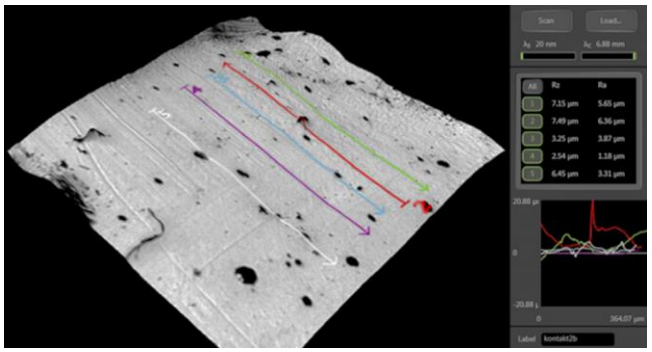

Fig. 11. Sample number 2, measurement 2 – 3D view of the test surface

Observations of the material of sample number 2 indicate a high presence of surface contaminants of various sizes but regular round shapes. Longitudinal cracks can be observed. In places of inclusions on the roughness profile, large differences in height appear (Fig. 11). In places without inclusions, the roughness profile shows very small differences in height. In the results for measurement 1 – line 5 (white) has a clearly increasing shape (Fig. 10). After analyzing this shape, this result is not considered a roughness measurement because the differences in profile height are too large – 79.3 µm – to qualify this shape irregularity as roughness. It is also not taken into account when calculating the average roughness value for the sample, which is for parameter Rz = 8.03 µm and for parameter Ra = 7.89 µm. The Ra value for gold coating is higher than that found in the literature, where it was 0.5715 µm and 0.3827 µm. The surface of the samples examined by Ren et al. was also less wavy and did not have large cracks and inclusions, which translates to lower roughness parameters [15].

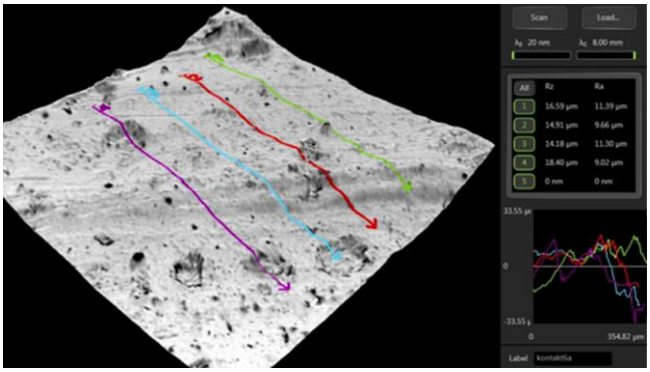

Fig. 12. Sample number 3, measurement 1 – 3D view of the test surface

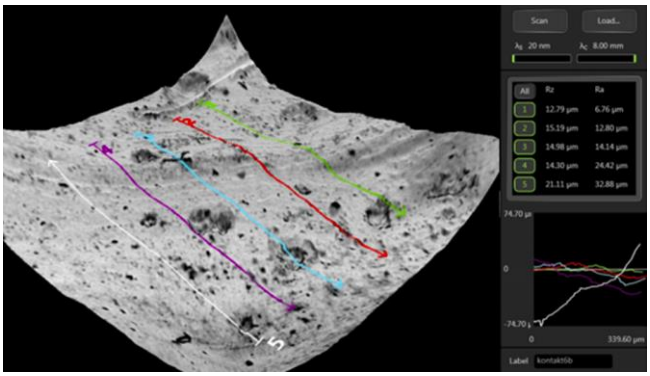

Fig. 13. Sample number 3, measurement 2 – 3D view of the test surface

The surface irregularities observed in the material of specimen number 3 are predominantly concave depressions – dark grey patches with irregular shapes visible in Fig. 12. and Fig. 13. A small number of convex, fine surface contaminations (black dots) with regular shapes and a small (several or even several times smaller) size compared to the depressions can also be observed. The sample has visible longitudinal scratches occurring in one direction. On the 3D image in places of surface roughness (convex and concave) on the roughness profile appear large differences in height. The indices of surface roughness for sample number 3 are for the parameter Rz = 13.58 µm and for the parameter Ra = 13.24 µm. Narayanan et al. examined the roughness of tin-coated connectors after 20000 fretting cycles at various temperatures. The Ra value they measured ranged from 1.71 to 2.77. This indicates that the samples they examined had lower roughness, despite being subjected to destructive testing, than sample number 3 [16].

Table 4. Surface roughness values

Sample	1st measurement – roughness values [μm]		2nd measurement – roughness values [μm]		Average roughness value [μm]	
	Rz	Ra	Rz	Ra	Rz	Ra
2	9.90	20.42	7.15	5.65	8.03	7.89
	13.53	9.09	7.49	6.36		
	8.43	8.68	3.25	3.87		
	10.80	8.60	2.54	1.18		
	~~17.43~~	~~18.11~~	6.45	3.31		
Average	10.67	11.70	5.38	4.07		
3	16.59	11.39	12.79	6.76	13.58	13.24
	14.91	9.66	15.19	12.80		
	14.18	11.30	14.98	14.14		
	18.40	9.02	14.30	24.42		
	~~0.00~~	~~0.00~~	~~21.11~~	~~32.88~~		
Average	12.82	8.27	14.32	14.53		

3.4. Corrosion tests

The corrosion resistance tests were carried out on two samples, number 2 and 3. The measurement of the stationary potential as a function of time for the open circuit of both samples showed that after 40 minutes both samples had very similar potential. The sample coated with gold, showed a potential E^0 = –421 mV, while the sample coated with tin, showed a potential E^0 = –422mV – the result is shown in Fig. 14.

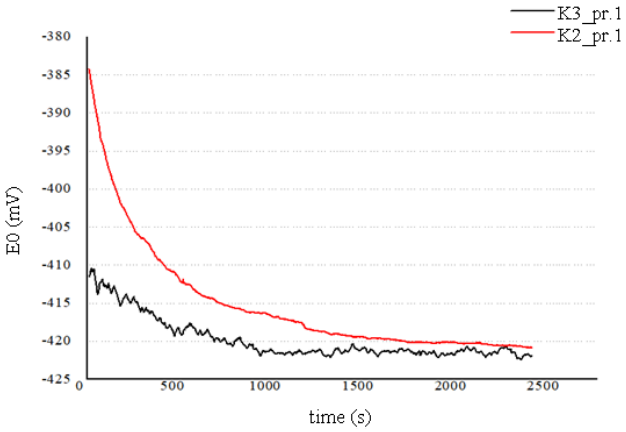

Fig. 14. Open circuit stationary potential as a function of time for samples number 2 and 3

Potentiodynamic results were obtained by performing anodic polarization and applying the Tafel method. These made it possible to obtain potentiodynamic curves, which were subsequently analyzed. On their basis the values of corrosion parameters were determined, i.e. corrosion potential (E_{cor}) and corrosion current (i_{cor}) – Table 5. The highest value of the corrosion potential was found for sample number 2 and the lowest value for sample number 3. The values of the corrosion potential translate into the results of the corrosion current. The values obtained for gold were similar to those in the literature, where E_{corr} was –359 mV and i_{corr} was $93 \cdot 10^{-6}$ A/cm^2. According to the authors, these parameters are unfavorable and imply the inability of the gold coating, made by the traditional method, to protect copper from corrosion and may even enhance it [17]. The values of polarization parameters reported by Arazna et al. differed from those obtained in this publication and were E_{corr} = –520 mV and $i_{corr} = 5.8 \cdot 10^{-6}$ A/cm^2 [18]. However, in both cases, the parameters indicated better corrosion resistance of tin than that of gold.

Table 5. Results of corrosion tests carried out on samples number 2 and 3

Sample	Coating material	E_{cor} [mV]	i_{cor} [A/cm^2]
2	Au	–572.61	$75.85 \cdot 10^{-6}$
3	Sn	–489.5	$12.65 \cdot 10^{-6}$

4. Conclusion

EDX analysis found inconsistencies in the manufacturer's specification. One connector was coated with a different metal than it should have been. The fact that sample number 1 according to the manufacturer is coated with gold, while the tests show that it is coated with silver, may lead to electrical harness damage, due to differences in electrochemical potential of these two elements. This mistake may lead to unreliable operation of receivers for which gold and not silver connector is dedicated. The cause of the mistake may be insufficient quality control at the production unit.

The chemical composition analysis of the gold coating (sample 2) revealed injections of copper. They were small, so they should not influence the maintenance of the correct connection between terminals and receivers. They can, however, have an influence on the quicker appearance of corrosion centers in the contact area than in the case of a coating with a lower level of copper contamination. With samples that are tin-plated (samples 3, 4 and 5) the copper content of the coating is higher than with precious metals (from 17 to 53%). This may be due to the greater ability of tin to react with other elements due to its lower (negative) electrochemical potential than the precious metals and copper (positive potential). This level of core element's presence in the coated layer may be a residue from chemical reactions occurring during the coating process. A break in the continuity of the tin coating is not detrimental to the beam as tin has a lower electrochemical potential than copper. It is the tin that will be chemically active so the quality of the bond will be maintained and will not be exposed to the environment and corrosion.

Observation of specimens performed by light microscope revealed very thin layers of coated metal, but did not allow for detecting coatings defects and measuring coating thickness due to insufficient magnification. SEM exposed many coating defects, such as impurities, injections, and delamination, which could not be revealed by light microscopy. It was also possible to measure coating thickness. Examination revealed the poor quality of all tin coatings. All samples had uneven coatings thickness. The coating on sample number 3 was not continuous. Many injections and impurities as well as delamination within the coating and between coating and core material were observed. The surface of the connector was not prepared correctly as there were lots of burrs and irregularities. Samples number 4 and 5 had continuous coatings, but also many injections and delamination. The gold coating was free from injections, delamination and discontinuities. The surface of the connector was prepared correctly for coating. The main issue with sample number 2 was the thickness of the coating. It was thinner than tin coatings, presumably due to the higher price of gold. It makes this coating vulnerable to mechani-

cal damage. While it is not crucial for tin coatings to be continuous, because they work as an anode and protect core material even with discontinuities, it is extremely important for a noble metal coating to cover protected material completely. Copper is a metal of lower electrochemical potential than gold, which means that if both of them are present in the same environment, copper will start to corrode. Every single discontinuity in the gold coating is a possible place for a corrosion pit.

The main irregularities concerning the coating itself are significant variations in layer thickness and delamination. Less common irregularities are pinholes which only occur in tin-coated samples. Differences in the preparation of the surface for the metal coating can also be observed. An unevenly prepared substrate significantly affects the difference in film thickness. The biggest problem in the use of connector terminals is the influence of the environment and thus the corrosion of the element, because all the above-mentioned defects and damages increase the susceptibility of the element to this phenomenon.

On the basis of the measurement of the surface roughness of the samples, it can be observed that the one coated with gold shows lower values of surface roughness for both indices (Ra and Rz) than the sample coated with tin. Sample number 2 has a greater difference in the height of the lowest and highest elevations examined on the roughness profile. The reason for this is point-like inclusions (black color in Fig. 10 and Fig. 11), which cause a peak change in the height of the roughness profile. Sample number 3 – coated with tin – shows a greater presence of pits on the surface than convexities on the surface. Sample number 2 shows a higher proportion of surface impurities in the form of inclusions, which are convex.

The surface roughness at the contact point of the connector is needed to ensure a connection at the contact point. However, large values of roughness (large peaks in the direction of lower or higher values) can have the opposite effect to that desired – they can cause surface deviation and poorer contact quality of the mating surfaces. All of the samples tested for roughness (samples 2 and 3) show significant surface irregularities at the roughness level. Inclusions or pits are present in each sample. Each sample is scratched – these are long straight scratches of varying depth. This damage is caused by the storage of the connector ends. They are stored in containers where they are exposed to each other. This causes scratches and micro-damage such as indentations. These containers are not particularly tightly sealed and are not isolated from the external environment, which gives rise to the possibility of contamination adhering to the surface. Spot contamination of the samples may also be a result of the chemical composition of the material used to coat the tips and the sterile conditions under which the coating process is carried out.

The corrosion resistance tests were conducted in a humid environment – in a 3% sodium chloride solution. This type of environment was chosen to imitate winter conditions of car operation in countries where winters with snow occur, and road salt is used on roads to prevent icing.

Research about the corrosion resistance of the samples has shown that the tin-coated tips have higher overall corrosion resistance. They have a higher corrosion potential (E_{cor}) and corrosion current (i_{cor}) than gold-plated samples. The higher the value of the corrosion potential, the higher the corrosion resistance of the metal and the lower the surface impact of the aggressive environment on the sample.

Research shows that gold-plated terminals, often chosen for responsible vehicle components, are actually a less safe choice than tin-plated connectors. In order to protect gold coated connector terminals well against corrosion, they should be very tightly manufactured to avoid discontinuities. Improving the quality of the coating can also be achieved by increasing its thickness, but this can result in a significant increase in production costs.

Bibliography

[1] Tilindis J, Kleiza V. The effect of learning factors due to low volume order fluctuations in the automotive wiring harness production. Procedia CIRP. 2014;19(C):129-134. https://doi.org/10.1016/j.procir.2014.05.019

[2] Kloch K, Kozak P, Mlyniec A. A review and perspectives on predicting the performance and durability of electrical contacts in automotive applications. Eng Fail Anal. 2021; (121):105143. https://doi.org/10.1016/j.engfailanal.2020.105143

[3] Swingler J, McBride J, Maul C. Degradation of road tested automotive connectors. IEEE Transactions on Components and Packaging Technologies. 2000;23(1):157-164. https://doi.org/10.1109/6144.833055

[4] LAM, Y., MAUL, C., MCBRIDE, J.W. Temperature, humidity and pressure measurement on automotive connectors. IEEE T Compon Pack T. 2006;29(2): 333-340. https://doi.org/10.1109/TCAPT.2006.875896

[5] Łoza Ł. The analysis of vibrations in the vehicle with naturally aspirated and turbocharged gasoline engine. Combustion Engines. 2020;181(2):19-23. https://doi.org/10.19206/CE-2020-203

[6] Abdi R, Benjemâa N. The effect of the temperature on the wear and resistance of automotive connectors subjected to vibration tests. P I Mech Eng D-J Aut. 2015;229(2):189-196. https://doi.org/10.1177/0954407014536379

[7] Osipowicz T, Lisowski M. The influence of corrosion phenomena on operational parameters of modern fuel injectors CI-engines. Combustion Engines. 2017;171(4):17-23. https://doi.org/10.19206/CE-2017-403

[8] Merkisz-Guranowska A. Product recycling of automotive parts – trends and issues. Combustion Engines. 2017; 171(4):24-28. https://doi.org/10.19206/CE-2017-404

[9] Blicharski M. Inżynieria powierzchni. Wydawnictwo Naukowe PWN. Warszawa 2016.

[10] Bahadori A. Principle of electrochemical corrosion and cathodic protection. Cathodic corrosion protection systems. Gulf Professional Publishing. 2014:1-34. https://doi.org/10.1016/B978-0-12-800274-2.00001-6

[11] Braunovic M, Konchits V, Myshkin N. Electrical Contacts: Fundamentals, Applications and Technology. CRC Press. Boca Raton 2006.

[12] Meyyappan K, Murtagian G, Kurella A, Pathangey B, McAllister A, Parupalii S. Corrosion studies on gold-plated electrical contacts. IEEE T Device Mat Re. 2014;14(3):869-877. https://doi.org/10.1109/TDMR.2014.2333758

[13] Monlevade E, Cardoso I, Maciel E, Alonso-Falleiros N. Galvanic corrosion of electroless nickel/immersion gold plated non-permanent electric contacts used in electronic devices–direct evidence of triggering mechanism. Eng Fail Anal. 2019; (96):562-569. https://doi.org/10.1016/J.ENGFAILANAL.2018.12.001

[14] Yuan H, Song J, Schinow V. Fretting corrosion of tin coated electrical contacts: The influence of normal force, coating thickness and geometry of sample configuration. IEEE 62nd Holm Conference on Electrical Contacts (Holm). 2016:33-38. https://doi.org/10.1109/HOLM.2016.7780003

[15] Ren W, Zhang C, Du Q, Du D, Wang H. Experimental investigation of cold adhesion failure physical mechanism of gold plated contact within the Micro-Electro-mechanical-Relay. Eng Fail Anal. 2021;(121):105-151. https://doi.org/10.1016/J.ENGFAILANAL.2020.105151

[16] Narayanan S, Park Y, Lee K. Fretting corrosion of lubricated tin plated copper alloy contacts: Effect of temperature. Tribol Int. 2008;41(2):87-102. https://doi.org/10.1016/J.TRIBOINT.2007.05.004

[17] Zhang X, Qian Q, Qiang L, Zhang B, Zhang J. Comparison study of gold coatings prepared by traditional and modified galvanic replacement deposition for corrosion prevention of copper. Microelectron Reliab. 2020;(110):113695. https://doi.org/10.1016/J.MICROREL.2020.113695

[18] Arazna A, Krolikowski A, Koziol G, Bielinski J. The corrosion characteristics and solderability of immersion tin coatings on copper. Mater Corros. 2012;64(10):914-925. https://doi.org/10.1002/maco.201106434

Paulina Adamczyk, MEng. – Faculty of Mechanical Engineering, Wrocław University of Science and Technology.
e-mail: *paulina.adamczyk@pwr.edu.pl*

Anna Zięty, DEng. – Faculty of Mechanical Engineering, Wrocław University of Science and Technology.
e-mail: *anna.ziety@pwr.edu.pl*

Dominika Grygier, DSc., DEng. – Faculty of Mechanical Engineering, Wrocław University of Science and Technology.
e-mail: *dominika.grygier@pwr.edu.pl*

Article citation info:
Regulski P. The material and economic assessment of the life cycle of city buses in the operational phase. Combustion Engines. 2023; 192(1):50-54. https://doi.org/10.19206/CE-151942

Paweł REGULSKI

Combustion Engines
Polish Scientific Society of Combustion Engines

The material and economic assessment of the life cycle of city buses in the operational phase

ARTICLE INFO

Received: 28 March 2022
Revised: 23 June 2022
Accepted: 7 July 2022
Available online: 9 August 2022

The aim of the article is the material and economic assessment of the life cycle of city buses with combustion engines. As part of the analysis, the analyzed parameters were optimized using neural networks with the use of a regression model. As part of the life cycle assessment criteria, three types of Solaris Urbino buses were analyzed. As a result of the research carried out for buses, the results were obtained regarding the optimal duration of operation, the number and cost of oil, air and fuel filter changes, and the replacement period of buses. The presented research and analyzes have a significant impact on the processes of purchasing and operating city buses.

Key words: *life cycle assessment, city buses, operation, neural networks, combustion engines*

1. Introduction

Life Cycle Assessment (LCA) concerns the assessment of potential environmental hazards. This model consists of three areas [12]:

1. produce the vehicle,
2. operation of the vehicle,
3. vehicle scrapping.

The area (phase) of vehicle operation will be analyzed.

The aim of the article is the material and economic assessment of the life cycle of city buses with combustion engines. The following parameters were analyzed: duration of operation, mileage, number and cost of filter changes: oil, air, fuel, and the period of replacement of buses. City buses often form the basis of the functioning of public transport. Solaris buses are operated in many Polish and European cities and meet the currently applicable emission standards. Low exhaust emissions from buses are of great importance for the protection of the environment.

2. Literature review

The use of the LCA cycle for vehicles has been presented in many publications. The publication [1] presents a set of key sustainable development indicators for various stages of the car's life cycle. The publication [2] uses the life cycle assessment methodology to determine whether the material composition strategy of the popular Volkswagen Golf model has reduced its environmental burden over the last 30 years. The publication [3] presents the supporting LCA method, within which fuel consumption was calculated. The application of the LCA cycle for internal combustion engines is presented in publications [4, 5]. The aim of the publication [4] was to present, using LCA analysis, the impact of changes in the material composition of engines on the environment under selected internal combustion conditions used in passenger cars. The simplified LCA model presented in the article presents energy consumption and total CO_2 emissions on the basis of the mass of materials from which the engine is made. The aim of the publication [5] was to demonstrate the environmental impact of changes in the material composition of Volkswagen Golf passenger cars in the last 30 years using the LCA methodology. The presented simplified LCA model of an engine shows the energy consumption and total CO_2 emissions based on the weight of the engine materials. The publication [6] presents the material and energy life cycle of a car. Changes in energy consumption and emission levels are presented. The publication [7] presents the application of the life cycle assessment to the analysis of ecological properties of a passenger car during its operation. The issues related to the operational efficiency of city buses are described in the publication [8]. The publication [9] presents research on the use of batteries in electric cars. The publications [10, 11] present a fleet management strategy that does not take into account the number and cost of replacing oil, air and fuel filters.

3. Research methodology

As part of the life cycle assessment criteria, three types of Solaris Urbino buses were analyzed. Figure 1 presents the Solaris Urbino 10.5 bus [17].

Figure 1. Solaris Urbino 10.5 bus [17]

Table. 1 presents the technical data of the Solaris Urbino 10.5 bus.

Table 1. Technical data of the Solaris Urbino 10.5 bus [20]

Type of Solaris Bus	Urbino 10.5
Years of production	Since 2017
Doors layout	2-2-0 2-2-2 1-2-0 1-2-2
Number of doors	2-3
The height of the floor	320 mm
Engines	Cummins ISB6.7E6C DAF MX-11
The power of the engines	Cummins: 187 kW (254 HP), 209 kW (277 HP), 224 kW (305 HP), DAF: 210 kW (286 HP), 240 kW (326 HP), 271 kW (368 HP)
Transmission	Automatic: ZF-EcoLife Voith DIWA.6
Length	10550 mm
Width	2550 mm
Height	3040 mm
Wheelbase	4450 mm
Number of seats	Up to 29
ABS	Yes
ASR	Yes
EBS	Yes
ESP	Yes
Air conditioning	Optional

Figure 2 presents the Solaris Urbino 12 bus. Figure 3 presents the Solaris Urbino 18 bus.

Table 2 presents the technical data of the Solaris Urbino 12 bus. Table 3 presents the technical data of the Solaris Urbino 18 bus.

Table 2. Technical data of the Solaris Urbino 12 bus [20]

Type of Solaris Bus	Urbino 12
Years of production	Since 1999
Doors layout	2-2-2 2-2-0 1-2-2 1-2-0
Number of doors	2-3
The height of the floor	320 mm
Engines	1) Cummins ISB6.7E6C 250B 2) Cummins ISB6.7E6C 280B 3) Cummins ISB6.7E6C 300B 4) DAF MX-11 210 5) DAF MX-11 240 6) DAF MX-11 271
The power of the engines	1) 189 kW (257 HP) 2) 209 kW (284 HP) 3) 224 kW (304 HP) 4) 210 kW (286 HP) 5) 240 kW (326 HP) 6) 271 kW (368 HP)
Transmission	1) ZF-EcoLife 2) Voith DIWA.6
Length	12000 mm
Width	2550 mm
Height	3040 mm
Wheelbase	5900 mm
Number of seats	Up to 43
ABS	Yes
ASR	Yes
EBS	Yes
ESP	Optional
Air conditioning	Optional

Fig. 2. Solaris Urbino 12 bus

Fig. 3. Solaris Urbino 18 bus

Table 3. Technical data of the Solaris Urbino 18 bus [20]

Type of Solaris Bus	Urbino 18
Years of production	Since 1999
Doors layout	2-2-2-0 2-2-2-2 1-2-2-0 1-2-2-2
Number of doors	3-4
The height of the floor	320 mm
Engines	1) DAF MX-11 240 2) DAF MX-11 271
The power of the engines	1) 240 kW (326 HP) 2) 271 kW (368 HP)
Transmission	1) ZF-EcoLife 2) Voith DIWA 6
Length	18000 mm
Width	2550 mm
Height	3090–3200 mm
Wheelbase	5130 mm 6770 mm
Number of seats	Up to 53
ABS	Yes
ASR	Yes
EBS	Yes
ESP	No
Air conditioning	Optional

For this purpose, neural networks were used to determine the optimal values of the operation duration, mileage, number and costs of replacement of selected consumables and the replacement period of buses. Neural networks can be used wherever there are tasks related to prediction, classification or control. In the conducted analysis, tasks related to prediction were used.

The analyzed parameters were determined on the basis of source data. The duration of operation was determined on the basis of the publication [20]. The mileage in one year was 100,000 km [18]. The engine oil filter was changed every 30,000 km [21], the air filter every 20,000 km, and the fuel filter every 100,000 km [19]. The cost of purchasing one engine oil filter was PLN 17 [14], one air filter PLN 220 [15], and one fuel filter PLN 32 [13]. The analyzed engine oil, air and fuel filters are used in all analyzed types of buses. As part of the costs of replacing individual filters, the costs of their purchases were taken into account. The bus replacement period was every 9 years [16]. Table 4 presents the values of the analyzed parameters of selected types of buses.

Table 4. Values of the analyzed parameters of selected types of buses

Type of Solaris Bus	Urbino 10,5				
Duration of operation[years]	4	3	2	1	
Mileage [1000·km]	400	300	200	100	
Number of filter changes [–]:					
the engine oil filter	13	10	7	3	
the air filter	20	15	10	5	
the fuel filter	4	3	2	1	
The cost of replacing [PLN*]:					
the engine oil filter	221	170	119	51	
the air filter	4400	3300	2200	1100	
the fuel filter	128	96	64	32	
Bus replacement period	0	0	0	0	
Type of Solaris Bus	Urbino 12				
Duration of operation [years]	9	8	7	6	
Mileage [1000·km]	900	800	700	600	
Number of filter changes [–]:					
the engine oil filter	30	27	23	20	
the air filter	45	40	35	30	
the fuel filter	9	8	7	6	
The cost of replacing [PLN*]:					
the engine oil filter	510	459	391	340	
the air filter	9900	8800	7700	6600	
the fuel filter	288	256	224	192	
Bus replacement period	1	0	0	0	
Type of Solaris Bus	Urbino 18				
Duration of operation[years]	9	6	5	4	3
Mileage [1000·km]	900	600	500	400	300
Number of filter changes [–]:					
the engine oil filter	30	20	17	13	10
the air filter	45	30	25	20	15
the fuel filter	9	6	5	4	3
The cost of replacing [PLN*]:					
the engine oil filter	510	340	289	221	170
the air filter	9900	6600	5500	4400	3300
the fuel filter	288	192	160	128	96
Bus replacement period	1	0	0	0	0
(*) 1 PLN = 0.2 EUR					

As part of the analysis, the analyzed parameters were optimized with the use of neural networks with the use of a regression model in the Statistica program.

The following signals are identified:

– quantitative input variables: operation time, mileage, number of engine oil filter replacements, number of air filter replacements, number of fuel filter replacements, cost of engine oil filter replacements, cost of air filter replacements

Table 5. Prediction sheet

No. – case	Output
1	0
2	0
3	0
4	0
5	1
6	0
7	0
8	0
9	1
11	0
12	0

– qualitative input variables: cost of fuel filter replacement,
– quantitative output variables: bus replacement period.

Table 5 presents the prediction sheet. Figure 4 presents the activation histogram. Table 6 shows the list of the qualities and errors in the regression model.

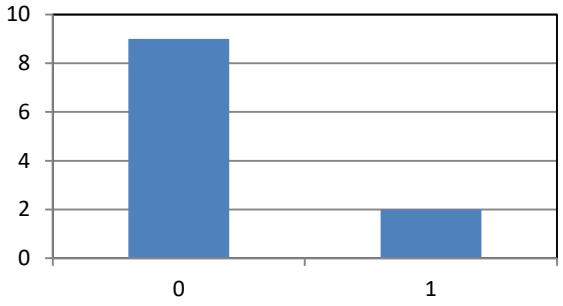

Fig. 4. Histogram of activation

Table 6. List of qualities and errors of the regression model

Quality (training)	Quality (testing)	Quality (validation)	Error (training)	Error (testing)	Error (validation)
1	0	0	0	0	0

4. Research analysis

The conducted research shows that for optimization equal to 1 for Solaris Urbino 12 and 18 buses with combustion drive, with a mileage of 900,000 km, the number of engine oil filter changes 30, the number of air filter changes 45 and the number of fuel filter changes 9 and the cost of engine oil filter replacements PLN 510, the cost of replacing the air filter PLN 9,900 and the cost of replacing the fuel filter PLN 288 and the replacement period for buses equal to 1, the optimal duration of operation is 9 years.

For Solaris Urbino 10.5 buses, the optimization results were below 1 and it was not possible to determine the optimal values of the analyzed parameters due to the shorter duration of operation compared to Solaris Urbino 12 and 18 buses.

5. Conclusions

On the basis of the conducted research and analyzes for the assessment of the life cycle of city buses in the operation phase, it has been shown that the optimal duration of operation is 9 years and is related to their mileage, the bus replacement period as well as the cost and number of filter replacements. The use of neural networks to determine the optimization of the analyzed parameters is an important source of information for the processes of planning the operating costs of bus companies. The presented research and analyzes have a significant impact on the processes of purchasing and operating city buses. Further research should be verified on the example of buses in operation in a specific company.

Nomenclature

ABS anti-lock braking system
ASR acceleration slip regulation
CO_2 carbon dioxide
EBS electronic braking system
ESP electronic stability program
LCA Life Cycle Assessment

Bibliography

[1] Arena M, Azzone G, Conte A. A streamlined LCA framework to support early decision making in vehicle development. J Clean Prod. 2013;41(2):105-113. https://doi.org/10.1016/j.jclepro.2012.09.031
[2] Danilecki K, Mrozik M, Smurawski P. Changes in the environmental profile of a popular passenger car over the last 30 years – results of a simplified LCA study. J Clean Prod. 2017;141(1):208-218. https://doi.org/10.1016/j.jclepro.2016.09.050
[3] Del Pero F, Delogu M, Pierini M. The effect of lightweighting in automotive LCA perspective: estimation of mass-induced fuel consumption reduction for gasoline turbocharged vehicles. J Clean Prod. 2017;154(6):566-577. https://doi.org/10.1016/j.jclepro.2017.04.013
[4] Mrozik M. Ecological comparative assessment of selected materials used for the construction of spark ignition engines. Combustion Engines. 2020;183(4):11-14. https://doi.org/10.19206/CE-2020-402
[5] Mrozik M, Danilecki K. Environmental assessment of the production process of internal combustion engines. Combustion Engines. 2017;171(4):117-120. https://doi.org/10.19206/CE-2017-419
[6] Mrozik M, Eliasz J, Terelak-Tymczyna A. Material-energy model of motor vehicle life cycle. Strojarstvo. 2013;55(2): 161-168.
[7] Mrozik M, Merkisz-Guranowska A. Environmental assessment of the vehicle operation process. Energies. 2021;14(1): 76. https://doi.org/10.3390/en14010076
[8] Niewczas A, Rymarz J, Debicka E. Stages of operating vehicles with respect to operational efficiency using city buses as an example. Eksploat Niezawodn. 2019;21(1):21-27. https://doi.org/10.17531/ein.2019.1.3
[9] Raugei M, Winfield P. Prospective LCA of the production and EoL recycling of a novel type of Li-ion battery for electric vehicles. J Clean Prod. 2019;213(3):926-932. https://doi.org/10.1016/j.jclepro.2018.12.237
[10] Redmer A. Strategic vehicle fleet management – a joint solution of make-or-buy, composition and replacement problems. J Qual Mainten Eng. 2022;28(2):327-349. https://doi:10.1108/JQME-04-2020-0026
[11] Redmer A. Strategic vehicle fleet management – the replacement problem. LogForum. 2016;b(1):17-24. https://doi:10.17270/J.LOG.2016.1.2
[12] Regulski P, Abramek KF. The application of neural networks for the life-cycle analysis of road and rail rolling stock during the operational phase. Tech Trans. 2022; e2022002. https://doi.org/10.37705/TechTrans/e2022002
[13] www.centrumauto.pl/czescisamochodowe/solaris/urbino/urbino-12-n9389/filtr-paliwa-100261 (accessed on 14.01.2022)

[14] www.esamochodoweczesci.pl/filtr-oleju-silnikowego-fast/FT38093,4938,FT38093~1FAST,a.aspx (accessed on 14.01.2022)
[15] www.otomoto.pl/czesci/q-filtr-powietrza-solaris/ (accessed on 14.01.2022)
[16] www.spak.pl/stantaboru/ (accessed on 1.06.2022)
[17] www.solarisbus.com/pl/pojazdy/napedy-konwencjonalne/grupa-urbino (accessed on 21.07.2022)
[18] www.teraz-srodowisko.pl/aktualnosci/Zielony-Transport-Publiczny-dotacje-11076.html (accessed on 4.06.2022)
[19] www.ucando.pl/blog/jakie-wystepuja-filtry-w-samochodzie-i-co-ile-je-wymieniac/ (accessed on 12.01.2022)
[20] www.wikipedia.org (accessed on 18.06.2021)
[21] www.wyborkierowcow.pl/co-ile-wymieniac-filtr-olejudlaczego-trzeba-zmieniac-filtrolejowy/ (accessed on 30.05.2022)

Paweł Regulski, MSc. – Faculty of Mechanical Engineering and Mechatronics, West Pomeranian University of Technology in Szczecin.
e-mail: *regulski85@gmail.com*

Article citation info:
Bienek F, Szczygiel I, Rutczyk B. Economical analysis of electric vehicles in Poland. Combustion Engines. 2023;192(1):55-62. https://doi.org/10.19206/CE-151941

Filip BIENEK
Ireneusz SZCZYGIEL
Bartłomiej RUTCZYK

Combustion Engines
Polish Scientific Society of Combustion Engines

Economical analysis of electric vehicles in Poland

ARTICLE INFO

Received: 19 April 2022
Revised: 15 June 2022
Accepted: 7 July 2022
Available online: 31 July 2022

The paper presents results obtained from calculations conducted to receive information on the capability of photovoltaic systems to power electric vehicles in regular use. The annual distance travelled was divided in nine categories. Every aspect of this analysis was suitable for Polish market and parameters given by the climate that is connected with geographical location of Poland. It is worth mentioning that one of the key elements is the law for renewable energy, that is the key aspect to economical benefits that come from so called green investments. Energy law was also taken into account during this simulation. All those aspects together summarized to a conclusions that Polish market is not as competitive as other European markets when electric propulsion is present in the system.

Key words: *PV system, electric vehicles, transportation economy*

1. Introduction

The growing number of photovoltaic systems (PV) in private possession demands an analysis of using such systems for powering electric vehicles (EV) or plug-in hybrids (PHEV). Each year the number of electrified vehicles on the roads in Poland is growing but to reach expected 1 million units there some encouragement is needed. Average range of an EV is not convincing enough for Polish citizens to pay a higher price for a less versatile vehicle [1]. This is one of the aspects that is analyzed in this paper. Another one is based on PV that can charge an EV in daily routine. It is an important aspect, because this can lead to higher interest in EV as the range would not be an issue anymore. Though certain studies have been carried out on the topic of the wider usage of EVs and their impacts, such as by Szymanski et al. [2] or the study on their influence on pollution [3], the question of their basic economy of use in the Polish market, still remains open.

The paper is focused mainly on Poland but similarly irradiated regions all around the world can be taken into consideration. Scrutiny provided by these calculations can be broadly compared only when the irradiation factor is comparable. Increasing number of EVs [4] on the roads can arise demand for new PV systems and larger energy supply needs. This creates another possibility, a usage of EVs as energy storage. Although some concerns are visible at first sight, for example preparation of power grid [5], as the one currently utilized in Poland is not ready for higher demand and power supply diversity. That is the main reason to convey such calculations, because according to European lawmakers future solutions should comply with the European Green Deal. This contrast can also serve the purpose of comparing EVs and plug-in hybrids with the upcoming competition created by hydrogen cells vehicles and hydrogen combustion engines currently under development in the automotive industry.

2. Analysis of range and availability of charging stations

Considering all the aspects of using a vehicle, it is worth taking into consideration the frequently chosen summer travel destinations. In this case, analysis conducted by Statistics Poland [6] was used to determine the most popular places for spending summer holidays by Polish citizens. It can therefore be concluded that Italy is the most common foreign destination, followed by Greece. When it comes to domestic trips, the Pomorskie Voivodeship is the undisputed leader. Using this information, exemplary routes to these places were created and compared with the parameters of an electric vehicle, which were made with the use of trip planning software [7].

2.1. Route Katowice–Venice

There has been some change to this route, the use of trip planning software [7] did not take into account road works, which slightly affects the length of the route. After comparing it with the route generated in "Google Maps" [8] and comparing the travel times (estimated for journeys without stops), the author decided to take into account the differences in order to refine the analysis.

Table 1. Route details generated for ICE vehicle in "Google Maps" [8]

Route	Katowice–Venice
Time of journey	10 h 12 min
Distance	964 km
Number of breaks	2
Break duration	20 min

The travel is determined by the time of 10 h 12 min, which should be enough to cover 964 km. This time should be supplemented with data from Daimler [9], in which it is mentioned that the average time of refueling an ICE vehicle takes the user about 6 minutes. In order to create realistic travel conditions, this time was increased to 10 minutes, which gives a travel time of 10 h 40 min. For comparison,

a simulation of driving this route with two vehicles representing the electric cars was created. One of them is Nissan Leaf (40 kWh) and the other is Tesla Model 3 Long Range (75 kWh). Additional information is a different distance (966 km) in relation to the journey of ICE car.

Table 2. Route details generated for Tesla Model 3 Long Range [7]

Route	Katowice–Venice
Time of journey	18 h 36 min
Distance	964 km
Number of breaks	2
Break duration	4 h 10 min

Table 2 presents data of a journey planned in EV. Usage of chargers providing low current values (1 phase, 50 kW) was the baseline in this case.

Table 3. Route details for Tesla Model 3 Long Range with the utilization of fastcharger [7]

Route	Katowice–Venice
Time of journey	11 h 6 min
Distance	964 km
Number of breaks	1
Break duration	1 h

The situation changes significantly when we consider fast charging (3 phase, >100 kW) [10], as the model allows it. This increases the comfort of traveling due to the readiness for further travel in a relatively shorter time, but the journey is extended by 26 minutes in comparison to ICE vehicle.

Table 4. Route details generated for Nissan Leaf [7]

Route	Katowice–Venice
Time of journey	27 h 12 min
Distance	964 km
Number of breaks	3
Break duration	5 h 30 min

A dramatic change in travel time occurs when there is a difference in the capacity of the batteries and charging scheme is based at 1 phase, < 50 kW devices. This parameter is almost 50% reduced (35 kWh, when compared to the capacity of Tesla's battery that has 75 kWh), while the travel time is extended to 27 h 12 min. It is therefore highly likely that people using this mode of transport would benefit from an overnight stay during the journey due to the long duration of the travel.

2.2. Route Katowice–Thessaloniki

This route was created because of the popularity of the holiday travel destination. Many people use air transport, but some people going in this direction use road vehicles.

Table 5. Route details generated for ICE vehicle in [8]

Route	Katowice–Thessaloniki
Time of journey	16 h 8 min
Distance	1579 km
Number of breaks	4
Break duration	40 min

For comparison purposes, a route with a travel time of 16 h 8 min was selected. All mapped routes follow the same roads. By enriching this time with stops for refueling [9], as in the case of the previous route, the time is extended to 16 h 45 min.

Table 6. Route details generated for Tesla Model 3 Long Range [7]

Route	Katowice–Thessaloniki
Time of journey	32 h 19 min
Distance	1579 km
Number of breaks	3
Break duration	5 h 30 min

The course of the route allows to notice one shorter stop, this is due to the possibility of using the Supercharger charging station (3 phase, > 100 kW) because this location has a rich infrastructure of these devices although other stops require usage of 1 phase, 50kW chargers. However, as can be seen at the bottom of Table 6, the travel time is 32 h 19 min, which means that the journey lasts almost twice as long as with the use of a ICE car.

Table 7. Route details generated for Tesla Model 3 Long Range with the utilization of fastcharger [7]

Route	Katowice–Thessaloniki
Time of journey	19 h 19 min
Distance	1579 km
Number of breaks	3
Break duration	1 h 30 min

When using Superchargers (3 phase, > 100 kW), the situation improves significantly, however, one must take into account an extended travel time (in comparison to ICE). It is worth noting that the route has been extended by over 500 km compared to the previous one (from Katowice to Venice), while the duration has increased by more than 1 hour. Compared to a combustion vehicle, the difference is less than 3 hours.

Table 8. Route details generated for Nissan Leaf [7]

Route	Katowice–Thessaloniki
Time of journey	47 h 42 min
Distance	1579 km
Number of breaks	5
Break duration	5 h 30 min

The travel time is almost two days, exceeding the travel time by an ICE car by more than 31 hours. This kind of

time difference can exclude a vehicle from range of interest if someone is looking for a fast mean of transport. This situation has place because of 1 phase, < 50 kW chargers used to recharge this vehicle.

2.3. Route Katowice–Gdańsk

Due to the popularity of the Pomeranian Voivodeship among people spending their holidays in Poland [6], it was chosen to analyze the route connecting the south with the north of the country.

Table 9. Route details generated for ICE vehicle in [8]

Route	Katowice–Gdańsk
Time of journey	5 h 26 min
Distance	519 km
Number of breaks	1
Break duration	10 min

In accordance with the previously adopted practice, the route should include the time for a stop to fill the tank, but the range of combustion vehicles allows one to travel this route without additional stops (if the driver's physiology allows it). The time taken for the comparison is 5 h 36 min.

The order of comparisons does not change, so in the first case the Tesla Model 3 Long Range is compiled, which (as the name of the model indicates – has a greater range) is characterized by better properties in terms of the distance that can be traveled on a single charge. The range specified by the manufacturer is 580 km, therefore, it makes it possible to cover the entire distance using only the pre-journey charging.

Table 10. Route details generated for Nissan Leaf [7]

Route	Katowice–Gdańsk
Time of journey	12 h 1 min
Distance	519 km
Number of breaks	1
Break duration	6 h 30 min

Due to the more modest range (389 km – declared by the manufacturer), it is not possible to cover the Katowice–Gdańsk route, requiring a stop (1 phase, < 50 kW charger) and an extension of the journey by 6 hours 30 minutes in order to ensure further mobility.

3. Costs comparison

3.1. Costs comparison charging station vs. household

The results developed for electric vehicles, which in this analysis would be charged using a charging station, are presented. It is worth mentioning that such stations are characterized by different charging parameters such as: direct current or alternating current and various power provided by these units: less than 50 kW, 50 kW, more than 50 kW [10, 11]. Such a difference affects the time required to charge the vehicle, but not every vehicle is adapted to such an activity, as shown in Table 12.

Table 11. Charging expenses at charging station

Vehicle	Battery capacity [kWh]	Charging cost [PLN]		
		AC < 50 kW 1 phase	DC 50 kW 3 phase	DC > 50 kW 3 phase
Nissan Leaf	40	57.20	79.60	95.60
	62	88.66	123.38	148.18
BMW i3	38	54.34	75.62	90.82
Audi e-tron	95	135.85	189.05	227.05
Renault Zoe	52	74.36	103.48	124.28
Tesla Model 3	52	74.36	103.48	124.28
	75	107.25	149.25	179.25

Table 12. Charging time

Vehicle	Battery capacity [kWh]	Charging time (according to producer) [h]		
		AC < 50 kW 1 phase	DC 50 kW 3 phase	DC > 50 kW 3 phase
Nissan Leaf	40	07:30:00	01:00:00	–
	62	11:30:00	01:30:00	No info.
BMW i3	38	04:54:00	00:42:00	–
Audi e-tron	95	08:50:00	01:24:00	00:30:00
Renault Zoe	52	20:00:00	06:00:00	–
Tesla Model 3	52	07:00:00	No info.	00:30:00
	75	09:00:00	No info.	00:45:00

Prices shown in Table 11 are calculated using values from Table 12 for a user that does not have the ability to charge EV in their household thus a charging process of 0–100% (using capacities given by manufacturer) was the benchmark for each vehicle. Large part of each price is created by parking fee that is added after 1 hour of AC charging and 45 minutes of DC charging in the amount of 0.4 PLN/min [11].

In comparison charging each of aforementioned vehicles using a traditional outlet would generate costs shown in Table 13.

Table 13. Costs of charging EV using traditional outlet

Vehicle	Battery capacity [kWh]	Cost of charging [PLN]	
		Lowest	Highest
Nissan Leaf	40	27.60	31.20
	62	42.78	48.36
BMW i3	38	26.22	29.64
Audi e-tron	95	70.30	74.10
Renault Zoe	52	35.88	40.56
Tesla Model 3	52	35.88	40.56
	75	51.75	58.50

The differences are notable, as even the most expensive option of charging the highest capacity battery (95 kWh Audi e-tron) generates costs about 1 PLN lower than charging the smallest battery (38 kWh BMW i3) at the charging station.

The density of charging stations in Poland is 0.0064 station/km^2 [12], while the density of the location of the charging stations operated by Orlen, taken into account in the calculations, can be seen in Fig. 1.

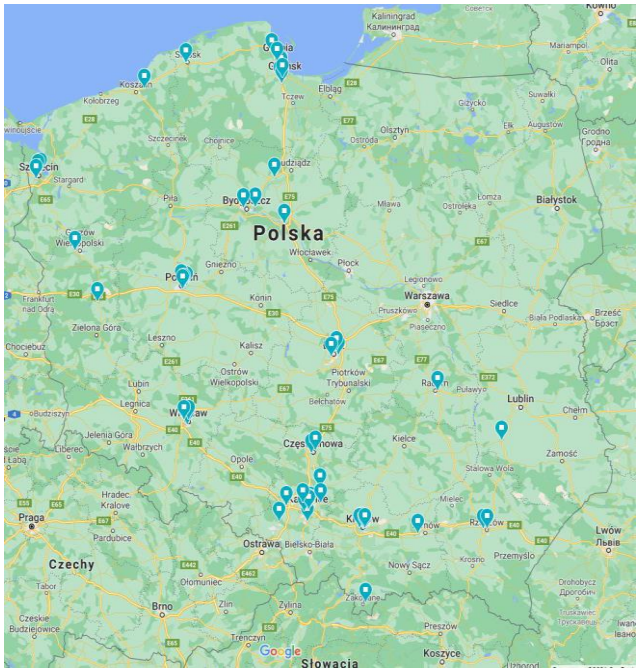

Fig. 1. Map of charging stations in Poland (provided by Orlen)

3.2. Costs comparison – ICE vehicles vs. EVs

Lists of cars has been prepared to present the costs and allow to clearly determine which vehicle is the cheapest in operation. This comparison refers only to the costs related to the source of power, all costs related to the depreciation of the vehicle are omitted, i.e. the costs of repairs, tire replacement, services, etc. The vehicles selected for this work allowed for the creation of four groups that are different from each other primarily by the segment they represent. There is also a difference between vehicles when it comes to the aspect of positioning certain vehicles as belonging to the premium segment, however this is not a measurable value and therefore it was not a parameter of this comparison.

The first group consists of representatives of the urban segment, otherwise known as the A and B segments. A characteristic parameter of these vehicles is their size and usually low power, due to the orientation of these cars towards economy, cost-effective use in the city and their easy use in such an environment. The performance is therefore not the determining aspect. It is also worth noting that vehicles in this segment are used in Poland as a means of transport for the whole family, even over long distances, which is a direct result of the ratio of purchase and use costs to the wealth of citizens.

Comparison presented in Table 14 shows that vehicles using combustion engines are able to compete directly with electric vehicles, if we take into account the economic conditions for charging vehicles with the use of charging stations available in the municipal infrastructure. This situation was taken into account due to the availability of such a solution for every user of an electric vehicle, regardless of the place of residence.

Table 14. Costs comparison – segment A and B

Vehicle	Propulsion type	km/PLN
Mini One	Petrol	3.42
Peugeot 208	Diesel	4.64
Hyundai i10	Petrol	3.97
Renault Zoe	Electric	3.82
BMW i3	Electric	3.47

Another group that has been generated for the purpose of comparison are compact vehicles, also referred to as the representatives of the C segment. These vehicles are quite small when it comes to external dimensions, but inside these vehicles are more spacious than products presented in Table 14. Such vehicles are undoubtedly suitable to travel long distances, because they allow four adult passengers to be comfortably carried with their luggage.

Table 15. Costs comparison – segment C

Vehicle	Propulsion type	km/PLN
Honda Civic 5D 2021	Petrol	2.59
Skoda Octavia IV 2.0 TDI	Diesel	4.75
Nissan Leaf (40 kWh)	Electric	4.89
Nissan Leaf (62 kWh)	Electric	3.56

This segment already shows a certain difference when we take into account the cost of 1 km, but these are not significant values, especially taking into account the prices of vehicles (in the case of electric vehicles they are much higher than in the case of internal combustion vehicles). It is also worth noting that a diesel vehicle (in this comparison – Skoda Octavia) generates lower travel costs compared to a gasoline engine vehicle. In direct competition with the more economical version of an electric vehicle, the situation for this segment differs significantly from, what was expected, the situation that takes place in the A and B segments. It can be concluded directly from the costs that only the diesel drive is an economic competition for the electric drive (in this comparison the Nissan Leaf with a 40 kWh battery).

Table 16 presents the representatives of another popular segment among the cars selected by customers, both new and used vehicles. Two vehicle models in two different configurations were compared.

Table 16. Costs comparison segment D

Vehicle	Propulsion type	km/PLN
BMW 318i	Petrol	3.09
BMW 316d	Diesel	4.06
Tesla Model 3 (52 kWh)	Electric	3.24
Tesla Model 3 (75 kWh)	Electric	3.24

The last group created for direct comparison is a very popular SUVs segment. This type of cars are intended to serve its owner in many different situations, as the abbreviation stands for Sport Utility Vehicle. Versatility brings slightly increased operating costs, which can be seen in Table 17.

Table 17. Costs comparison segment SUV

Vehicle	Propulsion type	km/PLN
Audi Q5 45 TFSI	Petrol	2.29
Audi Q5 35 TDI	Diesel	3.48
Audi e-tron	Electric	1.83

Multitude of applications for these vehicles also entails higher costs when it comes to traveling any given distance. In this case, the vehicle with electric drive is the least favorable, and its weight contributes to this, which directly affects the range offered by this solution. The difference here comes up to 1.65 km/PLN, which places this segment in the middle of the rate when it comes to coverage for PLN. Although the direct comparison of the values for the km/PLN parameter is definitely unfavorable for this segment, which allows to conclude that it is the least economical choice among those compared in this analysis.

4. PV system as charging source for EVs

Analysis of PV system usage to charge EVs was taken into consideration after comparing prices of the ICE counterparts and energy supply delivered by using public charging stations. Economical advantage provided by EVs were not significant and in some cases ICE vehicles are more budget friendly, which brings into question whether PV is the solution to this problem and what parameters should it fulfill to become a competitive option of transportation in the polish conditions.

4.1. Region of application

The regions chosen to investigate whether the PV system is suitable to power homestead and charge an EV are the three examples of irradiation diversity in Poland. Kołobrzeg presents the least solar radiation recorded during observation time, Katowice is the average irradiated region and Racibórz has the highest rate of sunlight according to the Ministry of Investment and Development [13] all of the parameters are presented in Fig 2. Data collected for the aforementioned regions can be a representation of large part of Europe according to Śmierzchalska et al. [14], thus making this paper applicable for different consumer markets.

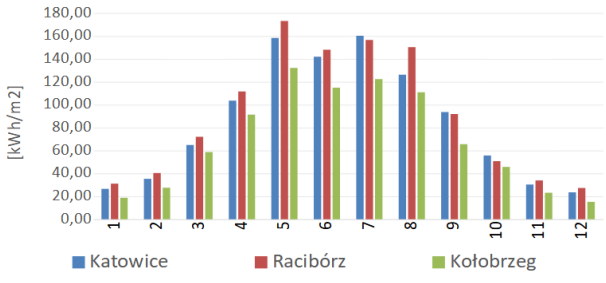

Fig. 2. Radiation magnitude for investigated regions (numbers at X axis represent months)

Summary of annual irradiation can give an insight to characteristics of each region. Kołobrzeg as the least irradiated city in this set is estimated to collect about 826.07 kWh/annum/m^2, Katowice is estimated to collect about 1019.70 kWh/annum/m^2 that is just above the average result for the territory of Poland and Racibórz can generate up to 1086.73 kWh/annum/m^2 [13].

4.2. PV system performance

Calculations were provided using PV system with nominal power of 10 kW, which is the highest power output for private use in Poland securing the highest power return rate possible. This kind of installation can also supplement the energy grid with its energy production. Polish law regulations create the possibility to use up to 80% of the power provided to power grid (by the prosumer from PV installation). In further calculations data from Gil and Wurfel [15, 16] is used as it is the most precise showing not only monthly intensity of radiation but also values recorded in time lapse, which were collected over the course of 30 years.

$$\eta_{ameff} = \eta_{pan} \cdot \eta_{inv} \cdot \eta_{am} \tag{1}$$

where: η_{ameff} – amended value of system efficiency, η_{pan} – efficiency of PV panel, η_{inv} – efficiency of inverter, η_{am} – amended coefficient.

Implementing the amended value of system efficiency for each month the values create efficiency of given system according to weather each month. Weather conditions such as temperature, humidity, precipitation were taken into account. This procedure helps to model the conditions of real environment in given area. Values obtained by calculations are presented in Fig 3. Values obtained from Daimler [8] and from formula (1) were used to calculate the amount of energy produced by the PV system taking into consideration the area of PV panels that were used in this simulation (49.5 m^2) suggested by Soleco [17], all three cities mentioned in chapter 4.1 were used to calculate the amount of energy that is possible to generate by such an installation.

$$E_m = \eta_{ameff} \cdot R_m \cdot A \tag{2}$$

where: E_m – energy produced in a period of one month [kWh], η_{ameff} – amended value of system efficiency, R_m – monthly irradiation [kWh/m^2], A – area of PV panels [m^2].

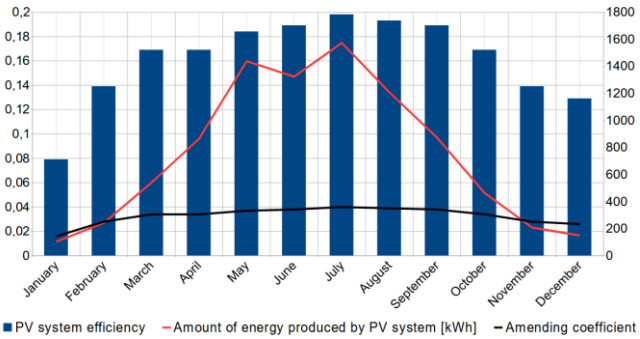

Fig. 3. PV system parameters (numbers at X axis represent months)

5. EV's market and energy demand

An important feature of a personal vehicle is mobility and independence. This chapter provides information about daily energy usage of 7 most popular EVs in Poland according to Fries et al. [2]. It creates an array of vehicles to compare with the ICE powered vehicles already in possession of a large number of commuters. Analysis was carried out for annual distance covered by vast majority of population, according to catalog data [19].

Table 18. Daily electricity demand for EVs

Vehicle	Battery capacity [kWh]	kWh/km	Thousand km/annum								
			2	5	8	12	17	25	30	35	40
			kWh/day								
Nissan Leaf	40	0.103	0.56	1.41	2.25	3.38	4.79	7.04	8.45	9.86	11.27
Tesla Model 3	52	0.113	0.62	1.55	2.48	3.72	5.27	7.74	9.29	10.84	12.39
Nissan Leaf	62	0.117	0.64	1.61	2.57	3.86	5.47	8.04	9.65	11.26	12.87
Tesla Model 3	75	0.129	0.71	1.77	2.83	4.25	6.02	8.86	10.63	12.40	14.17
Renault Zoe	52	0.132	0.72	1.80	2.89	4.33	4.13	9.02	10.82	12.62	14.43
BMW i3	38	0.145	0.79	1.99	3.18	4.77	6.76	9.93	11.92	13.91	15.89
Audi e-tron	95	0.229	1.25	3.14	5.02	7.53	10.66	15.68	18.81	21.95	25.09

$$M_D = \frac{C_{bat}}{R_{man}} \tag{3}$$

where: M_D – amount of electricity needed for every kilometer [kWh/km], C_{bat} – capacity of battery [kWh], R_{man} – range estimated by manufacturer.

Next step of calculations was to use (3) and calculate daily requisition for electricity, conducted using formula (4)

$$E_D = M_D \cdot D_{dist} \tag{4}$$

where: E_D – amount of electricity needed to cover the daily driven distance [kWh], M_D – amount of electricity needed for every kilometer [kWh/km], D_{dist} – daily distance [km].

Interesting conclusion comes to mind while analyzing the results. The first conclusion that appears obvious after analyzing the results is, that the heaviest car in the comparison (Audi e-tron) demands the highest power dose for every single day but right behind are Renault Zoe and BMW i3 which are both small and light (for EV standards) vehicles although one needs 0.53 kWh and the other 0.46 kWh (for annual mileage of 2000 km) less than the heavy Audi SUV. Growing number of kilometers generates higher differences between each vehicle, worth considering is the capacity of battery it indicates how often it is necessary to charge particular vehicle during given distance.

Table 19. Energy available to charge EV

Month	Amount of energy [kWh]
January	83.40
February	194.19
March	432.43
April	691.54
May	1150.41
June	1058.95
July	1258.88
August	966.39
September	699.02
October	371.78
November	166.64
December	120.03

Using the data presented at Fig. 3 and in Table 18 calculations that analyze how much kilometers it is possible to cover when one uses whole electricity produced by PV system in Katowice region were conducted. Including return factor of 0.8 and area of PV system mentioned in paragraph 4.2 results are as follows.

Combining results from Table 18 and 19 it was possible to calculate distance that can be covered by three exemplary cars: Nissan Leaf, Tesla Model 3 Long Range and Audi e-tron every month using the equivalent of power produced from solar energy.

An aspect of economy and difference between EV and ICE cars can be analyzed according to data received from examples shown in Table 20. Comparison fuel powered cars to EV's was based on models and specification from paragraph 3.2.

Table 20. Monthly distance provided by PV system for EV

	km/month		
Month	Nissan Leaf	Tesla Model 3	Audi e-tron
January	809.66	646.47	364.17
February	1885.31	1505.33	847.98
March	4198.37	3352.18	1888.35
April	6713.97	5360.77	3019.82
May	11169.06	8917.93	5023.64
June	10281.11	8208.95	4624.26
July	12222.15	9758.77	5497.30
August	9382.45	7491.42	4220.06
September	6786.57	5418.73	3052.47
October	3609.48	2881.99	1623.48
November	1617.82	1291.75	727.67
December	1165.34	930.46	524.15

Significant savings can be achieved when one uses PV system to power an EV, but amounts from Table 21 and 22 are extreme cases because these show annual distances equal to 31 to 69 thousand kilometers. Usually that kind of distance is covered by average citizen in 3 to 6 years time.

Table 21. Economical savings provided by PV system usage to power EV petrol vehicles compared

	PLN/month		
Month	Honda Civic	BMW 318i	Audi Q5 TFSI
January	311.72	209.07	158.89
February	725.85	486.82	369.97
March	1616.37	1084.10	823.89
April	2584.88	1733.67	131.55
May	4300.09	2884.06	2191.81
June	3958.23	2654.78	2017.56
July	4705.53	3155.99	2398.47
August	3612.25	2422.72	1841.21
September	2612.83	1752.42	1331.79
October	1389.65	932.04	708.32
November	622.86	417.75	317.48
December	448.65	300.91	228.69

Table 22. Economical savings provided by PV system usage to power EV Diesel vehicles compared

	PLN/month		
Month	Skoda Octavia	BMW 316d	Audi Q5 TDI
January	170.35	159.23	104.70
February	396.67	370.76	243.79
March	883.34	825.64	542.90
April	1412.62	1320.36	868.20
May	2349.97	2196.49	1444.30
June	2163.15	2021.87	1329.47
July	2571.54	2403.58	1580.47
August	1974.07	1845.14	1213.27
September	1427.89	1334.63	877.59
October	759.43	709.83	466.75
November	340.39	318.16	209.20
December	245.19	229.17	150.69

6. Solar panels area to fulfill the demand of an EV and an average household

Popularity of PV systems can be an asset worth considering, especially when someone is thinking about purchasing an EV. The following section contains information and data that verify how large of a solar array is needed to cover the need for electricity of an average household in Poland.

These calculations were conducted using data from the Polish Statistical Survey [19] and setting the average demand for electricity at 3500 kWh annually for a household. Given the aforementioned information the author performed simulations to achieve data that represents the area of solar panels needed to state all requirements linked to energy supply.

$$Y_E = E_D \cdot 365 \quad (5)$$

where: Y_E – annual energy demand of an EV [kWh], E_D – amount of electricity needed to cover daily driven distance [kWh/days].

EVs from two opposite points of spectrum were selected as the benchmark, to represent whole spectrum of energy usage generated by daily utilization of these vehicles**.**

The first finding that comes to mind after comparing the results is that as the annual mileage increases the demand for electricity grows heavily. Even the most economical vehicle from the array compiled in Table 18 requires energy from at least 20 m^2 of photovoltaic panels (case for 2000 km of annual travel). This occurs in the most irradiated city in Poland [13], and as it comes to the least irradiation (Kołobrzeg) the area increases to 30 m^2.

EV with higher demand for energy requires an installation of at least 25 m^2 that generates higher cost of such system and when this vehicle is used more intensively even the largest area of photovoltaic panels is not able to sustain the delivery of electricity needed. This means either the owner is going to create larger installation and receive only 0,7 of what has been produced or decides to exploit a system of power output up to 10 kW and feeds the remaining need from the power grid purchasing energy at regular prices.

7. Summary

Summarizing all obtained parameters of PV system usage, few conclusions can be made. At first the user needs to define if the system should support or be the only source of energy for the given household. In case such system is being built to be the sole source of energy, the size of the installation should be increased significantly over standard system recommended for an average household. This implicates larger number of solar panels and thus the price of whole unit is going to rise, changing the time of payback considerably. The second factor that is considered as the one responsible for price increment is the energy storage unit. Relative high price of this units is dictated by development stage of the technology connected to this sector and only upcoming innovations in battery production and materials used to create the storage can make the battery a competitor as it comes to price trade at the market.

According to calculations that compare using PV system to charge electric vehicle it can be noticed that large amount of monthly generated energy is consumed by this activity. Time required to generate enough savings to pay for the investment is estimated for 6–7 years (considering no further investments are needed and no damage to system is encountered) [20]. Given that not only EV usage should be powered by such system, a larger area of solar panels is needed. This complicates situation for individual user, because the power available to return from power grid reduces from 0.8 of produced energy to 0.7 [21]. The difference between these factors reduces savings and it can extend the return time significantly.

As the market of PV systems dynamically changes, constant observation and analysis is needed to encounter the most cost-effective method of energy generation.

Nomenclature

EV electric vehicle
ICE internal combustion engine
PHEV plug-in hybrid vehicle

Bibliography

[1] Friesa M, Kerlera M, Rohra S. et al. An overview of costs for vehicle components, fuels, greenhouse gas emissions and total cost of ownership update 2017. https://steps.ucdavis.edu/wp-content/uploads/2018/02/FRIES-MICHAEL-An-Overview-of-Costs-for-Vehicle-Components-Fuels-Greenhouse-Gas-Emissions-and-Total-Cost-of-Ownership-Update-2017-.pdf

[2] Szymanski P, Ciuffo B, Fontaras G, Martini G, Pekar F. The future of road transport in Europe. Environmental implications of automated, connected and low-carbon mobility. Combustion Engines. 2021;186(3):3-10. https://doi.org/10.19206/CE-141605

[3] Gis M, Bednarski M, Lasocki J. Determination of pollutant emission of electric vehicle in real traffic conditions in Poland. Combustion Engines. 2019;178(3):9-14. https://doi.org/10.19206/CE-2019-302

[4] Samar Vehicle Market Research Institution. https://www.samar.pl/__/3/3.a/111495/3.sc/11/Ponad-22-tys--wtyczkowozów---stan-parku-na-koniec-lutego-2021-roku.html?locale=pl_PL

[5] Kapustin NO, Grushevenko DA. Long-term electric vehicles outlook and their potential impact on electric grid. Energ Policy. 2020;(137):111103. https://doi.org/10.1016/j.enpol.2019.111103

[6] Statistics Poland „Tourism in 2019". Rzeszów, Warszawa 2020.

[7] PlugShare. https://www.plugshare.com

[8] Google maps. https://www.google.pl/maps

[9] Mercedes-Benz Group Media. https://www.media.daimler.pl/problemy-z-adowaniem-stereotypy-i-rzeczywistosc/ (accessed on 23.03.2021)

[10] Dujic D. Electric vehicles charging – an ultrafast overview. International Exhibition and Conference for Power Electronics, Intelligent Motion, Renewable Energy and Energy Management. Shanghai 2019. https://infoscience.epfl.ch/record/267807

[11] PKN Orlen Poland Price list for EV charging https://orlencharge.pl/#oferta (accessed on 23.03.2021)

[12] Guziński J, Adamowicz M, Kamiński J. Infrastruktura ładowania pojazdów elektrycznych. Automatyka, Elektryka, Zakłócenia. 2014;1(15):74-83.

[13] Polish Ministry of Investment and Development. https://archiwum.miir.gov.pl/strony/zadania/budownictwo/charakterystyka-energetyczna-budynkow/dane-do-obliczen-energetycznych-budynkow-1 (accessed on 09.04.2021)

[14] Śmierzchalska P, Chmielowiec M. Mapa usłonecznienia w Polsce. Pomerian Academy in Slupsk. Slupsk 2015. https://kierunkizamawiane.apsl.edu.pl/pliki/czystaenergia/raport4_II.pdf

[15] Gil P. Roczne wyniki pomiaru sprawności amorficznych kolektorów fotowoltaicznych w Rzeszowie. Rynek Energii. 2015;(4):75-83.

[16] Würfel P. Thermodynamic limitations to solar energy conversion. Physica E. 2002;14(1-2):18-26. https://doi.org/10.1016/S1386-9477(02)00355-7

[17] Soleco Polska. https://www.kolektory.com/instalacje-fotowoltaiczne-ceny/instalacje-fotowoltaiczneceny/zestaw-o-mocy-10-kw.html (accessed on 12.04.2021)

[18] Statistics Poland. Energy consumption in households in 2018, Warsaw 2019.

[19] Fotowoltaika. https://fotowoltaikaonline.pl/kalkulator

[20] Ustawa z dnia 20 lutego 2015 r. o odnawialnych źródłach energii. Dz.U. 2015, poz. 478, rozdz. 2, art. 4, ust. 2, Chancellery of the Sejm, 2015.

Filip Bienek, MSc. – Institute of Thermal Technology, Silesian University of Technology.
e-mail: *filipb50@wp.pl*

Prof. Ireneusz Szczygieł, DSc., DEng. – Institute of Thermal Technology, Silesian University of Technology.
e-mail: *ireneusz.szczygiel@polsl.pl*

Bartłomiej Rutczyk MSc. – Institute of Thermal Technology, Silesian University of Technology.
e-mail: *bartlomiej.rutczyk@polsl.pl*

Article citation info:
Fąfara J-M, Modliński N. Numerical study of internal flue gas recirculation system applied to methane-hydrogen powered gas micro-turbine combustor. Combustion Engines. 2023;192(1):63-77. https://doi.org/10.19206/CE-152236

Jean-Marc FĄFARA
Norbert MODLIŃSKI

Combustion Engines
Polish Scientific Society of Combustion Engines

Numerical study of internal flue gas recirculation system applied to methane-hydrogen powered gas microturbine combustor

ARTICLE INFO

Received: 9 May 2022
Revised: 11 July 2022
Accepted: 20 July 2022
Available online: 24 July 2022

Sources of renewable energy have been increasingly used all over the world. This kind of energy is highly desirable because of its unlimited availability. Unfortunately, renewable energy production very much depends on weather conditions. Consequently, it is necessary to store the produced excess energy in order to use it when needed. There is a technology able to produce a hydrogen/methane fuel from excess renewable energy, which may be stored. This technology is called the Power-to-Gas technology (P2G). Since the efficiency of this technological process depends on the hydrogen fraction in the renewable energy fuel, there is a need to increase this fraction. Concurrently, the gas microturbine technology is increasingly widely used in various industries (aviation, energy, automotive, military, etc). The P2G technology and the gas microturbine technology are likely to be integrated in the near future and, as mentioned above, the hydrogen fraction in the methane-hydrogen fuel will tend to increase. In order to power a gas microturbine with the methane-hydrogen fuel, it will be necessary to modify the combustor to avoid an excessive temperature increase and flashbacks. In this paper it is proposed to apply an autonomous internal exhaust gas recirculation system to resolve the hydrogen combustion problems indicated above. The operating principle and the proposed design of the recirculation system and the latter's impact on the combustor's operating parameters and emissivity (NO_x and CO) are presented.

Key words: *gas microturbines, combustor, power-to-gas, hydrogen, exhaust gas recirculation*

1. Introduction

1.1. Integration of power-to-gas technology and gas microturbine technology

An increase in electricity supply from renewable energy sources, especially from wind turbines, hydroelectric power plants and photovoltaic panels, can be observed in the power generation sector. Renewable energy sources present many advantages, such as unlimited energy production. One of the major drawbacks of all the energy sources is that the energy production is not constant over time, being variable and intermittent mainly due to weather conditions. This problem can be addressed by storing the excess energy and using it when convenient. It is possible to transform (through hydrolysis) the excess electrical energy into hydrogen and then to produce methane (using carbon dioxide, previously generated hydrogen and electrical power in a process called methanation). Finally, the two gases, i.e. hydrogen and methane, are mixed to obtain a renewable fuel. This technology is called "power-to-gas" ("P2G") [1]. The presence of methane gas in the renewable fuel makes the production of the latter less efficient than if solely hydrogen was used, but it is necessary because of the specific properties of hydrogen – hydrogen is more difficult and dangerous to store and transport and more demanding as regards its use in power devices [2]. In order to optimise the use of this renewable source energy, the percentage of hydrogen in the renewable fuel produced using the P2G technology needs to be increased.

Today, gas microturbines are increasingly often used in various industry sectors: in aviation to power drones, in the automotive industry to extend a car's range (e.g. Jaguar CX75, Pininfarina H600, etc.), in the energy industry to generate electrical (and heat) power for house applications, and so on [3]. Gas microturbines present many advantages, such as low noise level, cheap operation, limited number of moving parts, low emissions, etc. [4]. Consequently, the use of gas microturbine technology has spread to many industry sectors.

It can be beneficial to integrate the P2G technology and gas microturbine devices. For this purpose the efficiency of P2G should be increased by using a more hydrogen enriched fuel and the combustors of the latter need to be adapted. The use of a more hydrogen enriched fuel provokes higher local combustion temperatures and higher flame velocities [5], whereby if the combustors were unmodified, this would result in local overheating and increased NO_x emissions and provoke flame flashbacks in the direction of the fuel injection zone. All of this would have an adverse effect on the operation of the microturbine devices.

1.2. Exhaust gas recirculation applied to gas microturbines

In order to avoid the problems connected with the use of a more hydrogen enriched fuel in gas microturbines, conventional (diffusion) gas microturbine combustors must be made capable of reducing the combustion temperature and moving the combustion zone towards the exhaust outlet (to avoid flame flashbacks). In order to propose a solution to the above problems, a review of the literature on the subject was carried out and is presented below.

Guethe et al. [6] investigated the impact of exhaust gas recirculation (from the turbine outlet to the compressor inlet) in gas turbines. Turning back exhaust gases entails a reduction in the amount of oxygen in the combustion zone and an increase in carbon dioxide concentration. From the point of view of the chemical combustion process the re-

duction in the amount of combustion zone oxygen limits the concentration of O radicals which drive the combustion process. It is noted that carbon dioxide is not a gas "perfectly inert" in the combustion process. This means that some of the carbon dioxide present in the combustion process is subject to a certain reaction. The latter was identified as: $OH + CO \leftrightarrow H + CO_2$. Thus carbon dioxide can react with hydrogen atom H which is one of the radicals in the combustion process. Thanks to this reaction one can reduce the amount of hydrogen radicals in the combustion process and at the same time increase the OH and CO species. The research carried out by Liu et al. [7] drew attention to the fact that hydrogen radical H is involved in the combustion process in the following reaction: $H + O_2 \leftrightarrow O + OH$. Given that carbon dioxide reduces the amount of the hydrogen radicals present, the above-mentioned reaction is also reduced. This, in turn, limits the generation of O and OH substances (which are also radicals), whereby the combustion process reaction is significantly affected. According to Guethe et al. [6] and Liu et al. [7], limiting the concentration of hydrogen and oxygen radicals in the combustion zone carbon dioxide has a strong impact on the combustion process by inhibiting the combustion reaction, which results in a reduction in the combustion temperature and in a decrease in the laminar flame speed.

Ditaranto et al. in [8] showed that owing to the higher specific heat capacity of steam the use of steam dilution to limit the combustion temperature in gas turbine combustors is more effective than the use of nitrogen dilution. Hence by introducing a species whose specific heat capacity is higher than that of air one can reduce the combustion temperature in a gas turbine combustor. The recirculated turbine exhaust gases contain pure exhaust gases. The latter consist mainly of carbon dioxide and steam. Above 550 K the specific heat capacity of carbon dioxide and steam at a constant pressure is higher than that of air at the constant pressure [9–11]. Near the liner of the gas microturbine combustion chamber the temperature ranges from 770 K to as high as 2300 K [12]. The evolution of the specific heat capacity of the above-mentioned species at the constant pressure of 1 bar is presented in Fig. 1.

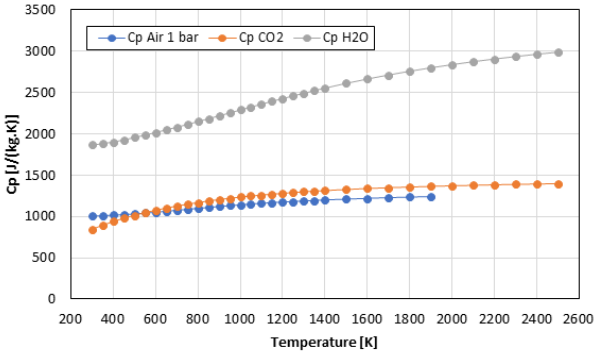

Fig. 1. Heat capacity of air, carbon dioxide and steam at constant pressure of 1 bar

In the combustion chamber operating conditions the specific heat capacity of the exhaust gases at a constant pressure is higher than that of the air supplied to the combustion chamber. Therefore the exhaust gases recirculated into the combustion zone will be able to absorb more combustion heat, whereby the temperature in the combustion zone will decrease. Hence it can be concluded that thanks to the physical action of the exhaust gases it will be possible to reduce the combustion temperature peak and gradient. As a result, the rate of combustion of the laminar flame will also be reduced (according to van't Hoff's law, as the temperature of a chemical reaction decreases, the reaction rate also decreases). Preliminary analyses indicate that the reintroduction of some of the exhaust gas into the combustion zone would provoke a reduction in both combustion temperature and flame speed.

Shi et al. [13] carried out research on a burner equipped with an Internal Flue Gas Recirculation (IFGR) system and demonstrated that by reintroducing some of the exhaust gas into the burner's air inlet one can increase the combustion zone volume, causing a reduction in combustion temperature, whereby the emission of nitrogen oxides can be reduced. The temperature reduction strongly depends on the combustion volume increased.

It emerges from the above that the introduction of an exhaust gas recirculation system into the gas microturbine combustor is an interesting solution. The presence of exhaust gases acts physically and chemically on the combustion process, limiting its combustion temperature, peak combustion temperature and combustion velocity. The recirculation of exhaust gases into the gas microturbine combustor would potentially reduce the combustion temperature and velocity, whereby hydrogen could be added to the fuel while keeping the nominal operating parameters and emissivity. Moreover, by adding more hydrogen to the fuel a reduction in the emission of carbon species, such as hydrocarbons and carbon monoxide, would be achieved. For the purpose of internal exhaust gas recirculation it is proposed to create a pipe system integrated into the combustor, able to autonomously move the exhaust gases from the exhaust outlet into the combustion zone. This concept is detailed in part II of this paper.

Other studies show that the application of exhaust gas recirculation may have a negative effect on the combustion process. These studies are presented below.

The fact that the exhaust gases contain some carbon monoxide needs to be taken into consideration. Jadidi et al. [14] and Taamallah et al. [15] presented the adiabatic temperatures of selected combustibles. The adiabatic combustion temperature of carbon monoxide is very high in comparison with that of hydrogen and can reach 2450 K. This temperature is higher than the adiabatic combustion temperature of methane fuel (2250 K) or hydrogen fuel (2400 K). This is why as a result of the recirculation of exhaust gases containing carbon monoxide the combustion temperature can increase in comparison with the case without recirculation.

One should also note that the recirculation of exhaust gases provokes a replacement of some of the "fresh" air coming from the compressor by a portion of the "hot" exhaust gases in the primary combustion zone. This results in an increase in the enthalpy of the gases supplied into the

combustion zone, increasing the peak temperature and the temperature gradients in the primary combustion zone.

Gieras [12] presented a concept of adapting the liner's holes to optimise the combustion process in a jet microturbine. In this way the mass flow passing through the combustor is effectively modified in various operating conditions. The introduction of an IFGR system into the combustor can modify the combustion process by creating or extending a combustion zone with an air-fuel equivalence ratio close to unity. This phenomenon can be responsible for an increase in combustion temperature.

The above three arguments show that the introduction of some of the exhaust gas into the combustion zone can have an opposite effect to the intended one. The replacement of some of the fresh air coming from the compressor by a part of the hot exhaust gases in the primary combustion zone and the potential modification of the air-fuel equivalence ratio may be responsible for an increase in combustion temperature.

It emerges from the above literature review that the introduction of an autonomous recirculation system (IFGR) into the gas microturbine combustor can have a positive or negative effect on the combustion process, particularly in the case of hydrogen enriched fuel. In order to determine the effect of the IFGR system on the combustion process (with and without hydrogen addition), the research presented below was carried out.

1.3. Novelty of this research

In the last decade of the 20th century a new approach to combustion, dedicated to industrial furnaces, was developed. This combustion method, referred to as High Temperature Air Combustion (HiTAC) [16], was developed by the Japanese company Nippon Furnace Kogyo (NFK) [17]. Other similar combustion technologies, diversely referred to as: Flameless Combustion (FLC), Flameless Oxidation (FLOX) and Moderate and Intense Low-oxygen Dilution (MILD) [18], were subsequently developed. All these methods are based on injecting hot air and fuel at high velocity into the combustion chamber. The air-fuel mixture temperature is higher than the auto-ignition temperature of the fuel. A recirculation zone is generated whereby the combustion products are diluted with the exhaust gases. As a result, the combustion zone spreads throughout the chamber volume. The temperature field is much more homogeneous than in the case of conventional combustion. Thanks to the homogeneous combustion zone the emissivity of NO_x and CO species is reduced [19]. All these combustion technologies are often grouped under the designation "MILD combustion" [18]. The MILD combustion process can be widely applied to various energy devices [20]. Recently this technology was studied to be applied to gas turbines [16] and even to gas microturbines [21]. The major challenge of conducting MILD combustion in a gas (micro)turbine is to keep the combustor inlet temperature above the auto-ignition temperature of the fuel [22]. This challenge inhibits the application of MILD combustion to gas microturbines. Considering this difficulty, an alternative concept to the MILD combustion design, suitable for the conventional gas microturbine combustor burning a more hydrogen enriched methane fuel is proposed in this paper.

The power-to-gas technology and the gas microturbine technology are very useful and widely used. In order to better integrate the two technologies, an effort must be made in the near future to increase the hydrogen fraction in the fuel mixture used in the gas microturbine. According to the presented literature review, this goal can be achieved by incorporating an autonomous internal flue gas recirculation system into the gas microturbine combustor. The aim of the present research was to assess through numerical analyses the usefulness of applying IFGR to a gas microturbine for the purpose of burning a more hydrogen enriched fuel. A conventional diffusion combustor was designed and then its design was modified by adding a pipe system enabling the autonomous exhaust gas recirculation inside the combustor. The following were assessed:

– the possibility of effecting autonomous IFGR inside the gas microturbine combustor
– the modification of the combustor's main operating parameters (the total pressure drop and the total exhaust gas temperature) by the IFGR system
– the impact of the IFGR system on the temperature field in the combustion zone
– the impact of the IFGR system on the CO and NO_x concentrations in exhaust.

Each of the evaluations was carried out for the hydrogen mass fraction in the methane fuel ranging from 0 to 0.5. The study was conducted using the numerical tools described further in this paper.

The novelty of this research consists in numerically investigating a novel IFGR system applied to the gas microturbine to evaluate its positive or negative impact on the combustor operation.

2. Case study combustor and operating conditions

A reference combustor was designed for a 40 kW gas microturbine powered by methane fuel. The combustor's approximate operating parameters are presented in Table 1. The combustor is schematically shown and described in Fig. 2.

Table 1. Reference gas microturbine and combustor operating parameters

Parameters	Combustor inlet	Combustor outlet
p^* [Pa]	324992.333	311992.640
p [Pa]	306584.082	301133.803
T^* [K]	433.834	1185
T [K]	426.666	1175.062
c [m/s]	120	155
$c_s = 4.874 \cdot 10^{-3} \frac{kg}{s}$; $\dot{m} = 0.251 \frac{kg}{s}$		

The first main objective of this study was to assess the possibility of effecting autonomous internal exhaust gas recirculation by adding a pipe system. The challenge consisted in moving exhaust gases from the combustor outlet zone to the top part of the liner. The pressure drop occurring in the combustor made this task difficult. Many IFGR pipe systems were analysed to find the ones most suitable for this application. Two IFGR systems (presented below) were selected.

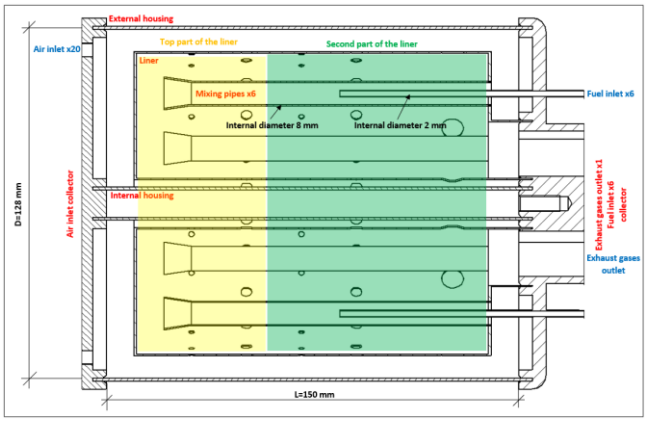

Fig. 2. Cross sectional view of 3D model of reference combustor

Figure 3 shows the first modified combustor equipped with an IFGR system (case A). In this case, a pipe system is installed between the liner and the combustor's external housing, whereby some of the exhaust gas can be transferred from the combustor outlet zone to the top part of the liner. The difference between the total pressure at the combustor outlet and the static pressure at the top of the liner is used to enable exhaust gas recirculation. Figure 4 shows the second modified combustor equipped with the IFGR system (case B). In this case, the mixing pipes are modified in two ways. Firstly, pipes taking some of the exhaust gas from the combustor outlet and introducing it into mixing pipe air are added to the mixing pipes. This design exploits the difference between the total pressure at the combustor outlet and the static pressure inside the mixing pipe. Secondly, the interior of the mixing pipes is shaped into a venturi, which increases the pressure difference and improves exhaust gas recirculation.

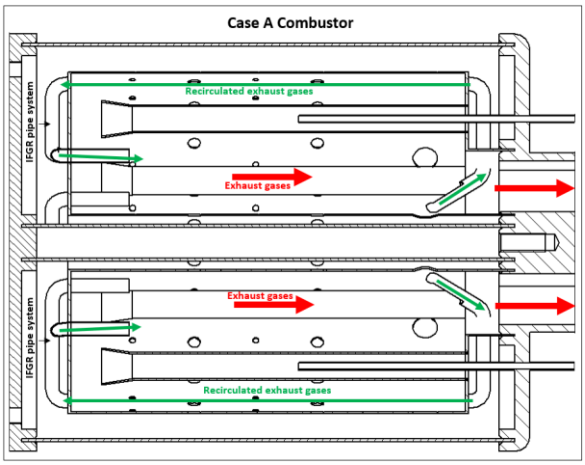

Fig. 3. Cross sectional view of 3D model of modified combustor (case A)

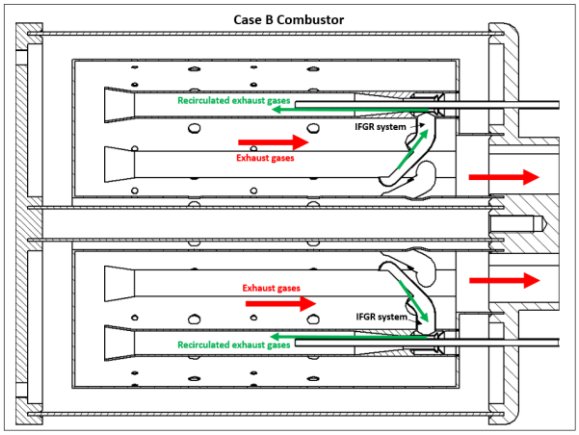

Fig. 4. Cross sectional view of 3D model of modified combustor (case B)

3. Numerical methods

3.1. Computational domain mesh system

3D combustor models were created using Solid Edge and the Ansys pre-processor [23]. Mesh generation is a major step in the simulation of the combustor. As it yields accurate results, the tetrahedral mesh structure is often used for gas microturbine combustor simulations [24–28]. The tetrahedral mesh can be applied to a complex geometry while maintaining acceptable values of quality parameters (skewness, orthogonality and aspect ratio). Recently, the polyhedral cell mesh has been intensively developed. Similarly as the tetrahedral mesh, polyhedral cells give relatively accurate results at better quality parameters [29–31]. A polyhedral mesh with the maximum cell length of 0.8 mm was selected for this study. After mesh volume generation the obtained mesh was improved by selecting the value of 0.45 as the desired minimum orthogonal quality. Finally, boundary layers were generated in order not to exceed the Y+ value of 300. According to the literature [24–25], the obtained grids (and the numbers of elements) constituting the calculation domains are sufficient to provide reliable results. The computational domain is shown in Fig. 5. Table 2 shows the quality parameters of the mesh.

Table 2. Mesh quality parameters

Case	Number of cells [millions]	Maximum aspect ratio	Maximum skewness	Minimum orthogonal quality
Reference	5.8	38.3	0.895	0.435
Case A	7.0	35.8	0.900	0.432
Case B	6.4	62.0	0.895	0.200

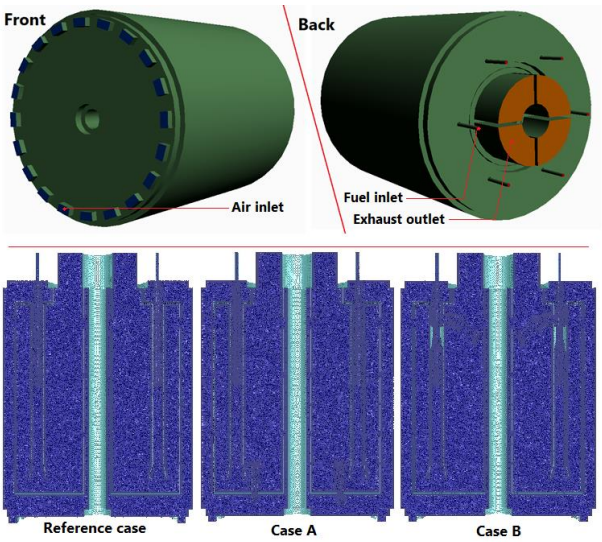

Fig. 5. External view of computational domain (external view is similar in all cases) and the mesh view in longitudinal cross sections for each combustor cases

3.2. Mathematical model

The simulations performed in this study were based on the CFD Ansys code [32]. The following processes: the turbulent flow, the non-premixed combustion in the gas phase and the radiative heat exchange, taking place within the calculation domain, were modelled as part of this study of the gas microturbine combustor.

The realizable k-ε model [12, 33] was used to model the turbulent flow through the combustor. This model is a Reynolds Averaged Stokes-Navier model (RANS). The realizable k-ε turbulence model is widely used to model flows in many industrial applications. This model yields acceptable results at a low computational cost. The enhanced wall treatment was enabled. The enhanced wall treatment makes it possible to fully resolve the flow on the wall boundary when Y+ is less or equal to 1, or to apply the enhanced wall function when Y+ is greater than unity. The enabled wall treatment model is a good compromise when wall phenomena are not of crucial importance for the studied flow properties, as it is the case in this study.

In the studied combustor cases the radiation model had to be enabled to model the heat exchanges inside the calculation domain, next to the heat transfer via conduction and convection. Radiation needs to be modelled in order to perform an accurate simulation and it is one of the most complex phenomena to be modelled. The Discrete Ordinate model [12, 25], which considers the calculation domain as a grey body, was used to model the radiation phenomena. The two major radiation absorbers and emitters in the combustor are steam and carbon dioxide. To perform a correct radiation simulation, it is necessary to use the Weighted Sum of Grey Gases method [12]. Emissivity coefficients extracted from the benchmark exponential wide-band model [34] were used in the simulation. The total gas phase absorption coefficient was calculated from the total emissivity with the mean path length calculated from the characteristic cell size. Wall emissivity was set to unity, which is a typical recommendation in gas microturbine combustor simulations [35].

The non-premixed steady diffusion flamelet [36] model was used to model turbulent combustion. In this model the flames in a turbulent flow are considered as a set of steady laminar flames referred to as "flamelets". Using this model one can apply a detailed chemistry model taking into account the kinetics effects. This combustion model also takes local turbulence phenomena into account through strain rates. A look-up table is generated before the calculations are run. Using the look-up table one can present the flame's all physical and chemical properties as a function of the mixture fraction in each location in the calculation domain. The local mixture fractions are determined on the basis of the flow turbulence. Hence the model enables one to determine the flame properties as a function of the mixture fraction and the local turbulence. The model yields sufficiently accurate results at a moderate computing cost.

The flamelets used in the non-premixed combustion model were generated on the basis of the detailed GRI-MECH 3.0 chemistry mechanism [37]. This mechanism takes into account 53 species involved in 325 reactions. From the GRI-MECH 3.0 website [37] the mechanism data and thermodynamic data files were freely downloaded and then inserted into the Ansys Fluent software using the non-premixed combustion model dialogue window. Before generating the flamelets, the hydrogen (H_2) and methane (CH_4) mass fractions in the fuel had been selected. In this study the hydrogen mass fraction evolved from 0 to 0.5 at a step of 0.1. For this range of the hydrogen mass fraction in the fuel the selected GRIMECH 3.0 mechanism gives sufficiently accurate results [38]. The oxidizer (air) composition was simplified to the 0.23 mass fraction of oxygen (O_2) and the 0.77 mass fraction of nitrogen (N_2). For each fuelling case individual set of flamelets was created. Based on the individual flamelet sets, the individual probability density function (PDF) tables were generated.

Finally, boundary conditions were determined. The inlet is the "mass flow" and the outlet is the "pressure outlet" (the values of the respective quantities were taken from the combustor design calculations).The x-velocity at the outlet was initially assumed to be the same as the velocities immediately upstream of the outlet plane and scaled appropriately to respond to the overall mass conservation. At the outlet plane $(\partial\varphi/\partial x)_{exit} = 0$. At the calculation domain's wall the no slip condition was enabled and the velocity values were set to zero. Near to the wall the flow is more affected by molecular viscosity than by turbulence phenomena. The wall function method presented in [39], which uses algebraic formulations to link the quantities at the wall to those occurring further away, was applied. The boundary conditions are described in Table 3.

Table 3. Boundary conditions obtained from simulations

Boundary condition designation	Type	Parameters
Air inlet	Mass-Flow Inlet	Mass flow = 0.251 kg/s | Turbulent Intensity = 15% | Turbulent Viscosity Ratio = 10 | Total Temperature = 433.834 K | Mean Mixture Fraction = 0 | Mixture Fraction Variance = 0
Fuel inlet	Mass-Flow Inlet	Mass flow = variable (see Table 4) | Turbulent Intensity = 15% | Turbulent Viscosity Ratio = 10 | Total Temperature = 300 K | Mean Mixture Fraction = 1 | Mixture Fraction Variance = 0
Exhaust	Pressure Outlet	Static Pressure = 0 Pa | Turbulent Intensity = 15% | Turbulent Viscosity Ratio = 10 | Backflow Total Temperature = 300 K | Mean Mixture Fraction = 0 | Mixture Fraction Variance = 0
Wall	Wall	Stationary Wall | No Slip | No Heat Exchange | Internal Emissivity = 1 | Opaque Wall | Diffuse Fraction of Radiation = 1
Operating conditions	–	Operating pressure = 301133.803 Pa | Gravity off

The second-order discretization [25] with the pressure-velocity coupled method and the pseudo-transient option enabled [40] was applied. The pressure-based solver [25, 40] was used for these series of simulations. Once the setup was completed the simulations were run.

In order to determine the fuel mass flow to be supplied into the combustor as a function of the hydrogen mass fraction in the fuel it was assumed that the total energy supplied into the combustor in the reference case (methane powered) had to be maintained. The lower heating values (LHV) of methane and hydrogen (LHV_{CH4} = 50 MJ/kg and LHV_{H2} = = 120 MJ/kg [1]) were used in formula 1. The calculation results are presented in Table 4.

$$c_s^{i_{H_2 mass_{fraction}}} = \frac{LHV_{CH_4} \cdot c_s^{0\_H_2 mass\_fraction}}{LHV_{H_2} \cdot H_2 mass\_fraction + LHV_{CH_4} \cdot (1 - H_2 mass\_fraction)} \quad (1)$$

Table 4. Fuel mass flows as function of hydrogen mass percentage in fuel

H_2 mass percentage [%]	$c_s^{i\_H_2 mass\_fraction}$ [kg/s]
10	0.004252
20	0.003787
30	0.003413
40	0.003107
50	0.002851

4. Results and discussion

As part of this study, the ability to effect autonomous exhaust recirculation was analysed for various hydrogen mass fractions in the methane fuel. The impact of the IFGR system implementation on the pressure drop and on the combustion processes was assessed by analysing the temperature fields, the air-fuel equivalence ratio and the evolution of CO and NO_x concentrations in exhaust.

4.1. Exhaust gas recirculation rate

The numerical simulation results for the three cases are discussed in this subsection. Numerical simulations showed that it was possible to obtain autonomous exhaust gas recirculation inside the gas microturbine combustion chamber at the maximum global rate of 0.53%. The IFGR system was found to affect the combustion processes without significantly modifying the combustor operating parameters. The pipe air, fuel and exhaust gas flows through the combustor's mixing pipes for different cases and different hydrogen mass fractions in the methane fuel are presented in Table 5. Figure 6 shows the recirculated exhaust gas mass flows for cases A and B and different hydrogen mass fractions in the methane fuel.

Table 5. Mass flows after IFGR system implementation

Case	Mass flow leaving all pipes [kg/s]	Exhaust mass flow recirculated by IFGR [kg/s]	Fuel mass flow entering in all pipes [kg/s]	Air mass flow entering in all pipes [kg/s]
R00H2	3.706E–02	0	4.874E–03	3.219E–02
R10H2	3.582E–02	0	4.252E–03	3.156E–02
R20H2	3.502E–02	0	3.787E–03	3.124E–02
R30H2	3.449E–02	0	3.413E–03	3.108E–02
R40H2	3.425E–02	0	3.107E–03	3.114E–02
R50H2	3.433E–02	0	2.851E–03	3.148E–02
A00H2	3.751E–02	8.236E–04	4.874E–03	3.263E–02
A10H2	3.613E–02	8.749E–04	4.252E–03	3.188E–02
A20H2	3.541E–02	8.703E–04	3.787E–03	3.163E–02
A30H2	3.490E–02	8.577E–04	3.413E–03	3.149E–02
A40H2	3.460E–02	8.588E–04	3.107E–03	3.149E–02
A50H2	3.463E–02	8.373E–04	2.851E–03	3.178E–02
B00H2	2.538E–02	1.344E–03	4.874E–03	1.916E–02
B10H2	2.476E–02	1.269E–03	4.252E–03	1.924E–02
B20H2	2.417E–02	1.208E–03	3.787E–03	1.917E–02
B30H2	2.383E–02	1.188E–03	3.413E–03	1.923E–02
B40H2	2.347E–02	1.154E–03	3.107E–03	1.920E–02
B50H2	2.316E–02	1.126E–03	2.851E–03	1.919Ev02

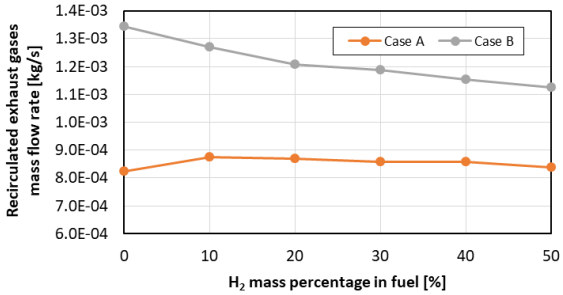

Fig. 6. Recirculated exhaust gas mass flows

The simulations yielded the recirculated exhaust gas mass flows for each of the combustor cases. IFGR ratios were calculated from equations 2 and 3. IFGR% stands for the ratio of the recirculated exhaust gas mass flow to the air mass flow passing through the mixing pipe, while IFGR%* stands for the ratio of the recirculated exhaust gas mass flow to the exhaust gas mass flow leaving the combustor. Figure 7 shows the calculated IFGR ratios.

$$IFGR\% = \frac{\text{Recirculated exhaust gas mass flow}}{\text{Air mass flow passing through mixing pipe}} \cdot 100 \quad (2)$$

$$IFGR\% * = \frac{\text{Recirculated exhaust gas mass flow}}{\text{Exhaust gas mass flow leaving combustor}} \cdot 100 \quad (3)$$

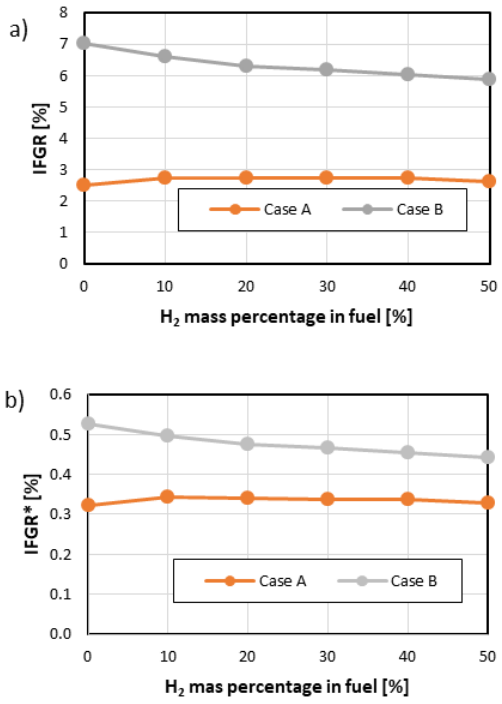

Fig. 7. a) IFGR ratio and b) IFGR* ratio

Firstly, it appears from the above that the IFGR% and IFGR%* ratios in case B are higher than in case A, regardless of the hydrogen mass fraction in the methane fuel. Figure 7 shows that in case A the IFGR% ratio ranges from 2.52 to 2.75%, whereas in case B it ranges from 5.87 to 7.01% . In case A the IFGR%* ratio is in the range of 0.32–0.34%, versus 0.44–0.53% in case B. The difference be-

tween these cases is due to design differences. In case A the recirculation of exhaust gases is accomplished by creating a pressure difference between the collection and injection locations. The difference between the total pressure (in the location where the exhaust gases are collected) and the static pressure (in the location where the exhaust gases are released) is exploited. In case B the recirculation of exhaust gases is driven not only by the total-static pressure difference, but also by an additional pressure difference generated by the venturi shaped mixing pipe. Due to this difference in the IFGR system design the amount of recirculated exhaust gases is greater in case B than in case A.

Secondly, one should note that in case A the IFGR ratios are constant, whereas in case B the IFGR ratios decrease as the hydrogen mass fraction in the fuel increases. In both cases this observation is fully concordant with the IFGR system design. In case A exhaust gases are recirculated by a pipe system located between the liner and the combustor's external housing, while in case B the IFGR system is directly connected to the mixing pipe inside the liner. The modification of the fuel's composition by adding hydrogen to the methane results in the diminution in the density of the fuel in the fuelling pipes and provokes an increase in the velocity of the fuel leaving the fuelling pipes. Once the fuel enters the mixing pipe, its velocity decreases, while its static pressure increases. In case B this results in a reduction in the pressure difference in the venturi fuelling pipe section, whereby the recirculated exhaust gas mass flow decreases as the hydrogen mass fraction in the fuel increases. In case A the IFGR system is independent of the phenomena arising inside the mixing pipes, whereby the IFGR ratios are constant regardless of the hydrogen mass fraction in the fuel.

Finally, let us consider the risk of IFGR system overheating depending on the IFGR system design. In case A, the IFGR system is a set of pipes located between the liner and the combustor's external housing. This design reduces the risk of IFGR system overheating since the set of IFGR pipes is constantly cooled by the air exiting the compressor. In case B, the IFGR system is located in the combustor outlet zone, far from the main combustion temperature, whereby the risk of IFGR system overheating is reduced. In both cases the IFGR system design reduces the risk of IFGR system overheating.

Summing up, it is possible to achieve autonomous exhaust gas recirculation inside a gas microturbine combustor for various hydrogen mass fractions in the fuel if an adequate IFGR pipe system is used. The IFGR ratios are constant in case A, while in case B the ratios decrease as the hydrogen mass fraction in the fuel increases. The case B IFGR system enables quantitatively larger exhaust gas recirculation than case A, regardless of the hydrogen mass fraction. In case A the IFGR%* ratio is about 0.33%, while in case B this ratio amounts to about 0.50%. In both cases the IFGR system design reduces the risk of IFGR system overheating.

4.2. Impact of IFGR system on pressure drop

In this subsection the total pressure drop in the combustion chamber is analysed. Figure 8 shows the total pressure drop for each combustor case and for various hydrogen mass fractions in the fuel. The total pressure drop is calculated from equation 4.

$$\Delta p^* = \frac{p_2{}^* - p_3{}^*}{p_2{}^*} \cdot 100 \tag{4}$$

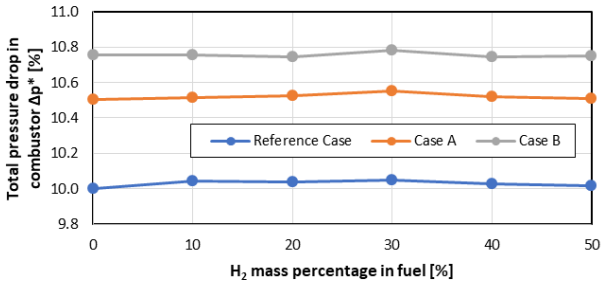

Fig. 8. Total pressure drop

Firstly, it can be noticed that regardless of the hydrogen mass fraction the pressure drop (ranging from 10.00% to 10.05%) is most advantageous in the reference case, intermediate (10.50–10.56) in case A and highest (10.74–10.78%) in case B. The total pressure drop in gas microturbine combustors of this type often amounts to about 10% [12]. The total pressure drop was expected to be higher in the IFGR cases than in the reference case as the IFGR pipe systems are extra elements, constituting additional sources of flow resistance, added to combustors A and B.

Secondly, it should be noted that the total pressure drop is quasi-constant in each case at the increasing hydrogen mass fraction in the fuel. This was also expected as the total pressure drop is closely connected with the combustor design.

Finally, the total pressure drop evolves from 10.00% (the reference case with pure methane fuel) to 10.78% (case B at a 0.3 hydrogen mass fraction in the fuel). The total pressure drop was found to increase maximally by about 0.78%. This increase in total pressure drop is very low considering the fact that the combustor internal design was modified. The differences in pressure drop between the considered IFGR cases can be neglected. Hence one can conclude that the IFGR system does not significantly affect the total pressure drop in the combustor.

Summing up, the implementation of the IFGR system into the combustor at various hydrogen fuelling options has no significant effect on the total pressure drop. This is a positive finding as keeping a low total pressure drop in the gas turbine combustor is one of the major challenges in designing. The fact that the IFGR system has no impact on this parameter is important since this means that the combustor's operating pressure will not be altered when the IFGR system is implemented.

4.3. Impact of IFGR system on temperature field

In the first part of this subsection the homogeneity of combustion static temperature is discussed. The designed combustors were considered as three-dimensional objects. In order to interpret the combustion phenomena occurring inside the combustion zone a representative plane for observing them had to be chosen. The selected plane corre-

sponded to the longitudinal cross section of the combustion chamber. The combustion static temperature field in each of the combustor design cases is shown below for pure methane fuelling (Fig. 9) and for a 0.5 hydrogen mass fraction in the methane fuel (Fig. 10).

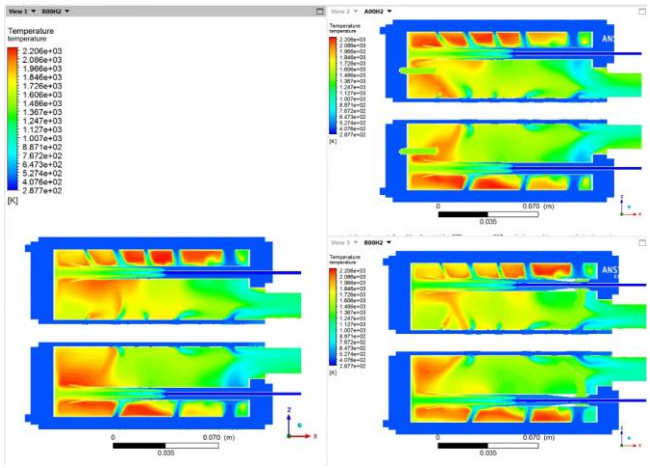

Fig. 9. Combustion static temperature field for pure methane fuelling option

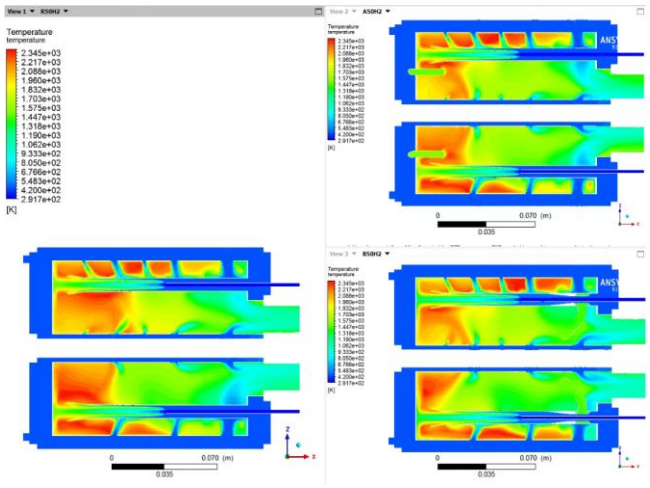

Fig. 10. Combustion static temperature field for 50% hydrogen mass percentage in fuel

Firstly, when comparing the combustion static temperature field (Figs 9 and 10) for the three cases, one can see that the hot spots are largest in the reference case, smallest in case B and intermediate in size in case A, regardless of the hydrogen mass fraction in the fuel. In all the cases the hot spots are located in the top part of the liner and along the liner's internal walls. In case A the temperature field is situated at the central top part of the liner in the place where the exhaust gases are introduced into the combustion zone, the temperature gradient is lower and the hot-spot area is reduced in comparison with the reference case. In case B the static temperature field in the top part of the liner is more homogeneous and the hot spots are smaller than in the reference case and in case A. In case B, combustion zone homogenization in the top part of the liner occurs in the whole section, not only in the central location (as in case A). This is due to the fact that the exhaust gases are mixed with fresh air in the mixing pipes. According to this visual analysis, case B is characterized by the best combustion static temperature field homogeneity, regardless of the hydrogen mass fraction in the fuel.

Secondly, when hydrogen is added to the fuel, the temperature gradient and the size of the hot spots increase. Thanks to the introduction of the IFGR system more homogeneous and smaller hot spots than in the reference case are obtained.

The visual observations are supported by the static temperature uniformity index on the mentioned-above plane, calculated for each of the cases at various hydrogen mass fractions. The uniformity index was calculated from formula 5.

$$\mathrm{UI}_{\mathrm{area}}^{\mathrm{plane}} = 1 - \frac{\sum_{i=1}^{N}\left[\left(\left|\mathrm{T}_{\mathrm{face}_i} - \mathrm{T}_{\mathrm{average}}\right|\right) \cdot \mathrm{A}_i\right]}{2 \cdot \mathrm{T}_{\mathrm{average}} \cdot \sum_{i=1}^{N}[\mathrm{A}_i]} \tag{5}$$

The values of the area weighted static temperature uniformity index (UI) are presented in Fig. 11, which validates the visual analysis carried out above. Case B is characterized by the best static temperature homogeneity, while the reference case shows the worst homogeneity, regardless of the hydrogen mass fraction in the fuel. When hydrogen is added to the fuel, homogeneity degradation occurs. The uniformity index values are very similar, which indicates that the IFGR system does not significantly affect the global static temperature homogeneity on the investigated plane of the combustor.

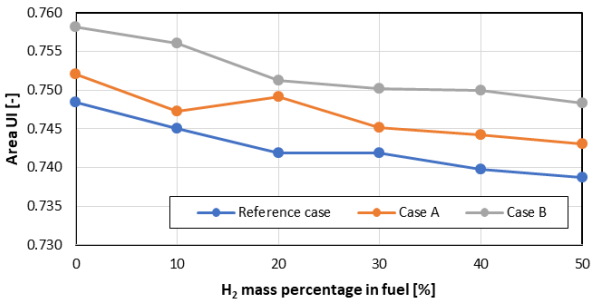

Fig. 11. Area weighted static temperature uniformity index for selected cross section

Summing up, thanks to the implementation of the IFGR system the combustion static temperature field is moderately homogenized and the size of the hot spots is reduced, especially in case B. This applies to all the hydrogen mass fractions in the fuel. The size of the hot spots and the temperature gradient increase with the amount of hydrogen added to the fuel. This applies to the selected representative cross section, but not necessarily to the whole volume of the combustor.

In the second part of this subsection, the maximum combustion static temperature is investigated. Figure 12 presents the combustion maximum static temperature occurring in the combustor.

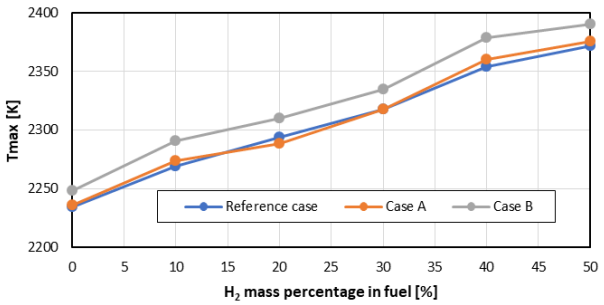

Fig. 12. Combustion maximum static temperature in combustors

Firstly, it can be noticed that the maximum combustion static temperature in the reference case and that in in case A are comparable, regardless of the hydrogen mass fraction in the fuel. In case B the maximum combustion static temperature is higher than in the reference case and in case A. The similarities between the reference case and case A stem from the fact that the amount of air supplied into the combustion zone is similar in both cases (see Table 5) and the recirculated exhaust gas mass flow is lower than in case B (see Fig. 7). As the IFGR ratio is low in case A, the chemical and physical effects (described in the Introduction) of the exhaust gases on the combustion zone are very poor and additionally, not only the reference case air mass flow through the liner, but also the air-fuel equivalence ratio and the combustion volume are maintained. This contributes to the maximum combustion static temperature similarity between the reference case and case A, regardless of the hydrogen mass fraction in the fuel. In case B the maximum combustion static temperature is higher than in the reference case and in case A and also the IFGR ratios (see fig. 7) are higher than in case A, but they are still very low (the IFGR%* ratio amounts to about 0.5%). This may indicate that the expected positive (chemical and physical) effects on the combustion processes are seriously limited. Considering that the mass flow of the recirculated exhaust gases is low, the exhaust gas enthalpy and the carbon monoxide reburn enthalpy added to the primary combustion zone can be neglected. According to the results presented in Table 5, in case B the air mass flow passing through the mixing pipes (primary combustion air) is reduced in comparison with the reference case and case A. For example, in the pure methane fuelling mode the primary air mass flow amounts to about 3.2E–2 kg/s in the reference case, to about 3.3E–2 kg/s in case A and to only about 1.9E–2 kg/s in case B. The primary combustion air mass flow modification in case B was identified as a major factor contributing to a change in combustion static temperature. The modification of the air supplied into the liner can affect the air-fuel equivalence ratio repartition in graduated combustion. An increase in the maximum combustion static temperature would indicate that there is a zone inside the liner where the air-fuel equivalence ratio is close to the stoichiometric condition (case B). This hypothesis will be tested in the next section of this paper.

Secondly, it can be noticed that the maximum combustion static temperature increases as the hydrogen mass fraction in the fuel is increased. The maximum combustion static temperature evolves from 2234–2248 K to 2371–2390 K. An increase in the maximum static temperature by about 140 K occurs when pure methane fuelling is changed to fuelling with a 0.5 hydrogen mass fraction in the fuel. The methane maximum adiabatic combustion temperature is 2250 K [14, 15], which corresponds to the result obtained in the cases with pure methane fuelling. The hydrogen maximum adiabatic combustion temperature is 2400 K [14, 15], which corresponds to the results obtained in the case with a 0.5 hydrogen mass fraction in the fuel. The increase in combustion temperature was expected for the hydrogen enriched fuel and the obtained results are consistent with the chemical and physical combustion properties of the fuel.

Summing up, one should note that the maximum combustion static temperature is lowest in the reference case and highest in case B, regardless of the hydrogen mass fraction in the fuel. At the same time the maximum combustion static temperature results for case A are closely comparable with the ones for the reference case. It emerges from the discussion of the results that the maximum combustion static temperature modification can be linked to the air-fuel equivalence ratio modification. This hypothesis will be tested in the next section of this paper. The addition of a 0.5 hydrogen mass fraction to the methane fuel provokes a rise in the maximum combustion static temperature by about 140 K. This observation is consistent with the chemical and physical combustion properties of the fuels.

In the third part of this subsection, the exhaust total temperature is analysed. This is one of the most important parameters describing a combustor. The evolution of the averaged exhaust gas total temperature is presented in Fig. 13.

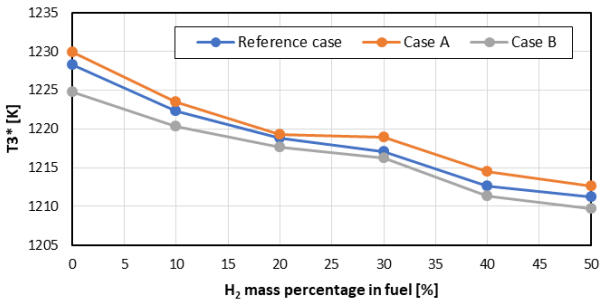

Fig. 13. Averaged exhaust gas total temperature

Firstly, it can be noticed that the averaged exhaust gas total temperature is highest in case A, lowest in case B and intermediate in the reference case, regardless of the hydrogen mass fraction in the fuel. In each of the fuelling cases the exhaust temperature values are relatively close. For example, in the pure methane fuelling mode the exhaust total temperature ranges from 1225 K to 1230 K. According to the preliminary simplified combustor calculations (see Table 1), the exhaust total temperature was to amount to about 1185 K. The relative difference in exhaust total temperature between the simplified gas microturbine design calculation result and the simulation result for the reference case amounts to about 3.65%. Considering that the design calculation model was much simplified and did not take into account the combustion chamber's shape which has a major impact on combustor exhaust total temperature, this difference is acceptable. Moreover, the difference in exhaust

total temperature between the reference case and the IFGR cases is negligible, regardless of the hydrogen mass fraction in the fuel. The fact that the exhaust total temperature remains at the same level in all the studied cases is highly important as it indicates that the implementation of the IFGR system will not alter this combustor operating parameter.

Secondly, one should note that the exhaust total temperature drops from the range of 1225–1230 K (pure methane fuelling) to the range of 1210–1213 K (for the 0.5 hydrogen mass fraction in the fuel). This means that the exhaust total temperature decreases by 15–17 K when hydrogen is added to the fuel. The decrease can be due to two factors: 1) a fuel supply calculation inaccuracy and 2) the fact that the addition of hydrogen to the fuel results in an extension of the flammability range and in incomplete combustion in the liner. This hypothesis needs to be tested since if incomplete combustion occurred in the liner, this would increase the risk of combustion in the turbine part of the gas microturbine. Although the decrease in exhaust total temperature can be neglected in terms of value, there is a need to check if this temperature drop stems from incomplete combustion. In the next subsection, for all the hydrogen mass fractions the total air-fuel equivalence ratio (in the combustion chamber) will be compared with the air-fuel equivalence ratios defining the range of flammability of the air-fuel mixture.

Summing up, one should note that the IFGR implementation does not significantly affect the exhaust total temperature, regardless of the hydrogen mass fraction in the fuel. When hydrogen is added to the methane fuel, a small decrease in exhaust total temperature occurs. Even though the decrease is negligible, it should be checked if it is linked with incomplete combustion in the liner (due to a flammability range extension caused by the addition of hydrogen to the fuel). This hypothesis will be tested in the next section of this paper.

From the above observations one can conclude that the implementation of the IFGR system into the gas microturbine combustor does not significantly affect the combustion temperature homogeneity and the exhaust total temperature, but it has an impact on the maximum combustion static temperature (especially in case B). The positive effect is that the exhaust total temperature is not significantly altered when the IFGR system is implemented. The fact that the combustion static temperature homogeneity is not significantly affected by the IFGR system implementation is of neutral consequence. Finally, the conservation or even augmentation (case B) of the maximum combustion static temperature when the IFGR system is implemented is a negative effect. This effect is probably due to the modification of the air-fuel ratio, which will be checked in the next subsection of this paper.

4.4. Impact of IFGR system on lambda ratio

This section is divided in two parts. The first part is dedicated to the analysis of the air-fuel equivalence ratio, aimed at explaining the increase in the maximum combustion temperature in case B. The air-fuel equivalence ratios occurring in the combustion chamber were determined on the basis of the liner air and exhaust gas mass flow repartition and the combustion properties of the fuel (methane and hydrogen) [41–43]. The oxygen present in the exhaust gases was taken into account in the air-fuel equivalence ratio calculations. The air-fuel equivalence ratio values are presented in Table 6. The primary zone is the liner's part which air and exhaust gases (coming from the IFGR system) enter. The hole series I to IV are perimetrical hole series located on the liner, enabling combustion to occur. The cooling hole series are holes located in the liner's end part, letting cooling air in. The "IFGR out" designation in table 6 is the liner outlet air-fuel equivalence ratio after some of the exhaust gas is taken by the IFGR system.

According to Table 6, the air-fuel equivalence ratios are closest to unity after liner hole series no. II. Figure 14 shows the air-fuel equivalence ratios for the second liner hole series.

One should note the decrease in the amount of oxygen supplied into the primary combustion zone in IFGR combustion case B in comparison with the reference case and case A. As a result of this decrease the augmentation of the

Table 6. Air-fuel equivalence ratios

Case	$\lambda^{Total}_{Prim.zone}$ [–]	$\lambda^{Total}_{Hole\ I}$ [–]	$\lambda^{Total}_{Hole\ II}$ [–]	$\lambda^{Total}_{Hole\ III}$ [–]	$\lambda^{Total}_{Hole\ IV}$ [–]	$\lambda^{Total}_{Cool.hole}$ [–]	$\lambda^{Total}_{IFGR\ out}$ [–]
R00H2	0.38	0.53	1.20	1.35	2.01	2.96	2.96
R10H2	0.39	0.55	1.24	1.40	2.10	3.09	3.09
R20H2	0.40	0.56	1.28	1.44	2.16	3.18	3.18
R30H2	0.40	0.57	1.30	1.47	2.21	3.25	3.25
R40H2	0.41	0.58	1.33	1.50	2.25	3.32	3.32
R50H2	0.42	0.60	1.36	1.53	2.29	3.37	3.37
A00H2	0.39	0.54	1.21	1.36	2.02	2.97	2.96
A10H2	0.40	0.56	1.25	1.41	2.10	3.09	3.09
A20H2	0.41	0.57	1.29	1.45	2.16	3.18	3.18
A30H2	0.42	0.59	1.32	1.49	2.22	3.26	3.25
A40H2	0.42	0.60	1.34	1.52	2.26	3.33	3.32
A50H2	0.44	0.61	1.37	1.54	2.30	3.38	3.37
B00H2	0.24	0.40	1.10	1.27	1.97	2.97	2.96
B10H2	0.25	0.42	1.15	1.32	2.05	3.10	3.09
B20H2	0.25	0.43	1.18	1.36	2.11	3.19	3.18
B30H2	0.26	0.44	1.21	1.39	2.16	3.26	3.25
B40H2	0.26	0.45	1.23	1.42	2.20	3.33	3.32
B50H2	0.27	0.45	1.26	1.44	2.24	3.39	3.37

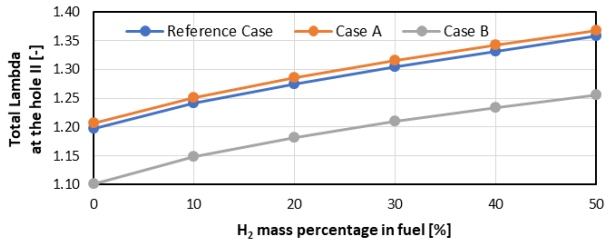

Fig. 14. Air-fuel equivalence ratios located after second liner hole series

total air-fuel equivalence ratio is delayed. Regardless of the hydrogen mass fraction in the fuel, case B has the lowest total lambda after the second liner hole series, which is closest to unity, especially in the pure methane fuelling mode. This observation is consistent with the temperature evolution described in the previous section. The augmentation of the maximum combustion static temperature in case B is connected rather with the modification of the air mass flow than with the exhaust gases recirculated by the IFGR system.

The second part of this section is dedicated to determining the evolution of the combustion zone in the studied combustor cases when hydrogen is added to the fuel. The fuel combustion ranges were determined [41–44] and compared with the air-fuel equivalence ratios in the liner's top part and its end part. As a result, it was found whether the combustion conditions were met in the two parts of the liner. The results of this analysis are presented in Table 7.

Firstly, according to the results presented in Table 7, the conditions in the primary combustion zone are met in the reference combustor and in the case A combustor when the hydrogen mass fraction in the fuel is larger than 0.2. Whereas in case B the combustion conditions in the primary combustion zone are not met. The main objective of the primary zone is to assure good air-fuel mixing in order to obtain a homogeneous mixture. Generally, combustion processes should be limited in this zone. When hydrogen, amounting to a 0.2 mass fraction, is added to the fuel, combustion occurs in the primary zone in the reference case and in case A. Only in case B combustion does not occur in the primary zone. This is due to a primary zone air mass flow reduction connected with the venturi shaped mixing pipes (Table 5). As regards the displacement of the flame into the top zone of the liner, the IFGR system case A does not present any advantages (in comparison with the reference case) and in case B the combustion conditions are not met in the top part of the liner (but this is just due to the primary air mass flow reduction).

Secondly, the addition of hydrogen to the fuel provokes an increase in the air-fuel equivalence ratio at which combustion can occur. According to the data presented in Table 7, beginning with the first hydrogen addition (a 0.1 mass fraction) the value of the total lambda at the combustion chamber's outlet is lower than the maximum lambda value at which fuel combustion can occur. This applies to the reference case and the IFGR cases. The addition of hydrogen alters the combustion design in the liner: combustion occurs in the whole liner, even in the cooling zone. When hydrogen is added, the temperature of the exhaust gases drops (Fig. 13) because the combustion is not complete yet. There is a risk that the combustion process will continue after the mass flow leaves the combustion chamber in the turbine. This risk cannot be reduced by implementing the IFGR system since the latter does not modify the final total air-fuel equivalence ratio.

Summing up, one should note that the increase in the maximum combustion static temperature in IFGR case B stems from the air-fuel equivalence ratio modification. When hydrogen amounting to a mass fraction of over 0.2 is added to the fuel, the combustion conditions in the primary zone are met in the reference case and in IFGR case A. In IFGR case B the combustion conditions in the primary zone are not met for the whole range of hydrogen additions. The drop in exhaust total temperature after hydrogen addition is the consequence of a combustion range extension resulting in a combustion zone expansion even to the turbine's inlet.

Table 7. Primary air zone and exhaust zone lambda vs flammability limit lambda

Case	λ_{min} [–]	$\lambda^{Total}_{Prim.zone}$ [–]	State	$\lambda^{Total}_{IFGR\,out}$ [–]	λ_{max} [–]	State
R00H2	0.592	0.38	No combustion	2.96	1.985	No combustion
R10H2	0.510	0.39	No combustion	3.09	3.441	Combustion
R20H2	0.442	0.40	No combustion	3.18	4.656	Combustion
R30H2	0.384	0.40	Combustion	3.25	5.685	Combustion
R40H2	0.334	0.41	Combustion	3.32	6.569	Combustion
R50H2	0.291	0.42	Combustion	3.37	7.335	Combustion
A00H2	0.592	0.39	No combustion	2.96	1.985	No combustion
A10H2	0.510	0.40	No combustion	3.09	3.441	Combustion
A20H2	0.442	0.41	No combustion	3.18	4.656	Combustion
A30H2	0.384	0.42	Combustion	3.25	5.685	Combustion
A40H2	0.334	0.42	Combustion	3.32	6.569	Combustion
A50H2	0.291	0.44	Combustion	3.37	7.335	Combustion
B00H2	0.592	0.24	No combustion	2.96	1.985	No combustion
B10H2	0.510	0.25	No combustion	3.09	3.441	Combustion
B20H2	0.442	0.25	No combustion	3.18	4.656	Combustion
B30H2	0.384	0.26	No combustion	3.25	5.685	Combustion
B40H2	0.334	0.26	No combustion	3.32	6.569	Combustion
B50H2	0.291	0.27	No combustion	3.37	7.335	Combustion

4.5. Impact of IFGR system on CO and NO_x concentrations

The CO concentrations in exhaust were calculated from formula 6 and are presented in Fig. 15.

$$CO = \frac{CO_{mole\_fraction}}{1 - H_2O_{mole\_fraction}} \cdot 10^6 \quad (6)$$

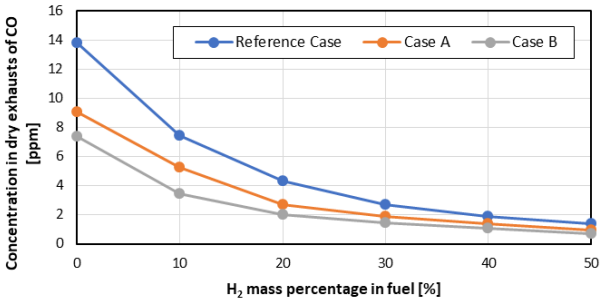

Fig. 15. CO concentrations in exhaust

Firstly, the CO concentrations show a decreasing trend from the reference case to case B. For all the IFGR cases CO concentrations are below 10 ppm. The decreasing values of CO concentrations correspond to an increase in the maximum combustion static temperature and to the recirculation of some of the exhaust gas mass flow. This reduction in CO concentrations can be due to two facts: 1) the combustion temperature increases from the reference case to case B and so the concentrations decrease and 2) some of the CO present in the exhaust gases is recirculated into the combustion zone and this CO is reburnt, which results in a reduction in CO concentration in the IFGR cases. The CO concentration trend is maintained for the whole range of hydrogen mass fractions in the fuel.

Secondly, the CO concentrations decrease as hydrogen is added to the fuel, regardless of the combustor case. This is due to the augmentation of the maximum combustion static temperature (see Fig. 12) and the degradation of combustion temperature homogeneity (see Fig. 11), resulting from hydrogen addition.

Finally, the reduction in CO concentrations is connected with the augmentation of the maximum combustion static temperature, which occurs in all the IFGR cases (especially in case B) and when hydrogen is added to the fuel.

The NO_x concentrations in exhaust were calculated from formula 7 and are presented in Fig. 16.

$$NO_x = \frac{NO_{mole\_fraction} + NO_{2\,mole\_fraction}}{1 - H_2O_{mole\_fraction}} \cdot 10^6 \quad (7)$$

Firstly, as regards NO_x concentrations, they increase from the reference case to case B. In this kind of power devices NO_x concentrations are strongly linked with the thermal NO mechanism. As the maximum combustion temperature increases from the reference case to case B (Fig. 12), so do NO_x concentrations. This is consistent with the CO concentrations and the maximum combustion temperature evolution. The NO_x concentration trend is maintained for the whole range of hydrogen mass fractions in the fuel.

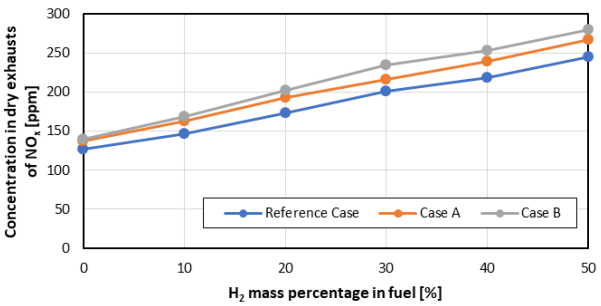

Fig. 16. NO_x concentrations in exhaust

Secondly, the NO_x concentrations decrease as hydrogen is added to the fuel, regardless of the combustor case. This is due to the augmentation of the maximum combustion static temperature (see Fig. 12) and the degradation of combustion temperature homogeneity (see Fig. 11), resulting from hydrogen addition.

Finally, the increase in NO_x concentrations in exhaust is connected with the augmentation of the maximum combustion static temperature, which occurs in all the IFGR cases (especially in case B) and when hydrogen is added to the fuel.

Summing up, the implementation of the IFGR system results in a reduction in CO concentrations and at the same time in an increase in NO_x concentrations. The most remarkable changes in pollutant concentrations in exhaust occur in case B. The changes are due to the increase in combustion temperature. The temperature augmentation is connected with the air-fuel equivalence ratio modification in the IFGR cases and with the increase in the hydrogen mass fraction in the fuel. The IFGR system does not affect the emissivity of the combustor through the expected chemical and physical effects (described in the Introduction) because the exhaust gas mass flow is too low to have a significant effect on the combustion process. The observed pollutant concentration modifications resulting from the implementation of the IFGR system are connected with the modification of the air-fuel equivalence ratio in the combustor's liner.

5. Conclusion

The observations and conclusions relating to the implementation of an autonomous IFGR system into the gas microturbine in the context of the co-combustion of higher hydrogen enriched methane fuel are listed below:

- it is possible to achieve autonomous exhaust gases recirculation inside a gas microturbine combustor at various hydrogen mass fractions in the fuel by applying an adequate IFGR pipe system;
- the maximum exhaust gases recirculation is obtained in combustor case B, regardless of the hydrogen mass fraction in the fuel;
- the IFGR ratios are constant in case A, whereas in case B they decrease as the hydrogen mass fraction in the fuel increases;
- the IFGR system design reduces the risk of overheating the IFGR pipes;
- the IFGR system implementation into the combustor does not significantly affect the total pressure drop at

various hydrogen fuelling options – the combustor's pressure operating parameters are not altered when the IFGR system is implemented;
- the implementation of the IFGR system into the gas microturbine combustor does not significantly affect the combustion temperature homogeneity at a constant hydrogen mass fraction in the fuel;
- the addition of hydrogen to the fuel results in the degradation of combustion static temperature homogeneity in the reference case and in the IFGR cases;
- the implementation of the IFGR system provokes maximum combustion static temperature augmentation, especially in case B, regardless of the hydrogen mass fraction in the fuel;
- the addition of hydrogen to the fuel provokes maximum combustion static temperature augmentation in all the combustor cases;
- the maximum temperature augmentation, especially in case B, is due to the fact that the local air-fuel equivalence ratio approaches unity owing to the IFGR system design;
- for a constant hydrogen mass fraction in the fuel the exhaust total temperature in the reference case and in the IFGR cases is comparable;
- the addition of hydrogen to the fuel results in a decrease in the exhaust total temperature in all the combustor cases;
- the exhaust total temperature drop after hydrogen addition is due to a combustion range extension provoking a combustion zone expansion even to the inlet of the turbine;
- when hydrogen amounting to a mass fraction of over 0.2 is added to the fuel, the combustion conditions in the mixing pipes are met in the reference case and in IFGR case A;
- in IFGR case B the combustion conditions in the mixing pipes are not met for the whole range of hydrogen additions;
- the implementation of the IFGR system results in a reduction in CO concentrations and at the same time in an increase in NO_x concentrations (especially in case B);
- the addition of hydrogen to the fuel results in a reduction in CO concentrations and at the same time in an increase in NO_x concentrations (especially in case B);
- the pollutant concentration modifications are connected with the increase in combustion temperature;
- the IFGR system does not affect the emissivity of the combustor through the expected chemical and physical effects (described in the Introduction) because the exhaust gas mass flow is too low to have a significant effect;
- the observed pollutant concentration modifications resulting from the implementation of the IFGR system are connected with the modification of the air-fuel equivalence ratio in the combustor's liner.

The investigated IFGR system enables the recirculation of exhaust gases, but the recirculated exhaust gas mass flow is too low to act as expected on the combustion processes. The observed temperature and pollutant concentration modifications result from the modification of the combustion air-fuel equivalence ratio due to the modification of the combustor design. The autonomous IFGR system does not seem to be an efficient way of improving the combustion process in the gas microturbine combustor with or without adding hydrogen to the fuel. This concept would work if the recirculated exhaust gas mass flow was increased, for example, by an additional pumping system [12], but this would entail powering the latter and so power losses would occur. At this stage of the investigations, the MILD combustion design seems to be one of the most promising ways to reduce the combustion temperature and so the emissivity.

Nomenclature

A_i area of facet defining analysed surface [m^2]
c air stream velocity [m/s]
CO carbon monoxide concentrations in exhaust [ppm]
$CO_{mole\_fraction}$ carbon monoxide mole fraction [–]
c_s fuel mass flow for pure methane fuelling mode [kg/s]
$c_s^{i\_H_2 mass\_fraction}$ fuel mass flow for hydrogen mass fraction i in fuel [kg/s]
$H_{2_{mass\_fraction}}$ hydrogen mass fraction in fuel [–]
$H_2O_{mole\_fraction}$ water vapor mole fraction [–]
$IFGR\%$ primary zone combustion IFGR ratio [%]
$IFGR\%*$ global combustion IFGR ratio [%]
LHV_{CH_4} lower heat value of methane fuel [kJ/kg]
LHV_{H_2} lower heat value of hydrogen fuel [kJ/kg]
Mass percentage [%] = Mass fraction [–] × 100
$\dot{m}$ air mass flow entering combustor [kg/s]
$\dot{m}_{fuelling\_pipe}$ air mass flow passing through fuelling pipes [kg/s]
$NO_{mole\_fraction}$ nitrogen oxide mole fraction [–]
NO_x nitrogen oxides concentrations in exhaust [ppm]
$NO_{2_{mole\_fraction}}$ nitrogen dioxide mole fraction [–]
p^* total pressure [Pa]
$p_2{}^*$ total pressure at combustor's inlet [Pa]
$p_3{}^*$ total pressure at combustor's outlet [Pa]
Δp^* total pressure drop in combustor [%]
UI_{area}^{plane} area averaged uniformity index [–]
$T_{average}$ average static temperature in analysed cross-section [K]
T_{face_i} static temperature on i-th facet defining analysed surface [K]
$Tmax$ static maximum temperature in combustor [K]
$T3^*$ total exhaust temperature [K]
T^* total temperature [K]
$\lambda_{Hole\_serie\_i}^{Total}$ total air-fuel equivalence ratio for i-th hole series location [–]
$\lambda_{max(min)}$ explosive limit air-fuel equivalence ratio [–]

Bibliography

[1] Boudellal M. Power to Gas. De Gruyter. 2018. https://doi.org/10.1515/9783110559811

[2] Sterner M, Jentsch M, Holzhammer U. Energiewirtschaftliche und ökologische Bewertung eines Windgas-Angebotes. Fraunhofer Institute Raport. Kassel 2011.

[3] Fąfara J-M, Modliński NJ. Internal flue gas recirculation system in the gas microturbine as a way for the co-combustion of higher enriched hydrogen fuel. In: Kudela H, Cholewiński M, Machalski A. (Eds.). II edition of the XII Conference Young Scientists In Power Engineering – Book of abstracts. 153-154. Publishing House of the Wroclaw University of Science and Technology. Wroclaw 2020.

[4] Lav C, Kaul C, Singh R, Rai A. Potential of micro turbines for small scale power generation. Int J Adv Infor Sci Tech. 2013;2(5):35-39. https://doi.org/10.15693/ijaist/2013.v2i5.77-81

[5] Jerzak W. Adiabatic flame temperature and laminar burning velocity of CH_4/H_2/air mixtures. Archiwum Spalania. 2011; 11(3-4):197-206. https://www.researchgate.net/publication/260244139_Adiabatic_flame_temperature_and_laminar_burning_velocity_of_CH4H2air_mixtures_in_Polish

[6] Güthe F, García M, Burdet A. Flue gas recirculation in gas turbine: Investigation of combustion reactivity and NO_x emission. Proceedings of the ASME Turbo Expo. Orlando 8-12.06.2009. https://doi.org/10.1115/GT2009-59221

[7] Liu F, Guo H, Smallwood G. The chemical effect of CO_2 replacement of N_2 in air on the burning velocity of CH_4 and H_2 premixed flames. Combust Flame. 2003;133(4):495-497. https://doi.org/10.1016/S0010-2180(03)00019-1

[8] Ditaranto M, Li H, Løvås T. Concept of hydrogen fired gas turbine cycle with exhaust gas recirculation: Assessment of combustion and emissions performance. Int J Greenh Gas Con. 2015;(37):377-383. https://doi.org/10.1016/j.ijggc.2015.04.004

[9] Engineering ToolBox. Carbon Dioxide Gas – Specific Heat. 2005. https://www.engineeringtoolbox.com/carbon-dioxide-d_974.html (accessed on 28.06.2020).

[10] Engineering ToolBox. Water Vapor – Specific Heat. 2005. https://www.engineeringtoolbox.com/water-vapor-d_979.html (accessed on 28.06.2020).

[11] Engineering ToolBox. Air – Specific Heat at Constant Pressure and Varying Temperature. 2004. https://www.engineeringtoolbox.com/air-specific-heat-capacity-d_705.html (accessed on 28.06.2020).

[12] Gieras M. Miniaturowe silniki turboodrzutowe (Microturbojet engine). Publishing House of the Warsaw University of Technology. Warsaw 2016.

[13] Shi B, Hu J, Peng H, Ishizuka S. Effects of internal flue gas recirculation rate on the NO_x emission in a methane/air premixed flame. Combust Flame. 2018;(188):199-211. https://doi.org/10.1016/j.combustflame.2017.09.043

[14] Jadidi M, Moghtadernejad S, Dolatabadi A. A comprehensive review on fluid dynamics and transport of suspension/liquid droplets and particles in high-velocity oxygen-fuel (HVOF) thermal spray. Coatings. 2015;5(4):576-645. https://doi.org/10.3390/coatings5040576

[15] Taamallah S, Vogiatzaki K, Alzahrani FM, Mokheimer EMA, Habib MA, Ghoniem AF. Fuel flexibility, stability and emissions in premixed hydrogen-rich gas turbine combustion: technology, fundamentals, and numerical simulations. Appl Energ. 2015;(154):1020-1047. https://doi.org/10.1016/j.apenergy.2015.04.044

[16] Wang L, Qi D, Sui X, Xie X. Analysis of re influence on MILD combustion of gas turbine. Energ Power Eng. 2013;(5):92-96. https://doi.org/10.4236/epe.2013.54B018

[17] Karpiński B, Szkodo M, Stąsiek J et al. High temperature air combustion. Energetyka. 2014;12(726):735-737.

[18] Mi J, Li P, Wang, F., Cheong K-P, Wang G. Review on MILD combustion of gaseous fuel: its definition, ignition, evolution, and emissions. Energ Fuel. 2021;35(9):7572-7607. https://doi.org/10.1021/acs.energyfuels.1c00511

[19] Mameri A, Tabet F, Aggab Y et al. MILD Combustion of hydrogenated biogas in opposed jet configuration. Proceedings of the 2nd International Workshop on CFD and Biomass Thermochemical Conversion. Leipzig 9.09.2016. https://www.researchgate.net/publication/340310099_MILD_Combustion_of_hydrogenated_biogas_in_opposed_jet_configuration

[20] Webera W, Guptab AK, Mochidac S. High temperature air combustion (HiTAC): how it all started for applications in industrial furnaces and future prospects. Appl Energ. 2020; (278):115551. https://doi.org/10.1016/j.apenergy.2020.115551

[21] Fortunato V, Giraldo A, Rouabah M, Nacereddine R, Delanaye M, Parente A. Experimental and numerical investigation of a MILD combustion chamber for micro gas turbine applications. Energies. 2018;11(12):3363. https://doi.org/10.3390/en11123363

[22] Albin T, Aguiar Da Franca A, Varea E et al. Potential and challenges of MILD combustion control for gas turbine applications. In: King R. (Eds.). Active Flow and Combustion Control – Notes on Numerical Fluid Mechanics and Multidisciplinary Design. 2015, 127. Springer.

[23] Ansys website. https://www.ansys.com/ (accessed on 25.05.2021).

[24] Gieras M, Stańkowski T. Computational study of an aerodynamic flow through a micro turbine engine combustor. J Power Technol. 2012;92(2):68-79.

[25] Suchocki T, Lampart P, Klonowicz P. Numerical investigation of a GTM 140 turbojet engine. Open Eng. 2015;(5): 478-484. https://doi.org/10.1515/eng-2015-0053

[26] Dias FLG, Do Nascimento MAR, De Oliveira Rodrigues L. Reference area investigation in a gas turbine combustion chamber using CFD. J Mech Eng Autom. 2014;4(2):73-82. https://doi.org/10.5923/j.jmea.20140402.04

[27] Vilag V, Vilag J, Carlanescu R, Mangra A, Florean F. CFD application for gas turbine combustion simulations. In: Ji G,, Zhu J. (Eds.). Computational Fluid Dynamics Simulations. IntechOpen. 2019. https://doi.org/10.5772/intechopen.89759

[28] Gonzalez C, Wong KC, Armfield S. Computational study of a micro turbine engine combustor using Large Eddy Simulation and Reynolds Averaged turbulence models. ANZIAM Journal. 2008;49(2007):407-422. https://doi.org/10.21914/anziamj.v49i0.338

[29] Sosnowski M, Krzywanski J, Gnatowska R. Polyhedral meshing as an innovative approach to computational domain discretization of a cyclone in a fluidized bed CLC unit. E3S Web Conf. 2017;(14):01027. https://doi.org/10.1051/e3sconf/20171401027

[30] Qureshi Z, Chan A. A study of the effect of element types on flow and turbulence characteristics around an isolated high-rise building. Eleventh International Conference on CFD in the Minerals and Process Industries. CSIRO. Melbourne 7-9.12.2015. https://www.cfd.com.au/cfd_conf15/PDFs/035IQB.pdf

[31] Matyushenko A, Stabnikov A, Garbaruk A. Criteria of computational grid generation for turbulence models taking into account laminar-turbulent transition. J Phys: Conf Ser. 2019;(1400):077047. https://doi.org/10.1088/1742-6596/1400/7/077047
[32] Ansys, Inc. Ansys Fluent Theory Guide – Release 15.0. 2013.
[33] Suchocki T, Lampart P, Surwiło J. Designation of operating characteristics for micro-jet engine and CFD validation. Mechanik. 2015;(7):813-820. https://doi.org/10.17814/mechanik.2015.7.301
[34] Smith T, Shen Z, Friedman J. Evaluation of coefficients for the weighted sum of gray gases model. J Heat Transfer. 1982;104(4):602-608. https://doi.org/10.1115/1.3245174
[35] Fuchs F, Meidinger V, Neuburger N, Reiter T, Zündel M, Hupfer A. Challenges in designing very small jet engines fuel distribution and atomization. International Symposium on Transport Phenomena and Dynamics of Rotating Machinery. Honolulu 10-15.04.2016. https://hal.archives-ouvertes.fr/hal-01891309/document
[36] Peters N. Turbulent Combustion. Cambridge University Press. 2000.
[37] Smith GP, Golden DM, Frenklach M et al. Welcome to the GRI-Mech Home Page! http://www.me.berkeley.edu/gri_mech/ (accessed on 25.05. 2021).
[38] Ji C, Du W, Yang J, Wang S. A comprehensive study of light hydrocarbon mechanisms performance in predicting methane/hydrogen/air laminar burning velocities. Int J Hydrogen Energ. 2017;(42):17260-17274. https://doi.org/10.1016/j.ijhydene.2017.05.203
[39] Launder BE, Spalding DB. The numerical computation of turbulent flows. Comput Method Appl M. 1974;3(2):269-289. https://doi.org/10.1016/0045-7825(74)90029-2
[40] Ansys, Inc. Ansys Fluent Tutorial Guide – Release 18.0. Ansys 2017.
[41] Air liquid. Gas encyclopedia – Méthane. 2021. https://encyclopedia.airliquide.com/fr/methane (accessed on 19.06.2021).
[42] Air liquid. Gas encyclopedia – Hydrogène. 2021. https://encyclopedia.airliquide.com/fr/hydrogene (accessed on 19.06.2021).
[43] Air liquid. Gas encyclopedia – Oxygène. 2021. https://encyclopedia.airliquide.com/fr/oxygene (accessed on 19.06.2021).
[44] PDF4PRO. AFC International, Inc. – Gas Detection&Air Monitoring Specialists – Combustibles. 2017. https://pdf4pro.com/view/combustible-gas-chart-596617.html (accessed on 20.06.2021).

Jean-Marc Fąfara, MEng. – Faculty of Mechanical and Power Engineering, Wroclaw University of Science and Technology.
e-mail: *jean-marc.fafara@pwr.edu.pl*

Norbert Modliński, DSc., DEng. – Faculty of Mechanical and Power Engineering, Wroclaw University of Science and Technology.
e-mail: *norbert.modlinski@pwr.edu.pl*

Article citation info:
Stępień Z. Synthetic automotive fuels. Combustion Engines. 2023;192(1):78-90. https://doi.org/10.19206/CE-152526

Zbigniew STĘPIEŃ

Combustion Engines
Polish Scientific Society of Combustion Engines

Synthetic automotive fuels

ARTICLE INFO

Received: 14 June 2022
Revised: 28 July 2022
Accepted: 31 July 2022
Available online: 3 August 2022

The article explains the differences between synthetic fuels of first and second generation. The potential of e-fuels to reduce GHG emissions was indicated. The application requirements that synthetic fuels need to meet in order to be used for powering internal combustion engines have been described. The possibility of using synthetic fuels as "drop-in" fuels, in blends with conventional petroleum-derived fuels as well as by themselves was discussed. E-fuels developed and optimized to power compression ignition and spark ignition engines were characterized. The possibilities of synthetic fuels to reduce emissions of regulated and unregulated exhaust components and to improve the work and operational parameters of the engine were also analyzed using the research carried out so far as basis. At the end of the article, forecasts for synthetic fuels development and applications were presented in the form of a SWOT analysis.

Key words: *synthetic fuels, combustion engines, synthetic fuel applications, exhaust emissions*

1. Introduction

The statutory requirements for climate protection result in an increasing need for a drastic reduction of greenhouse gases (GHG) generated by the transport sector. At the same time, the current and future limit values for exhaust emissions from regulated internal combustion engines must be met. Given the need to diversify future types of powertrains, several technological options are being considered. In particular, battery electric vehicles (BEV), fuel cell electric vehicles (FCEV), and advanced low-emission fuels, such as synthetic fuels and renewable biofuels [8, 11, 18, 23, 29, 30, 39, 40–43, 46], are mentioned as potential solutions to reduce greenhouse gas emissions in the transport sector. In order to minimize the total CO_2 emissions, it is necessary to rationally use various drive systems technologies, including internal combustion engines powered by synthetic fuels. It should not be forgotten that greenhouse gas emissions and climate change are inherently a global and complex problem that requires an integrated approach, one that encourages innovation and avoids dependence on a single technology. Meanwhile, the current EU legal regulations focus solely on e-mobility, leaving no room for other technologies or technological competition to achieve climate goals. This approach indicates a departure from the current practice of adopting a balance between different technologies. The significant potential to reduce CO_2 from the existing vehicle fleet is also being ignored. However, looking at the future development of the global vehicle fleet, even assuming a significant level of electrification of all newly registered vehicles in the coming years, a significant reduction in CO_2 emissions could still be achieved using even low levels of synthetic fuels admixture with classic fuels. The use of fully synthetic fuels to power internal combustion engines could bring even greater benefits, provided that the vehicles are properly adapted and optimized for the use of such fuels [11, 18, 23, 29, 30, 39, 40–43, 47]. Contrary to the complex influence of various factors on CO_2 emissions accompanying the rapid take-up of BEVs, where introducing large amounts of BEV too early may increase overall CO_2 emissions, the situation is almost linear for synthetic fuels. The sooner and more of them are introduced, the greater the benefits will be achieved in terms of reducing CO_2 emissions.

Synthetic fuels make it possible to integrate mobility into the sustainable energy systems of the future. They are assessed according to five criteria: I – CO_2 neutrality, II – sustainable availability, III – environmental impact, IV – cost effectiveness and V – functionality. Synthetic fuels appear in the literature under various names, such as: PtL (Power-to-Liquid), PtX (Power-to-X), Power-to-Gas (PtG), SynFuels, e-fuels.

Generally speaking, when synthetic fuels are used, the reduction in well-to-wheel CO_2 emissions depends on the production methods of these fuel components and can be as high as 100% when the CO_2 emitted by the synthetic fuel vehicle is fully neutralized by atmospheric CO_2 capture systems, given the electricity was also generated using renewable energy sources [18].

The sustainable production of Fischer-Tropsch diesel fuel using CO_2 and H_2 makes first-generation synthetic fuels, whose main components are isoalkanes and n-alkanes with a chain length of 11–22 [10]. However, these fuels are classified as harmful to human health and the environment. The ecological situation forces the introduction of fuels which are neutral in terms of CO_2 emissions, so having net zero emissions, but at the same time pose less of a threat to people and the environment. Since first-generation synthetic fuels (SynFuels) were classified as hazardous substances, they cannot achieve this goal. Therefore, it is necessary to introduce the second generation of fuels with further reduced ecological impact.

E-fuels are synthetic fuels, resulting from the combination (synthesis) of "green hydrogen" produced by water electrolysis (e.g. using sea water) powered with renewable electricity and CO_2 captured from a concentrated source (e.g. exhaust fumes from an industrial plant) or directly from the air by carbon capture. Thus, fuels that are synthesized using renewable electricity, often using inorganic raw materials, are classified as e-fuels. E-fuels include liquid and gaseous hydrocarbons such as methane and various

gasoline-like fuels, diesel fuel, alcohols such as ethanol and methanol, and non-carbon fuels such as hydrogen and ammonia. Once refined, the produced e-fuels can be used as e-petrol, e-diesel, e-fuel oil and e-kerosene – and can completely replace conventional fuels in their roles. Due to their "drop-in" properties (can be used directly to power in-service internal combustion engines without the need for modification or tuning), e-fuels can be mixed with conventional fuels in any proportion for better effect.

They offer high energy parameters, are easy to transport and enable long-term storage without energy losses, and therefore have significant advantages over propulsion technologies based on either hydrogen or electric batteries [23, 29, 30, 39, 40–43, 48]. The analysis of the potential offered by synthetic fuels, in particular second-generation fuels (e-fuels) in automotive applications, became the motivation behind this article.

2. Requirements set for synthetic fuels

Synthetic fuels that are currently in production, including e-fuels, must meet the requirements of EN 228 or EN590 norms. In this case, they are referred to as "drop-in" fuels and therefore directly applicable for use in current internal combustion engines as single fuels or as admixtures to conventional hydrocarbon fuels.

Conventional petroleum fuels are complex mixtures of hundreds of individual components, separated through various stages of crude oil refining, the purpose of which is to achieve specific target fuel properties optimized for the requirements of internal combustion engines. Therefore, the baseline feature of each developed e-fuel should be its ability to as closely as possible resemble the properties of fuels (both physical and chemical) specified in the EN 228 or EN 590 norms [34]. This can be achieved through the proper selection and optimisation of the most important fuel properties presented in Table 1, which are relevant to the efficiency, performance, handling characteristics and emissions of harmful engine exhaust components [22].

The synthetic fuels production technology allows for selectively influencing the final properties of the obtained fuel. In this way, within certain limits, it is possible to produce a fuel that reduces harmful exhaust components and/or allows to achieve higher engine efficiency. Examples include the C/H/O ratio and the aromatic content of the fuel. If the C/H/O ratio is shifted slightly in favor of a higher hydrogen content and a higher oxygen content, it will significantly reduce the amount of toxic components emitted by the engine they are fed to. Another example are diesel fuels in which a homogeneous, uniform combustible mixture is created [22]. The processes of homogeneous charge combustion require stable conditions of ignition, for which the fuel has a relatively large range of ignition delay times independent of the temperature. In addition, the fuel in question must have appropriate auto-ignition properties. This can be achieved by using to the optimal composition of carbon, hydrogen and oxygen, as well as by managing the chain lengths of alkanes and alkenes. In this respect, the composition of e-fuel may also be a starting point for the development and implementation of alternative combustion processes, optimized to reduce emissions of harmful exhaust components (including GHG) or to improve engine efficiency.

Table 1. List of fuel properties that have significance with respect to the engine design and operation [22]

Fuel properties	Influences	Technical measures
Calorific value	Engine efficiency	–
Octane number	Irregular combustion/ engine knock/engine efficiency	Optimization of compression ratio and fuel composition
Cetane number	Flammability/ignition start/efficiency/ injectors contamination	Compression ratio control, fuel improvement admixture optimization
Oxygen content	Engine efficiency/ harmful contamination of the engine's fuel supply and combustion system elements	Mixture formation processes optimization
Excess air coefficient	Engine power and efficiency	Fuel injection and mixture preparation processes optimization
Flammability limits	Engine efficiency/ harmful contamination of the engine's fuel supply and combustion system elements	Ignition energy and compression ratio optimization
Boiling temperature	Engine efficiency/ harmful contamination of the engine's fuel supply and combustion system elements	Fuel injection and mixture preparation processes optimization
Enthalpy of evaporation	Preparation of the mixture/engine efficiency/ harmful contamination of elements of the engine's fuel supply and combustion system	Improving the quality of fuel atomization and mixture formation
Aromatics content	Harmful contamination of the engine's fuel supply and combustion system components	Fuel injection and mixture preparation processes optimization

If e-fuels are only to be used as "drop-in" fuels, the first stage of their use should include the optimization of various aspects of gasoline and diesel combustion processes. The aim is to obtain higher knock resistance in SI engines or high oxygen content, as well as a low content of aromatic compounds in order to reduce the formation of soot in the combustion processes of both diesel and gasoline [45, 51]. This will save fuel by, among others, reducing the necessary frequency of the diesel particulate filter regeneration. The introduction of singular, standardized e-fuels could further change the direction of the development of fuels, but also engines, allowing them to be optimized both to the requirements of combustion processes and those related to the reduction of harmful exhaust emissions.

In the case of spark ignition (SI) engines, the research and motor octane number determines the resistance of a given fuel to unplanned detonation (engine knock), and thus the engine's ability to operate in the most effective conditions [34, 37]. While the specifications for octane numbers around the world vary slightly, e-fuels should have a Research Octane Number (RON) above 90–95 and a Motor Octane Number (MON) above 85–90. Density and boiling point are also important fuel properties ensuring the proper formation of a combustible mixture in the combus-

tion chamber in terms of its formation rate and mixing quality and thus preventing excessive amounts of leftover unburned hydrocarbons. These properties are usually determined by the molecular weight distribution of the fuel. The aromatics content of SI engine fuels is usually below 25% to avoid excessive particulate formation, and the alkene content is limited to 5% to maintain the required oxidation stability. Taking these limitations into account, an ideal e-fuel would be a suitable mixture of straight-chain and branched C_5–C_9 alkanes, C_5–C_6 cycloalkanes and/or C_7–C_9 aromatics [8]. The fraction of straight chain alkanes is usually restricted to the lower carbon chains as the octane number decreases with increasing chain length. Branched alkanes that have multiple methyl isomers are preferred, as this increases the octane number [4].

For compression ignition (CI) engines, the cetane number (CN) is an indicator of the ability of diesel fuels to ignite. Currently, typical CN values are in the range exceeding 50–55. A high CN allows achieving high combustion efficiency and high EGR (Exhaust Gas Recirculation) rates. Taking this into account, a CN of at least 55 is currently recommended [3, 57], and since the reduction of NO_x emissions is influenced by a high EGR factor, it is desirable to increase the minimum CN up to even 70 if possible [57]. Density, viscosity and final boiling point are also important properties that regulate the combustion processes of the atomized fuel, engine performance and the formation of toxic components. The initial boiling point being above 150°C reduces the negative effects that the fuel has on the elements of the fuel injection system, such as wear of its components due to cavitation. For Category 5 diesel fuels, WWFC (Worldwide Fuel Charter) also recommends a final boiling point of 350°C. Eventually, efforts will be made to lower the final boiling point to 260°C in order to facilitate fuel vaporization and to better homogenize the combustible mixture formed in the combustion chambers, as well as to reduce dilution of the lubricating engine oil.

3. E-fuels for SI engines

So far, the only e-fuel for SI engines to meet the requirements of second-generation synthetic fuel in terms of complete combustion, without the formation of soot particles and without products that are harmful to the environment and human health, is a mixture of dimethyl carbonate (DMC) and methyl formate (MF), called DMC+. DMC+ has very good anti-knock properties (RON/MON >110). Its vapor pressure is within the range required by the EN 228 norm, as is the final boiling point of 90°C [3, 45, 47, 48]. The significant reduction of the final boiling point, from 210°C for EN 228 gasoline to 120°C, improves the homogenization of the mixture formation and combustion process. Pre-ignition resistance, and limited pre-ignition related to the so-called "hot-spots", is the result of the full (almost complete) combustion of the DMC+ fuel. Hence, impurities are not deposited in the fuel injectors and in the combustion chambers.

Potentially CO_2 neutral fuels are most easily synthesized from carbon oxides, mainly CO_2 and CO. Methanol is a fuel for SI engines with excellent combustion properties. It is always a basic product, whose direct use as a fuel for vehicles (SynFuel of the first generation) is limited in scope due to its toxicity. The conversion of methanol to non-toxic DMC using CO_2 and to MF using CO significantly reduces the fuel's harmful effects on the environment. In the case of DMC+ fuel with the composition of DMC 65/MF 35% (v/v), the so-called negative fuel sensitivity of > 3 should be noted. Negative fuel sensitivity (MON > RON) means that the anti-knock properties of the fuel increase with the thermal load present. The advantage of DMC+ when used in SI engines is the improvement of their efficiency. This is possible thanks to the very good anti-knock properties and the cooling effect of DMC+ fuel vapors injected directly into the combustion chamber of the engine, three times higher than that of petrol. Downsized engines powered by DMC+ were found to have the engine efficiency increase by 10%, and at full load by about 19% [13].

The DMC admixture of 5–15% (v/v) to gasoline lowers HC emission [53]. DMC is a component that can be mixed with conventional gasoline. However, the negative properties of aromatic and olefin compounds (main high boiling point substances) present in gasoline that does meet the EN 228 requirements are further enhanced when mixed with oxygenates. This applies in particular to the soot particles number (PN) emission when 10% EtOH or DMC is added to the mixture. In a comparative study, in which DIN EN 228 gasoline was replaced with an alkyl fuel (E DIN 51641), free from aromatics and olefins, the final boiling point was found at: 180°C along with a significant reduction in PN emission [24].

MF admixture in gasoline increases its octane number [12]. However, mixtures of MF with benzene undergo hydrolysis in the presence of water [12]. Research is currently being carried out on the behavior and properties of fuel mixtures containing MF.

In the case of gasoline used in blends with DMC and MF it is recommended to change the formula of the base fuel by eliminating aromatics and olefins and lowering the final boiling point from 210°C to 170–180°C. Knock resistance is guaranteed by the addition of MF and/or DMC. For fuel blends containing MF intended for use in SI engines, additives are developed to inhibit the undesirable hydrolysis of MF.

4. E-fuels for CI engines

As a result of many studies, oxymethylene ether ($OME_{3–5}$) was selected as a second-generation synthetic fuel for compression ignition engines [10]. A special molecular feature of OME is the alternating sequence of carbon and oxygen atoms. The absence of C–C bonds and the high oxygen content lead to almost complete elimination of soot formation during combustion. The boiling range of $OME_{3–5}$ is within the limits of 150–250°C which, combined with high volatility, promotes the formation of homogeneous flammable mixtures. The boost pressure requirements can be reduced without adversely affecting particulate emissions resulting from the delayed boost pressure build-up. In addition, the complexity of the fuel injection system can also be reduced by depressurizing the common rail and by using an appropriately configured split injection strategy. However, to counterbalance the lower energy density (when used as pure $OME_{3–5}$ fuel), the total fuel injection dose should be increased by 80% compared to diesel fuel

by using larger diameter injector nozzle openings. Doubling the amount of fuel supplied into the cylinder also leads to a correspondingly increased cooling of the fuel dose in the cylinder through evaporation, and decreases the flame adiabatic temperature [32].

Standard $OME_{3–5}$ has a flash point of 60°C, a cetane number CN ≥ 70, and a boiling point range between 150 and 260°C [54, 55]. The final boiling point of the fuel is approximately 100°C lower than that of conventional diesel fuels, which leads to $OME_{3–5}$ evaporating easily. For further testing and possible market introduction of $OME_{3–5}$ as a standalone fuel or blend component, the quality of the $OME_{3–5}$ has to be standardized.

$OME_{3–5}$ can be a component of a diesel fuel blend while being in accordance with the EN 590 norm. A 20% (v/v) admixture of $OME_{3–4}$ into diesel fuel that meets the EN 590 B7 norm requirements results in a varied (throughout the engine operating range) reduction of the generated soot particulate mass, which can be found in the range of 50–80% of the original value [27]. This effect has been confirmed multiple times in the studies of mixtures containing 5–35% (v/v) $OME_{3–5}$ [2, 9, 20, 25, 31, 35]. However, in order not to exceed the limits specified in EN 590, the maximum admixture of $OME_{3–5}$ must not exceed 5–7% (v/v). The highly polar OME has a limited miscibility with the less polar diesel fuel, especially at higher proportions of OME content in the mixture and at low temperatures [7, 31, 52, 54]. The hygroscopic properties of OME facilitate water penetration of the substance. This leads to a significant increase in the polarity of OME [38]. Therefore, it is necessary to investigate the stability of mixtures with OME in cold conditions in more detail. Effective dissolving agents must be found to prevent phase separation in the mixtures.

5. The potential of synthetic fuels in reducing exhaust emissions and improving engine operational parameters

So far, one of the most comprehensive studies on the impact of e-fuels on regulated as well as unregulated exhaust emissions (taking into account the future requirements of Euro 7 norm), and the GHG of SI engines, was carried out in 2021 by IFP Energies nouvelles (IFPEN) based in France, which was commissioned by T&E (Transport & Environment). The tests were performed both on the chassis dynamometer as well as in simulated and real driving conditions [21]. As no e-fuels were commercially available at the time of the tests, IFPEN developed custom fuel blends for testing, representing e-fuels that could be placed on the EU market in the future [21].

Three different e-fuel mixtures have been prepared:

E-fuel 1: 100% paraffinic e-fuel, i.e. a mixture consisting of 100% hydrocarbon chains, which had no ring-shaped hydrocarbons with delocalized electrons such as benzene (i.e. aromatic hydrocarbons). It is a fuel that ensures efficient combustion and is representative of the basic e-fuels blend that could potentially be made available on the EU market [1, 21].

E-fuel 2: 90% paraffinic e-fuel, 10% aromatic e-fuel. 10% of aromatic compounds were included in this mixture in order to check what influence this may have on the emission of harmful exhaust components [21].

E-fuel 3: 90% paraffinic e-fuel, 10% second-generation ethanol. However, the addition of ethanol to the paraffinic e-fuels blend caused significant miscibility problems. Looking for a solution to this problem, eventually it was found that adding 1% of fusel oil to the mixture would prevent ethanol separation [21].

The E10 homologation fuel mixture was used as the reference fuel, being representative for the current European fuel market, the fuel mixture was in accordance with the EN228 standard and the EU regulation 2008/692/EC [1, 5, 6, 21, 57]. The tests were carried out using a Mercedes A180 vehicle, which met the Euro 6d-temp exhaust emission norms. All tests measured both the raw engine exhaust emissions (upstream of the three-way catalytic converter) and the exhaust emissions after passing through the aftertreatment system (tailpipe exhaust) [21].

The results obtained from NO_x emission tests measured in the exhaust, carried out according to the WLTC (Worldwide Light Duty Test Cycle) procedure were, in the case of the above-described four fuels, all within the limits required by the Euro 6 norm and were very similar to each other in value. The average exhaust emission measured in WLTC was 24 mg/km for the E10 fuel, and 22–23 mg/km for e-fuels – Fig. 1 (variations in exhaust emissions were presented in percentage terms). The NO_x emission results obtained in the RDE (Real Driving Emissions) road cycle test was 21 mg/km for E10, compared to 21–22 mg/km for e-fuels mixtures – Fig. 1 [14, 21].

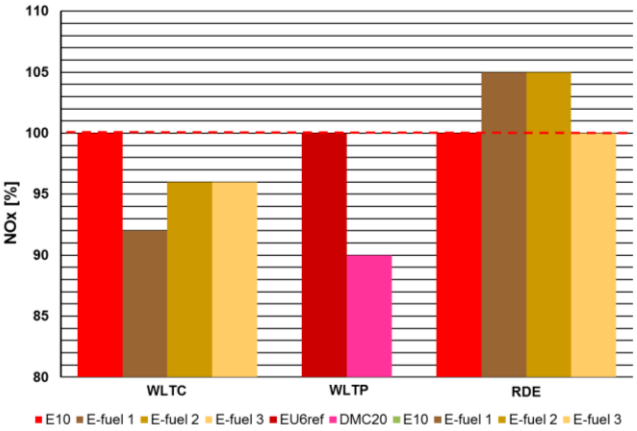

Fig. 1. Changes in the mean NO_x exhaust emissions for various synthetic fuels compared to conventional petroleum fuels as measured in the WLTC, WLTP and RDE tests [14, 21]

Thus, the tested e-fuels did not have a large impact on NO_x exhaust emissions from the tailpipe, which remained at the same level as for conventional fuel (E10) [21]. It is worth noting that the currently applicable Euro 6 norm sets the upper limit of nitrogen oxides (NO_x) emission at 60 mg/km. CLOVE (a consortium working on behalf of the European Commission on the development of emission norms for new vehicles) proposed to lower this limit to at least 30 mg/km or even 20 mg/km for the upcoming Euro 7 norm [5, 14, 16, 21, 28].

Exhaust emissions of particulates from cars equipped with SI engines are governed by two different parallel restrictions, relating to:

– total particulate mass (PM) below the Euro 6 limit value of limited to 4.5 mg/km,
– total particulate number (PN) more than 23 nm in diameter, below the Euro 6 limit value of 6×10^{11}/km.

The measured PM emissions for the four tested fuel types were very low, at < 0.1 mg/km. Since the obtained result was lower than the measurement uncertainty it was not possible to assess the possible impact that the tested fuel (in particular e-fuels) could have had on the exhaust emissions. PN23 emissions, measured for all fuels, were below the Euro 6 limit value of 6×10^{11}/km. At the same time, three e-fuels showed a large reduction in PN emissions compared to the base E10 fuel throughout the test. In the WLTC tests, the mean exhaust emissions of PN23 for the three e-fuels were 97–98% lower than the corresponding emissions for E10 – Fig. 2 (changes in emissions were presented in percentage terms). In RDE tests, the reduction of PN23 when using e-fuels was less significant and amounted to 82–87% of the base fuel value – Fig. 2 [21, 38].

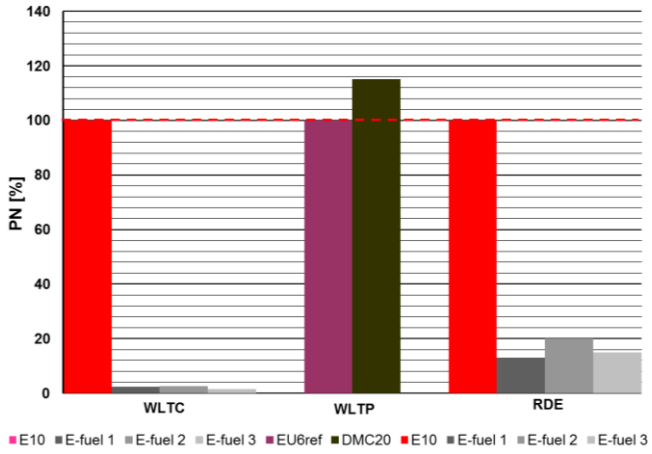

Fig. 2. Changes in the mean level of PN emissions (> 23 nm) for various synthetic fuels compared to conventional petroleum fuels measured in the WLTC, WLTP and RDE tests [21, 38]

It can be hypothesized that the reduction in particulate exhaust emissions observed for e-fuels was probably mostly the result of the low aromatics content in e-fuels, < 0.1% in the case of e-fuel 1 and 3 and 10% in the case of e-fuel 2 compared to 26% for E10. It is likely that future e-fuels will be low in aromatics. It has been shown that as the content of aromatic compounds in gasoline blends increases, the exhaust emission of particulate matter also increases [5, 16, 26, 28], and this effect was through to have been caused by the incomplete combustion of large (heavy) aromatic compounds [15, 16, 28, 33]. The aromatic have a lower hydrogen to carbon ratio compared to aliphatic hydrocarbons and require a higher excess air ratio to enable efficient combustion. Therefore, aromatic hydrocarbons are more likely to cause incomplete combustion and particulate/soot formation than aliphatic hydrocarbons.

During the IPFEN test program described in the article, the emission of solid particles with a size reduced to 10 nm (PN10) was also measured [21]. After taking into account the measured emission of PN10 particles, the total number of particles emitted in the WLTC test increased 1.7 times for E10 fuel and 2.1–2.3 times for e-fuels, with the largest proportional increase observed for e-fuel 3 [21]. For the RDE test the increase in PN emissions, after taking into account PN10, was similar for all fuels, i.e. about 2 times (in the case of e-fuels it was about 5% higher compared to E10). These results indicate that the SI engines emitted more of the currently unregulated particulates in the range 10-23 nm than the regulated particulates > 23 nm for all four fuels tested in the RDE test and all e-fuels tested in the WLTC. The proportion of particles with a size of 10–23 nm compared to PN23 is higher for e-fuels than for E10 fuels. In general, the total exhaust emissions of particulate matter were significantly lower for the three tested e-fuels than for the E10 in both test cycles [21]. In the future Euro 7 norm, CLOVE proposed to lower the limit of particulate matter emissions for cars powered by SI engines from the current 6×10^{11}/km to 1×10^{11}/km [5, 6, 16, 33], which is a very significant reduction.

During the tests [21], all three e-fuels resulted in a significant increase in CO emissions from the tailpipe measured in the WLTC. The increase measured was about a 2.5-fold more CO emissions compared to the values resulting from the combustion of E10 fuel. This increase in CO emissions was mainly in line with the expected significant increase in exhaust emissions during the cold engine start phase and in urban driving. In this engine phase, CO emissions from e-fuels exceeded the allowable CO emission limits, set by the Euro 6 norm, by as much as 23% [40]. It is interesting that such a large increase was not observed when using the base fuel, only about 10% increase in CO emissions in the case of e-fuels compared to E10 – Fig. 3 (changes in exhaust emissions were presented as a percentage) **[**21, 38**]**.

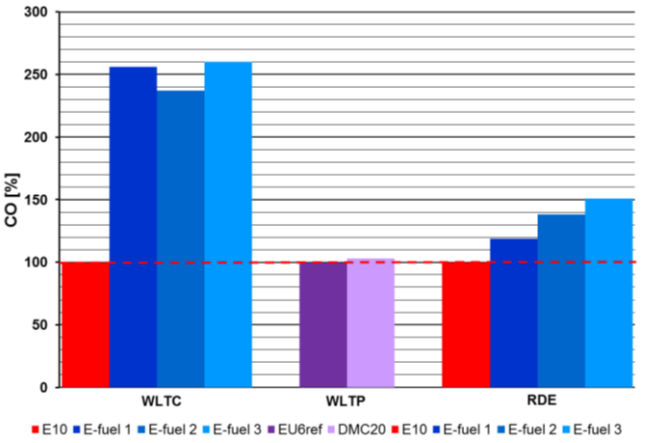

Fig. 3. Changes in the mean CO exhaust emissions for various synthetic fuels compared to conventional petroleum fuels measured in the WLTC, WLTP and RDE tests [21, 38]

This suggests that the large increase in CO emissions may have been caused by an exhaust aftertreatment system that was not optimized sufficiently for e-fuels to be used with an engine powered by such fuels. The increase in CO emissions from the exhaust pipe in the case of the tested e-fuels was lower in the RDE test, although in this case the overall CO exhaust emission when using the e-fuels was 20–50% higher than in the case of E10 – Fig. 3 [5, 21].

HC emission results obtained for e-fuels were favorable in both test cycles [5, 21, 33]. Switching to e-fuels reduced the mean HC emissions in the WLTC test by 23–40% compared to the E10 fuel – Fig. 4 (exhaust emission changes were shown as a percentage), with all emissions below the Euro 6 limit values. The most notable decrease was observed for high driving speeds in the case of the WLTC cycle – 54–77% [40]. Due to the very low HC emission measured in the RDE test for all tested fuels (< 5 mg/km), the differences in exhaust emissions between the various fuels in this test could not be discerned – Fig. 4 [21, 38]. Overall, the obtained results indicate a possibility to reduce hydrocarbon emissions when using e-fuels for compression ignition engines.

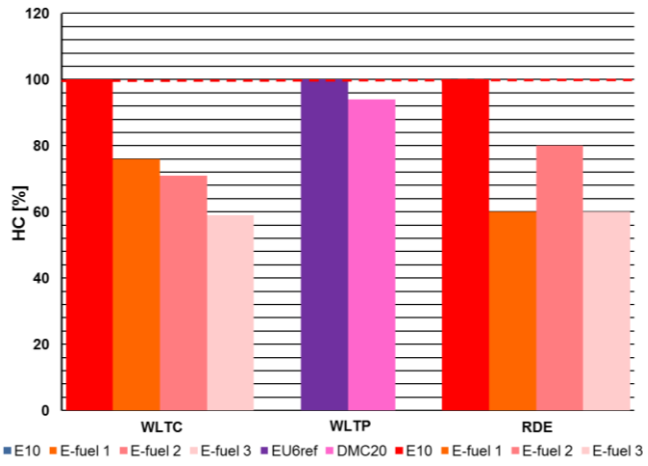

Fig. 4. Changes in the mean HC exhaust emissions of various synthetic fuels compared to conventional petroleum fuels measured in the WLTC, WLTP and RDE tests [21, 38]

Currently, the limit for total hydrocarbon emissions (Euro 6) for cars with SI engines is 100 mg/km. CLOVE proposed to introduce a reduction in the emission of non-methane organic gases (NMOG) at the level of 25–45 mg/km to be added into the Euro 7 exhaust emission norm [14, 21].

Ammonia (NH_3) emissions were also measured as part of the IPFEN research program. Overall, in the WLTC test, ammonia emissions for all tested fuels were low and amounted to about 1 mg/km, except for e-fuel 3, for which the emissions were higher (at 2 mg/km) [21]. However, a significant increase in ammonia emissions from e-fuels compared to E10 was observed in the cold start phase and urban driving (early test phase). The mean emissions for each of the three e-fuels in that time period were 3.5 to 7 times higher than the emissions measured for E10 [21]. In the RDE test, a significant increase in NH_3 emissions was observed for e-fuels 2 and 3, 1.7 and 2.2 times greater, respectively [21]. Also in this test, the greatest increase in emissions for the engine when powered by e-fuels, compared to E10, was observed during the cold start and urban driving section in the first 2 km of the test. These results suggest that the use of e-fuels may contribute to an increase in ammonia emissions, especially during the shorter journeys that are more typical of urban driving.

Ammonia emissions from cars are not regulated by the current Euro 6 norm, however CLOVE has proposed to place a limit on ammonia emissions at the level of 10 mg/km, which would be included in the future Euro 7 norm [5, 14, 21, 38].

The overall level of formaldehyde emissions was very low for each of the tested fuels and was below 0.3 mg/km in the WLTC test and 0.2 mg/km in the RDE test [21]. The highest exhaust emission of formaldehyde was observed during the engine cold start and in the initial phase of the WLTC and RDE tests, when it increased rapidly, even up to about 4 times the base value, most probably due to the catalyst temperature being too low, thus preventing optimal reduction of harmful exhaust components [1, 5, 21, 26].

Exhaust emissions of formaldehyde are also not regulated based on the Euro 6 emission norm, but an emission limit of 5 mg/km has been proposed to be included in the upcoming Euro 7 norm [14, 21, 33].

The presence of acetaldehyde when measured in the exhaust during the performed tests was below the detection limit for most of the test cycle run time for both the WLTC and RDE tests, with the exception of the engine cold start period [21]. Emissions measured in the so-called early phase (the first 3 km of the test) for the WLTC test was 3.0 mg/km in the case of fueling the engine with E10 fuel, and in the case of e-fuels it was lower by about 36–70%. In the case of the RDE test, the acetaldehyde emission for e-fuels was about 55–80% lower relative to the emissions from the E10 fuel.

Acetaldehyde emissions are also not regulated by the Euro 6 norm. So far, no proposal was made to introduce a direct acetaldehyde exhaust emission limit in the future Euro 7 norm. However, acetaldehyde emissions could be regulated under the Euro 7 as part of the CLOVE proposed non-methane organic gas emission limit (NMOG) of 25–45 mg/km [14, 21, 33].

The IPFEN research program included a portion measuring the exhaust emissions of three greenhouse gases, i.e. carbon dioxide (CO_2), methane (CH_4) and nitrous oxide (N_2O). Currently, apart from the regulated emissions of carbon dioxide, emissions of other greenhouse gases are not regulated.

The test results showed that for all three of the e-fuels tested in the WLTC, carbon dioxide emissions were reduced by 3–4% compared to the emissions from the combustion of the regular E10 fuel. This is thought to have been caused by the higher ratio of hydrogen to carbon in the hydrocarbons making up the e-fuels compared to the E10 fuel, due to the lower content of aromatic compounds [16, 19, 33]. Furthermore, the higher energy content of e-fuels 1 and 2 (indicated by the increased lower calorific value) helped lower the fuel consumption and thus reduce the CO_2 emissions. The exhaust emission of methane (CH_4) in both tests (WLTC and RDE) were low and amounted to 1 mg/km for each of the fuels. During the cold engine start period, the exhaust emission values increased to about 10 mg/km, while after the exhaust aftertreatment system reached its operating temperature the emission dropped below the measurement uncertainty value [21]. Similar results were recorded for the emission of N_2O in the WLTP

test, which was very low and similar for all the fuels tested (at around 1 mg/km). As with the other exhaust components, the highest N_2O emission values were observed during the cold engine start. In the RDE test, nitrous oxide emissions were slightly higher (in the case of E10, e-fuel 2 and 3, the emission was measured at 2 mg/km, and in the case of e-fuel 1, at about 3 mg/km) [21].

Currently, the companies Mahle and Porsche are investigating the possibility of using DMC mixtures both in engine test benches as well as in vehicles, in road tests [5, 26, 33]. The results obtained so far on the engine test bench indicated a great potential of DMC mixtures, especially where the engine and its software was adapted to such a fuel, and determined all the effects the application of such a fuel could have on engine components [38]. On the other hand, the test results have shown that DMC should not be used as a standalone fuel, due is its melting point (~4°C) and a low calorific value of 15.8 MJ/kg, which would necessitate adapting the engine accessories, especially for the injection system as well as ECU reprogramming. The mixture of methyl formate (MF) and ethanol, as proposed in [17], solves the melting point problem, but not the low calorific value problem, so such a fuel would also require an adaptation of the engine hardware and injection system. To avoid this, an admixture of DMC to conventional fuel can be used. Tests were carried out to investigate this option, in which the base fuel was E5 SuperPlus98 gasoline (E5-SP98), to which DMC was added as an admixture of 5 to 20% (v/v) in the case of tests on an engine stand, or up to 50% (v/v) for laboratory tests [38]. While most of the relevant properties of the DMC20 blend were within the EN 228 norms, there still were slight variations in the density (slightly higher for the DMC20 fuel) as well as large variation in the oxygen content. When using a higher permitted oxygen content (for Super E10) in accordance with EN 51 626-1, an admixture of 5% (v/v) DMC to the E0 base would meet the requirements of EN 228. After introducing Super E20, it would be possible to add 10% DMC (v/v) to the E0 base. The DMC blend has advantages in terms of aromatic content.

One of the important technical aspects is the material compatibility of the components directly in contact with the fuel, especially the sealing and filtering materials. To test material compatibility with DMC20, the sealing materials widely used in combustion engines, such as hydrogenated acrylonitrile butadiene rubber (HNBR) and fluorinated rubber (FKM), were treated with E5-SP98 and DMC20 fuels for 500 hours at 60°C, and filter materials for 2000 hours at 60°C [38]. Before and after exposure to these fuels, the sealing materials were evaluated for changes in hardness, tensile strength, fracture strain, and volume changes. The obtained results showed that the addition of 20% (v/v) DMC to E5-SP98 adversely affected the hardness of the elastomers, but the effect was found to be small. As a consequence, the materials were concluded to meet the limit value requirements, so no reduction in functionality was to be expected. These materials show neutral or moderately better behavior when subject to tensile strength and strain at break for the DMC20 versus E5-SP98. On the other hand, the visible increase in volume in the case of HNBR and FKM materials subjected to DMC20 treatment may cause a problem from the functionality perspective. Similarly, the swelling tendency, which in the case of DMC20 may be even 80% greater than in the case of E5-SP98 [1, 38], should be noted. The test results prove that DMC20 cannot be assumed to be compatible with all the relevant materials (elastomers). Therefore, for each material exposed to DMC, its compatibility with DMC should be verified. Similarly to the sealing materials, tests were carried out on representative, single-layer filter papers used in fuel filters, both with natural and fully synthetic fibers [1, 38, 40]. All filter materials treated with the tested fuels passed the folding test. The expansion and contraction of the tested materials was negligible when exposed to both fuels. Visual inspection indicated no significant differences. The tear resistance of the filter materials has exceeded the threshold value of 0.1 N/mm^2, irrelevant of the type of fuel used [38].

Further studies of the impact of adding 20% (v/v) DMC to the E5-SP98 fuel showed that such an admixture of DMC reduces the calorific value of the fuel from 42.2 MJ/kg for the base fuel down to 37.1 MJ/kg for the DMC20 mixture [1, 38]. Therefore, the fuel injection duration should be extended for the same engine load when using the new fuel mixture. However, despite the lower calorific value of the DMC20 fuel and the need to inject more fuel, the engine rated power was not affected by this change. A more detailed analysis of the engine test results showed no influence of the DMC content, up to 20% (v/v), on the ignition timing, combustion duration, peak cylinder pressure or pressure gradient values. However, as the share of DMC was increased, the specific fuel consumption also increased due to the extension of the injection duration [1, 38]. Summarizing, it can be stated that from the thermodynamic point of view, it is possible to operate the engine on fuel containing up to 20% (v/v) DMC without the need for changes to the engine design or the control unit software. However, given the high knock resistance of the DMC20 fuel, a slight software modification of the engine control unit (ECU) could increase the engine performance.

In order to make an assessment of the DMC20 mixture's averaged impact on exhaust emissions, measurements were carried out on a chassis dynamometer using a Porsche 911 Carrera GTS with a manual gearbox. No changes were made to the software of the engine control unit for the measurements. The exhaust emissions comparison was based on measurements performed as a part of the WLTP procedure [1, 5, 33, 38]. For emission measurements, reference fuel EU6 (EU6ref) was used, which met the requirements of the EN 228 norm, both as the base fuel and the fuel to which 20% (v/v) DMC was added [1, 5, 33, 38].

When assessing the obtained HC and CO emissions results, no significant difference between the tested fuels was found – Figs 3 and 4. However, in the case of NO_x, the exhaust emission of that component for the DMC20 fuel was about 10% lower – Fig. 1. The emission of particulate matter (PN) was assessed based on the cumulative exhaust emission values in the WLTP test [38]. A significant increase in PN emission was observed for the DMC20 mixture during engine start and in the initial phase of its warm-up, up to about 100 seconds into the test. In that time peri-

od, the DMC20 produced around 70 percent more particulate matter than the reference fuel EU6ref. However, once the engine warm-up phase was complete, the changes in the exhaust emission of particulate matter in dynamic engine operating conditions, were clearly smaller in the case of the mixed fuel than in the case of the pure reference fuel. By the end of the study, the combined increase in particulate emissions from the DMC20 fueled engine dropped to around 15 percent – Fig. 2 [38]. When changing the fuel injection time during the tests it was found, that the PN exhaust emission value was characterized by a much greater sensitivity in the engine powered by DMC20 fuel (when compared to EU6ref). This increased response of PN emissions could result in increased particulate emissions during engine warm-up phase. Thus, the improvement of the particulate matter emissions result could be obtained through optimizing the fuel injection time control [38].

The research on the impact of using e-fuels to power compression ignition engines was carried out at several institutions, such as Ford [56]. The test vehicle was a Ford Mondeo equipped with a 1.5-liter diesel engine. It uses a Denso low-pressure fuel injection system optimized for DME fuel (max. injection pressure: 35 bar, max. fuel flow rate: 80 kg/h). Testing for changes in the measured mass of particulate matter (PM), NO_x and CO_2 exhaust emissions from a test vehicle powered by standard commercial diesel fuel and DME fuel was conducted in accordance with the WLTC guidelines. It was found that by supplying the engine with DME fuel, it is possible to reduce the PM emission to a level close to zero, while at the same time significantly reducing the NO_x emission (by about 30%). The exhaust emission of CO_2 for an engine fueled by DME remained at close to the same level as for the diesel fueled engine [56].

A synthetic fuel with 33% organic content marked as R33 BlueDiesel has already been made available at some gas stations throughout Europe, and is approved for use in all compression ignition engines. Taking into account the methods used for the production of this fuel (in terms of the energy source used for the fuel production and the amount of atmospheric CO_2 capture involved), it can help reduce CO_2 emissions (measured as well-to-wheel) by 20% [11]. For synthetic diesel fuels, HVO (Hydrogenated Vegetable Oil) and Fischer-Tropsch middle distillates (GtL – Gas to Liquids) are already widely available. These fuels were standardized under the general label of paraffinic diesel oil (PD – Paraffinic diesel) in accordance with the EN 15490 norm. Due to its high purity, especially the low content of sulfur and aromatic compounds, PD fuel is an environmentally friendly alternative to conventional diesel oil for compression ignition engines.

6. Synthetic fuels prognosis – SWOT analysis

6.1. Strengths

- E-fuels are produced using renewable electricity, as well as atmospheric CO_2 captured from the air and hydrogen obtained from water, thus significantly reducing GHG emissions.
- E-fuels can reach the market quickly through existing flexible distribution networks, making them easily accessible to consumers.
- A wide range of e-fuels can be produced, ranging from drop-in fuels to fuels optimized for engine efficiency increase or to minimize the regulated, unregulated and GHG emissions.
- E-fuels can be used both as admixtures to conventional fuels and as standalone fuels.
- E-fuels are suitable for use in all means of transport: cars, trucks, airplanes and ships. In addition, they can be used as a substitute for petroleum in the chemical industry.
- Renewable synthetic fuels (e-fuels) of the "drop-in" variety may in a very short time contribute to improving the CO_2 exhaust emission balance of the existing vehicle fleet, since there is no need to introduce any modifications in the vehicles, thus avoiding incurring large investment costs in refueling infrastructure and operation. The reduction in CO_2 emissions depends on the synthetic fuel production technology and can be as high as 100% when the CO_2 emitted by a synthetic fuel vehicles is fully captured from the atmosphere while using only electricity from renewable sources to power fuel production.

6.2. Weaknesses

- If only drop-in admixture e-fuels that meet the requirements of EN228 and EN590 are used to power vehicles, only a slight decrease in the regulated emissions and harmful exhaust components such as HC, CO and NO_x will be achieved, compared to the emissions of petroleum-powered piston combustion engines.
- The current e-fuel production technology is still in the demonstrative phase. Solving some of the more serious challenges to the development of large-scale commercial installations will require an installation scaling of up to 100,000 times what has been demonstrated so far, or 100 times the scale of the project recently announced in Norway. Currently, there are only a few full-scale pilot or production plants, operating or planned in Europe and worldwide, to produce e-fuels for road transport. However, in order to fully decarbonize the new cars from the existing vehicle fleet a huge amount of e-fuels would be needed.
- Renewable electricity is a prerequisite for the development of low-carbon e-fuels production to the extent necessary to have a measurable effect on reducing the greenhouse gas emissions. Therefore, the plan requires a significant increase in the production of electricity from renewable sources.
- The low efficiency of e-fuels means that they are a very costly technology to use in decarbonizing road transport. In 2030, the cost of energy needed to power a car with an SI engine and e-fuel will be nearly four times higher than in the case of an electric vehicle (BEV).

6.3. Opportunities

- Despite the plans made by many governments to ban the sale of cars with internal combustion and hybrid en-

gines, some experts believe that the transition to electric vehicles will not happen soon enough to meet the environmental targets. The provision of carbon-neutral synthetic fuel for passenger cars, trucks and airplanes with internal combustion engines would therefore be a welcome step along the way towards the goal of being carbon-neutral.

- Combustion of synthetic fuel releases CO_2 back into the atmosphere, but because it can be recovered (through carbon capture) and reused to make e-fuels once again, the process is forms a closed loop that can help reduce 10 billion tons of carbon added to the atmosphere per year. E-fuels have also been shown to reduce particulate emissions and are sulfur-free, helping to reduce the local air pollution.
- Siemens Energy and Porsche have already started their production of synthetic fuel, setting up a pilot plant in Chile. The factory will produce e-fuels that are almost completely CO_2 neutral. At the same time, the German government has created a special program to reduce CO_2 emissions by 10 million tons per year starting from 2030 and based on the production and use of e-fuels. The German government will allocate 1.54 billion euros for this purpose until 2024.
- Currently, there are no alternatives to synthetic fuels in aviation and maritime transport, while in the automotive industry a huge advantage is the fact that synthetic fuel can be used for both vehicles already in use (drop-in fuel) as well as new vehicles, optimized to run on synthetic fuels with a special formulation, in order to further reduce the exhaust emissions.
- E-fuels will be critical for transportation applications, for which there are currently no electric propulsion systems commercially available. Therefore, it is now up to policymakers and industry to create a framework that would make e-fuels economically attractive enough for the market.
- Without developing and employing e-fuels, meeting the ambitious goals of climate neutrality by 2045 might not be achievable, and the milestones set will not be met. The reason is the huge number of vehicles with internal combustion engines in operation. Internal combustion engines, especially when combined with e-fuels, still offer great development potential and can therefore make a significant contribution to the global reduction of CO_2 emissions.
- All the studies carried out so far and the forecasts developed have shown that in the future, even in markets with a very high share of electrified vehicles, e-fuels would still be needed to cover energy demand in transport. This is mainly related to aviation and shipping, but also to the supply of e-fuels for commercial vehicles and passenger cars (ICE, PHEV, REEV, FCEV).

6.4. Threats

- The current EU regulation of CO_2 emission only considers the CO_2 reduction achieved by the engine itself, not the fuel or energy that is used to propel it. This is not in line with the principle of technological neutrality pursued by the EU. It is not the internal combustion engine itself that causes the vehicle exhaust emissions, but the fuel used to propel it. With the upcoming revision of CO_2 emission norms, the European Commission indicated that it would investigate the possibility of including a new mechanism in the regulation, which would allow for the emissions reduction achieved by clean fuels, such as synthetic fuels. It should be considered a good step forward. It should not be forgotten that greenhouse gas emissions and climate change are inherently a global and complex problem that requires an integrated approach that encourages innovation while avoiding overdependence on a single technology.
- From a technical point of view, in addition to renewable H_2, also other renewable liquid energy sources such as synthetic fuels (e-fuels) – should be considered as an integral part of the program enabling the use of renewable energy sources on a large scale. However, the political reality is different – quite often e-fuels are seen as an ineffective option aimed only at extending the lifetime of internal combustion engines.
- Greenhouse gas (GHG) emissions from synthetic fuels depends to a large extent on the type of electricity used to produce the fuel. CO_2-based synthetic fuels produced from coal-based electricity are likely to increase the overall greenhouse gas emissions compared to those produced from crude oil. In contrast, CO_2-based synthetic fuels (e-fuels) produced using excess renewable electricity – for example, off-peak night-time wind power that has no other use aside from storage – could have a much lower carbon footprint compared to the fuels produced from crude oil [44].
- Some sources indicate that advanced biofuels and liquid fuels will not make a significant contribution to reducing GHG emissions by 2030, and will be limited in the medium term by land availability and insufficient renewable energy sources to produce sufficient amounts of synthetic fuels [49].
- Presently, any forecast of future e-fuel production is burdened with high uncertainty – these are assumptions rather than factual forecasts. In addition to legal uncertainty and political perception, the enormous investment costs and the expected decline in the number of passenger cars with internal combustion engines over the next decades are also significant obstacles to the development of e-fuels production.
- The assumption that e-fuels will contribute to the automotive exhaust emissions decarbonization in the next 10 years bears a high risk as there are currently no widely available e-fuels on the market for either spark ignition or compression ignition engines.
- The current EU legal regulations focus on e-mobility, leaving no room for other potential technologies or technological competition in achieving the set climate goals. However, this approach means a departure from the current practice and the adoption of a balance between different technologies. Worse, the issue will not be discussed again in the EU until 2023. Moreover, the potential for CO_2 reduction in the existing vehicle fleet has been so far largely ignored, and the major contribution of CO_2 exhaust emissions from transport has hardly

been taken into account. Looking at the future development of the road vehicle fleet, even assuming a significant level of electrification of newly registered vehicles in the coming years, significant reductions in CO_2 emissions could be achieved even at low levels of e-fuels blending with classic fuels. Especially considering the huge worldwide population of vehicles with conventional drive systems, not to mention the benefits of using clean e-fuels to power internal combustion engines as long as they are adapted and optimized for the use of such fuels.

- The production and distribution of e-fuels will not be possible without political support. All scenarios indicate that significant amounts of e-fuels can only be produced and sold with a subsidy level of 1.0–1.5 EUR per liter or greater. This corresponds approximately to a cost of 300–500 EUR for every ton of CO_2 savings, which is more than most, if not all, of the current biofuel subsidies. Thus, a significant support of the e-fuels production technology development would require an unprecedented level of political support to reduce the EU's CO_2 emissions by less than 0.2%. It seems possible that reductions in greenhouse gas emissions in the transport and industrial sectors could be achieved at a lower cost with other measures. Therefore, policymakers are considering the legitimacy and possibilities of supporting the development of production and distribution of synthetic fuels.

7. Conclusions

1) The current ecological situation forces the introduction of CO_2-neutral fuels with a reduced potential harm to human health and the environment. First generation synthetic fuels, classified as hazardous substances, cannot meet these requirements. Therefore, it is necessary to introduce the second generation of fuels (e-fuels), which will be less harmful to the human health and the environment. In order to achieve this, as a result of an extensive selection process, C1 $OME_{3–5}$ fuels and DMC/MF (DMC+) have been proven to be particularly suitable for CI and SI engines respectively.
2) Synthetic fuels are technically feasible and commercially viable, especially provided the availability of renewable energy. Synthetic fuels will support the production of H_2 and the circular CO_2 economy.
3) Synthetic fuels produced with electricity obtained from renewable energy sources can significantly reduce the carbon footprint of combustion engine vehicles that are already in operation.
4) E-fuels make it possible to optimize the use of the global potential of solar and wind energy around the world.
5) E-fuels can be easily stored and safely transported over long distances without any waste of energy. They solve one of the main problems related to the energy transformation: the inability to continuously supply the grid with renewable energy, and thus its continuous availability.
6) The use of e-fuels in cars with internal combustion engines (ICEs) will not solve the air pollution problems to the extent set by the EU. Tests of three different e-fuels, in a Euro 6d-temp compliant car on a chassis dynamometer in WLTC and RDE cycles, described in detail in [21], have shown that e-fuels are not clean combustion fuels and, apart from particulate emissions, they will not significantly contribute to reducing the exhaust emission of both regulated and unregulated toxic pollutants, relative to E10 fuel. However, other studies show significant benefits in terms of reducing CO_2 emissions in the life cycle of an e-fuel vehicle [38]. Some studies point to the great potential of e-fuels to improve engine efficiency [13].
7) The conducted tests have shown that e-fuels do not have a large impact on the amount of NO_x emissions released, and therefore one of the most harmful components of exhaust emitted by internal combustion engines of vehicles remains mostly unaffected. No significant effect of e-fuels use on hydrocarbon emissions was observed in RDE tests. On the other hand, the emission of toxic carbon monoxide increased significantly, as well as the emission of ammonia, which contributes to the increase in the emission of particulate matter [21]. However, other studies emphasize that even the admixture of e-fuels to conventional gasoline is enough to reduce PM, NO_x and HC emissions from an SI engine [38].
8) The results of the greenhouse gas emissions measurements carried out in the performed WLTC and RDE tests indicated that the use of e-fuels in road transport is unlikely to be entirely climate neutral. While it is widely assumed that CO_2 emissions from burning e-fuels produced through the use of direct atmospheric CO_2 capture are carbon neutral, the production of the two more potent greenhouse gases – methane and nitrous oxide – in the engine and the exhaust emission control system is not taken into account. At the same time, the research described in [6] proves that the cumulative GHG emissions of e-fuels powered vehicles are fully competitive to the corresponding emissions generated in the BEV or FCEV in their whole life cycle.
9) The results of the research that has been carried out on the impact of e-fuels on the exhaust emissions of regulated and unregulated exhaust components and GHG from internal combustion engines often present inconsistent results. These conflicting assessments are caused by testing e-fuels of different origins, composition, use of different test methods, different engine generations and different adaptation (optimization) of the engines themselves and their exhaust aftertreatment systems to be powered by e-fuels.
10) Second-generation synthetic fuels (e-fuels) can provide a significant reduction in the exhaust emission of harmful components and greenhouse gases from internal combustion engines, making them potentially useful even after 2050.

Acknowledgements

This work is supported by the Ministry of Science and Higher Education Republic of Poland. Grant number INiG-PIB/0037/TE/22.

Nomenclature

BEV	battery electric vehicles
CH_4	methane
CI	compression ignition
CN	cetane number
CO	carbon monoxide
CO_2	carbon dioxide
DMC	dimethyl carbonate
EGR	exhaust gas recirculation
FCEV	fuel cell electric vehicles
FKM	fluorinated rubber
GHG	greenhouse gases
HC	hydrocarbon
HNBR	hydrogenated acrylonitrile butadiene rubber
HVO	hydrogenated vegetable oil
MF	methyl formate
MON	motor octane number
NH_3	ammonia
NMOG	non-methane organic gases
N_2O	nitrous oxide
NO_x	nitrogen oxides
OME	oxymethylene ether
PD	paraffinic diesel
PM	particulate mass
PN	particle number
PtG	power-to-gas
PtL	power-to-liquid
PtX	power-to-x
RDE	real driving emissions
RON	research octane number
SI	spark ignition
WLTC	worldwide light duty test cycle
WLTP	worldwide harmonized light vehicles test procedure
WWFC	worldwide fuel charter

Bibliography

[1] Aakko-Saksa P, Brink A, Happonen M et al. Future combustion technology for synthetic and renewable fuels in compression ignition engines (REFUEL) – Final report. 2012. Aalto University publication series: 21/2012. http://urn.fi/URN:ISBN:978-952-60-4942-7 (accessed on 22.05.2022).

[2] Beidl C, Münz M, Mokros A. Synthetische Kraftstoffe – Anwendung von Oxymethylenether (OME) am Dieselmotor. 814-849. Springer Vieweg, Berlin, Heidelberg 2019. https://doi.org/10.1007/978-3-662-58006-6_32

[3] Bogatykh I, Goral T, Seidenspinner P et al. Synthetic fuels against climate change and environmental pollution. 41st. International Vienna Motor Symposium. 22-24.04.2020. https://doi.org/10.51202/9783186813121

[4] Boot MD, Tian M, Hensen EJM, Sarathy SM. Impact of fuel molecular structure on auto-ignition behavior – design rules for future high performance gasolines. Prog Energ Combust. 2017;(60):1-25. https://doi.org/10.1016/j.pecs.2016.12.001

[5] Bosch. synthetic fuels – the next revolution. 2017. https://www.bosch.com/stories/synthetic-fuels/ (accessed on 07.04.2022).

[6] Calendini P-O, Rankovic N, Gaillard P et al. Synthetic fuel: a promising H_2 carrier for transport sector. 42nd International Vienna Motor Symposium. 29-30 April 2021. Vienna 2021.

[7] Crusius S, Müller M, Stein H et al. Oxymethylen dimethyl ether, (OMEx) as an alternative for diesel fuel and blend compound: Properties additizing and compatibility with fossil and renewable fuels, Proceedings International Colloquium Fuels, TAE. Stuttgart-Ostfildern 25-26.6.2019.

[8] Czerwinski J, Comte P, Stepien Z, Oleksiak S. Effects of ethanol blend fuels E10 and E85 on the non-legislated emissions of a flex fuel passenger car. SAE Technical Paper 2016-01-0977. 2016. https://doi.org/10.4271/2016-01-0977

[9] Damyanov L. Diesel-OME-blends. Springer Berlin Heidelberg 2019. https://doi.org/10.1007/978-3-662-58006-6_39

[10] De Klerk A. Fischer-Tropsch refining, Wiley. Wiesbaden 2011. https://doi.org/10.1002/9783527635603

[11] Erdmann L et al. Roadmap for the substitution of critical raw materials in electric motors and drives. European Commission 2015. https://doi.org/10.13140/RG.2.1.3564.1206

[12] Forbes AD, Powell KG. Applicant: BP: Gasoline Composition, 1975, GB1411947.

[13] Wagner C, Grill, M, Keskin MT, Bargende M, Cal L, Pitsch H. Potential analysis and virtual development of SI engines operated with synthetic fuel DMC+. SAE Technical Paper 2020-01-0342. 2020. https://doi.org/10.4271/2020-01-0342

[14] Grisstede I, Kunert S, Müller W et al. EU7 legislation – challenges for the exhaust aftertreatment of gasoline engines. 43rd. International Vienna Motor Symposium. 27-29.04.2022. Vienna 2022.

[15] Zhang S, Geng P, Han L, Tian H, Guo X, Li B et al. Effects of oxygenates and aromatics in gasoline on vehicle particulate emissions. SAE Technical Paper 2021-01-0542, 2021. https://doi.org/10.4271/2021-01-0542

[16] Härtl M, Seidenspinner P, Wachtmeister G, Jacob E. Synthetic diesel fuel OME1 a pathway out of the soot-NO_x trade-off. MTZ Worldwide. 2014;(7/8):48-53. https://doi.org/10.1007/S38313-014-0173-1

[17] Härtl M, Stadler A, Blochum S et al. DMC+ as particulate free and potentially sustainable fuel for DI SI engines. 39th International Vienna Motor Symposium 26-27.04.2018. Vienna 2018. https://doi.org/10.1007/978-3-658-21015-1_29

[18] Hartung S. Powertrains of the future – how we will meet our climate goals through technology neutrality. 42nd International Vienna Motor Symposium 29-30.04.2021. Vienna 2021.

[19] Karavalakis G, Short D, Russell R, Hajbabaei M, Asa-Awuku A, Durbin TD. Evaluating the effects of aromatics content in gasoline on gaseous and particulate matter emissions from SI-PFI and SIDI vehicles. Environ Sci Technol. 2015;49(11):7021-7031. https://doi.org/10.1021/es5061726

[20] Kastner O, Avolio G, Rösel G. OME – Diesel Blends für niedrigere Well-to-Wheel CO_2 Emissionen in Pkw Motoren. Springer Berlin Heidelberg. 2019:928-941. https://doi.org/10.1007/978-3-662-58006-6_40

[21] Krajinska A, Poliscanova J, Earl T, Gimbert Y, Decock G, Rangaraju S. Magic green fuels. Transport & Environment. 2021. https://www.transportenvironment.org/wp-content/uploads/2021/11/2021_12_TE_e-fuels_cars_pollution.pdf (accessed on 07.04.2022).

[22] Kratzsch M, Wukisiewitsch W, Sens M et al. The path to CO_2-neutral mobility in 2050. 40th International Vienna Motor Symposium. 15-17.05.2019. https://doi.org/10.51202/9783186811127-II-343

[23] Kuchling T, Awgustow A, Kureti S. Treibhausgasreduzierte Energieträger – Herstellung und anwendungstechnische Eigenschaften. EEK-Erdgas, Erdöl, Kohle. 2019, 7-8, 304-315.

[24] Lensch-Franzen C. Emission potential of operating fluids and powertrain functions. 5. International Motorenkongress 2018. 27-28.2.2018. Proceedings. Springer Vieweg, Wiesbaden. https://doi.org/10.1007/978-3-658-21015-1_35

[25] Liu H, Wang Z, Wang J, He X, Zheng Y, Tang Q et al. Performance, combustion and emission characteristics of a diesel engine fueled with polyoxymethylene dimethyl ethers ($PODE_{3-4}$)/diesel blends. Energy. 2015;(88):793-800. https://doi.org/10.1016/j.energy.2015.05.088

[26] Liu H, Wang Z, Li Y, Zheng Y, He T, Wang J. Recent progress in the application in compression ignition engines and the synthesis technologies of polyoxymethylene dimethyl ethers. Appl Energ. 2019;(233-234):599-611. https://doi.org/10.1016/J.APENERGY.2018.10.064

[27] Lumpp B, Rothe D, Pastötter CR, Lämmermann R, Jacob E. Oxy-methylene ethers as diesel fuel additives of the future. MTZ Worldwide. 2011;72(3):35-38. https://doi:10.1365/S38313-011-0027-Z

[28] Maier T, Härtl M, Jacob E, Wachtmeister G. Dimethyl carbonate (DMC) and methyl formate (MeFo): emission characteristics of novel, clean and potentially CO_2-neutral fuels including PMP and sub-23 nm nanoparticle-emission characteristics on a spark-ignition DI-engine. Fuel. 2019; (256):115925. https://doi.org/10.1016/J.FUEL.2019.115925

[29] Maus W, Jacob E. Synthetic fuels – OME1: a potentially sustainable diesel fuel. 35th International Vienna Motor Symposium. 8-9.05.2014. Fortschritt-Berichte VDI Reihe 2014;12(777):325-347.

[30] Maus W. Zukünftige Kraftstoffe. Energiewende des Transports als ein weltweites Klimaziel. Springer Vieweg Berlin, Heidelberg. 2019. https://doi.org/10.1007/978-3-662-58006-6

[31] Omari A, Heuser B, Pischinger S, Rüdinger C. Potential of long-chain oxymethylene ether and oxymethylene ether-diesel blends for ultra-low emission engines. Appl Energ. 2019;(239):1242-1249. https://doi.org/10.1016/j.apenergy.2019.02.035

[32] Pélerin D, Gaukel K, Härtl M, Jacob E, Wachtmeister G. Potentials to simplify the engine system using the alternative diesel fuels oxymethylene ether OME1 and OME3-6 on a heavy-duty engine. Fuel. 2020;(259):116231. https://doi.org/10.1016/j.fuel.2019.116231

[33] Porsche and Siemens Energy. (2020, December 2). Siemens Energy and Porsche, with partners, advance climate-neutral e-fuel development. https://www.porsche.com/uk/aboutporsche/pressreleases/pcgb/?id=619733&pool=international-de&lang=none (accessed on 07.04.2022).

[34] Ramirez A, Sarathy M, Gascon J. CO_2 derived e-fuels: research trends, misconceptions, and future directions. Trends in Chemistry. 2020;2(9):785-795. https://doi.org/10.1016/j.trechm.2020.07.005

[35] Richter G, Zellbeck H. OME as an alternative for passenger car diesel engines. MTZ Worldwide. 2017;78(12):60-67. https://doi.org/10.1007/s38313-017-0126-6

[36] Richter G. Oxymethylendimethylether: Ein CO_2-neutraler Kraftstoff zur Auflösung des Ruß-NO_x-Zielkonflikts. Dissertation. TU Dresden 2018. Verlag Dr. Huth, München, 2019.

[37] Sarathy S, Farooq A, Kalghatgi GT. Recent progress in gasoline surrogate fuels. Prog Energ Combust. 2018;(65): 67-108. https://doi.org/10.1016/j.pecs.2017.09.004

[38] Scharrer O, Wieske P, Warth M et al. Uncompromisingly fun to drive thanks to synthetic fuel blend. 40th International Vienna Motor Symposium. 15-17.05.2019. Vienna 2019. https://doi.org/10.51202/9783186811127

[39] Schlögl R. Synthetic fuels: a buzzword or a relevant contribution to the turnaround to energy policy? 35th International Wiener Motorensymposium. 8-9.05.2014. Vienna 2014.

[40] Schlögl R. CO_2 to fuels – chemical perspectives. 37th International Vienna Motor Symposium. 28-29.04.2016. Vienna 2016. https://doi.org/10.51202/9783186799128

[41] Schlögl R. Erneuerbare Energien in der Mobilität: Das Potenzial synthetischer Kraftstoffe auf der Basis von CO_2. 39th International Vienna Motor Symposium. 26-27.04. 2018. Vienna 2018. https://doi.org/10.51202/9783186807120-191

[42] Schlögl R. Methanol as synfuel. 6th MTPCC – Methanol Technology and Policy Commercial Congress. Frankfurt 4.12.2019. https://pure.mpg.de/pubman/faces/ViewItemFullPage.jsp?itemId=item_3313871_1 (accessed on 16.05.2022).

[43] Schlögl R. Liquid fuels as chemical batteries. 7. Internationaler Motoren-Kongress. 16.02.2020. Baden-Baden 2020. http://hdl.handle.net/21.11116/0000-0008-5FAC-D

[44] Schmidt P, Weindorf W, Roth W, Batteiger V, Riegel F. Power to liquids: potentials and perspectives for the future supply of renewable aviation fuel. Tech. rep. German Environment Agency (Umwelt Bundesamt). 2016. https://books.google.pl/books/about/Power_to_liquids.html?id=20YnzgEACAAJ&redir_esc=y (accessed on 11.04.2022).

[45] Stępień S. Intake valve and combustion chamber deposits formation – the engine and fuel related factors that impacts their growth. Nafta–Gaz. 2014l(4);236-242.

[46] Stepien Z, Czerwinski J, Comte P, Oleksiak S. Nanoparticle and non-legislated gaseous emissions from a gasoline direct-injection car with ethanol blend fuels and detergent additives. Energy&Fuels. 2016;30(9):7268-7276. https://doi.org/10.1021/acs.energyfuels.6b00583

[47] Stępień S. The influence of particulate contamination in diesel fuel on the damage to fuel injection systems. Combustion Engines. 2019;177(2):76-82. https://doi.org/10.19206/CE-2019-213

[48] Stępień S. Influence of physicochemical properties of gasoline on the formation of DISI engine fuel injector deposits. Combustion Engines. 2021;184(1):16-24. https://doi.org/10.19206/CE-133730

[49] Transport & Environment. Published: April 2018. European Federation for Transport and Environment AISBL. https://www.transportenvironment.org (accessed on 10.04. 2022).

[50] Teng H, McCandless J. Comparative study of characteristics of diesel-fuel and dimethyl-ether sprays in the engine. SAE Technical Paper 2005-01-1723. 2005. https://doi.org/10.4271/2005-01-1723

[51] Urzędowska W, Stępień Z. Prediction of threats caused by high FAME diesel fuel blend stability for engine injector operation. Fuel Process Technol. 2016;(142):403-410. https://doi.org/10.1016/j.fuproc.2015.11.001

[52] Wang D, Zhu G, Li Z, Xia C. Polyoxymethylene dimethyl ethers as clean diesel additives: Fuel freezing and prediction. Fuel. 2019, 237, 833-839. https://doi.org/10.1016/j.fuel.2018.10.014

[53] Wen I, Xing CY, Yang SC. The effect of adding dimethyl carbonate (DMC) and ethanol to unleaded gasoline on exhaust emission. Appl Energ. 2010;(87):115-121.

http://www.sciencedirect.com/science/article/pii/S0306-2619(09)00240-2 (accessed on 11.04.2022).
[54] Wilharm T, Jacob E. The way to an OME specification: where do we stand? 6th MTPCC – Methanol Technology and Policy Commercial Congress. Frankfurt 12.2019.
[55] Wilharm T, Stein H, Bogatykh I. Roadmap to an OME-Spezification. 7. International Motorenkongress Baden-Baden. 16.2.2020. https://doi.org/10.1007/978-3-658-30500-0_13
[56] Willems W, Weber J, Herrmann OE et al. DME/OME1 – Sustainable fuels for compression ignition engines for passenger car and heavy-duty applications. 40th International Vienna Motor Symposium. 15-17.05.2019. https://doi.org/10.51202/9783186811127
[57] Worldwide Fuel Charter. 6th Edition, Gasoline and Diesel Fuel. ACEA. 28.10.2019. https://www.acea.be/uploads/publications/WWFC_19_gasoline_diesel.pdf (accessed on 07.04.2022).

Zbigniew Stępień, DSc., DEng. – Performance Testing Department, Oil and Gas Institute – National Research Institute, Poland.
e-mail: *stepien@inig.pl*

Article citation info:
Żurawski P. Optimization of the combustion chamber strength of aluminum pistons in diesel engines using the DuralBowl technology. Combustion Engines. 2023;192(1):91-96. https://doi.org/10.19206/CE-153000

Paweł ŻURAWSKI

Combustion Engines
Polish Scientific Society of Combustion Engines

Optimization of the combustion chamber strength of aluminum pistons in diesel engines using the DuralBowl technology

ARTICLE INFO

Received: 8 June 2022
Revised: 12 August 2022
Accepted: 25 August 2022
Available online: 2 September 2022

The article focuses on the problem of loading the combustion chamber of diesel engine pistons together with the method of its optimization using the DuralBowl technology. Along with the growing requirements of exhaust emission standards, the increasing competition in the efficiency of internal combustion engines, the load on the combustion pistons increases due to the increase in pressure and temperature of fuel combustion and the tendency to slim the structure. Numerical analyzes and analyzes of damaged pistons in diesel engines have shown that one of the places most exposed to piston damage are the combustion chambers. There is a concentration of thermomechanical stress at the edge of the combustion chamber, which may lead to the destruction of the piston and the necessity to carry out overhaul of the drive unit. One of the technologies that optimizes the strength of this zone is the DuralBowl local remelting process. This process allows for several timesimprovement in the fatigue strength of pistons in internal combustion engines. The article analyzes the thermomechanical load on the combustion chamber along with the impact of this load on the durability of pistons in diesel engines. An analysis of the DuralBowl process was also performed, aimed at eliminating the negative effects of loading the combustion chamber, extending the piston life. The analysis focused on the microstructure of the material before and after the DuralBowl process.

Key words*: diesel engines, DuralBowl, piston, combustion chamber, chamber melting*

1. Introduction

The rapid development of the automotive industry determines the search for newer directions in the development of car components and the technology of their production at the designers of cars with internal combustion engines. In addition, there is a tendency to constantly increase the performance of the internal combustion engine, which forced the creation of more effectively working pistons of internal combustion engines through the use of more durable materials, better technological treatments and by improving the engine operating conditions [1]. It is one of the factors determining the market success of the engine and the possibility of its use on world markets. Its ability to reduce the harmfulness to the environment by meeting the required exhaust emission standards is fundamental for its admission to global markets. Over the years, exhaust emission standards have changed to reduce the limits of toxic exhaust gas components, fuel consumption, and lengthening the life cycle of the engine [2]. Optimization of new design and operation solutions for internal combustion engines is often associated with increasing thermal and mechanical loads on the elements surrounding the combustion chamber of the internal combustion engine. One of the significant factors affecting the strength of the internal combustion engine components and the degradation of the oil film is the thermal load [3]. By using more durable materials is meant replacing aluminum alloys with alloy steels or ductile iron. You can also influence technological procedures, i.e. the use of coatings, changes in the structure of the material, heat treatment, change of the surface of the pistons. Assuming staying with aluminum alloys in the production of pistons of internal combustion engines, the use of coatings and influencing the structure of the material are particularly interesting, as is the case with the DuralBowl technology. It allows you to improve fuel efficiency and minimize exhaust emissions from diesel engines [4].

The piston of diesel engines is expected to withstand thermal and mechanical loads, correct thermal conductivity, resistance to high temperature gradient, low friction coefficient, low weight. The most popular material in internal combustion engines is aluminum alloy. It owes its popularity to low weight, low production cost and sufficient resistance to the conditions in the engine cylinder. As the requirements increase, diesel engines are increasingly loaded, which leads to the operation of the pistons at the limit of their endurance [5].

2. Combustion chamber damage analysis

One of the most stressed parts of the piston is the combustion chamber which is most exposed to pressure and temperature. Many studies present the edge of the combustion chamber as a stress build-up [6–8]. The deformations due to pressure are different in the main plane of the piston along the pin bore than in the plane perpendicular thereto. With proper engine operation, the force reaches 60,000 N for passenger cars and up to 360,000 N for trucks. However, these forces can be even twice as high if the internal combustion engine is not working properly. As a result, in diesel engines, cracks and chipping may appear on the piston crowns [9]. For a better illustration of the zones most exposed to destruction, Fig. 1 presents a numerical analysis of the temperature gradient of a piston in a diesel engine. It shows that the rim of the combustion chamber is the place of concentration of thermal intensities, the most vulnerable to damage.

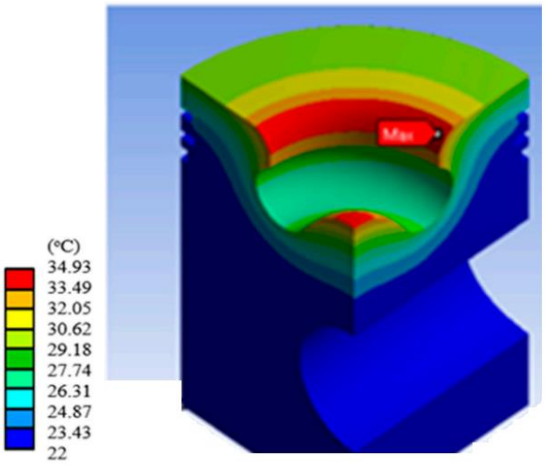

Fig. 1. Numerical analysis of the temperature gradient of a piston in a diesel engine [10]

Of course, the influence of high temperature on the rim of the combustion chamber of diesel pistons can be eliminated by changing the engine operating parameters, changing the piston material, changing the piston structure, etc. One of such design changes is the addition of a cooling duct, as shown in Fig. 2. This design change was introduced. caused that about 50% of the heat from the piston is dissipated through the cooling channel, and to a much lesser extent is dissipated by the piston ring part. The addition of a cooling channel to the piston of the diesel engine also reduced the maximum temperature of the rim of the combustion chamber by approximately 30 degrees. The temperature of the working medium in the combustion process can reach even 2000°C [11]. However, with increasing environmental requirements, increasing combustion pressures and temperatures, the addition of a combustion chamber may not be sufficient to provide the required strength for aluminum diesel pistons. Other possible design changes of the combustion chamber are shown in Table 1, together with the determination of their influence on the durability and performance of the piston.

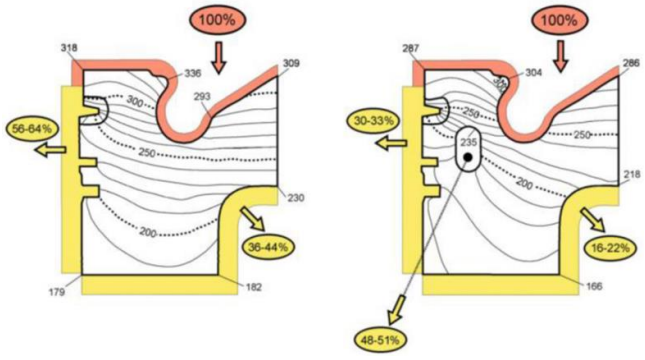

Fig. 2. Temperature distribution of the combustion chamber of a diesel engine piston with and without a cooling channel [11]

Stress concentration in the bottom area results in numerous failures and damage to the pistons, often resulting in engine stoppage and the need for a major overhaul. The most common types of damage include: chipping, cracks, melting, which are very often the result of improper engine operation. Figure 3 shows the piston of a diesel engine with a damaged edge of the combustion chamber. The damage was caused by thermal fatigue associated with material stress caused by a change in the thermal gradient of the piston. The thermal stresses in the piston result from the difference in temperature across the piston crown with the flow of hot gases and the impact of the fuel. The edge of the combustion chamber is an area of elevated temperature, and the thermal deformation of this area is limited by the surrounding piston material, which causes significant compressive stresses over the entire area of the combustion chamber, often exceeding the yield strength of the piston material. After relaxation of the compressive stresses of the cold piston occurs, the creep effect causes an increase in the tension of the residual stresses at the edge of the combustion chamber. The occurrence of these cyclic stresses causes fractures of the edges of the combustion chamber.

Table.1. Influence of changes in individual features of the combustion chamber of a piston of a diesel engine [10]

Parameter	Effect
Bowl depth	Reduce emissions of soot, hydrocarbons, carbon, monoxide, nitrogen oxides and specific fuel consumption [13]
Throat diameter	Reduce specific fuel consumption and increase crushing [14]
Bowl diameter/ depth ratio	Increase crushing, improve air fuel mixture, and generate higher efficiency [15]
Lip radius	Increase performance and reduce the generation of polluting emissions [16]
Outside diameter	Decrease throat diameter ratio to increase swirl and increase turbulence [17]
Protrusion height	Reduce emissions of nitrogen oxides [18]
Bowl diameter	Reduce the generation of smoke and generate greater crushing [19]

Fig. 3. Diesel engine piston with a chipped edge of the combustion chamber [20]

Figure 4 shows the piston of a diesel engine with a crack at the bottom from the combustion chamber to the shell in the plane of the bolt hole. The crack originated in the piston's combustion chamber. In pistons with a combustion chamber on the inner edge of the combustion chamber, there are two stress concentration areas in the plane of the pin bore.

Fig. 4. Diesel engine piston with a crack on the bottom [21]

Figure 5 shows a diesel engine piston with a melted bottom. This type of damage occurs most often in direct injection diesel engines. It was created as a result of not maintaining the proper injection pressure, which causes vibrations that can raise the needles again, allowing the fuel to enter the combustion chamber. Then, after the remaining oxygen is used up, the fuel droplets flow to the piston crown, where they burn at high temperature, causing the piston crown material to soften. Erosive and mass forces acting on the fast-flowing exhaust gas tear particles of the softened material from the piston crown.

Fig. 5. Diesel engine piston with a melted bottom [21]

3. DuraBowl process analysis

The combustion process in diesel engines takes place in the combustion chamber, where the pressure can reach over 200 bars and the temperature over 400 degrees. The presented analyzes of thermal and mechanical damage have shown that the rim of the combustion chamber is particularly vulnerable to damage. By analyzing the microstructure in this area, the presence of free silicon particles decomposed on aluminum can be detected. It should be noted that aluminum expands eight times more than silicon, which causes stresses inside the piston material as the temperature changes. Repeated heating and cooling of the piston material by ignition in the cylinder can fatigue the combustion chamber material. This type of failure is referred to as thermomechanical fatigue due to excessive high and low cycle fatigue loads. That is why Federal Mogul has developed the DuralBowl technologies, which place particular emphasis on the local improvement of the microstructure of the combustion chamber rim in order to improve the strength of the aluminum piston and increase the resistance to multiphase thermomechanical fatigue load. Diesel pistons are subjected to a low-cycle thermal load and a high-cycle mechanical-thermal load due to a combustion load per engine cycle.

The DuraBowl technology enables about ten times greater fragmentation of the microstructure than in the case of the cast structure. The fragmentation of the structure significantly improves the fatigue strength of the optimized combustion chamber surface. Validation tests of pistons with a remelted chamber and without remelting have shown an increase in service life from 4 to 8 times [22]. The increase in strength of aluminum pistons makes it possible to ensure sufficient strength despite increasing ignition pressures and temperatures in the fuel combustion process. The process itself can be described as a local process of remelting critical zones of the combustion chamber with a modified form of tungsten inert gas welding. The DuraBowl process is performed by a welding robot with strictly defined process parameters.

The smelting process requires one pass if only the edges of the combustion chamber are to be strengthened, and the base of the chamber also needs to be strengthened several times. Rapid heating of the piston surface by a welding robot using the TIG method and then its very rapid cooling causes fragmentation of the microstructure of the melted chamber surface. Figure 6 shows simulations of smelting the edge of the combustion chamber of a piston in a diesel engine.

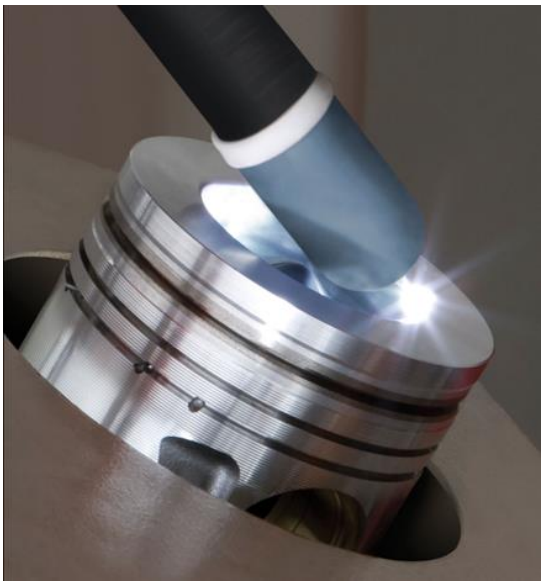

Fig. 6. Simulation of the fistula at the rim of the combustion chamber [22]

Figure 7, 8 shows the edge of the combustion chamber of an aluminum piston before and after the local DuralBowl remelting process. Figure 7 shows the combustion chamber before local remelting. It is a roughly machined piston. Figure 8 shows the same piston, but after the local melting of the combustion chamber edge. You can see the surface change caused by the TIG melting method. The surface is smooth, uniform without any discontinuities. The following parameters play the most important role in this process: current type and intensity, arc voltage, welding speed, type and flow rate of shielding gas, diameter, shape and type of non-consumable electrode, balance and frequency of current, method of cooling. Appropriate selection and stability of these parameters guarantees obtaining the appropriate structure of the melted material.

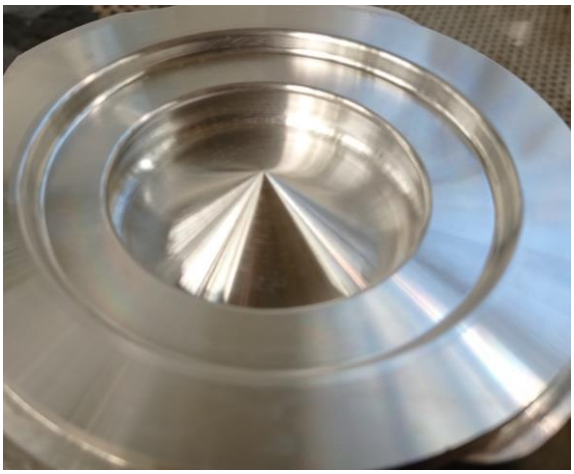

Fig. 7. Combustion chamber of an aluminum piston before the local DuralBowl remelting process

Fig. 8. Combustion chamber of an aluminum piston after the local DuralBowl remelting process

Figure 9 shows the structure of the melted rim of the piston combustion chamber. The depth of the penetration is about 3 mm in depth. The transition of the fragmented microstructure into the native material of the piston casting is smooth. The hardness measured on the Brinell scale in the remelted zone is about 140 HB, while in the zone of the piston parent material it is about 110 HB.

The comparison of materials before and after the DuralBowl process showed that the microstructure of the aluminum piston casting material after the remelting process is ten times smaller than the microstructure of the remaining casting. The microstructure of the silicon and intermetallic phases was fragmented. The silicon phase in the piston casting has a size of 50 μm, after the DuralBowl process, the microstructure of the silicon phase is 4–5 μm. Figure 10 shows the transition of the microstructure of the melted rim of the combustion chamber into the microstructure of the native casting of the piston. On the left side of the drawing you can see the microstructure of the casting, while on the right side the fragmented microstructure after the local remelting of the DuralBowl process.

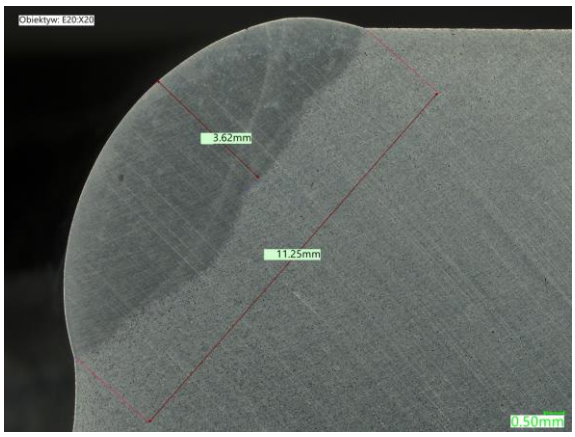

Fig. 9. cross-section of the rim of the melted combustion chamber

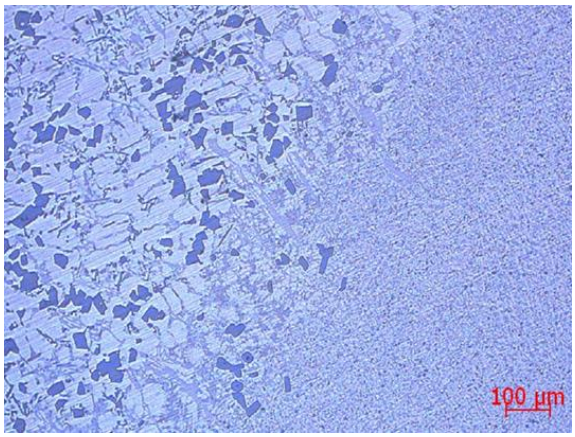

Fig. 10. DuralBowl remelting microstructure

The fatigue strength tests to temperature changes showed that the change of structure in the DuralBowl process increased the resistance to microcracks and microplasticity caused by sudden changes in the operating temperature many times over. This is due to a mismatch in thermal expansion between the aluminum alloy phases of the pistons of internal combustion engines. The differences in thermal expansion between the phases are eightfold, which causes fatigue in the event of a sudden temperature change [23].

Conclusions

The growing requirements of customers regarding the efficiency of combustion engines and exhaust emissions

have forced engine designers to design new construction solutions working at the limit of their endurance. The operating pressure and the fuel combustion temperature are increased. As a result, aluminum pistons, especially in diesel engines, work at the limit of their strength. Numerical analyzes and analyzes of damaged pistons have shown that the area most vulnerable to damage to the piston of a diesel engine is the edge of the combustion chamber. It is subjected to the highest thermal and mechanical loads.

In order to meet these growing requirements, it was necessary to introduce changes in the structure of aluminum pistons or the technology of their production. Changing the material is not always advisable as steel is much heavier and economically more expensive to produce. Therefore, in order to improve the strength of aluminum pistons in diesel engines, a team of engineers at Federal Mogul developed the DuralBlowl technology, which consists of pretoping the rim of the combustion chamber. The much higher cooling speed than in the casting will make the microstructure of the melted rim much smaller than in the rest of the aluminum piston. The change in structure results in an increase in hardness and resistance to thermal and mechanical microcracks. Melted combustion chamber pistons in diesel engines are more durable and reliable than standard pistons.

In the current application, the DuralBlowl local remelting technology is used especially for large aluminum pistons for diesel engines. However, a significant increase in the requirements of exhaust gas standards results in increasing the pressure and temperature of fuel combustion in passenger cars. For this reason, part of the market for aluminum pistons has been replaced with steel pistons, however, in the further part aluminum pistons show great development potential, supported by new technologies such as DuralBlowl.

Bibliography

[1] Walczak M, Bieniaś J, Stradomska B, Jankowski A, Bielecki D. Wear of engine pistons – microstructural characteristics of materials used to produce them. Innovatio Press Wydawnictwo Naukowe Wyższej Szkoły Ekonomii i Innowacji. Lublin 2011;1(1):59-72. https://wydawnictwo.wsei.eu/serie-naukowe/transport-i-informatyka/

[2] Merkisz J. Some trends in the evolution of combustion engines. Combustion Engines. 2004;118(1):28-39. https://doi.org/10.19206/CE-117422

[3] Stanik W, Jakóbiec J. Environmentally friendly development of diesel (compression-ignition) engine technologies. Bezpieczeństwo i ekologia. 2012;36(7-8). http://yadda.icm.edu.pl/baztech/element/bwmeta1.element.baztech-article-BWAK-0032-0040

[4] Uczak De Goes W, Somhoorst J, Markocsan N, Gupta M, Ilikova K. Spension plasma-sprayed thermal barrier coatings for light duty diesel. J Therm Spray Tech. 2019;(28):1674-1687. https://link.springer.com/article/10.1007/s11666-019-00923-8

[5] Siadkowska K, Majczak A, Barański G. Studying a construction of pistons for the aircraft CI engine. Combustion Engines. 2017;168(1):161-167. https://doi.org/10.19206/CE-2017-126

[6] Mysłowski J, Talaga K. Thermal loads a piston in a diesel engine during startup. Combustion Engines. 2008;133(2): 20-25. https://doi.org/10.19206/CE-117242

[7] Kalke J, Szczeciński M, Mazuro P. Unsteady conjugated heat transfer in cylinder of highly loaded opposed-piston engine. Combustion Engines. 2016;167(4):64-72. https://doi.org/10.19206/CE-2016-407

[8] Pietrykowski K, Magryta P, Skiba K. Finite element analysis of a composite piston for a diesel aircraft engine. Combustion Engines. 2019;179(4):107-111. https://doi.org/10.19206/CE-2019-417

[9] Bąkowski H, Stanik Z. Application of the FEM analytical practice for explanation of the effect of service conditions on emergency wear of the self-ignition engine piston. Mechanik. 2010;4(83). http://yadda.icm.edu.pl/baztech/element/bwmeta1.element.baztech-article-BOS2-0021-0102

[10] Noriega Lozano JI, Paredes Rojas JC, Romero Ángeles B, Urriolagoitia Sosa G, Contreras Mendoza BA, Torres San Miguel CR et al. Redesign of a diesel combustion engine to use biodiesel blends. Materials. 2021;14(11):2812. https://doi.org/10.3390/ma14112812

[11] Wróblewski E, Iskra A, Babiak M. Minimizing wear of components piston-cylinder group. Autobusy: technika, eksploatacja, systemy transportowe. 2017;18(16):1137-1141.

[12] Miguel A, Drummond H, Copeland C. Improving heat transfer and reducing mass in a gasoline piston using additive manufacturing. SAE Technical Paper 2015-01-0505. 2015. https://doi.org/10.4271/2015-01-0505

[13] Ganji PR, Singh RN, Raju VRK, Srinivasa Rao S. Design of piston bowl geometry for better combustion in direct-injection compression ignition engine. Sadhana. 2018; 43(92):1-9. https://doi.org/10.1007/s12046-018-0907-x

[14] Paramvir VS, Kumar ST, Singh R, Kumar N. Modification in combustion chamber geometry of ci engines for suitability of biodiesel: A review. Renew Sust Energ Rev. 2017; (79):1016-1033. https://doi.org/10.1016/j.rser.2017.05.116

[15] Ramesh-Bapu BR, Saravanakumar L, Durga-Prasad B. Effects of combustion chamber geometry on combustion characteristics of a DI diesel engine fueled with calophyllum inophyllum methyl ester. J Energy Inst. 2017;90(1):82-100. https://doi.org/10.1016/j.joei.2015.10.004

[16] Vedharaj S, Vallinyagam R, Yang WA, Saravanan CG, Lee PS. Optimisation of combustion bowl geometry for the operation of kapok biodiesel – Diesel blends in a stationary diesel engine. Fuel. 2015;(139):561-567. https://doi.org/10.1016/j.fuel.2014.09.020

[17] Yan B, Wang H, Zheng Z, Qin Y, Yao M. Experimental and numerical investigation of the effects of combustion chamber reentrant level on combustion characteristics and thermal efficiency of stoichiometric operation natural gas engine with EGR. Appl Therm Eng. 2017;(123):1473-1483. https://doi.org/10.1016/j.applthermaleng.2017.05.139

[18] Dimitriou P, Wang W, Peng Z. A piston geometry and nozzle spray angle investigation in a di diesel engine by quantifying the air-fuel mixture. Int J Spray Combust. 2015;7(1):1-24. https://doi.org/10.1260/1756-8277.7.1.1

[19] Yaliwal VS, Banapurmath NR, Gireesh NM, Hosmath RS, Donateo T, Tewari PG. Effect of nozzle and combustion chamber geometry on the performance of a diesel engine operated on dual fuel mode using renewable fuels. Renew Energ. 2016;(93):483-501. https://doi.org/10.1016/j.renene.2016.03.020

[20] Dhamak CS, Patil BD, Chavaan N, Dharmashale VR. Piston analysis of IC engine. International Journal of Advance Research and Innovative Ideas in Education. 2015;(2):317-325. http://ijariie.com/AdminUploadPdf/Piston_Analysis_of_IC_Engine_ijariie1180_volume_1_11_page_317_325.pdf
[21] Piston damage – recognising and rectifying. MS Motorservice International GmbH. 2018. https://mam.ms-motorservice.com/mc/epaper?guid=14c0122387e59c2c (20.05.2022)
[22] Hellstern U. New Mercedes-Benz V6 diesel engines use DuraBowl® piston technology from Federal-Mogul. Cision Distribution. 1.09.2011.
[23] Federal-Mogul introduces new diesel piston design to support downsized engines with higher output. Green Cars Congress Energy, technologies and policies for sustainable mobility. 11.2009. https://www.greencarcongress.com/2009/11/durabowl-20091115.html

Paweł Żurawski, MEng. – Federal Mogul Gorzyce
e-mail: *zurawskipawel15@gmail.com*

Article citation info:
Krakowski R. The effect of adding effective microorganism and silver compounds to flash point of engine oil. Combustion Engines. 2023;192(1):97-104. https://doi.org/10.19206/CE-153001

Rafał KRAKOWSKI

Combustion Engines
Polish Scientific Society of Combustion Engines

The effect of adding effective microorganism and silver compounds to flash point of engine oil

ARTICLE INFO

Received: 23 June 2022
Revised:3 August 2022
Accepted: 25 August 2022
Available online: 2 October 2022

The article presents the effect of the effective microorganisms and silver compounds addition on the flash point of new and used oil. The work describes environmentally friendly additives to engine oil. Next the ignition point of the engine oil were described. In the further part, the research stand and methodology were presented. In the main part of the article the flash point values for new and used oil compared to oils with the effective microorganisms and silver compounds addition were shown. New and used oil samples were mixed with effective microorganisms in the form of a liquid (2.5 ml and 5 ml) and ceramic tubes (3 pcs and 6 pcs). In addition, silver solution and silver compounds were mixed in the same amounts as the liquid effective microorganisms. In summary it was stated, that adding of the effective microorganisms to the fresh oil in liquid form causes the flash point to drop significantly. It follows that effective microorganisms in liquid form have a very negative effect on the properties of the oil. In the case of microorganisms in the form of ceramic tubes, which in this larger amount slightly increase this point compared to oil without additives. Regardless of the type of silver and its quantity, very low flash point values were obtained. For used oil the best results are obtained with the addition of microorganisms in liquid form. For the used oil the addition of silver compounds does not have the beneficial effect of restoring the original properties.

Key words: *engine oil, flash point, oil properties, effective microorganisms, silver compounds*

1. Introduction

Currently an increasing influence, in connection with the tightening of regulations on the emission of toxic compounds and carbon dioxide (CO_2) into the atmosphere, have alternative drives that are under intense development. Nevertheless, internal combustion piston engines, including marine engines, are still developed and improved to meet these stringent standards [3, 4, 6, 8, 11, 18].

Due to its design, the operation of the piston engine is not possible without a properly selected lubricating oil. Lubricating oil is an integral part of any internal combustion engine and must meet all the design requirements set by the engine constructor [2, 17, 22].

As a result of work in the engine, the oil undergoes the processes of oxidation, aging and destruction. The oil oxidation products and aging create sludges, carbon deposits and varnishes that change the physicochemical properties of the oil and are highly corrosive to metal parts of the engine. In order to counteract these phenomena, the oil is mixed with additives. One of them are biocides that are harmful to the environment. Therefore, additives are currently being sought that will fulfill this role at the current level and will be environmentally friendly [1, 7, 9, 20, 23].

For this purpose, it was decided to check the effect of the addition of effective microorganisms and colloidal silver on the value of the ignition point of engine oil. The flash point is the lowest temperature at which airborne oil vapors can ignite on contact with a flame and should be as high as possible because it affects oil consumption. So it is very important to check that these additives will not deteriorate the properties of the oil in this regard. The flash point is another parameter investigated because the influence of these additives on the acid number, base number and viscosity of the engine oil [12–14] was previously investigated. These studies show that it is worth conducting research in this direction, with better results improving the properties of the oil obtained for effective microorganisms than for nanosilver. For used oil, it is better to add microorganisms in liquid form, and to new oil, microorganisms in the form of ceramic tubes, from which they are slowly released into the engine oil. As for nanosilver, the results were similar for used oil and new oil, which shows that the addition of silver does not have such a positive effect on the improvement of oil properties as effective microorganisms.

The article presents the research results for new and used oil with and without the addition of effective microorganisms and silver compounds as oil enriching agent to slow down the process of microbiological degradation of lubricating oil [21].

2. Engine oil and additives improving the properties of the oil

The primary task of the oil is to lubricate the moving parts of the engine over a wide temperature range. This is done by creating a durable and break-resistant oil film. Its role is to separate the mating engine parts from each other and reduce the friction coefficient, which will significantly reduce the wear of mating engine parts. This function is related to the viscosity of the oil, i.e. its ability to separate the cooperating elements from each other. Immediately after starting the engine, the oil should reach all friction nodes and create an oil film of appropriate thickness and strength. At the same time, its continuity must be maintained in order to prevent even point contact of the mating metal parts.

The second very important function of engine oil is heat dissipation, which is especially important in modern turbo-

charged combustion engines. Due to the fact that some engine components can reach very high temperatures, the task of the oil is to extract large amounts of heat from them. For this reason, a high flash point of the lubricant, adequate temperature stability and protection against oxidation at high temperatures are important.

A very important function is to keep the engine clean, which has a positive effect on the technical condition of the engine. The oil prevents the build-up of low- and high-temperature contaminants that remain dissolved in the oil. It is important to properly add improvers so that the oil does not become the cause of its degradation due to, for example, increased microbial contamination that may occur in petroleum products. For this reason, an important element is the prevention and protection of petroleum products against microbial contamination. Such protection may include physical methods such as settling, fuel filtration or thermal decontamination, and a chemical method. Physical methods are less burdensome to the environment, but unfortunately their use is limited. For this reason, other agents are used, which include biocides, i.e. compounds of synthetic or natural origin. Biocides are pesticides that are used, inter alia, to combat or limit the growth of microorganisms in petroleum products. Xbee cleaners are also used in the storage of petroleum products to help eliminate water, reducing deposits such as rust [43, 44].

Due to the fact that physical and thermal methods are ineffective, and chemical methods use highly concentrated substances that have a detrimental effect on the natural environment, it is necessary to develop effective, environmentally friendly methods of combating the phenomenon of microbiological contamination of fuels and oils. These methods should take into account both technical aspects and the specificity of the processes taking place in the fuel and lubricating systems [15].

One of such measures may be effective microorganisms, that is, specially and properly selected smallest organisms on Earth. The composition of 81 different strains of aerobic and anaerobic microorganisms (Fig. 1), incl. lactic acid bacteria, yeast, photosynthetic bacteria, mold or actinomycetes. It was developed by Professor of Horticulture Teruo Higa from the Agricultural Academy of Ryukyus University in Okinawa, Japan. According to the creator, properly and systematically introduced into the environment give it the potential of biodynamic self-renewal and regeneration [10, 27].

Photosynthetic bacteria using available conditions, eg CO_2, temperature, produce useful biochemical active compounds from organic matter or toxic gases. Lactic acid bacteria also slow down the growth of harmful bacteria. Another important component of the mixture is yeast. Thanks to fermenting mushrooms, organic matter is decomposed and unpleasant odors are neutralized. The principle of operation of EM is based solely on natural processes, they are not genetically modified and completely environmentally friendly [16, 18, 19, 34, 35, 37, 40].

Another environmentally friendly measure can be the use of silver. This chemical element has long been used for protective and healing purposes. Silver is also used in filters, as well as to clean the air of microbes and water in closed spaces, e.g. in airplanes. The silver ionization method contributed to the enhancement of the disinfecting effect of this element. Silver ionization, like copper ionization, has found application in the elimination of some bacteria [5, 32]. Silver is also used in the form of nanosilver.

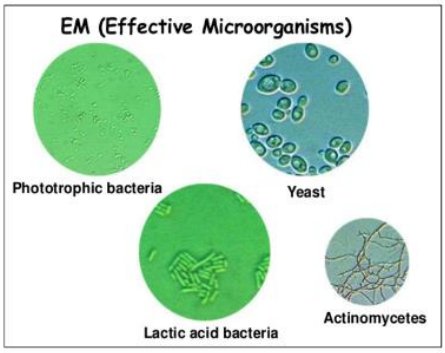

Fig. 1. A composition composed of various strains of aerobic and anaerobic microorganisms that are part of effective microorganisms [39]

Nanosilver is microscopic particles - silver ions that can only be observed through an electron microscope. Thanks to the fragmentation of silver into nanoparticles with a size of 1 to 5 nm, the effectiveness of using the bactericidal, fungicidal and virucidal properties of silver has increased incomparably. Crushed silver to nanoparticles has a disproportionately larger active surface, and thus a previously unattainable biocidal potential. The effectiveness of nanosilver includes the elimination of over 99.99% of bacteria, fungi, viruses and mold. Nanosilver is able to attach to bacterial cell membranes and block their production of enzymes necessary for reproduction and growth.

3. Flash point as one of the parameters characterizing engine oil

The flash point for oil is the lowest temperature at which an oil sample develops sufficient vapours under specified conditions for the air-vapour mixture above the sample to ignite for the first time without continuing to burn afterwards. If the oil-air mixture burns for at least five seconds or longer, this is referred to as the focal point of the oil. The focal point is usually only a few degrees Celsius above the flash point. The flash point alone is not a sufficient quality feature of oil, nor does it allow conclusions about the suitability of the oil. Moreover, they cannot be drawn on the subject of oil consumption in internal combustion engines. The flash point is an important constant for any type of lubricant, therefore each oil is tested for its flash point. The flash point contributes significantly to the scope of the lubricant application. Each oil has a different flash point. Depending on the application, a certain flash point may also be required. Basically, it can be said that the flash point of paraffin-based oils with a density between 860 and 890 kg/m^3 is between 200 and 280°C. For naphthene-based oils with a density between 890 and 960 kg/m^3 flash points of 235°C and lower are reached [24, 25, 36, 38].

In the case of engine oils for passenger cars, flash points of 200°C to 270°C are usually achieved. Some special oils

for industrial applications can reach flash points above 300°C.

Particularly in combustion engines, the oil may mix with fuel after prolonged periods of use, resulting in oil dilution. The entry of foreign substances, fuel or water is also the reason why the flash point of other oils could drop. If the flash point of the oil sample falls below 150°C, the oil should be changed to reduce the risk of fire.

As shown in Table 1, flash points for conventionally refined mineral oils can range from 165°C for an ISO 22 viscosity oil to a high 260°C for an ISO 1000 viscosity oil. Flash points also vary somewhat within viscosity grades as influenced by the crude oil type and refining process [33].

Table 1. Typical flash points of industrial lubricants [33]

Oils ISO VG	Flashpoint	
	°C	F
22	165	329
100	224	435
150	226	439
220	232	450
320	236	457
460	236	460
680	238	460
1000	260	500

As previously mentioned, synthetic lubricants typically exhibit higher flash points than their mineral-oil counterparts. Therefore, it is sometimes possible to detect a wrong or mixed oil with the use of flash point testing. However, from a practical standpoint, other routine tests such as infrared spectroscopy, TAN viscosity and color are more effective in alerting users to wrong or mixed lubricants. In these instances, the flash point test better serves in a confirming role.

4. The research stand, materials and metodology

5W30 synthetic oil was used for the tests, which slightly changes its viscosity during temperature changes. As a result, it perfectly lubricates engine parts, while protecting it against deposits of carbon deposits, sludge and other harmful impurities that can accelerate its wear. At the same time, the specificity of 5W30 oil allows it to maintain its fluidity even at very low temperatures, which significantly facilitates engine start-up in winter.

The new oil had a dynamic viscosity at 2°C at the level of 598 mPa·s, while at 63°C (the maximum temperature obtained on the viscometer), it was 26 mPa·s. In addition, the flash point was measured, which is 212.44°C.

Used oil, the same type as the new one, i.e. 5W30 synthetic, was also used for testing. This oil was used in a compression ignition engine under variable conditions and had a mileage of approx. 15,000 km.

The dynamic viscosity of the oil at 2°C is 697 mPa·s, while at 63°C – 24.5 mPa·s, additionally, the ignition point was measured, which was 198.8°C.

Before starting the research, effective microorganisms and silver were added to the oil about 4 weeks earlier.

Figures 2 and 3 show samples of new oil, new oil with additives and used oil. In the case of used oil, the color and appearance were the same no matter what additives were added.

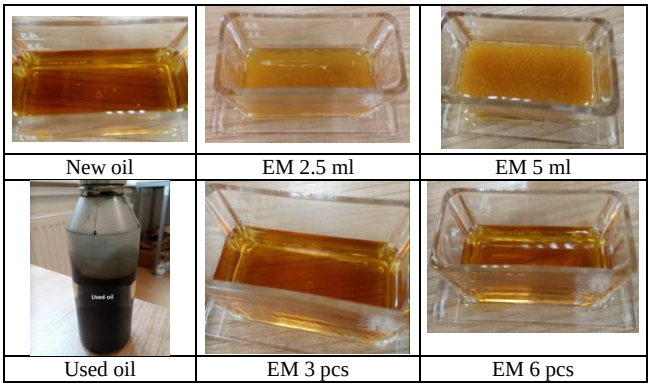

Fig. 2. Fresh oil, with the addition of effective microorganisms in liquid form and ceramic tubes and used oil

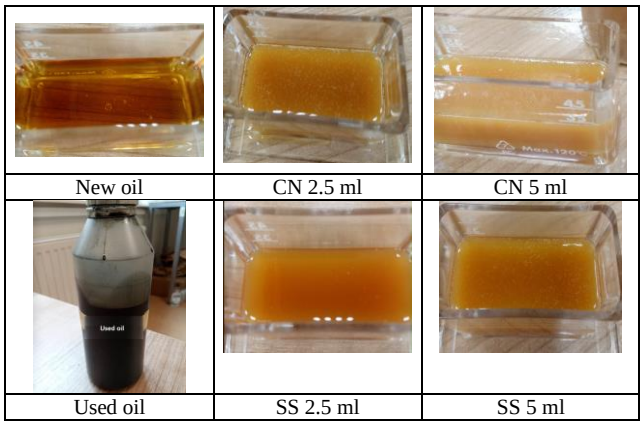

Fig. 3. Fresh oil, with the addition of silver solution (SS) and colloidal nanosilver (CN) in liquid form and used oil

Effective microorganisms in liquid form (2.5 ml and 5 ml per 100 ml of oil) and in the form of ceramic tubes (3 pieces and 6 pieces with a diameter of 9 mm and a height of 11 mm for 100 ml of oil) was added to fresh and used oil.

Effective microorganisms of the commercial form presented in Fig. 4 were used for the research.

Fig. 4. The commercial form of effective microorganisms in liquid form and ceramic tubes [29, 31]

In addition, silver solution and colloidal nanosilver were added to fresh and used oil in the same proportions as for effective microorganisms (2.5 ml and 5 ml per 100 ml of oil). Nanosilver was used for the tests in the commercial form shown in Fig. 5.

Determination of the flash point for new and used oil using an automatic apparatus for testing the flash point in a closed crucible – EraFLASH was carried out (Fig. 6). The device advantages are the speed and precision of determina-

tions, the patented technology of heating and cooling from –25°C to +420°C (in one apparatus), and the applied methods of determination according to the standards: ASTM D 6450 and D 7094.

Fig 5. The commercial form of colloidal nanosilver and silver solution [26, 30]

Fig. 6. Apparatus for testing the flash point in a closed cup – EraFLASH [41, 42]

ERAFLASH is a device that enables the measurement of the flash point for all types of fuels, such as diesel oil, fuels, biofuels, solvents, fragrances and flavors, paints, varnishes, residual fuels, marine fuels, tars, asphalts and solid substances. The apparatus can also be used to determine the degree of fuel dissolution in the engine oil. Besides, it is easy and convenient to use also in the field.

A small amount of sample: 1 ml for the ASTM D 6450 method or 2 ml for the ASTM D 7094 method and the crucible closed during the test, guarantee the highest safety for the laboratory. The sample is heated in the closed measuring chamber from above. An electric arc is used for ignition. This device uses neither open flame nor electric filament. The flash point is measured as the point where the pressure of the gases in the measuring chamber increases rapidly. The use of small samples reduces the costs of collecting, storing and disposing of samples and beakers after analysis, and also facilitates the cleaning of the device [28].

As for the tests of the samples that were used to make the graphs and analysis, they were carried out in accordance with the ASTM D7094 standard.

5. Results and analysis of research

In order to analyse oil flash point for each samples, the test results are presented in the form of graphs in Figs 7, 9, 11 and 13. These graphs show the variation in the value of the oil's flash point after adding to fresh and used oil effective microorganisms in liquid form and in the form of ceramic tubes. In addition, silver solution and colloidal nanosilver were added to fresh and used oil in the same proportions as for effective microorganisms. Each sample of pure oil and oil with additives were tested three times. However, the article presents the average result for each case.

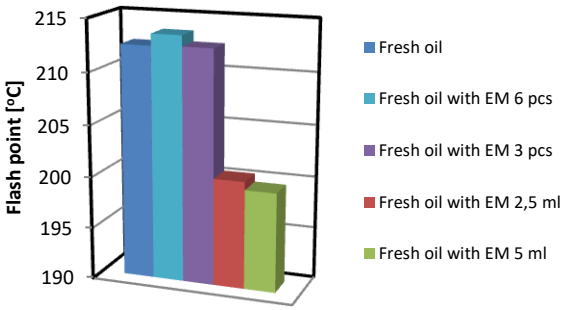

Fig. 7. Flash point oil of fresh oil and fresh oil with EM in liqiud form and ceramic tubes

Analyzing the results obtained, it can be seen in Fig. 7, that for fresh oil the flash point is 213°C. On the other hand, adding of the effective microorganisms to the oil in the amount of 2.5 ml causes the flash point to be lowered to 200°C, while the greater amount of liquid additive, i.e. 5 ml, lowers this value further to 199°C. It follows that effective microorganisms in liquid form have a very negative effect on the oil properties, so they should not be added to the new oil. The situation is different in the case of microorganisms in the form of ceramic tubes. The analysis of the graph shows that the addition of three pieces of ceramic tubes has no effect on the oil, because the flash point value is at the same level as for oil without the addition of microorganisms. A larger number of ceramic tubes, i.e. in this case six pieces, even slightly increases this point to the value of 231.5°C. The graphs in Fig. 8 for acid and base numbers also show that the effective microorganisms in the form of ceramic tubes do not increase the acid number and do not significantly reduce the base number of new oil. This confirms that the best choice will be to add effective microorganisms to the new oil, but only in the form of ceramic tubes.

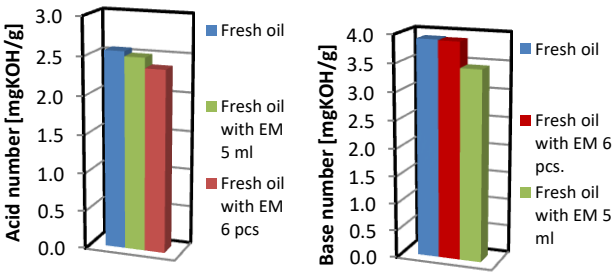

Fig. 8. Acid and base number of fresh oil and fresh oil with EM in liquid form and ceramics tubes

In Fig. 9 is shown the oil flash point for fresh oil and fresh oil with the addition of colloidal nanosilver and silver solution. Regardless of the type of silver and its quantity, very low flash point values were obtained, i.e. for colloidal nanosilver 2.5 ml and 5 ml – 200°C and 198°C, respectively, while for silver solution 2.5 ml and 5 ml – 207°C and 201°C compared to 213°C for oil without any additives. The highest value of the flash point can be observed for the silver solution of 2.5 ml, but this temperature level is still unacceptable due to the fact that oil vapors may ignite in such conditions when they come into contact with a flame. Larger amounts of additives result in even lower flash point values.

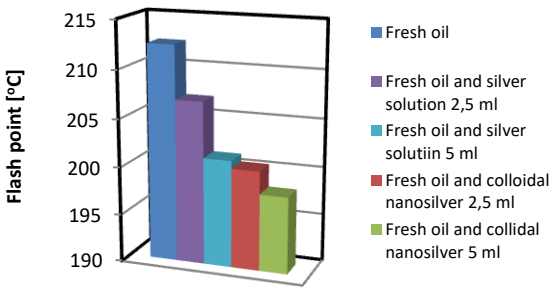

Fig. 9. Flash point oil of fresh oil and fresh oil with colloidal nanosilver and silver solution

The acid and base number graphs presented in Fig. 10 confirm the negative effect of such an addition to the oil, because the addition of silver, for example in the amount of 5 ml, increases the acid value and significantly reduces the base number of new oil. This phenomenon occurs regardless of the type of silver added. Basically, adding silver to new oil does not have any justification, because even before pouring it in the internal combustion engine, we have much worse properties than new oil, and the operation of engine oil in difficult conditions will only accelerate its decomposition.

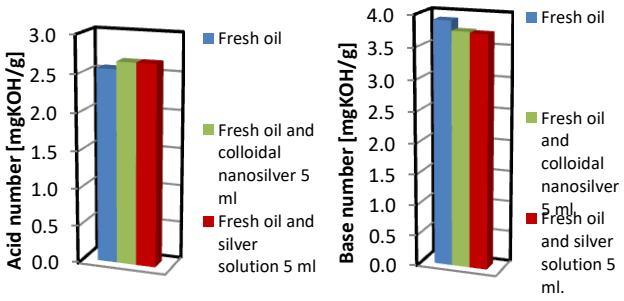

Fig. 10. Acid and base number of fresh oil and fresh oil with colloidal nanosilver and silver solution

Figure 11 shows the flash point for used oil without additive and comparison with used oil with the addition of effective microorganisms, the same as for fresh oil, i.e. in liquid form and in the form of ceramic tubes. In order to visualize, how much the flash point dropped for used oil, the results were compared with the value for fresh oil. The analysis of the graphs shows that, unlike for fresh oil, the best results are obtained for oil with the addition of microorganisms in a liquid form, because the flash point of used oil without any additives is 199°C (for fresh oil it is 213°C), while with the addition of effective microorganisms in the amount of 2.5 ml and 5 ml, respectively 203°C and 202°C, and for effective microorganisms in the form of ceramic tubes in the amount of 3 pcs and 6 pcs, respectively 197°C and 198°C. This means that the effective microorganisms in the form of ceramic tubes lower this flash point even more compared to the original value.

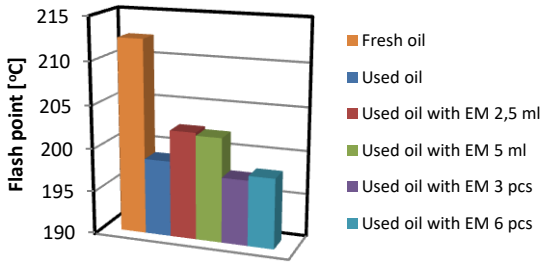

Fig. 11. Flash point oil of used oil and used oil with EM in liquid form and ceramic tubes

The acid and base numbers presented in Fig. 12 also confirm that the use of effective microorganisms in liquid form in the used oil gives better parameters, because effective microorganisms in the form of ceramic tubes increase the acid number much more, while reducing the base number. This is very disadvantageous for the components of the internal combustion engine.

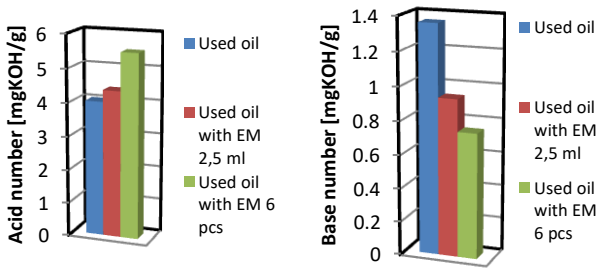

Fig. 12. Acid and base number of used oil and used oil with EM in liquid form and ceramic tubes

Graphs for used oil without additives and with silver additives as colloidal nanosilver and silver solution are shown in Fig. 13. Their analysis shows that without any additives the oil flash point is 199°C (for new oil it is 213°C) and the oil with the 5 ml silver solution addition, for which the flash point is almost 198°C, is the closest to this value.

Also for the amount of 5 ml, but this time for the colloidal nanosilver, this point is 194°C. The smaller amount of silver, i.e. 2.5 ml, significantly lowers the flash point to a temperature of 186°C for colloidal nanosilver and 191°C for silver solution. In general, the addition of silver does not

improve the properties of the oil, so it makes no sense to add such compounds to the used oil. It follows that in this case both types of silver in this larger amount, i.e. 5 ml, have the least negative influence on the flash point.

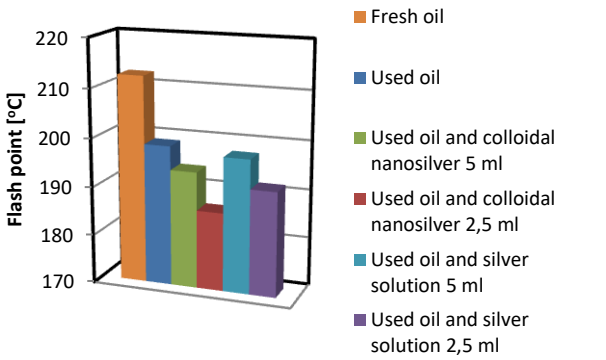

Fig. 13. Flash point oil of used oil and used oil with colloidal nanosilver and silversolution

The acid and base number graphs (Fig. 14) show that better values were obtained for colloidal nanosilver in the amount of 5 ml. This applies to both acid number and base number. On the other hand, the addition of the silver solution resulted in the highest value of the flash point, but also, unfortunately, a further increase in the acid number and a decrease in the base number. This makes this additive unsuitable for improving the properties of the oil, causing a counterproductive effect. In general, the addition of silver compounds does not have the beneficial effect of restoring the original properties, preferably those of the new oil.

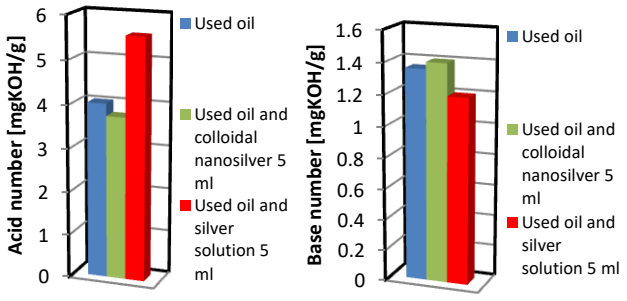

Fig. 14. Acid and base number of used oil and used oil with colloidal nanosilver and silver solution

Figure 2 shows the color of the samples, which shows that after adding microorganisms in a liquid form to the new oil, they became an oil-water emulsion and in this form are not suitable for use as a lubricating oil (there is probably some decomposition and release of water bound in the oil or a chemical reaction that resulted in the formation of such a large amount of water, which is related to the composition of the liquid additive of effective microorganisms).

The situation is different for the addition of microorganisms in the form of ceramic tubes, in which the microorganisms are bound and do not mix with the oil as in liquid form. It follows that only effective microorganisms are released into the oil, and due to the fact that they are not in liquid form, the oil has a clean and clear appearance. Silver solution and colloidal nanosilver were also added to the fresh oil in the amounts of 2.5 ml and 5 ml.

These photos in Fig. 3 show that additives caused the formation of a water-oil emulsion. In this form, the lubricating oil will not properly perform the tasks for which it was intended.

In used oil additives were added after using the oil. Previous research show that better parameters for used oil are obtained by adding EM in liquid form. The best additive for new oil are effective microorganisms in the form of ceramic tubes, and for used oil, the addition of effective microorganisms in the liquid form works best. As for silver, they adversely affect the parameters of both new and used oil.

6. Conclusions

The article presents research of flash points for new and used oil with the addition of effective microorganisms and silver solution. Additionally, the acid and base numbers for selected mixtures were presented in order to confirm the obtained results.

This work shows the variation in the value of the oil's flash point after adding to fresh and used oil effective microorganisms in liquid form and in the form of ceramic tubes. In addition, silver solution and colloidal nanosilver were added to fresh and used oil in the same proportions as for effective microorganisms. Each sample of pure oil and oil with additives were tested three times. However, the article presents the average result for each case.

Analyzing the results obtained, it can be seen, that for fresh oil the flash point is 213^{o}C. On the other hand, adding of the effective microorganisms to the oil in the amount of 2.5 ml causes the flash point to be lowered to 200^{o}C, while the greater amount of liquid additive, i.e. 5 ml, lowers this value further to 199^{o}C. It follows that effective microorganisms in liquid form have a very negative effect on the oil properties, so they should not be added to the new oil. The situation is different in the case of microorganisms in the form of ceramic tubes. Three pieces of ceramic tubes has no effect on the oil, because the flash point value is at the same level as for oil without the addition of microorganisms. A larger number of ceramic tubes, i.e. in this case six pieces, even slightly increases this point to the value of 231.5^{o}C.

The acid and base number charts also confirm that adding effective microorganisms to the new oil in the form of ceramic tubes is the best choice.

Regardless of the type of silver and its quantity, very low flash point values were obtained, i.e. for colloidal nanosilver 2.5 ml and 5 ml – 200^{o}C and 198^{o}C, respectively, while for silver solution 2.5 ml and 5 ml – 207^{o}C and 201^{o}C compared to 213^{o}C for oil without any additives. The highest value of the flash point can be observed for the silver solution of 2.5 ml, but this temperature level is still unacceptable due to the fact that oil vapors may ignite in such conditions when they come into contact with a flame. Larger amounts of additives result in even lower flash point values. Basically, adding silver to new oil does not have any justification, because even before pouring it in the internal combustion engine, we have much worse properties than new oil, and the operation of engine oil in difficult conditions will only accelerate its decomposition.

The acid and base number diagrams only confirm the negative effect of such an oil additive, because the addition of silver increases the acid value and significantly lowers the base value of the new oil. This phenomenon occurs regardless of the type of silver added.

In order to visualize, how much the flash point dropped for used oil, the results were compared with the value for fresh oil. For fresh oil, the best results are obtained for oil with the addition of microorganisms in a liquid form, because the flash point of used oil without any additives is 199°C (for fresh oil it is 213°C), while with the addition of effective microorganisms in the amount of 2.5 ml and 5 ml, respectively 203°C and 202°C, and for effective microorganisms in the form of ceramic tubes in the amount of 3 pcs and 6 pcs, respectively 197°C and 198°C. This means that the effective microorganisms in the form of ceramic tubes lower this flash point even more compared to the original value.

The acid and base number presented in the graphs also confirm that when microorganisms are applied to used oil, better parameters are obtained for oil in the liquid form of this additive, because in the ceramics form they increase the acid number much more, while lowering the base number, which is very unfavorable for internal combustion engine components.

Then an analysis was made for used oil without additives and with silver additives as colloidal nanosilver and silver solution, where without any additives the oil flash point is 199°C (for new oil it is 213°C) and the oil with the 5 ml silver solution addition, for which the flash point is almost 198°C, is the closest to this value.

Also for the amount of 5 ml, but this time for the colloidal nanosilver, this point is 194°C. The smaller amount of silver, i.e. 2.5 ml, significantly lowers the flash point to a temperature of 186°C for colloidal nanosilver and 191°C for silver solution. In general, the addition of silver does not improve the properties of the oil, so it makes no sense to add such compounds to the used oil. It follows that in this case both types of silver in this larger amount, i.e. 5 ml, have the least negative influence on the flash point.

Nomenclature

ASTM	American Society for Testing and Materials	ISO	International Organization for Standardization
CO_2	carbon dioxide	TBN	total base number
EM	effective microorganisms		

Bibliography

[1] Baczewski K, Kałdoński T. Paliwa do silników o zapłonie samoczynnym. WKiŁ, Warszawa 2008.

[2] Benner JJ, Sadeghi F, Hoeprich MR, Frank MC.Lubricating properties of water in oil emulsions. J Tribol. 2006;128(2): 296-311. https://doi.org/10.1080/10402008908981921

[3] Bielaczyc P, Klimkiewicz D, Woodburn J, Szczotka A. Exhaust emission testing methods – BOSMAL's legislative and development emission testing laboratories. Combustion Engines. 2019;178(3):88-98. https://doi.org/10.19206/CE-2019-316

[4] Bielaczyc P, Woodburn J. Global trends in emissions regulation and reduction (perspectives from the 1st International Exhaust Emissions Symposium). Combustion Engines. 2010;142(3):3-27. https://doi.org/10.19206/CE-117132

[5] Dzikowska A, Gościańska J, Nowak I. Synteza, właściwości fizykochemiczne oraz zastosowania nanocząstek srebra w kosmetyce. Kosmetyki – chemia dla ciała. Wydawnictwo Cursiva. 2011:163-182.

[6] Gawron B, Białecki T, Janicka A, Górniak A, Zawiślak M. An innovative method for exhaust gases toxicity evaluation in the miniature turbojet engine. Aircr Eng Aerosp Tec. 2017;89(6):757-763. https://doi.org/10.1108/AEAT-06-2016-0091

[7] Gaylarde CC, Bento F, Kelley J. Microbial contamination of stored hydrocarbon fuels and its control. Rev Microbiol. 1999;30(1):1-10. https://doi.org/10.1590/S0001-37141999000100001

[8] Janicka A, Zawiślak M. New technology for toxicity investigation of vehicle indoor air with BAT-CELL. Toxicol Lett. 2015;238(2):S372. https://doi.org/10.1016/j.toxlet.2015.08.1062

[9] Jiang H, Wang Y, Nie C, Yan F, Ouyang X, Gong J. Oil sludge deposition in storage tanks: a case study for Russian crude oil in Mo-He Station. Appl Sci. 2021;11(1):321. https://doi.org/10.3390/app11010321

[10] Kolasa-Więcek A. Czy efektywne mikroorganizmy zrewolucjonizują świat? Postępy Techniki Przetwórstwa Spożywczego. 2010, 1, 66-69.

[11] Keska A, Janicka A. Application of bat-cell bio-ambient tests in exhaust gas emissions examinations for euro and euro 6 combustion engines. J Mach Eng. 2017;17(4):83-90. https://doi.org/10.5604/01.3001.0010.7007

[12] Krakowski R. Research on the effect of the effective microorganisms, silver solution and colloidal nanosilver addition on the engine oil acid number (TAN). Combustion Engines. 2021;186(3):59-63. https://doi.org/10.19206/CE-140730

[13] Krakowski R. Research on the effect of the effective microorganisms, silver solution and colloidal nanosilver addition on the engine oil base number (TBN). Combustion Engines. 2021;187(4):8-11. https://doi.org/10.19206/CE-140112

[14] Krakowski R. Research into the effects of the effective microorganisms addition on the engine oil viscosity. Journal of Kones. 2019;26(3):105-112. https://doi.org/10.2478/kones-2019-0063

[15] Lasocki J, Karwowska E. Wpływ mikroorganizmów bytujących w środowisku oleju napędowego i biodiesla na układ paliwowy pojazdów napędzanych silnikami o zapłonie samoczynnym. Archiwum Motoryzacji. 2010;(3):167-183.

[16] Lawrowski Z. Tribologia, tarcie, zużycie i smarowanie. Wydawnictwo Politechniki Wrocławskiej. Wrocław 2008.

[17] Ljubas D, Krpan H, Matanovic I. Influence of engine oils dilution by fuels on their viscosity, flash point and fire point. Nafta. 2010;61(2):73-79.

[18] Mazanek A. An overview of engine and exploitation research methods taking into account the current and future quality requirements on motor fuels. Paraffin-Gas. 2014;(8): 534-540.

[19] Młynarczak A. Modelling of alkalinity changes in lubricating oils used in marine diesel engines. Journal of KONES. 2009;16(2):329-335.

[20] Passman FJ. Microbial contamination and its control in fuels and fuel systems since 1980 – a review. Int Biodeter Biodegr. 2013;(81):88-104. https://doi.org/10.1016/j.ibiod.2012.08.002
[21] Ptak S, Jakóbiec J. Ropa naftowa jako główny surowiec energetyczno-przemysłowy. Nafta-Gaz. 2016;72(6):451-460.
[22] Shao H, Lam W, Remias J, Roos J, Choi S, Seong HJ. Effect of lubricant oil properties on the performance of gasoline particulate filter (GPF). SAE Int J Fuels Lubr. 2016; 9(3):650-658. https://doi.org/10.4271/2016-01-2287.4
[23] Tarasova G, Grigoryeva E. Research on destruction of oil-containing emulsion waste by hard solid demulsinators based on industry waste, E3S Web Conf (CATPID-2019). 2019;138(8):01020. https://doi.org/10.1051/e3sconf/201913801020
[24] Vijayakumar AP, Sarath PS, Nidhin PS et al. Experimental determination of flash point of lubricating oil. International Refereed Journal of Engineering and Science (IRJES). 2018;7(4):1-3. https://www.irjes.com/Papers/vol7-issue4/A0704010103.pdf
[25] Addinol. https://addinol.de/en/service-en/expert-tip/flash-point/ (accessed on 17.06.2022).
[26] Allegro. https://allegro.pl/oferta/srebro-koloidalne-jonowe-ag-500ml-9929512556 (accessed on 17.06.2022).
[27] Aptekarzpolski. https://www.aptekarzpolski.pl/2015/01/01-2015-technologia-efektywnych-mikroorganizmow/ (accessed on 17.06.2022).
[28] ASTM. https://www.astm.org/d7094-04.html (accessed on 17.06.2022).
[29] Ecoshop. https://www.ecoshop.com.pl/mikroorganizmy/3556-greenland-em-melasa-1l-5907738935220.html (accessed on 17.06.2022).
[30] Enaturalnie. https://enaturalnie.pl/argentum200-niejonowe-srebro-100-ppm-plyn-tonik-500-ml-aura-herbals_2838.html (accessed on 17.06.2022).
[31] Falaem. https://falaem.pl/rurki-ceramiczne-uzdatnianie-wody (accessed on 17.06.2022).
[32] Hsewatch. https://hsewatch.com/flash-point (accessed on 17.06.2022).
[33] Machinery Lubrication. https://www.machinerylubrication.com/Read/19/flash-point-test (accessed on 17.06.2022).
[34] Medium. https://medium.com/@veedolindia/5-main-functions-of-engine-oil-83134430a3e9\ (accessed on 17.06.2022).
[35] Motofaktor. https://www.motofaktor.pl/funkcje-oleju-silnikowego/(accessed on 17.06.2022)
[36] Mydelkoznanosrebrem. https://www.mydelkoznanosrebrem.pl/nanosrebro.php (accessed on 17.06.2022).
[37] Rymax-lubricants. https://www.rymax-lubricants.com/updates/the-function-of-engine-oil/ (accessed on 17.06.2022).
[38] Semanticscholar. https://www.semanticscholar.org/paper/Influence-of-engine-oils-dilution-by-fuels-on-their-Ljubas-Krpan/3605e76fb43ec911dc60cf2d7cfaca59975ad5e8 (accessed on 17.06.2022).
[39] Slideshare. https://www.slideshare.net/AllahDadKhan/effective-microorganism-technology-by-allah-dad-khan (accessed on 17.06.2022).
[40] Totalenergies. https://totalenergies.ke/products/lubricants/engine-oil-guides/engine-oil-role-benefits (accessed on 17.06.2022).
[41] Tusnovics. https://www.tusnovics.pl/static/tsvc-gear-search/files/ERAFLASH/Tusnovics_ERAFLASH.pdf (accessed on 17.06.2022).
[42] UMG. http://wm.umg.edu.pl/sites/default/files/files/laboratoria/KPT/Lab%20Reologii/Era%20Flash%20temp%20zaplonu.pdf (accessed on 17.06.2022).
[43] Xbee. www.xbee.com.pl/specyfikacja-techniczna/dzialanie (accessed on 17.06.2022).
[44] Xbee. www.xbee.com/enzyme-fuel-treatment/reduce-fuel-consumption-additive/ (accessed on 17.06.2022).

Rafał Krakowski, DEng. – Faculty of Marine Engineering, Gdynia Maritime University.
e-mail: *r.krakowski@wm.umg.edu.pl*

AIR FORCE INSTITUTE OF TECHNOLOGY
INSTYTUT TECHNICZNY WOJSK LOTNICZYCH

ul. Księcia Bolesława 6, 01-494 Warszawa, Poland
tel.: +48 261 851 300; fax: +48 261 851 313
www.itwl.pl e-mail: poczta@itwl.pl

SUPPORTING OPERATIONS & MAINTENANCE OF AERONAUTICAL ENGINEERING:

- tribological diagnostics of lubrication systems in power units and hydraulic systems
- endoscopic examinations of power units
- measurements of operation parameters of power units using one's own and company systems and their analysis

DEVISING AND DEVELOPING NEW DIAGNOSTIC METHODS:

- CT examinations – V/tome/X CT system
- blade vibration measurements using the tip-timing method

NEW TECHNOLOGIES FOR UNMANNED AERIAL VEHICLES:

- technical condition monitoring system of mini jet engine
- hybrid drive of unmanned aerial vehicle

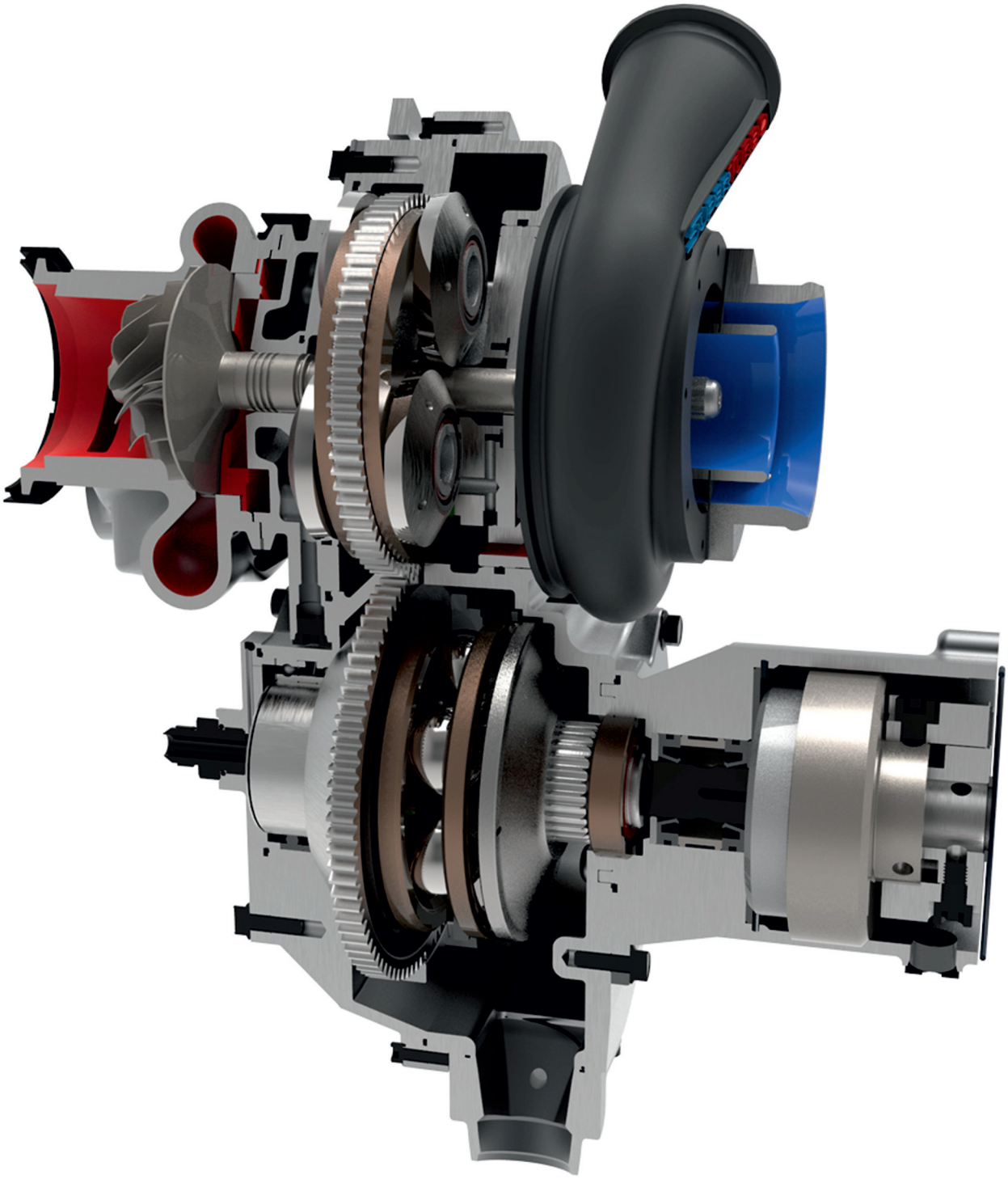

Publisher:

Polish Scientific Society of Combustion Engines

ISSN: 2300-9896
eISSN: 2658-1442

Combustion Engines

Polskie Towarzystwo Naukowe Silników Spalinowych

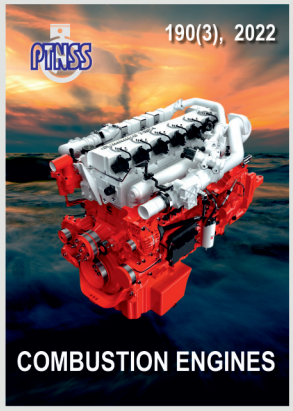

www.combustion-engines.eu